



Infra-red study of lipid-water systems.

WILFORD, Leslie D.R.

Available from the Sheffield Hallam University Research Archive (SHURA) at:

<http://shura.shu.ac.uk/20535/>

A Sheffield Hallam University thesis

This thesis is protected by copyright which belongs to the author.

The content must not be changed in any way or sold commercially in any format or medium without the formal permission of the author.

When referring to this work, full bibliographic details including the author, title, awarding institution and date of the thesis must be given.

Please visit <http://shura.shu.ac.uk/20535/> and <http://shura.shu.ac.uk/information.html> for further details about copyright and re-use permissions.

POND STREET
SHEFFIELD S1 1WB

TELEPEN

100250758 8



**SHEFFIELD POLYTECHNIC
LIBRARY SERVICE**



MAIN LIBRARY

Sheffield City Polytechnic Library

REFERENCE ONLY

Books must be returned promptly, or renewed, on
or before the last date stamped above.

FAILURE TO DO SO WILL INCUR FINES

PL/17

ProQuest Number: 10701182

All rights reserved

INFORMATION TO ALL USERS

The quality of this reproduction is dependent upon the quality of the copy submitted.

In the unlikely event that the author did not send a complete manuscript and there are missing pages, these will be noted. Also, if material had to be removed, a note will indicate the deletion.



ProQuest 10701182

Published by ProQuest LLC (2017). Copyright of the Dissertation is held by the Author.

All rights reserved.

This work is protected against unauthorized copying under Title 17, United States Code
Microform Edition © ProQuest LLC.

ProQuest LLC.
789 East Eisenhower Parkway
P.O. Box 1346
Ann Arbor, MI 48106 – 1346

A thesis entitled

INFRA-RED STUDY OF LIPID-WATER
SYSTEMS

presented by

LESLIE DOUGLAS REID WILFORD B.Tech.

in part fulfilment of the requirements
for the degree of

DOCTOR OF PHILOSOPHY

of the

COUNCIL FOR NATIONAL ACADEMIC AWARDS

Department of Chemistry and Biology,
Sheffield Polytechnic,
Pond Street,
Sheffield, S1 1WB.

September 1973



~~74-15597~~

ACKNOWLEDGEMENTS

This work was carried out in the Department of Chemistry and Biology, Sheffield Polytechnic.

My sincere thanks are expressed to my supervisor Dr. M.P. McDonald, for his help and guidance throughout this research work.

I would also like to thank the late Professor Lawrence for his interest in the work carried out, and for supplying samples of 1-monodecanoin, 1-monododecanoin, and 1-mono-octadecanoin.

I am grateful to Professor D. Chapman, Assistant Director of Research, Reckitt & Colman Ltd., for acting as industrial supervisor, and to Dr. R.G. Laughlin of Procter & Gamble, Ohio, U.S.A. for supplying a sample of dimethyldodecylphosphine oxide.

I wish to thank the Local Education Authority of the City of Sheffield for their financial support during my research assistantship.

L.D.R. Wilford

SUMMARY

The work described in this thesis has been divided into two parts.

In part one the infra-red spectra of pinacol, a model compound with two OH groups, and its monohydrate and hexahydrate have been recorded at the beam temperature and low temperature and assignments made of the principle vibrations in each case. Also low temperature spectra of pure and partly deuterated substances have been recorded. These spectra are discussed in terms of their crystal structures which have been investigated previously by X-ray diffraction. Certain features of the hydrogen bonding in pinacol and its hydrates have been elucidated from a study of the decoupled OD stretching vibrations.

In part two a number of lipids and lipid/water systems have been studied. The polymorphism of four 1-monoglycerides has been investigated. Transition temperatures have been determined and the thermal stability of the various polymorphs has been investigated. The structure of the various polymorphs has been investigated using infra-red spectroscopy. Assignments of the principle vibrations have been made of the most stable form of the pure and partly deuterated 1-monooctanoin.

Infra-red spectra of 1-monooctanoin in solution have been obtained and conclusions have been drawn about the hydrogen bonding of 1-monooctanoin in the dissolved state.

The 1-monoundecanoin/D₂O phase diagram has been determined and the structure of the neat liquid crystalline phase of this system, along with that of the 1-monooctanoin/D₂O system, have been investigated using polarized and unpolarized infra-red spectroscopy.

Polarized and unpolarized infra-red spectra and X-ray long spacings of dimethyldecyl - and dimethyldodecylphosphine oxide

have been obtained. Assignments of the principle vibrations have been made and the results are discussed in terms of a model structure.

The dimethyldecylphosphine oxide/ H_2O phase diagram has been determined and the structures of the neat and middle liquid crystalline phases of this system and the dimethyldodecylphosphine oxide/ H_2O system, as well as the hydrated solid phase of the dimethyldecylphosphine oxide/ H_2O system have been investigated using polarized and unpolarized infra-red spectroscopy.

Useful information has been obtained on the hydrogen bonding in most of these systems.

CONTENTS

PART I

MODEL SYSTEM

	<u>PAGE</u>
CHAPTER IINTRODUCTION	1
CHAPTER IIEXPERIMENTAL	
(i) Theory	7
(ii) Preparation and purification of materials	9
(iii) Growing of single crystals	11
(iv) Running of spectra	11
CHAPTER IIIRESULTS AND DISCUSSION	13
CHAPTER IVCONCLUSIONS	33

PART II

LIPID AND LIPID-WATER SYSTEMS

CHAPTER IINTRODUCTION	
(I) Lipid Systems	34
(II) Structure of Lipids	35
(III) Hydration of Lipids	42
(IV) Structure of Water from Infra-red and Raman spectroscopy	45
(V) Lyotropic Liquid Crystalline Phases	49
CHAPTER IIEXPERIMENTAL	
(I) Preparation and purification of materials	59
(II) Methods	64
CHAPTER IIIANHYDROUS LIPIDS	
(I) 1-monoglycerides	69
(II) Unsymmetrical Trialkylphosphine Oxides	99
CHAPTER IVPHASE BEHAVIOUR	
(I) Results	119

(II) Discussion	120
CHAPTER VHYDRATED DIMETHYLDECYL-	
PHOSPHINE OXIDE	
(I) Results	130
(II) Discussion	130
CHAPTER VILIQUID CRYSTALLINE	
PHASES	
(I) Neat phase	136
(II) Middle phase	165
CHAPTER VIICONCLUSIONS	
(I) Anhydrous Lipids	172
(II) Hydrated dimethyldecylphosphine oxide	173
(III) Liquid Crystalline Phases	174
REFERENCES	177
Postgraduate course of studies	191

CHAPTER I

INTRODUCTION

In recent years the study of the structure of polar lipids and their interaction with themselves and water has intensified considerably.

Industrially and academically they are of great interest. From the industrial point of view they are important not only as surface active agents for cleansing purposes but they are used in the production of stable emulsions and also to promote solidification of fats in suitable crystal forms. From an academic point of view a study of these systems leads to an understanding of the Van der Waals forces between the alkyl chains, the electrostatic forces between ionic head groups of lipids and water, as well as the hydrogen bonding (H-bonding) which takes place between lipids containing one or more polar groups of the type $-OH$, $-NH_2$, $-COOH$, $\geq P=O$, $\geq N=O$ and water.

Polar lipids are of great biological importance. The extent to which polar lipids interact with water is crucial to the organisation, structure and function of the living cell. The basic unit of life is really an aqueous system in which there are suspended various lipids and complex proteins, the organisation and structure of which ultimately dictate its function.

The work recorded in this thesis involves a study of the structure of certain polar lipids which contain $-OH$ and $\geq P=O$ groups, and the systems formed when they interact with water. A hydroxylic model compound, pinacol, which forms two definite crystalline hydrates has also been investigated.

The number of crystalline hydrates of monohydric alcohols

known is small (1). Hatt (1) gives a list of monohydric alcohols of an aliphatic nature which are known to form hydrates.

All the alcohols forming hydrates have a compact molecular shape and most of them are tertiary alcohols possessing considerable symmetry. Methanol, tertiary butanol and pentamethylethanol (P.M.E.) are the only saturated aliphatic alcohols which form crystalline hydrates. The replacement of three methyl groups in P.M.E. with three chlorine atoms still preserves the ability to form a hemihydrate. This fact suggests that spatial factors and not electronic factors are important in the formation of alcohol hydrates. Hatt (1) has inspected some alcohols closely related to P.M.E. which do not form hydrates and has concluded that these spatial factors can be closely defined.

The aliphatic glycols that have been reported to form hydrates (1) are methyl substituted glycols and show a striking correspondence to the hydrate forming monohydric alcohols. The series ethylene glycol, meso-2,3-butanediol, 2-methyl-2,3-butanediol and pinacol being analogous to methanol, tertiary butanol and P.M.E.

Pinacol (2,3-dimethylbutan-2,3 diol) forms two hydrates, the mono- and hexahydrate. The existence of these two hydrates was first shown by Pushin et al (2). The phase diagram of Pushin et al (2) is shown in figure 1. There are two compounds with congruent melting points clearly shown by the maxima at 50 molar per cent and 41.25°C (pinacol monohydrate) and 14.3 molar per cent and 45.4°C (pinacol hexahydrate).

O'Connor (3) has proposed, using X-ray diffraction that pinacol crystallizes in an orthorhombic structure with sixteen

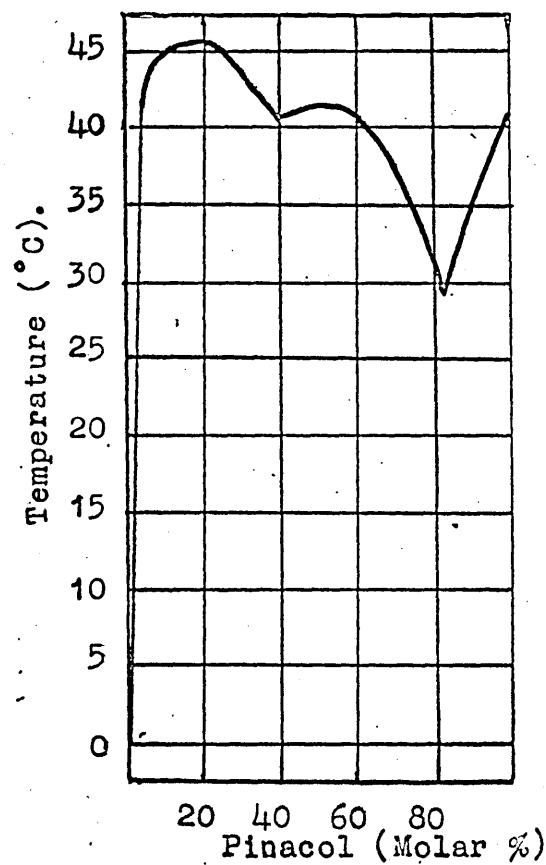


Figure 1.

Pinacol/water phase diagram.(2)

molecules per unit cell. Figures 2a, **b** and c show the proposed structure assuming all the molecules are in the gauche configuration. In figure 2a each symbol of the type $\text{C} \begin{array}{c} \text{O} \\ | \\ \text{---} \text{C} \end{array} \text{C}$ or $\text{O} \begin{array}{c} \text{C} \\ | \\ \text{---} \text{O} \end{array} \text{C}$ represents a pinacol molecule. The C-C part represents the central carbon-carbon bond of the pinacol molecule. O-O represents an imaginary line joining the two oxygen atoms of the pinacol molecule. The methyl groups have been excluded for convenience. The dotted lines represent the H-bonding system. The molecules are oriented in space in one of two positions. The first type of molecule have their C-C bond parallel to the 'a' crystallographic axis. The second type of molecule have their O-O connecting line parallel to the 'a' crystallographic axis. Going across the unit cell in the 'b' crystallographic direction the molecules are alternately above and below the central layer of oxygen atoms.

Figure 3 shows a cross section of pinacol monohydrate structure suggested by Hatt (1). Rotation through 90° gives the arrangement in the adjacent layers of the pinacol molecules. O'Connor (3) using X-ray diffraction has shown the monohydrate to crystallize in the tetragonal system with two molecules per unit cell and with a structure similar to that suggested by Hatt (1). Figures 4a and **b** show the structure proposed by O'Connor (3). Figure 4a shows the tetrahedrally positioned water molecule, the oxygen of that molecule being represented by O_w with the three water molecules W_1 , W_2 and W_3 occupying positions vertically below each other. The line connecting O_{A3} O_{A4} oxygen atoms is in the 'ac' plane and the line connecting O_{A2} O_{A1} oxygen atoms is in the 'bc' plane. Figure 4b shows the chain structure of the monohydrate with pinacol in the trans configuration.

O'Connor (3) has also shown using X-ray diffraction that

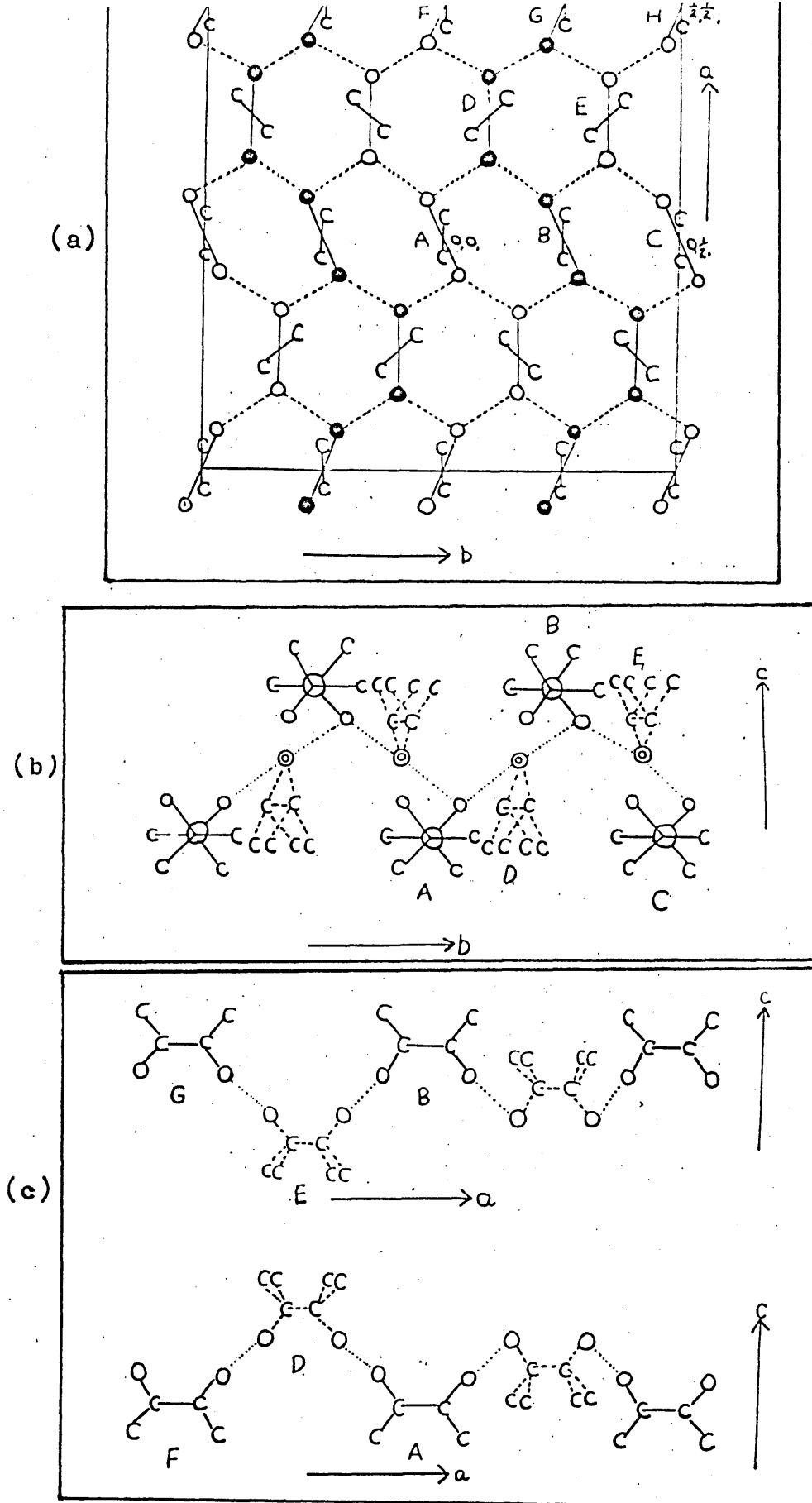


Figure 2.
Structural diagram of pinacol projected onto the
(a) ab, (b) bc, (c) ac planes. (3)

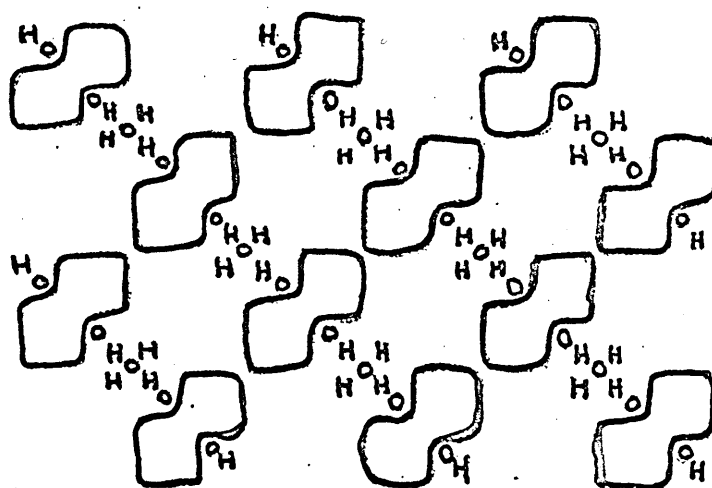


Figure 3.

A cross section of the pinacol monohydrate structure suggested by Hatt(1).

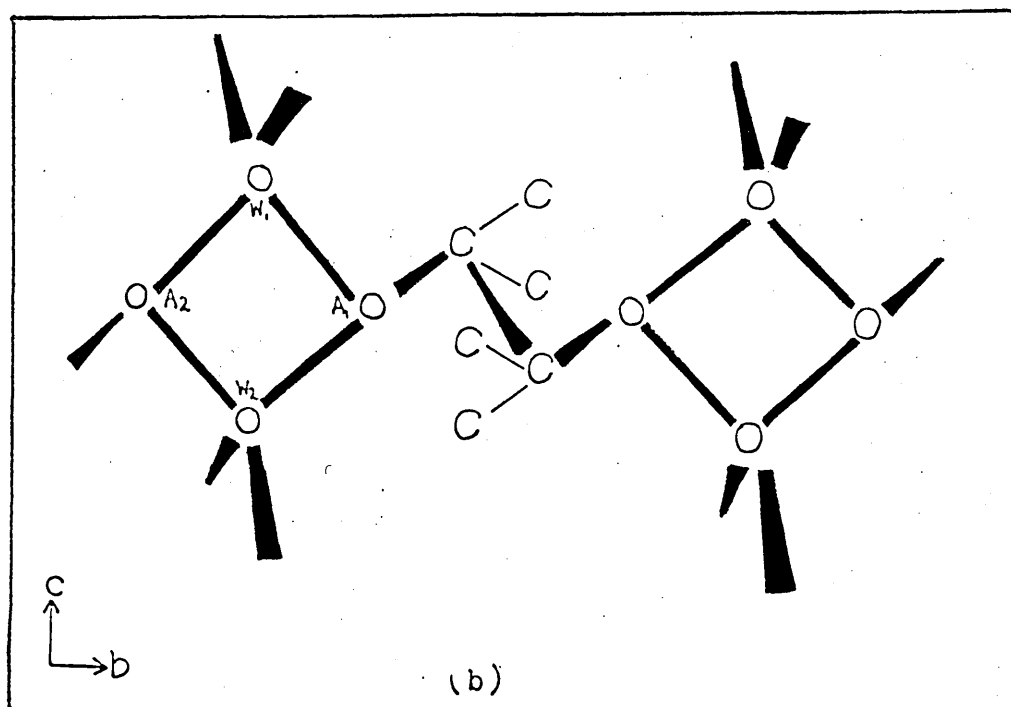
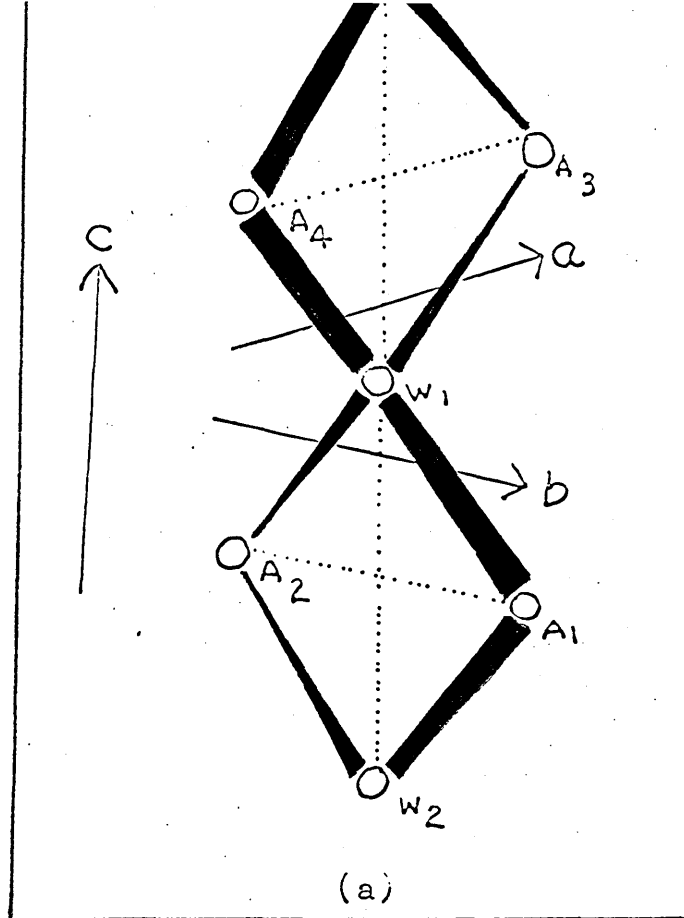


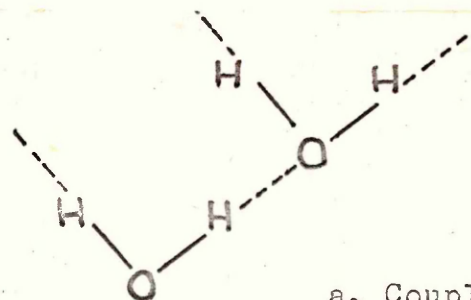
Figure 4.
Structural diagram of pinacol monohydrate (3)

the hexahydrate crystallizes in the monoclinic system with eight molecules per unit cell. He also concludes that possibly the structure of the hexahydrate has some similarity to that of the monohydrate.

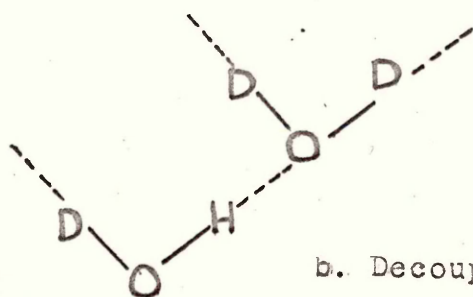
To date no infra-red spectroscopic studies have been carried out on any of the above organic hydrates. However several have been made on inorganic hydrates (4-11). In some of these studies (6-11) the isotope dilution technique has proved very useful for sensing the environment about the water molecules in the hydrates, the number of $\nu(\text{OH})$ and $\nu(\text{OD})$ bands directly reflecting the number of physically different OH and OD bonds in the hydrate.

Several unpolarized (12, 13, 14) and polarized (12, 15-18) infra-red studies of the monohydric alcohols themselves have been reported. In some cases complete analysis of the vibrational modes has been carried out in relation to their structure (12, 13, 15). Some studies have also been carried out on the H-bonding in solid monohydric alcohols (16, 17). In these studies use has been made of the decoupled $\nu(\text{OH})$ and $\nu(\text{OD})$ modes. The physical basis of coupling and decoupling is as follows.

The oscillations of weakly connected vibrations having nearly the same characteristic frequency are said to be coupled. Two pendulums suspended from a taut string are examples of such a coupled system (figure 5), since displacement in one vibrator produces forces in the other vibrator



a. Coupled systems



b. Decoupled systems



Figure 5
Coupled and decoupled vibrating systems.

and this sort of interaction can occur between neighbouring molecules in a crystal.

If the frequencies of the decoupled vibrators are nearly the same, then the introduction of a physical connection between them will produce a much larger shift in the frequencies of the system than if the frequencies of the decoupled vibrators are quite different. The frequency changes produced by connecting two pendulums of very different length or bob mass are therefore small and the pendulums are said to be decoupled. Similarly the OH bond in a particular alcohol molecule is strongly coupled with the other OH bonds in a crystal of ordinary alcohol but if all the other protons in the environment of the particular OH bond are replaced by deuterons then the OH is decoupled from the lattice.

Both decoupled and coupled $\nu(\text{OH})$ and $\nu(\text{OD})$ bands of monohydric alcohols have been studied by Brasch et al (16, 17) using unpolarized and polarized infra-red spectroscopy, both at normal and high pressures. The polarized spectra of the

coupled $\nu(\text{OH})$ vibrations showed two components polarized at right angles. Spectra of the partially deuterated alcohols demonstrated that the appearance of two bands was due to crystal splitting. This splitting was explained in terms of nearest neighbour coupling of the vibrations of the OH groups along the H-bond chain. The decoupled $\nu(\text{OH})$ vibration of these alcohols gave a narrow singlet absorption with a half band width ($\Delta\nu_{\frac{1}{2}}$) of approximately 30cm^{-1} . Thus it was inferred that $\nu(\text{OH})$ was not inherently broad but that it gained breadth as a result of coupling between OH groups. A further study of the partially deuterated liquid alcohols indicated that the coupling was responsible for only a small part of the $\nu(\text{OH})$ band widths in liquids. It was therefore concluded that different mechanisms controlled the $\nu(\text{OH})$ band widths in liquid and solid alcohols.

The hydrates of pinacol suggest themselves as model systems for looking at the possible structure of water in the solid 1-monoglyceride/ water systems as well as in the liquid crystalline phases. Therefore the object of the work incorporated in this part of the thesis was to study the structure of pinacol and its hydrates using polarized and unpolarized infra-red spectroscopy. Also to make use of the isotope dilution technique to derive information about the environment of the hydroxyl protons in these substances.

CHAPTER II

EXPERIMENTAL

(i) Theory

Infra-red spectra arise from the interaction between electromagnetic radiation and matter, the fundamental range of frequencies for this interaction being $5000 - 550\text{cm}^{-1}$. For an infra-red band to occur by absorption of energy it is essential that there should be a change in the dipole moment of the absorbing molecule during its vibration. The number of normal modes of vibration for non-linear molecules is equal to $3N-6$ (where N is the number of atoms in the molecule).

The vast majority of infra-red spectra have been recorded in the liquid, solution or solid state. The major difference from those in the vapour state is the disappearance in nearly all cases of any rotational structure.

In the liquid state of polymethylene compounds the molecules are curled and bent into a variety of conformations and thus give rise to poorly resolved spectra. Therefore in these states there is no resultant direction of vibration. In the crystalline state, on the other hand, the methylene chains are generally extended, the carbon atoms lying uniformly spaced on two parallel straight lines and the different chains parallel to one another. Consequently the vibrational spectra are better resolved and often simpler even though more bands may appear.

Polarized infra-red spectroscopy has been used extensively to study oriented films and single crystals of polymers (19-27),

n paraffins (22, 23, 24, 28), carboxylic acids (29-39) and alcohols (12, 15-18) and the technique has provided essential information for the complete assignments of bands in the infra-red spectra and also aided structural elucidation. In single crystals the direction of the transition moment may be found using polarized infra-red radiation. If the electric vector, E , of the radiation is parallel to the direction of the transition moment, M , maximum absorption will occur, but if they are perpendicular the absorption will be zero. For cases in-between a gradual change occurs.

In polarized infra-red work it is necessary to be very careful as to the interpretation of the resulting dichroism. This is because whilst it is convenient to speak of 'bond' vibrations, eg. N-H, the normal vibrations in polyatomic molecules involve the movement of all the atoms to some extent, especially those atoms which are adjacent to the 'bond' involved. Further Coulson (40) has pointed out that it is necessary to take into consideration the displacement of the electrons as well as nuclei. Also it is not free molecules but crystalline arrays of molecules which are involved. Hence uncertainties are introduced because of the perturbations which occur through interaction and coupling of vibrations. These difficulties are inherent in the exact determination of directions of transition moments and limit the accuracy in determining the directions of bonds from polarization measurements.

The most satisfactory way of producing polarized radiation in the infra-red region is by the use of a suitable transmission polarizer. This usually consists of a pile of infra-red transparent plates set at Brewsters (polarizing) angle so that the angle of incidence, θ , on the front face of each

plate is given by

$$n = \tan \theta$$

Where n is the refractive index of the dielectric for the wavelength of the light.

Under the conditions stated above the reflected beam contains only the component with electric vector perpendicular to the plane of incidence. Therefore the transmitted beam will be enriched in the component with electric vector parallel to the plane of incidence. Both silver chloride (41) plates or selenium sheet (42,43) are commonly used as the dielectric. Silver chloride polarizers are to be preferred because of their robustness even though they are not as efficient as the selenium type and produce more beam displacement.

Prisms (44) and gratings (45) introduce some polarization into an unpolarized beam. It is therefore necessary to position the polarizer with the E vector of the radiation either parallel, perpendicular or at 45° (44) to the exit slit.

(ii) Preparation and purification of materials

Pinacol was obtained from Koch light laboratories and was first dried by refluxing it for 24 hours over calcium oxide, which had been ignited for 24 hours at 900°C . The pinacol was then distilled, the material collected being that which boiled at 172.5°C at 750mm pressure.

The purity of this distilled material was checked using a Pye 104 gas chromatograph (G.L.C) with flame ionisation detector. An 11ft. column was used and the oven temperature was set at approximately 5°C below the boiling point of the pinacol sample. The stationary phase used was polyethylene glycol adipate. The purity was found to be at least 99.5%. The pure anhydrous pinacol was subsequently stored in a dessicator over P_2O_5 .

To prepare the monohydrate and hexahydrate forms, pure anhydrous pinacol was melted, mixed with water in the required ratio by molecular weight and allowed to solidify. To test whether the correct hydrate had been prepared, melting points were carried out on a Du Pont 900 Differential Scanning Calorimeter (D.S.C). The melting points of the monohydrate and hexahydrate were found to be 41.1°C and 45.2°C respectively (Literature values 41.25°C and 45.4°C (2)). The hydrates thus prepared were stored in sealed flasks in a dessicator over P_2O_5 . The pure water utilized in the preparation of the hydrates was obtained by refluxing distilled water over alkaline permanganate and then distilling, the water collected having a conductivity of less than $2\mu\text{S cm}^{-1}$.

To investigate the decoupled $\nu(\text{OD})$ vibration it was necessary to prepare samples of pinacol, pinacol monohydrate and pinacol hexahydrate containing approximately 4% of OD referred to as pinacol-d, pinacol-d monohydrate, and pinacol-d hexahydrate in the following text. Pinacol-d was prepared by refluxing pinacol with a small amount of D_2O , in the presence of freshly ignited calcium oxide for 24 hours. Pinacol-d was then distilled, the fraction collected being that which boiled at 172.5°C at 750mm pressure.

Pinacol-d monohydrate was prepared by adding pure water to pinacol in just under the correct mole proportion. The remainder of the mole proportion was then added as D_2O . The addition of D_2O was carried out in a dry box desiccated by P_2O_5 under an atmosphere of dry nitrogen. Pinacol-d hexahydrate was prepared in a similar manner. Again a check of the hydrate prepared was made by carrying out a melting point on the D.S.C. The melting points of the pinacol-d monohydrate and hexahydrate

- 11 -

were found to be 41.1°C and 45.2°C respectively.

In the three cases above sufficient D_2O was added to give a 4% deuteration if 100% exchange had taken place.

(iii) Growing of single crystals

Single crystals of pinacol and pinacol monohydrate were grown from the melt between silver chloride windows kept at a constant temperature of 30°C . Single crystal portions were then detected using a polarizing microscope and the remainder of the cell blanked off with cardboard.

Extreme difficulty was encountered in trying to grow a single crystal of the hexahydrate in this way. This was due to the hexahydrate becoming what may be a glass when cooled just below its melting point. This glass was found to be very stable when kept between the plates for a period of days and did not transform into the crystalline form. Several methods of crystallization were tried including seeding from the melt, crystallization at a constant temperature and gradient cooling, none of which were successful. A method was devised finally which gave the crystalline hexahydrate, but not as a single crystal. This involved melting the hexahydrate between silver chloride windows and then pouring liquid nitrogen over the sample. This method only produced polycrystalline samples.

All the samples between silver chloride windows were sealed around the edges with insulating tape to prevent moisture being absorbed or lost. When not in use the sealed samples were stored in a desiccator over P_2O_5 .

(iv) Running of Spectra

The liquid and polycrystalline samples were produced as thin films between silver chloride windows.

Single crystal polarized spectra were obtained with a silver chloride, six plate polarizer, mounted between the monochromator and detector (figure 6) so that the polarized radiation produced had the electric vector parallel to the exit slit. Dichroisms were observed by rotation of the sample.

Two methods were utilized in variable temperature runs.

- (1) For temperatures above ambient an electrically heated jacket ((J-2) - R11C) was used.
- (2) For temperatures between -170°C and ambient the VLT2 (R11C) cell enclosure was used (figure 7). This is a Dewar cell maintained at a pressure of less than 0.05mm by constant pumping. Liquid nitrogen was used as a coolant and a built in electrical heating jacket used for fine adjustment of temperature.

In both cases the temperature was controlled and monitored by the TEM 1 (R11C) temperature controller. All temperatures measured were accurate to $\pm 2^{\circ}\text{C}$.

Solution spectra were obtained in cells of pathlength 1.0mm with NaCl windows. These spectra were run with a balanced reference cell containing the solvent.

All the infra-red spectra were run on a Grubb Parsons 'Spectromaster' double beam spectrometer, the range of the scan covered being $4000\text{-}550\text{cm}^{-1}$. Calibration of the spectromaster was accurate to $\pm 1\text{cm}^{-1}$.

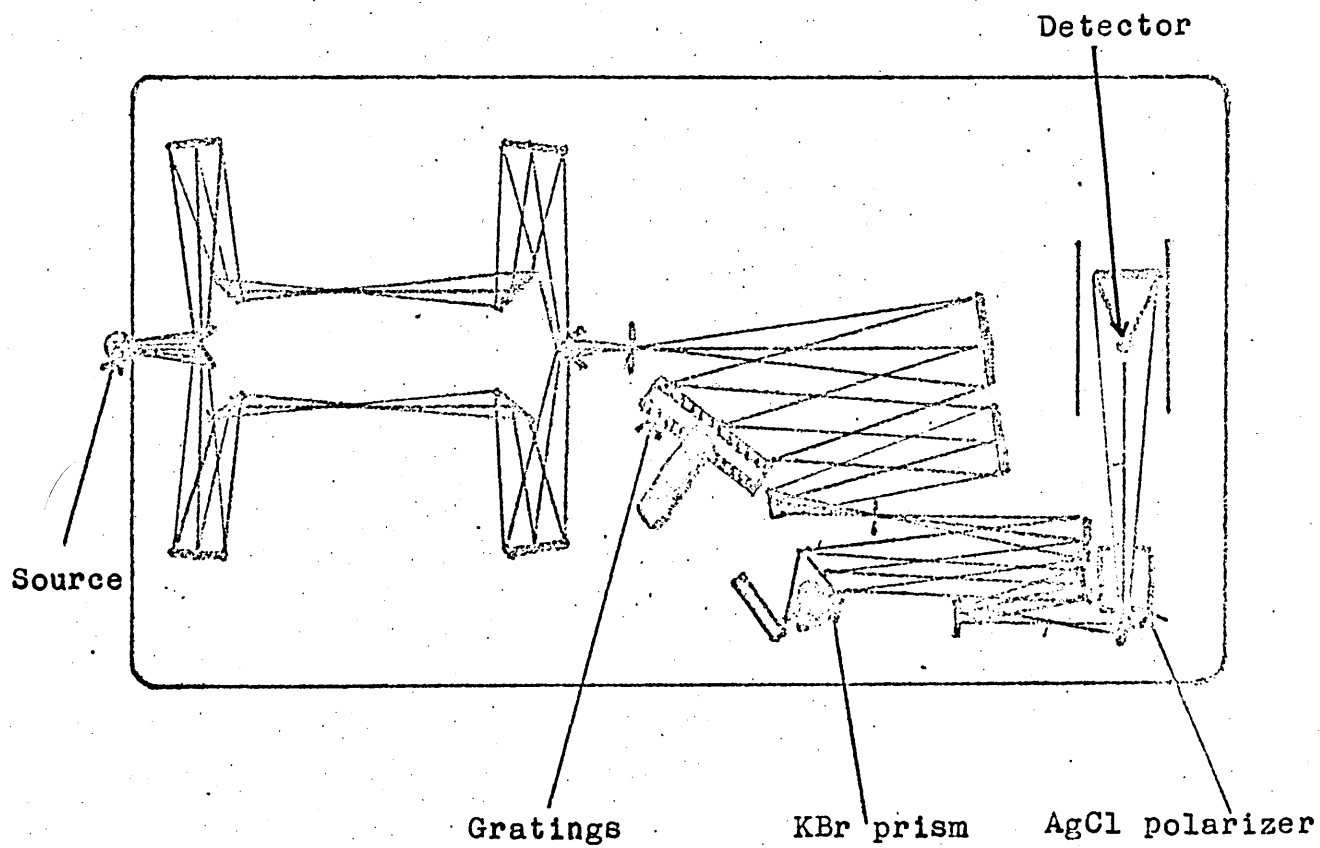


Figure 6.

Diagram showing the position of the AgCl polarizer.

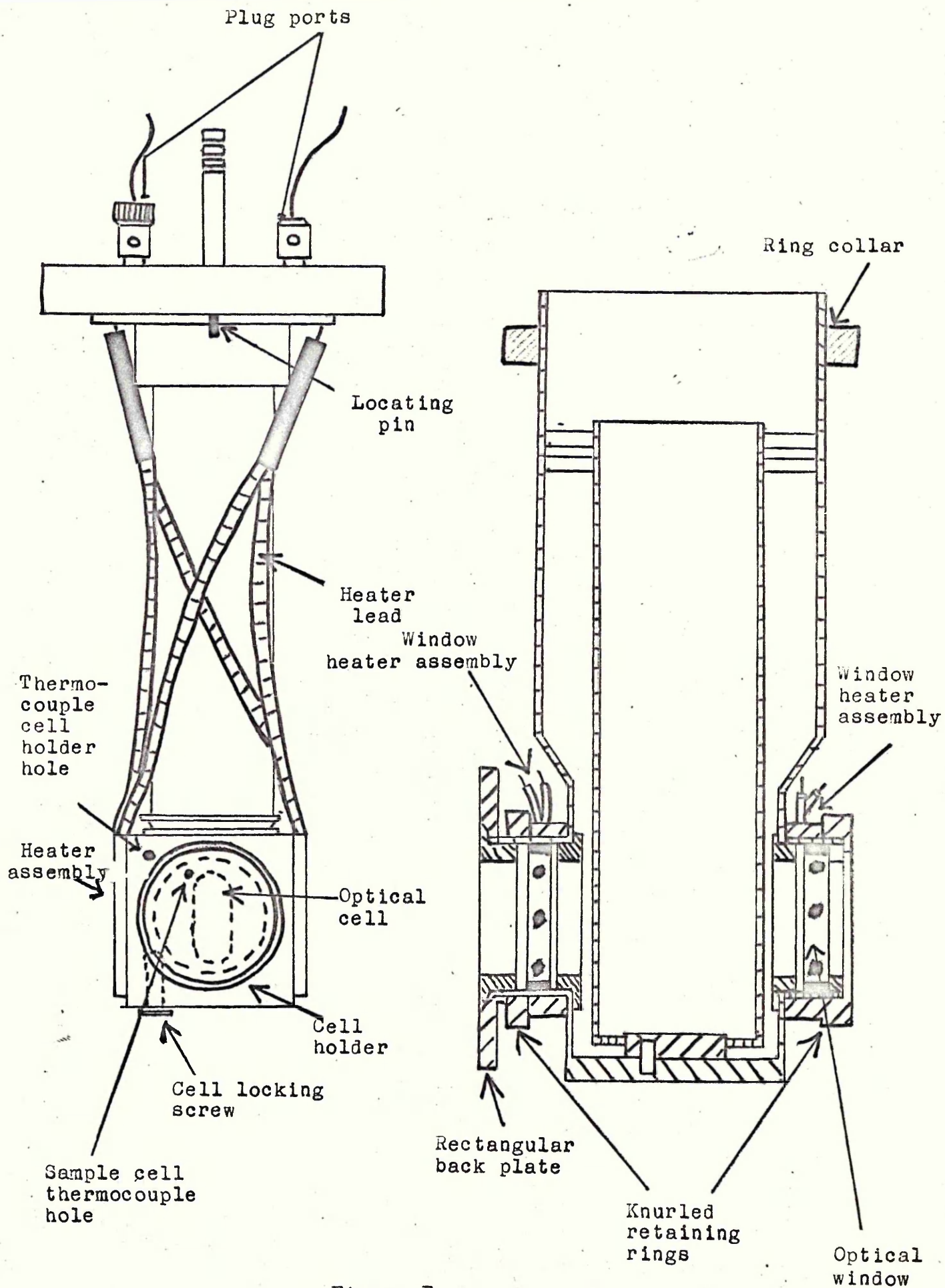


Figure 7.

VLT2(RIIC) cell enclosure.

CHAPTER III

RESULTS AND DISCUSSION

(I) Results

The unpolarized infra-red spectra have been obtained of pinacol (figure 9) and its two hydrates in the liquid state at 50°C and as crystalline solids at the beam temperature (figure 10, 12 and 14) and -170°C (figure 11, 13 and 14). Also the infra-red spectrum of pinacol in dilute solution (0.005M) in CCl₄ (figure 9) has been obtained at the beam temperature as well as that of the crystalline hexadeuterio-hydrate at the beam temperature and -170°C (figure 14).

Polarized infra-red spectra of single crystal samples of pinacol and the monohydrate were obtained at beam temperature (figures 10 and 12) and -170°C (figures 11 and 13).

The proposed assignments of the absorption bands of pinacol and its hydrates are shown in tables I and II.

The unpolarized infra-red spectra of the decoupled $\nu(\text{OD})$ in crystalline pinacol-d, pinacol-d monohydrate and pinacol-d hexahydrate were obtained at the beam temperature and -170°C and are shown as figure 17.

(II) Discussion

(a) Beam Temperature

(i) In the unpolarized spectrum of pinacol (figure 10).

$\nu(\text{OH})$ is resolved as two components at 3441cm^{-1} and 3390cm^{-1} . In the polarized spectra these components are polarized at right angles to one another, the higher frequency band being narrower than the band at lower frequency (figure 10).

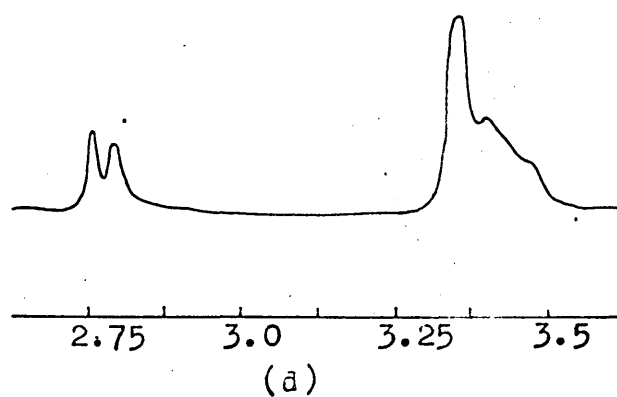
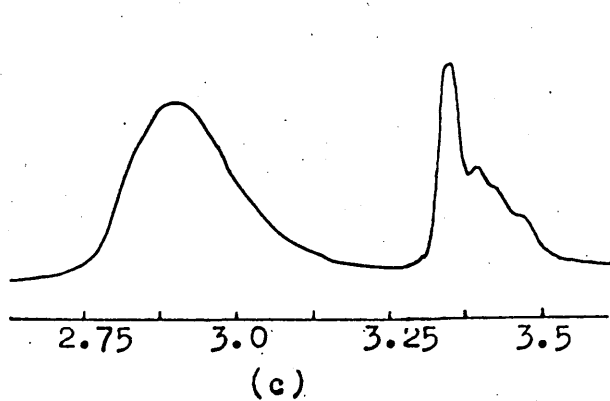
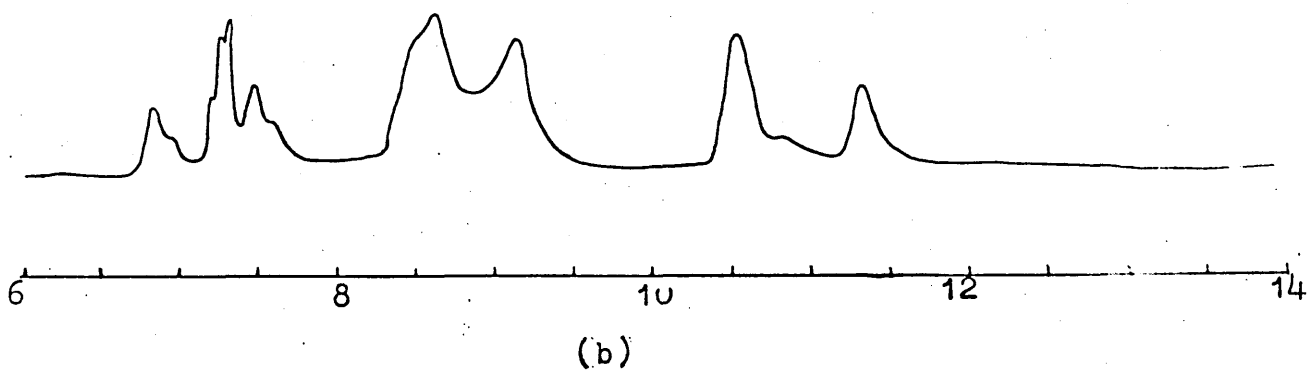
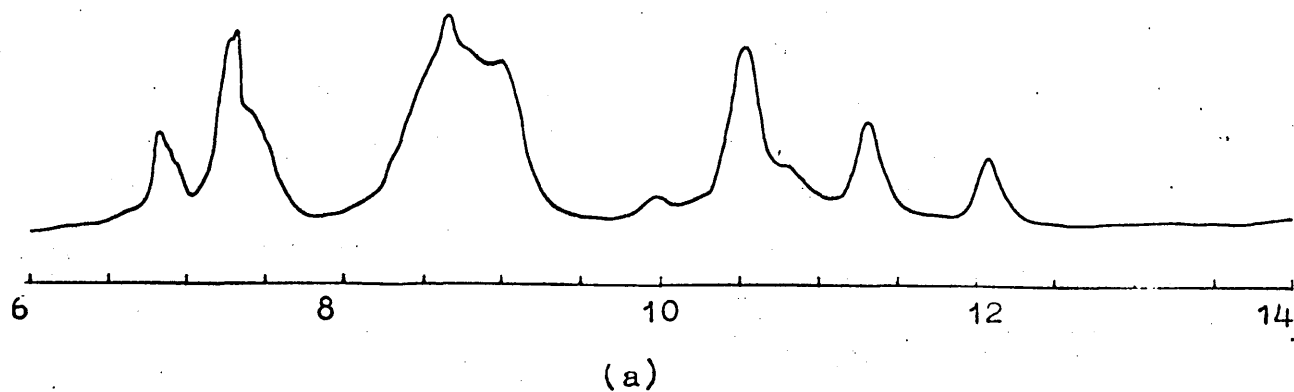
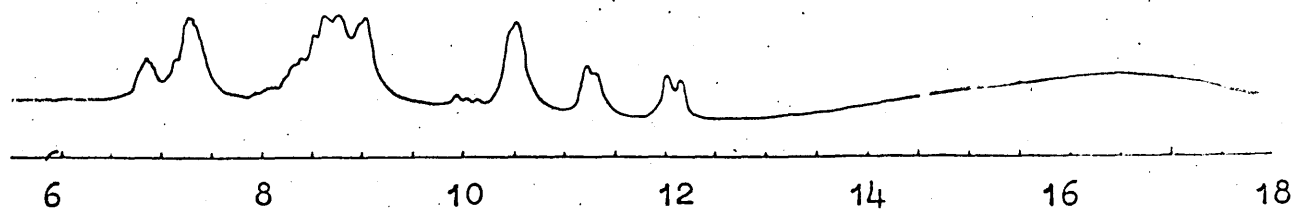
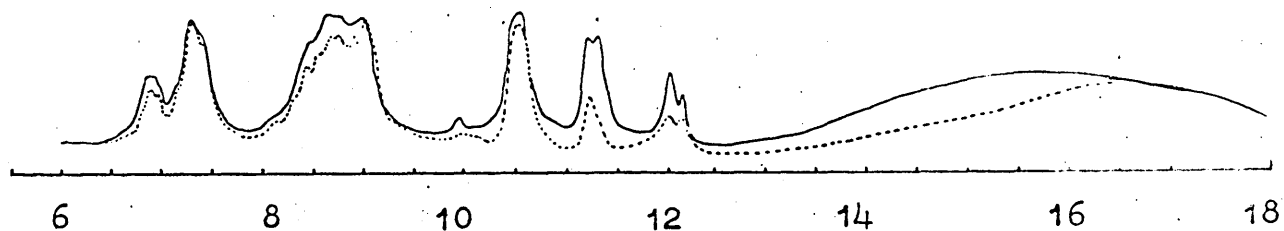


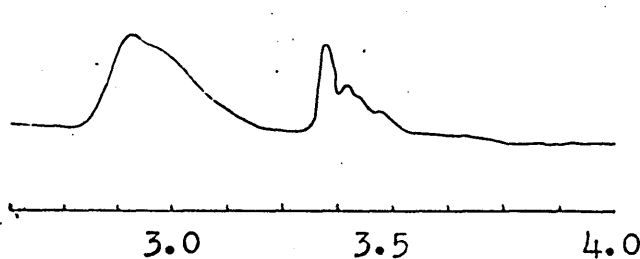
Figure 9.
 Infra-red spectra of pinacol as:- Liquid (50°C), Wavelength (a) 6-14 μ .
 (c) 2.75-3.5 μ .
 Solution (0.005M in CCl₄),
 Wavelength (b) 6-14 μ , (d) 2.75-3.5 μ .



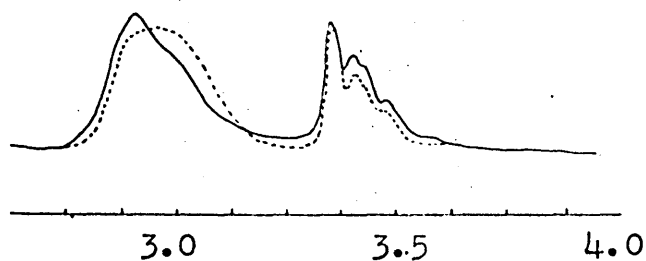
(a)



(b)



(c)



(d)

Figure 10.

Infra-red spectra of pinacol at beam temperature:-

Polycrystalline, Wavelength(a) 6-18 μ , (c) 2.625-4.0 μ .

Polarized single crystal, Wavelength(b) 6-18 μ , (d) 2.625-4.0 μ ,

alignment of sample ; 0° ----; 90° —.

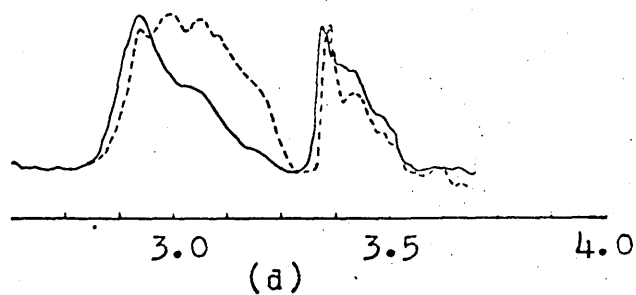
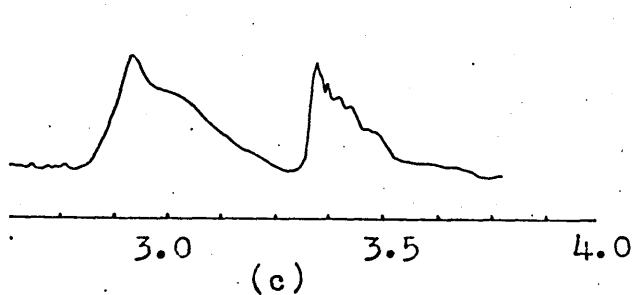
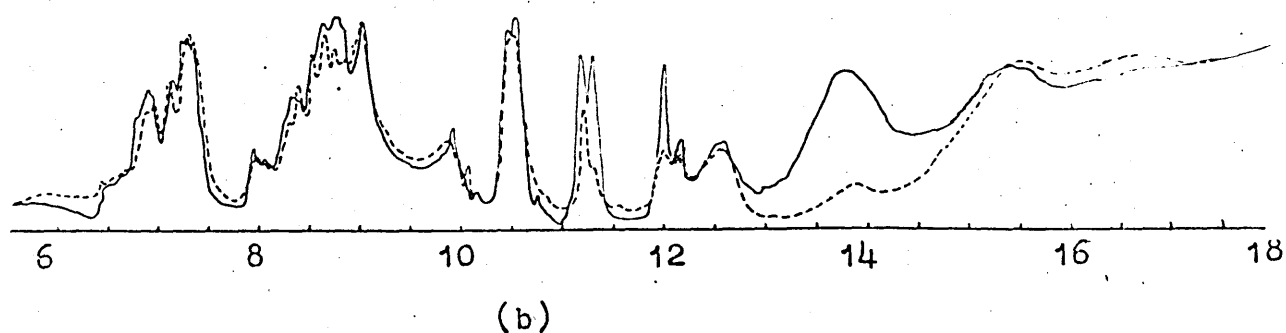
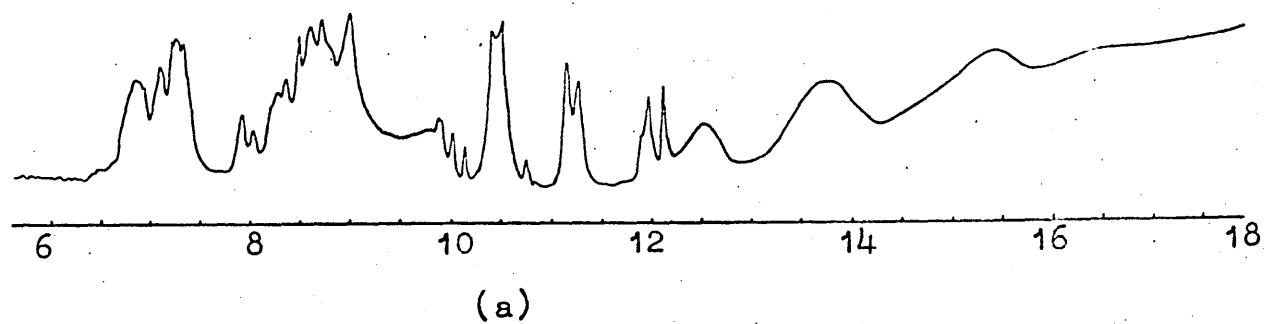


Figure 11.

Infra-red spectra of pinacol at -170°C :-

Polycrystalline, Wavelength (a) $6-18\mu$, (c) $2.625-4.0\mu$.

Polarized single crystal, Wavelength, (b) $6-18\mu$, (d) $2.625-4.0\mu$,

alignment of sample ; 0° ----; 90° —.

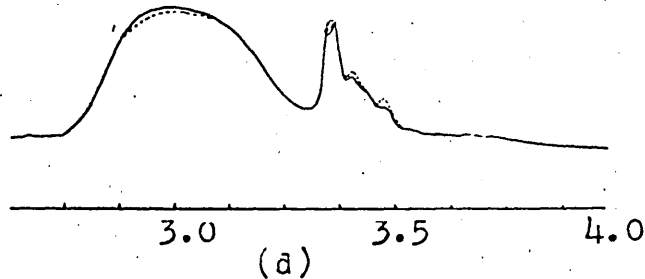
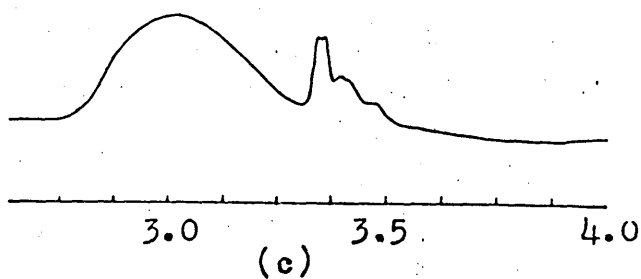
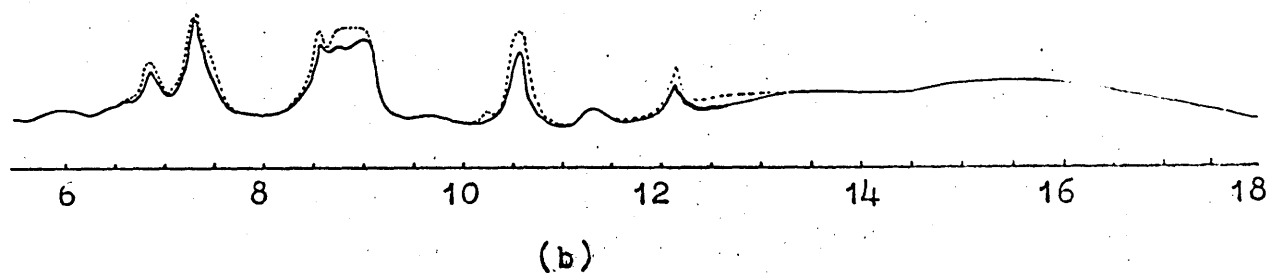
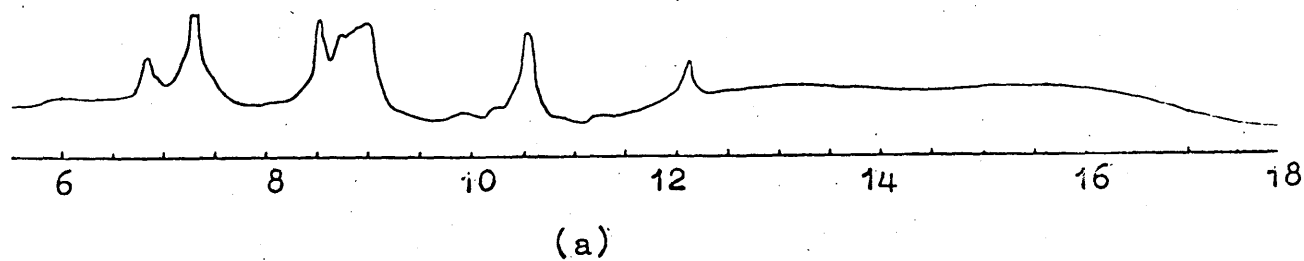


Figure 12.

Infra-red spectra of pinacol monohydrate at beam temperature:-
 Polycrystalline, Wavelength(a) 6-18 μ , (c) 2.625-4.0 μ .
 Polarized single crystal, Wavelength(b) 6-18 μ , (d) 2.625-4.0 μ ,
 alignment of sample ; 0°----; 90°—.

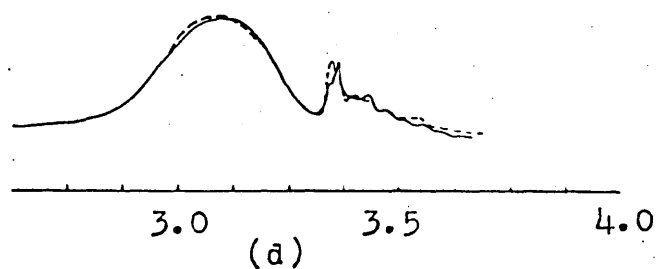
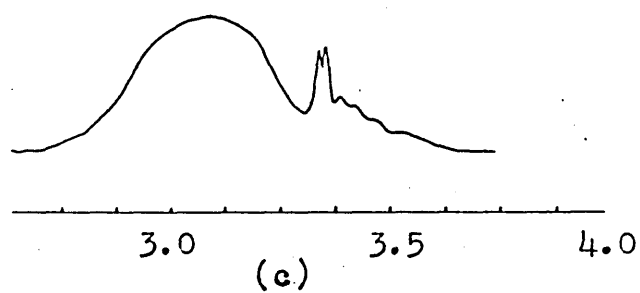
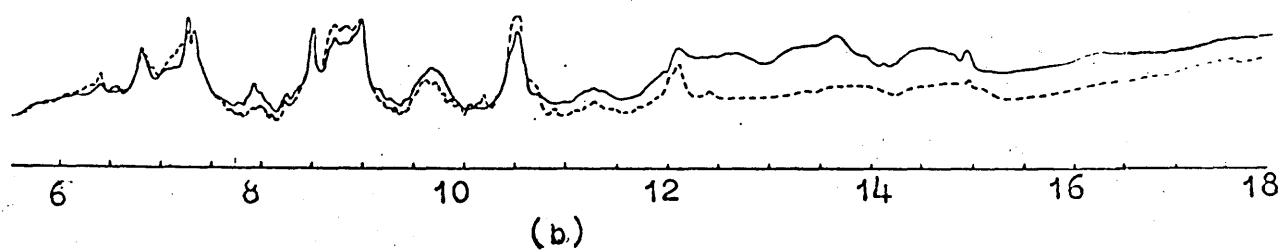
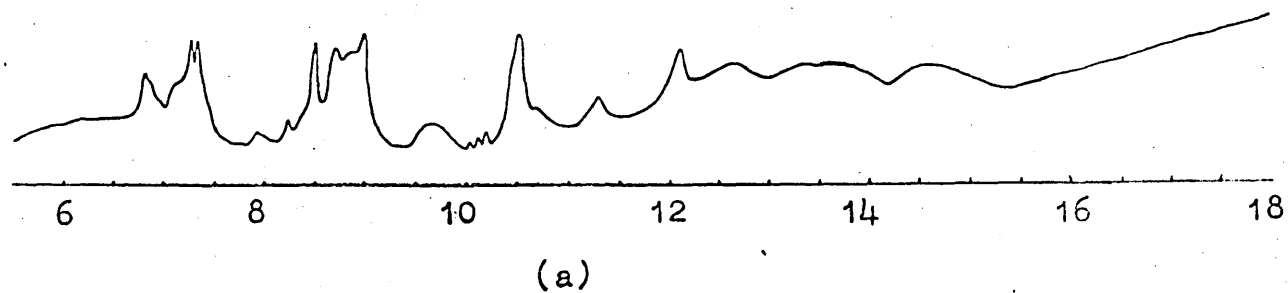
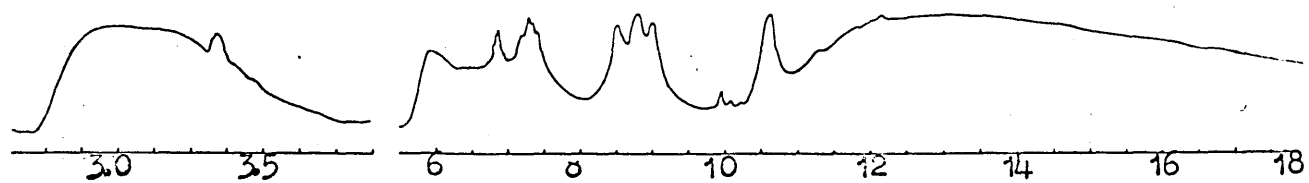


Figure 13.

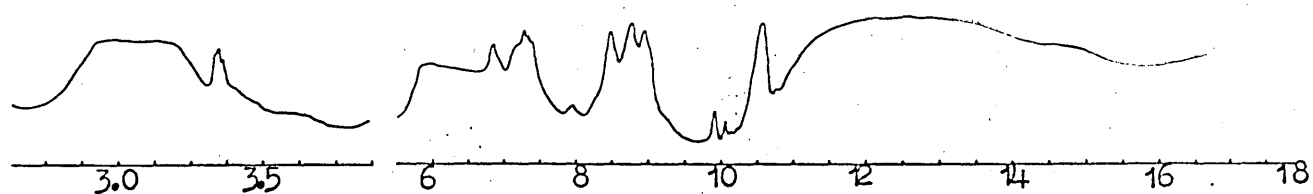
Infra-red spectra of pinacol monohydrate at -170°C :
 Polycrystalline, Wavelength(a) 6-18 μ , (c) 2.525-4.0 μ .
 Polarized single crystal, Wavelength(b) 6-18 μ , (d) 2.525-4.0 μ ,
 alignment of sample; 0° ----; 90° —.

Pinacol hexahydrate at beam temperature



(a)

Pinacol hexahydrate at -170°C



(b)

Pinacol hexadeuteriohydrate at -170°C



(c)

Figure 14.

Infra-red spectra of polycrystalline pinacol hexahydrate and hexadeuteriohydrate.

Wavelength $2.625\text{--}3.875\mu$ and $6\text{--}18\mu$.

Similar behaviour to this has previously been observed in the polarized spectra of single crystals of monohydric alcohols (16,17). In that work Brasch et al (16,17) observed two components in the spectrum of $\nu(\text{OH})$, a narrow component at a higher frequency than a broad component, polarized at right angles. The appearance of these two components (16,17) was interpreted in terms of crystal splitting since only a single component was observed in the spectrum of the partially deuterated alcohol. To account for the polarization of the two components at right angles, nearest neighbour coupling of OH groups along the H-bond chain was postulated (figure 8). Thus it was said (16,17) that the broader lower frequency component was due to an in-phase vibration of adjacent OH groups involving tautomerization, whereas the narrower band was due

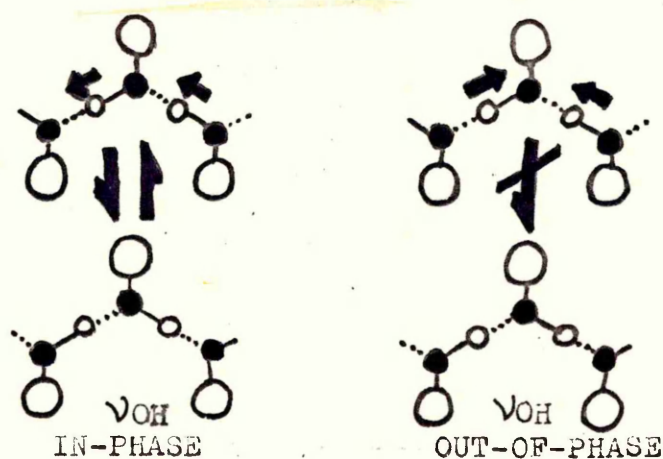


Figure 8.

Stretching vibration in H-bonded chain of a solid alcohol, (O), hydrocarbon portion of alcohol molecule; (●), oxygen atoms; (o), hydroxyl hydrogen atom. (17)

to an out-of-phase vibration and did not involve tautomerization.

It is therefore thought that the appearance of two components in the beam temperature spectrum of pinacol and their

polarization at right angles may be due to a similar tautomerization effect along the intermolecularly H-bonded chain as described by Brasch et al (16,17). However referring to the proposed (3) structure of pinacol shown in figure 2 the spectra do not help us to decide which way the crystal samples were aligned with respect to the polarized beam since the above effect might be expected to arise along all three crystallographic directions.

Significant dichroisms have been observed for the skeletal modes of the pinacol molecule (figure 10) at 891cm^{-1} , 883cm^{-1} , 832cm^{-1} , and 822cm^{-1} whilst only very small dichroisms have been observed for the symmetrical and asymmetrical CH_3 stretching bands, $\nu_s(\text{CH}_3)$ and $\nu_a(\text{CH}_3)$, in the range 2985 - 2878cm^{-1} . Also only very small dichroisms are observed for the symmetrical and asymmetrical CH_3 bending vibrations, $\delta_s(\text{CH}_3)$ and $\delta_a(\text{CH}_3)$, in the range 1455 - 1361cm^{-1} and CH_3 rocking mode, $\rho(\text{CH}_3)$, at 957cm^{-1} and 951cm^{-1} .

Figures 2a and c show the proposed structure of pinacol (3) projected onto the 'ab' and 'ac' planes. It would appear, referring to this structure that the resultant components of the skeletal vibrations may give rise to a predominant contribution in the 'a' direction and that the observed dichroisms of these skeletal modes are parallel and perpendicular to the 'a' direction.

If this is the case with the crystal aligned with the 'a' axis in the plane of the silver chloride plates it can be seen that the resultant components of the $\nu(\text{CH}_3)$, $\delta(\text{CH}_3)$ and $\rho(\text{CH}_3)$ modes may be approximately the same for both positions of the sample and hence give rise to only very small dichroisms.

(ii) The symmetry of the monohydrate structure compared

to that of pinacol is reflected in the smaller dichroisms observable in the beam temperature spectrum (figure 12). The structure of the monohydrate proposed by Hatt (1) was recently confirmed by O'Connor using X-ray diffraction (3) and figure 4b shows a section of the structure in the 'bc' plane. The H-bonded chains of pinacol OH groups linked by water molecules extend along the 'c' axis. The pinacol molecule takes up a trans conformation so that its two oxygen atoms become involved with two different H-bonded chains and it forms a cross-link between the chains. This cross-linking occurs in the 'a' and 'b' directions on alternate planes perpendicular to the 'c' axis.

A negligible dichroism is observed for the $\nu(\text{OH})$ band in the monohydrate spectrum (figure 12). Also small but significant dichroisms are observed for the bands associated with the OH-in-plane deformation, $\beta(\text{OH})$ at 1346cm^{-1} , $\nu(\text{CH}_3)$ in the range $2990\text{--}2882\text{cm}^{-1}$ and $\delta(\text{CH}_3)$ in the range $1467\text{--}1363\text{cm}^{-1}$, as well as the skeletal vibrations at 891cm^{-1} and 824cm^{-1} .

Referring to figure 4b it seems likely that this magnitude of dichroism would arise if the single crystal samples were aligned with their 'c' axes in the plane of the silver chloride plates.

(iii) In dilute solution (figure 9) two bands are observed for $\nu(\text{OH})$, a sharp band at 3630cm^{-1} associated with 'free' $\nu(\text{OH})$ and a broader band at 3580cm^{-1} associated with the intramolecular H-bonded $\nu(\text{OH})$. The appearance of these two components in dilute solution has been previously observed by Khun (46).

(iv) In the solid state there is a progressive broadening of $\nu(\text{OH})$ towards lower frequency with increasing hydration of pinacol (figures 10, 12 and 14, table I). In pinacol the

highest frequency peak occurs at 3441cm^{-1} which is much lower than the intramolecular H-bond frequency of 3580cm^{-1} observed in dilute solution. In solid sucrose which contains two intramolecular H-bonds (47) a sharp peak does occur at 3564cm^{-1} . It would therefore appear that there is no intramolecular H-bonding in the solid pinacol nor in the two hydrates whose highest frequency peaks are below 3441cm^{-1} .

(v) Bands due to HOH bending (ν_2) of water are visible in both the hydrate spectra (figures 12 and 14) and the association band of water (ν_A) also appears at 2210cm^{-1} in the hexahydrate spectrum. There is a shift in the ν_2 band in the hexahydrate to a higher frequency (table I) relative to the monohydrate indicating an increase in the strength of the H-bonding in the hexahydrate. ν_2 occurs at 1645cm^{-1} in liquid water at 30°C (48) and 1650cm^{-1} in ice I at -160 (49) whilst ν_A is found at 2125cm^{-1} in liquid water and at 2270cm^{-1} in ice I. It would therefore appear that the H-bond strength in these hydrates is above that in liquid water as well as in ice I, although it must be added that these bands are extremely broad and have indistinct maxima. Therefore the positioning of these bands may be in error $\pm 10\text{cm}^{-1}$ for ν_2 and $\pm 20\text{cm}^{-1}$ for ν_A .

(vi) In the light of present evidence the OH-in-plane deformation frequency, $\beta(\text{OH})$, in alcohols occurs in the region $1400\text{--}1300\text{cm}^{-1}$ (50(a)). A shoulder is seen in the liquid spectra of pinacol and the hexahydrate at 1350cm^{-1} and 1346cm^{-1} in the monohydrate and these have been assigned to $\beta(\text{OH})$. In methanol (14) $\beta(\text{OH})$ occurs at 1346cm^{-1} in the vapour, 1420cm^{-1} in the liquid and is split into two components at 1492cm^{-1} and 1514cm^{-1} in the solid at low temperature. It therefore appears that increasing the strength of H-bonds causes an increase in the

frequency of $\beta(\text{OH})$ and it might be expected therefore that in the crystalline pinacol and its hydrates, $\beta(\text{OH})$ would occur at a much higher frequency than in the liquid. However $\beta(\text{OH})$ cannot be identified with certainty in the spectra of the solids at ambient temperature.

In the crystalline monohydrate spectrum (figure 12) a weak shoulder is observed at 1346cm^{-1} with a significant dichroism and has been assigned to $\beta(\text{OH})$, although this is at the same frequency as the band assigned to this vibration in the liquid.

Stuart et al (51) observed a pair of bands for monohydric alcohols in solution in this region of the spectrum due to intermolecularly H-bonded and non-bonded $\beta(\text{OH})$, the latter band being at a lower frequency than the former. In the dilute solution spectrum of pinacol (figure 9), where only intramolecular H-bonding is taking place, two weak bands are observed at 1338cm^{-1} and 1316cm^{-1} which have been assigned to intramolecularly H-bonded and non-bonded $\beta(\text{OH})$.

(vii) The out-of-plane OH deformation, $\gamma(\text{OH})$, in the bonded state is known to absorb very broadly and diffusely near 650cm^{-1} (51). In the pinacol spectrum (figure 10) $\gamma(\text{OH})$ is visible as a very broad band centred at 626cm^{-1} and shows quite a strong dichroism, whilst in the monohydrate it is centred at 651cm^{-1} and shows no dichroism (figure 12).

The broad band centred at 760cm^{-1} in the monohydrate and hexahydrate is undoubtedly the librational band of water, ν_{L} , which appears in pure water at 685cm^{-1} at 30°C (48) and at 840cm^{-1} in ice I at -160°C (49). In the monohydrate ν_{L} is not dichroic.

(viii) Most oxygen containing compounds show bands due

to CH_3 asymmetric stretch, $\nu_a(\text{CH}_3)$, in the range $2990\text{--}2922\text{cm}^{-1}$ (50(b)) and the average position for the band associated with the CH_3 symmetric stretch, $\nu_s(\text{CH}_3)$, in these compounds is 2880cm^{-1} (50(b)). Also in this region of the spectrum occur overtones of the asymmetric and symmetric CH_3 bend, $\delta_a(\text{CH}_3)$ and $\delta_s(\text{CH}_3)$. Bands occur in this region of the spectrum of pinacol and its hydrates and they have been assigned to $\nu_a(\text{CH}_3)$ and $\nu_s(\text{CH}_3)$. It is noticeable that there is a significant increase in the frequency of $\nu_a(\text{CH}_3)$ with degree of hydration (table I).

(ix) Bands due to the asymmetrical CH_3 deformation, $\delta_a(\text{CH}_3)$ occur around 1460cm^{-1} (50(c)). The position of the symmetrical CH_3 deformation, $\delta_s(\text{CH}_3)$, lies in the region of 1380cm^{-1} and its position is dependent on the nature of the element attached to it (52). For example in the case of methyl ketones bands associated with $\delta_s(\text{CH}_3)$ are found in the vicinity of 1359cm^{-1} (52). Also a characteristic splitting occurs when two methyl groups are found on the same carbon atom (52). Therefore the $\delta_s(\text{CH}_3)$ mode gives rise to at least two bands in the spectrum of pinacol and its hydrates due to the in-phase and out-of-phase interaction of the two methyl groups on the same tertiary carbon atom. In the monohydrate spectrum (figure 12) there are only two bands at 1370cm^{-1} and 1363cm^{-1} but in pinacol (figure 10) there seem to be five components at 1399cm^{-1} , 1379cm^{-1} , 1375cm^{-1} , 1370cm^{-1} and 1361cm^{-1} and in the hexahydrate (figure 14) four at 1394cm^{-1} , 1375cm^{-1} , 1365cm^{-1} and 1356cm^{-1} . The large number of $\delta_s(\text{CH}_3)$ bands present in the spectra of pinacol and the hexahydrate may be due to crystal splitting since it is known (3) that pinacol crystallizes with sixteen molecules per unit cell and the hexahydrate with eight molecules per unit cell.

Although it is tempting to assign the bands at approximately 1390cm^{-1} to the $\beta(\text{OH})$ mode there is still a band at 1399cm^{-1}

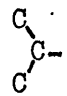
in pinacol hexadeuteriohydrate (figure 14) and so there must be at least one $\delta_s(\text{CH}_3)$ band at that frequency. There is also a band at 1389cm^{-1} in the dilute solution spectrum (figure 9) in addition to those at 1379cm^{-1} and 1370cm^{-1} which must arise from the $\delta_s(\text{CH}_3)$ mode since the $\beta(\text{OH})$ bands are at a lower frequency in this spectrum. The number of bands associated with $\delta_s(\text{CH}_3)$ in the dilute solution spectrum is not surprising since there may be both trans and gauche conformers present (53).

(x) In isopropyl groups in hydrocarbons a band involving the CH_3 rocking mode, $\rho(\text{CH}_3)$, usually occurs at $922\text{-}919\text{cm}^{-1}$ and in t-butyl groups in hydrocarbons at $932\text{-}926\text{cm}^{-1}$ (54(a)). In non hydrocarbons the regions are wider $950\text{-}875\text{cm}^{-1}$ and $935\text{-}810\text{cm}^{-1}$. Strong bands might be expected in a compound containing four methyl groups. A strong doublet is observed at 957cm^{-1} and 951cm^{-1} in the pinacol spectrum (figure 10) while single strong bands are observed at 947cm^{-1} and 943cm^{-1} in the mono and hexahydrate spectra (figures 12 and 14) which have been assigned to $\rho(\text{CH}_3)$. Also in solution a strong $\rho(\text{CH}_3)$ band is observed at 956cm^{-1} in the same position as in the liquid spectrum (figure 9).

(xi) The C-O stretching vibration, $\nu(\text{CO})$, in tertiary alcohols usually gives rise to a band of strong intensity and is found in the region $1210\text{-}1100\text{cm}^{-1}$ (54(b)). Strong bands at 1111cm^{-1} in the pinacol spectrum (figure 10) and 1114cm^{-1} in the mono-hydrate and hexahydrate spectra (figure 12 and 14) have been assigned to $\nu(\text{CO})$. In the spectrum of the hexadeuteriohydrate (figure 14) the band at 1114cm^{-1} in the hexahydrate is missing and appears at 950cm^{-1} therefore confirming the assignments.

In solution it is known that tertiary alcohols give rise to association and monomer $\nu(\text{CO})$ bands (51), the monomer band being at a lower frequency than the intermolecularly H-bonded component.

In the dilute solution spectrum of pinacol (figure 9) where only monomer $\nu(\text{OH})$ and intramolecular $\nu(\text{OH})$ are observed there is no band at 1111cm^{-1} and it is assumed that the 1095cm^{-1} band is due to monomer $\nu(\text{CO})$, the intramolecular band being eclipsed by the higher frequency bands.

(xii) The remaining bands are more difficult to assign. All three substances have strong absorptions between 1200cm^{-1} and the $\nu(\text{CO})$ band at approximately 1111cm^{-1} (figures 10, 12 and 14). This region is simplest in the dilute solution spectrum (figure 9) where only two significant bands occur at 1173cm^{-1} and 1159cm^{-1} . It is well known that strong bands occur in this region in branched chain hydrocarbons (53) and alcohols (55) due to the interaction of C-C and  skeletal modes with CH_3 rocking or CO stretching modes. It is therefore thought that bands in this region are due to various mixtures of these modes. The strong band which appears at 1140cm^{-1} in all the solids including the hexadeuteriohydrate (figure 14) and liquid pinacol (figure 9) appears to be absent in the dilute solution spectrum. It is assumed that this band arises from a coupling which only occurs in the intermolecularly H-bonded state of the solids and pure liquid pinacol but not in dilute solution where only intramolecular H-bonding occurs.

(xiii) In the study of modes associated with the tertiary butyl group in tertiary butoxide derivatives, Ory (56) assigned bands in the $920\text{-}820\text{cm}^{-1}$ region to skeletal modes of the tertiary butyl group. There are two quite dichroic doublets at 891cm^{-1} , 883cm^{-1} and 832cm^{-1} , 822cm^{-1} in solid pinacol (figure 10) with corresponding singlet absorptions at 885cm^{-1} and 829cm^{-1} in the liquid pinacol (figure 9). In the monohydrate spectrum (figure 12) only a band at 824cm^{-1} is significant and is quite dichroic whilst in the hexahydrate there is no strong absorption in the

vicinity of 885cm^{-1} or 829cm^{-1} possibly because of ν_L of water which is already quite significant in intensity at these frequencies (figure 14). This is confirmed by the fact that these bands are present at 888cm^{-1} and 829cm^{-1} in the spectrum of the hexadeuteriohydrate. In the dilute solution spectrum of pinacol (figure 9) there is a band at 883cm^{-1} but not in the 829cm^{-1} region. These bands are undoubtedly associated with the skeletal modes of pinacol and are typical of those observed in branched chain hydrocarbons (53). However it appears that the occurrence of a band at 829cm^{-1} , like that at 1140cm^{-1} , seems to be strongly dependent on the nature of the H-bonding in these systems.

(b) Low Temperature

(i) A considerable narrowing of the absorption bands occurs in the low temperature spectra (figures 11,13,14) and there is generally a small increase in the size of the dichroisms in the polarized spectra of pinacol and the monohydrate (figure 11 and 13).

(ii) It is known from X-ray measurements (3) that pinacol crystallizes in an orthorhombic structure with sixteen molecules in the unit cell. On the other hand the monohydrate is tetragonal with two molecules in the unit cell and the hexahydrate is monoclinic with eight molecules in the unit cell. It is therefore not suprising to find a larger number of bands in the spectrum of pinacol than in those of the two hydrates. Infact it can be clearly seen in the low temperature spectra of the monohydrate (figure 13) that a single band occurs at 1375cm^{-1} , 1361cm^{-1} , 948cm^{-1} , 885cm^{-1} and 825cm^{-1} in the same region as doublet absorptions occur in the pinacol spectrum (figure 11).

(iii) There are several distinct peaks in the $\nu(\text{OH})$ region of the pinacol spectrum (figure 11) and a number of these are appreciably dichroic. In the low temperature spectrum of the

monohydrate and hexahydrate (figures 13 and 14) however no structure is resolved, the $\nu(\text{OH})$ bands being broad and featureless. However they have shifted to lower frequency, the monohydrate $\nu(\text{OH})$ from 3306cm^{-1} at the beam temperature to 3225cm^{-1} at the low temperature and the extremely broad band in the hexahydrate from $3441\text{--}3181\text{cm}^{-1}$ to $3413\text{--}3125\text{cm}^{-1}$. This is indicative of an increase in the H-bonding at a lower temperature and this sort of shift has been observed previously in methanol (14) and ethylene glycol (57).

(iv) The band due to ν_2 of water at 1688cm^{-1} in the beam temperature spectrum of the hexahydrate (figure 14) is now observed at 1690cm^{-1} in the low temperature spectrum (figure 14). However in the low temperature spectrum of the monohydrate ν_2 is not observed (figure 13).

The band due to ν_A of water at 2210cm^{-1} in the beam temperature spectrum of the hexahydrate now occurs at 2275cm^{-1} . Bearing in mind the likely error involved in determining the peak position it would appear that the H-bond strength in the case of the hexahydrate is greater than that found in ice I (49).

(v) The dichroic band assigned to $\beta(\text{OH})$ at 1346cm^{-1} in the beam temperature spectrum of the monohydrate is not present in that position at low temperature (figure 13). However a shoulder is observed at the much higher frequency of 1380cm^{-1} which is extremely dichroic and is not present at beam temperature. It is therefore thought to be the $\beta(\text{OH})$ band showing a low temperature shift similar to that observed in the case of methanol (14) and ethanol (58).

(vi) It is noticeable that there are at least three $\gamma(\text{OH})$ bands in the low temperature spectrum of pinacol (figure 11) at 795cm^{-1} , 725cm^{-1} and 650cm^{-1} and these bands are more intense than the single band observed at 626cm^{-1} at beam temperature (figure

10). Furthermore the 725cm^{-1} band is very dichroic.

In the spectrum of the monohydrate (figure 13) several weak broad bands are now observed at 787cm^{-1} , 745cm^{-1} , 730cm^{-1} and 684cm^{-1} , where previously at the beam temperature (figure 12) there had only been two at 760cm^{-1} and 651cm^{-1} due to ν_L and $\gamma(\text{OH})$. These bands show a small dichroism. Also at low temperature in the hexahydrate spectrum where previously only one intense broad band due to ν_L had been observed at 762cm^{-1} at the beam temperature several bands are now observed (figure 14). Intense broad bands are seen at 854cm^{-1} and 793cm^{-1} with weak shoulders at 675cm^{-1} and 570cm^{-1} .

The increase in frequency and intensity of $\gamma(\text{OH})$ vibrations with decreasing temperature and resolution into multiple bands has been observed previously in the case of methanol (14), ethanol (58) and ethylene glycol (57) and has not been explained. Although it was pointed out by Pimentel and McClellan in 1960 (59) that there are interesting parallels between the increase in frequency of $\gamma(\text{OH})$ and the decreasing frequency of $\nu(\text{OH})$ with increasing strength of H-bonding, no systematic investigation of the relationship has been made since that time.

In the hexahydrate spectrum the bands at 854cm^{-1} , 793cm^{-1} , 675cm^{-1} and 570cm^{-1} may be due to the components of ν_L which occur in ice I, at -160°C , at 840cm^{-1} , 770cm^{-1} , 660cm^{-1} and 555cm^{-1} (49). However in the monohydrate there is a more complex situation because both ν_L and $\gamma(\text{OH})$ bands are present and it is not possible to distinguish between them.

(c) Decoupled Spectra

(i) The use of curves relating the distance between oxygen atoms involved in a hydrogen bridge, $R_{\text{O-H-O}}$, and the frequency of the $\nu(\text{OH})$ stretching vibration in X-ray and spectroscopic investigations has already become widely accepted (60-64).

A relationship between $\nu(\text{OH})$ and the interatomic separation, $R_{\text{O-O}}$, was first noticed by Rundle et al (65). Since this early investigation several groups of workers have studied this problem (66-70). In spite of the large spread in experimental points extremely similar correlation curves were obtained.

However in recent years a considerable proportion of the interatomic separations, $R_{\text{O-O}}$, used in the earlier correlation curves have proved to be incorrect and some doubt has arisen on the reliability of spectroscopic data used. In the light of this information Efimov et al (71) have critically re-examined the relationship and figure 15 shows the correlation curve they produced from the data they consider to be reliable. Furthermore they have also produced a correlation curve for $\nu(\text{OD})$ v's $R_{\text{O-O}}$ from a limited number of data points. This curve was found to agree well with the $\nu(\text{OH})$ v's $R_{\text{O-O}}$ correlation when the scale of the abscissa was multiplied by 1.33 (71) and is shown as figure 16.

In the single crystal spectra of pinacol at low temperature (figure 11) there are at least eight components of the $\nu(\text{OH})$ band while in the decoupled $\nu(\text{OD})$ band of the polycrystalline sample at -170°C there are four distinguishable peaks (figure 17).

In Brasch's original work on solid alcohols (16,17) it was shown that the breadth of the $\nu(\text{OH})$ band was principally due to nearest neighbour coupling between OH groups along a H-bonded chain. Single crystal studies show that coupling between identical OH groups leads to two bands separated by between 90cm^{-1} and 160cm^{-1} in the undeuterated alcohol studied. On progressive deuteration these two bands diminish in intensity and a new band appears at a point midway between the original bands. In a 95% deuterated sample only a small narrow $\nu(\text{OH})$ band remains, the two

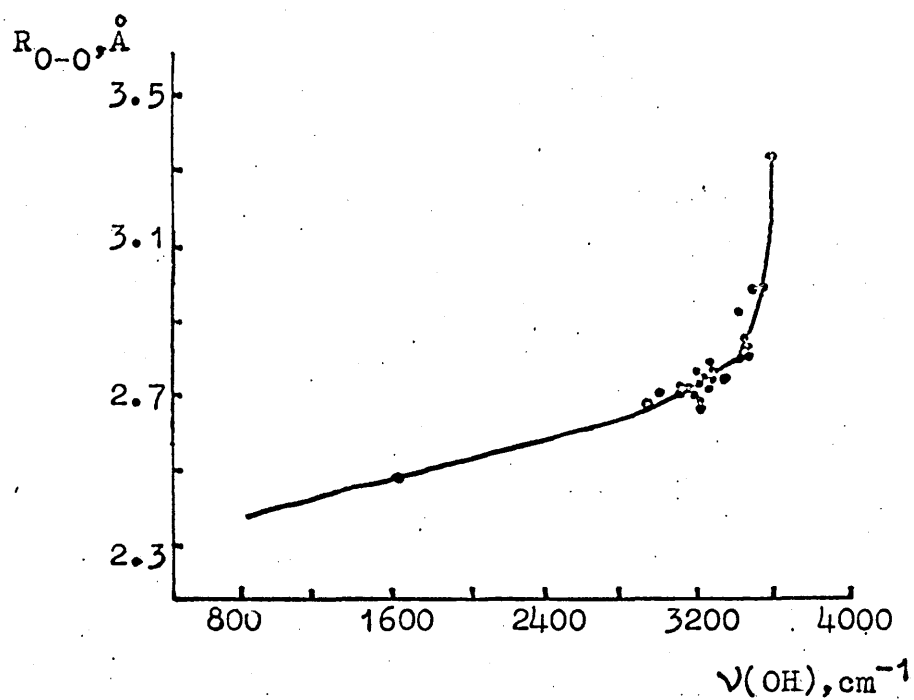


Figure 15.

$\nu(OH)$ v's R_{O-O} correlation curve. (71)

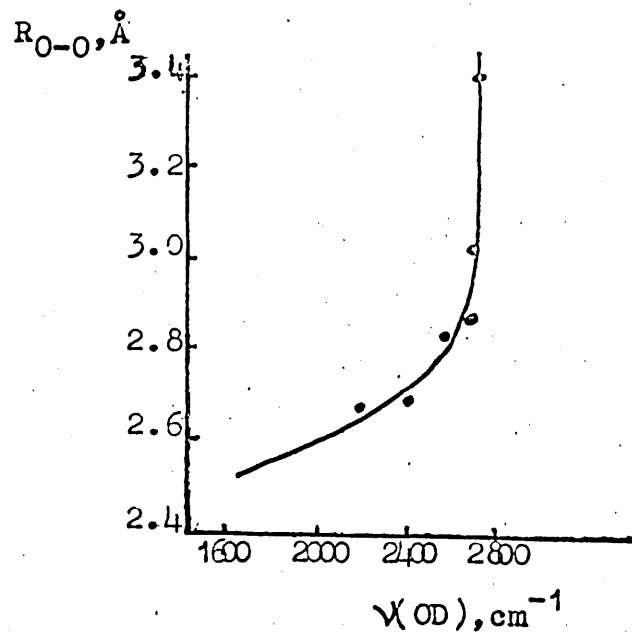


Figure 16.

$\nu(OD)$ v's R_{O-O} correlation curve. (71)

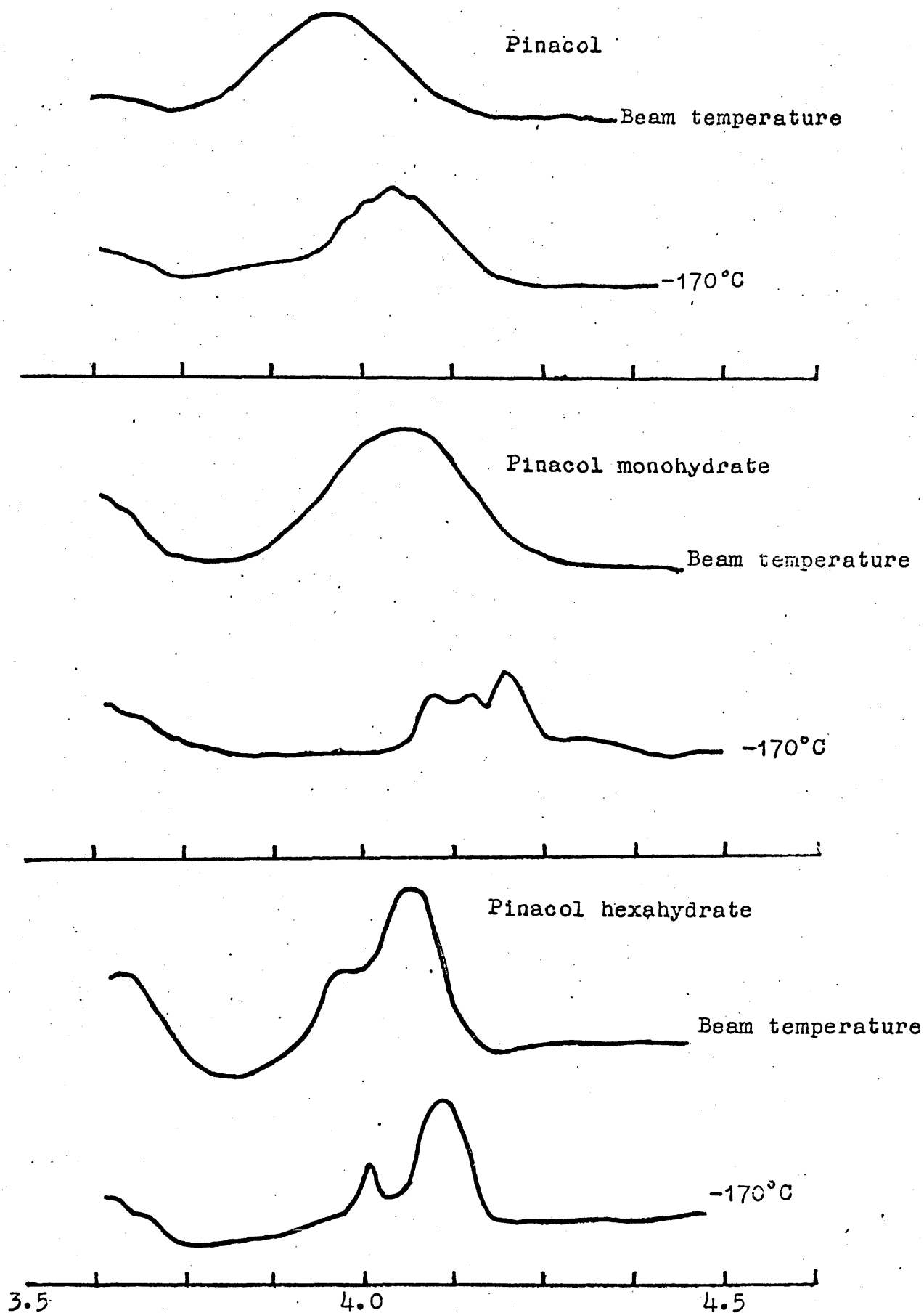


Figure 17.
 $\nu(\text{OD})$ bands of 4% deuterated pinacol, monohydrate, and hexahydrate. Wavelength 3.5-4.5 μ .

- 20 -

original bands having disappeared. The same effect can be observed on the $\nu(\text{OD})$ vibration for a sample which has been deuterated to only a small extent say 5%.

Since there are eight peaks in the $\nu(\text{OH})$ band and four in the decoupled $\nu(\text{OD})$ band of pinacol at low temperatures it has been possible to select four pairs of $\nu(\text{OH})$ peak frequencies and relate the mean frequency of each pair to one of the components of the $\nu(\text{OD})$ band, bearing in mind the likely isotopic ratio. The result of this procedure is shown in table III. The splitting $\Delta\nu$, between components of the $\nu(\text{OH})$ pairs increases as the frequencies decrease until the final pair when there is an abrupt decrease in $\Delta\nu$. The isotope ratios for the first three pairs are also very similar and compare favourably with the values 1.34 found for decanol (17), 1.35 for methanol (14) and 1.33 for ice I (49). The low value for the fourth pair may be due to the inaccuracies in measuring peak frequencies in the rather extended tails of $\nu(\text{OH})$ and $\nu(\text{OD})$.

The appearance of the four decoupled $\nu(\text{OD})$ bands indicates possibly that there are four distinctly different OD environments in pinacol. Using the correlation curve relating $\nu(\text{OD})$ to $R_{\text{O-O}}$ in figure 16 it has been possible to obtain $R_{\text{O-O}}$ values corresponding to these frequencies. The results of this procedure are shown in table III. It must be added that values obtained using the correlation curves involve a likely error of $\geq 0.04\text{\AA}$ since this is the size of the error involved in many of the X-ray determined $R_{\text{O-O}}$ distances. However since the data used for comparison with these results from the correlation curves has similar errors it was thought that use of the correlation curve was not invalidated.

The R_{O-O} values obtained for pinacol lie in the range 2.75-2.78 Å and are of a similar size to that of pentaerythritol of 2.74 Å (72) but are much longer than that of 2.66 Å for methanol (73).

In view of the rather complex structure (figure 2) proposed (3) for pinacol the fact that there are four R_{O-O} distances corresponding to the four $\nu(OD)$ frequencies is not surprising.

As a check of the validity of $\nu(OD)$ v's R_{O-O} correlation curve in view of the relatively few data points used in the plot, the mean $\nu(OH)$ frequencies of the pairs of bands was related to R_{O-O} distances using the $\nu(OH)$ v's R_{O-O} correlation curve shown in figure 15. The results of this procedure are also shown in table III. It can be seen that in general there is very good agreement except in the last case. The discrepancy here could arise from inaccuracies in measuring peak frequencies in the rather extended tails of $\nu(OH)$ and $\nu(OD)$ as previously mentioned. On the basis of this analysis it seemed reasonable to utilize the R_{O-O} v's $\nu(OD)$ correlation curve further.

(ii) For pinacol monohydrate and hexahydrate the low temperature $\nu(OH)$ bands are broad and featureless and yield very little structural information, but the decoupled $\nu(OD)$ bands can be seen to comprise a number of distinguishable peaks (figure 17).

In the case of the hexahydrate there are only two resolvable bands associated with the decoupled $\nu(OD)$, the higher frequency component being much sharper and less intense than the low frequency component (figure 17).

The lower frequency $\nu(OD)$ band occurs at about the same frequency as the decoupled $\nu(OD)$ band in partly deuterated ice I (49). From the correlation curve (figure 16) the value of

R_{O-O} corresponding to this frequency is 2.74\AA and this is identical with that found for ice I (74). The higher frequency component of $\nu(\text{OD})$ gives rise to an R_{O-O} value of 2.77\AA .

It would therefore appear that the majority of the water molecules in the pinacol hexahydrate occupy similar sites in an ice like lattice, which confirms the suggestion of Cook et al (75).

(iii) There are three components in the decoupled $\nu(\text{OD})$ band of the monohydrate. The bands may arise in the following way. Figure 4b shows a section of the chain structure of the monohydrate in the 'bc' plane with the pinacol molecules in the trans configuration. In this structure the water oxygen atoms may be covalently bonded either to two protons in the same chain segment or to two protons in adjoining segments (figure 4a). It is possible that these arrangements correspond to the presence of two distinct sets of water molecules which will therefore give rise to two $\nu(\text{OD})$ bands at slightly different frequencies (64). Since the decoupled $\nu(\text{OD})$ band in ice I (49) occurs at 2421cm^{-1} it is proposed to assign the 2443cm^{-1} and 2411cm^{-1} components of the monohydrate $\nu(\text{OD})$ band to water molecules and the 2385cm^{-1} component to pinacol.

(iv) In the hexahydrate the broad $\nu(\text{OD})$ component at 2434cm^{-1} is in the same range as the highest frequency $\nu(\text{OD})$ bands at 2443cm^{-1} and 2411cm^{-1} in the monohydrate. It therefore appears that there is a similar strength of H-bonds in these hydrates. However in the case of the hexahydrate the weaker band observed at 2496cm^{-1} is probably due to lower strength H-bonded OD groups. These points do not support fully the fact suggested by the higher ν_2 value in the hexahydrate that the water in this material is involved in stronger H-bonding than the case of the monohydrate.

Table I

Assignments of the absorption bands of Pinacol and its hydrates at the beam temperature.

Pinacol			Pinacol Monohydrate			Pinacol Hexahydrate			(c) Assignments
cm ⁻¹	(a) Intens	(b) Polarization	cm ⁻¹	(a) Intens	(b) Polarization	cm ⁻¹	(a) Intens		
3441	s	90°				3441-		} ν(OH)	
3390	s	0°	3306	s	0°	3181	s.br.		
						3003	s		
2985	s	90°	2990	s	0°	2994	s	} ν _a (CH ₃)	
2978	s	-	2980	s	0°				
2963	sh	90°							
2941	m	90°	2945	m	0°	2929	sh		
2914	m	90°							
2878	w	90°	2882	w	90°	2882	sh	} ν _s (CH ₃)	
			1667	w	-	2210	m.br.		
			1467	m	0°	1688	s.br.		
			1460	m	0°	1460	m		
1455	m	90°				1394	sh	} δ _s (CH ₃)	
1399	m	90°							
1379	s	90°							
1375	s	90°				1375	s		
1370	s	-	1370	s	-	1365	s		
1361	s	-	1363	s	0°	1356	sh	} β(OH)	
			1346	sh	0°				
1258	sh	90°							
1235	w	90°	1240	w	90°				
1208	w	90°							
1198	sh	90°	1198	sh	0°				
1187	sh	90°							
1180	m	90°				1176	s		
1170	m	90°	1170	s	0°				
1156	s	90°							
1139	s	90°	1143	s	0°	1139	s		
			1130	sh	0°				
			1124	sh	0°				
1111	sh	90°	1114	s	0°	1114	s	ν(CO)	
1105	s	0°							
1008	w	90°	1005	w	-	1007	w		
995	w	90°				993	v.w.	} δ(CH ₃)	
985	w	90°	975	w	0°	978	v.w.		
957	s	90°							
951	s	90°	947	s	0°	943	s		
891	m	90°	891	w	0°				
883	m	90°							
832	m	90°	824	m	0°	823	w		
822	m	90°							
			760	w.br.	-	762	s.br.	ν _L (H ₂ O)	
626	w.br.	90°	651	w.br.	-			δ(OH)	

Table II

Assignments of the absorption bands of Pinacol and its hydrates
at -170°C .

Pinacol			Pinacol Monohydrate			Pinacol Hexahydrate		
cm ⁻¹	(a) Intens	(b) Polariz- ation	cm ⁻¹	(a) Intens	(b) Polariz- ation	cm ⁻¹	(a) Intens	(c) Assignm- ents
3419	s	90°				3413-	s.br.	} $\nu(\text{OH})$
3376	sh	0°				3125		
3355	s	0°						
3339	s	0°						
3266	s	0°						
3226	s	0°	3225	s	0°			
3163	s	0°						
3124	m	0°						} $\nu_a(\text{CH}_3)$
2994	s	90°	2994	sh	0°	3002	sh	
2990	s	0°	2988	s	0°	2990	s	
2980	s	0°	2977	s	0°	2980	s	
			2955	w	90°			
2941	m	90°						
2931	m	90°						
2920	m	90°	2920	w	-			} $\nu_s(\text{CH}_3)$
2914	m	90°						
2878	w	90°	2885	w	0°	2888	w	
2857	v.w.	90°	2848	v.w.	-			} $\nu_a(\text{H}_2\text{O})$ $\nu_2(\text{H}_2\text{O})$
						2275	w.br.	
						1690	m.br.	} $\delta_a(\text{CH}_3)$
1471	m	90°	1465	m	90°			
1450	m	90°	1455	m	0°	1460	s	
1430	sh	90°	1439	w	0°			} $\delta_s(\text{CH}_3)$ $\beta(\text{OH})$
1403	s	90°				1394	sh	
			1380	sh	0°			} $\delta_s(\text{CH}_3)$
1379	s	90°	1375	s	90°	1370	s	
1365	s	90°						
1361	s	90°	1361	s	90°	1361	s	} $\delta_s(\text{CH}_3)$
1351	s	0°				1351	sh	
1258	w	90°	1262	w	90°	1258		
1242	w	90°	1250	w	90°			} $\nu(\text{CO})$
1235	w	90°	1235	v.w.	90°			
1205	m	90°						
1194	s	-						} $\nu(\text{CO})$
1173	s	90°	1176	s	0°	1180	s	
1156	s	90°	1152	sh	0°			
1143	s	90°	1146	s	0°			} $\nu(\text{CO})$
1139	s	90°				1139	s	
1130	s	90°	1126	s	0°			
			1117	sh	0°			} $\nu(\text{CO})$
			1111	s		1117	s	
1108	s	90°						
			1033	w.br.	90°			} $\nu(\text{CO})$
1015	w	-						
1010	w	90°						
1008	sh	90°				1008	w	

Pinacol			Pinacol Monohydrate			Pinacol Hexahydrate			(c) Assignments
cm ⁻¹	(a) Intens	(b) Polarization	cm ⁻¹	(a) Intens	(b) Polarization	cm ⁻¹	(a) Intens		
995	w	90°	995	v.w.	0°	995	w	} ρ (CH ₃)	
			990	v.w.	0°				
985	v.w.	90°	980	v.w.	0°				
960	s	90°							
955	s	90°							
951	s	90°	948	s	0°	946	s	} ν _L (H ₂ O)	
			935	w	-				
930	v.w.	-							
893	m	90°						} ν _L (H ₂ O)	
888	m	90°	885	w	-	854	s.br.		
839	sh	90°						} γ (OH) and ν _L (H ₂ O)	
833	m	90°	833	sh	90°				
823	m	90°	825	m	90°				
818	sh	90°							
795	w.br.	90°	787	m.br.	90°	793	s.br.		
			745	m.br.	90°			}	
725	m.br.	90°	730	m.br.	90°				
			684	m.br.	90°				
650	m.br.	90°				675	w.sh	} ν _L (H ₂ O)	
						570	w.sh		

(a) The following abbreviations are used:

s - strong, m - medium, w - weak, v - very,
sh - shoulder, br - broad

(b) Polarizations 0° and 90° indicate perpendicular alignments of the sample.

(c) The meanings of the symbols used are as follows:

ν - stretching
 δ - bending
 β - in-plane bending
 ρ - rocking
 γ - out-of-plane bending

Wavelength To Frequency Conversion Table

cm^{-1}	μ	cm^{-1}	μ	cm^{-1}	μ
4000	2.5	1299	7.7	775	12.9
3846	2.6	1282	7.8	769	13.0
3704	2.7	1266	7.9	763	13.1
3571	2.8	1250	8.0	758	13.2
3448	2.9	1235	8.1	752	13.3
3333	3.0	1220	8.2	746	13.4
3226	3.1	1205	8.3	741	13.5
3125	3.2	1190	8.4	735	13.6
3030	3.3	1176	8.5	730	13.7
2941	3.4	1163	8.6	725	13.8
2857	3.5	1149	8.7	720	13.9
2778	3.6	1136	8.8	714	14.0
2703	3.7	1124	8.9	709	14.1
2632	3.8	1111	9.0	704	14.2
2564	3.9	1099	9.1	699	14.3
2500	4.0	1087	9.2	694	14.4
2439	4.1	1075	9.3	690	14.5
2381	4.2	1064	9.4	685	14.6
2326	4.3	1053	9.5	680	14.7
2273	4.4	1042	9.6	676	14.8
2222	4.5	1031	9.7	671	14.9
2174	4.6	1020	9.8	667	15.0
2128	4.7	1010	9.9	662	15.1
2083	4.8	1000	10.0	658	15.2
2041	4.9	990	10.1	654	15.3
2000	5.0	980	10.2	649	15.4
1961	5.1	971	10.3	645	15.5
1923	5.2	962	10.4	641	15.6
1887	5.3	952	10.5	637	15.7
1852	5.4	943	10.6	633	15.8
1818	5.5	935	10.7	629	15.9
1786	5.6	926	10.8	625	16.0
1754	5.7	917	10.9	621	16.1
1724	5.8	909	11.0	617	16.2
1695	5.9	901	11.1	614	16.3
1667	6.0	893	11.2	610	16.4
1639	6.1	885	11.3	606	16.5
1613	6.2	877	11.4	602	16.6
1587	6.3	870	11.5	599	16.7
1562	6.4	862	11.6	595	16.8
1538	6.5	855	11.7	592	16.9
1515	6.6	848	11.8	588	17.0
1493	6.7	840	11.9	585	17.1
1471	6.8	833	12.0	581	17.2
1449	6.9	826	12.1	578	17.3
1429	7.0	820	12.2	575	17.4
1408	7.1	813	12.3	571	17.5
1389	7.2	807	12.4	568	17.6
1370	7.3	800	12.5	565	17.7
1351	7.4	794	12.6	562	17.8
1333	7.5	787	12.7	559	17.9
1316	7.6	781	12.8	556	18.0

Table III

Frequencies and corresponding Ro-o distances for the decoupled $\nu(\text{OD})$ of pinacol and its hydrates.

	$\nu(\text{OH})$ (cm^{-1})	Ro-o (\AA)	$\nu(\text{OD})$ (cm^{-1})	Ro-o (\AA)	Ratio $\frac{\nu(\text{OH})}{\nu(\text{OD})}$
Pinacol	3419 } 3339 }	3379	2510	2.78	1.34
	3376 } 3266 }	3321	2496	2.77	1.33
	3355 } 3226 }	3290	2473	2.76	1.33
	3163 } 3124 }	3144	2447	2.75	1.29
			2443	2.75	
	3225		2411	2.73	
			2385	2.72	
			2496	2.77	
Pinacol mono- hydrate			2434	2.74	
Pinacol hexa- hydrate	3413-3125				

CHAPTER IV

CONCLUSIONS

Infra-red spectra of pinacol and its hydrates have been obtained at the beam and low temperature and assignments of the principle vibrations made. More bands are observed in the pinacol spectra than its hydrates which is to be expected in view of the proposed crystal structures, with sixteen molecules in the unit cell of pinacol whilst there are only two and eight molecules respectively in the unit cells of the monohydrate and hexahydrate. Also the dichroisms observed in the polarized spectra of pinacol and the monohydrate have assisted in deciding the orientation of the molecules in the single crystal samples. The dichroisms observed for $\nu(\text{OH})$ of pinacol are discussed in terms of tautomerization along the intermolecularly H-bonded chain of OH groups.

The decoupled $\nu(\text{OD})$ bands of pinacol and its hydrates have been obtained at low temperature. In pinacol four bands are observed corresponding to the eight observed in the undeuterated molecule. In the monohydrate three bands are observed and in the hexahydrate only two. The number of bands present, the frequency positions and $R_{\text{O-O}}(\text{\AA})$ values are discussed in terms of the proposed crystal structures.

CHAPTER I

INTRODUCTION

(I) Lipid Systems

Polar lipids contain hydrocarbon chains which are hydrophobic (water hating) terminating in one or more polar groups which are hydrophilic (water loving). Because of this dual nature such molecules are described as amphiphilic. All of these amphiphilic lipids crystallize in bimolecular layers.

The amphiphilic lipids can be classed in three main groups on the basis of their molecular make up and their interaction with water (76, 77, 78). Figure 18 abstracted from the paper by Lawrence (76), shows the skeleton formulae of some amphiphilic lipids placed in the group classification. Group I consists of the monofunctional unionized fatty acids and alcohols and includes the important cholesterol and other sterols. Group II, also unionized, includes the monofunctional alkylamines, the bifunctional diols such as 1,2 hexadecane diol, 1,2 and 1,3 monoglyceride diols, α -hydroxy acids as well as the biologically important lecithins, phosphatidyl ethanolamines, inositols and sphingomyelins. Group III may be split into two sections and these are group III(a) and (b). Group III(a) includes many of the classic anionic, cationic and non-ionic detergents as well as the important biological compound lysolecithin. Group III(b) in general are aromatic compounds with three or more fused rings and although these molecules may have definite hydrophobic and hydrophilic regions, these regions may occur randomly throughout the molecule leaving no overall polarity. Compounds in this group include the sulphated bile alcohols and bile salts which are steroids.

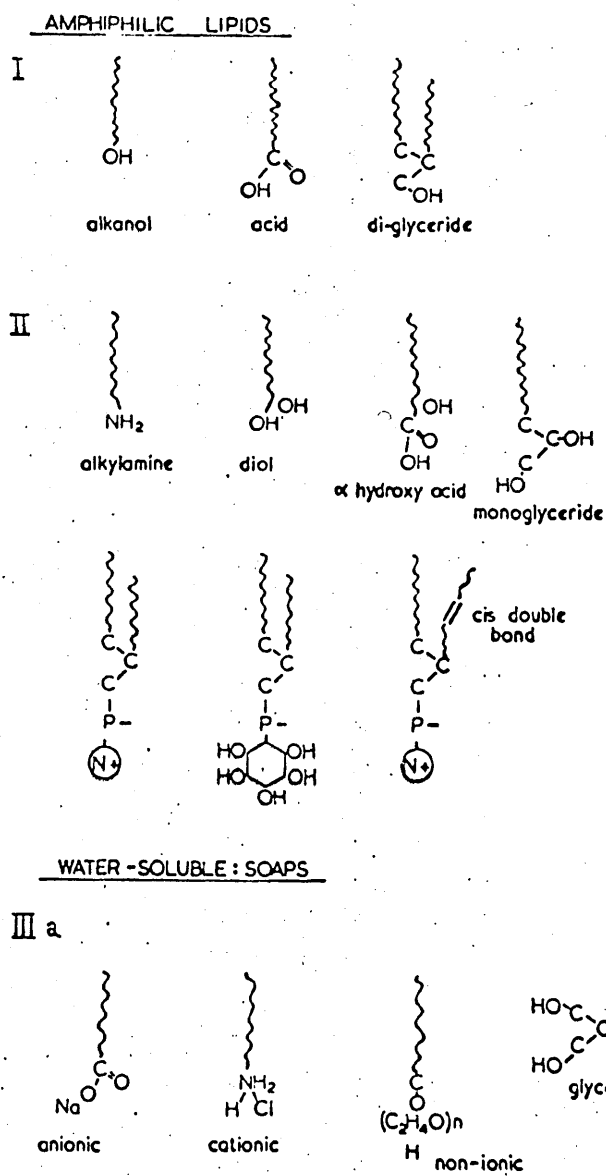


Figure 18 Amphiphilic lipids; skeleton formulae showing shape of molecules and location of hydrophilic groups. (76)

The physical interaction with water varies from group to group. Group I dissolve up to 2.5% water to form either liquid or solid solutions of water in lipid; the fatty alcohols reach saturation at the composition of a quarter hydrate. In the bulk they are virtually insoluble in water but they form stable monolayers on water. Much more water dissolves in the group II lipids which then form certain well defined liquid crystalline phases (79), for instance with the monoglycerides, up to 50% by volume is dissolved in liquid and liquid crystal phases. These substances are virtually insoluble in water and spread on water, as do those in group I to form stable monolayers. In group III(a) the lipids possess one distinct hydrophilic region and can be distinguished from group III(b) lipids by the fact that they form liquid crystalline phases when small quantities of water are added to them, whereas group III(b) do not. Both these groups are soluble in water, do not form stable monolayers at the air/water interface but demonstrate an equilibrium between molecules in the bulk phase and those on the surface.

In this thesis the polar lipids studied belong to group II. These soluble amphiphiles interact with water to form liquid crystalline phases and spread to form monolayers at the air/water interface. These systems will be described in greater detail in part V.

(II) Structure of Lipids

In most lipid material the polymorphism arises because of the different ways in which the hydrocarbon chains can pack together in bimolecular layers and the different angles of tilt to the plane of the layer which these modes of packing produce.

The different polymorphic forms of 1-monoglycerides have

been studied by various techniques including thermal analysis (80-87) and X-ray diffraction (82,84,85,86,88) as well as infra-red (89,90) and broad line N.M.R. spectroscopy (91) and dielectric measurements (92,93).

(i) l-monoglycerides

The polymorphism of racemic l-monoglycerides and other glycerides has been reviewed by Chapman (94) and later new information has been provided by the work of Larsson (95,96) and Lutton (97).

The pioneer work on the polymorphism of l-monoglycerides was carried out by Fischer et al (80) and Rewadikar et al (81). The work was extended by Malkin et al (82) who deduced from X-ray and thermal measurements that there existed three modifications for the l-monoglycerides. These were a low melting alpha (α) form and two higher melting modifications beta-prime (β') and beta (β). Later Lutton et al (85) after a re-investigation gave a further description of the crystallization phenomena. They not only observed the α , β' and β forms but also a sub-alpha (sub- α) form. The main points of the controversy over the polymorphism centred around whether the sub- α form is or is not crystalline, whether the sub- α to α transformation is genuinely reversible and whether in fact the α form is stable down to the lower transition temperature (86). A brief outline of the data reported on the polymorphic forms of l-monoglycerides is given below. The infra-red spectra of the different polymorphic forms of l-monostearin are shown as figure 19. The frequencies of the OH and C=O stretch, $\nu(\text{OH})$ and $\nu(\text{C=O})$, of the different polymorphs of l-monostearin are shown in table IV. The melting points of the polymorphic forms of some l-monoglycerides are shown in figure 20.

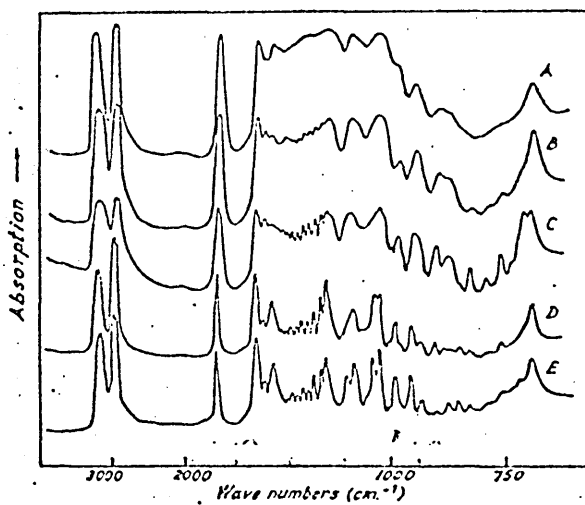


Figure 19.
Polymorphic forms of 1-monostearin.
A, Liquid; B, α ; C, Sub- α ; D, β' ; E, β . (90)

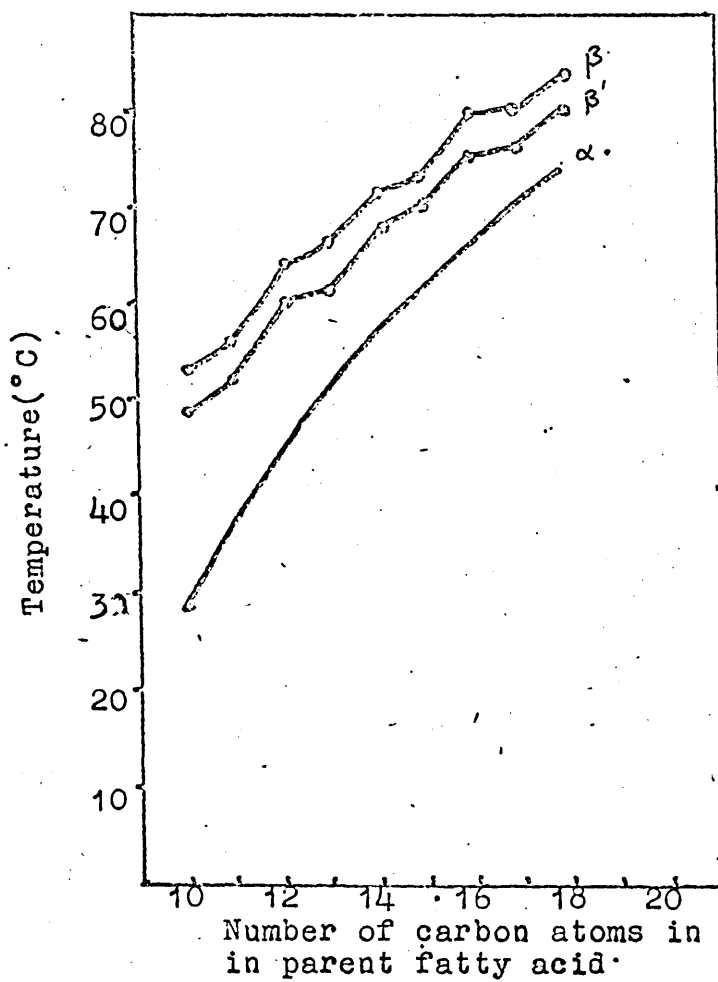


Figure 20.

Melting points and transition temperatures of the polymorphic forms of 1-monoglycerides. (82)

Table IV $\nu(\text{OH})$ and $\nu(\text{C=O})$ band position
in 1-monostearin (90).

Phase	$\nu(\text{OH})$ (cm^{-1})	$\nu(\text{C=O})$ (cm^{-1})
Liquid	3453	1706
α	3360	1721
Sub- α	3342	1730
β'	3342 3243	1736
β	3307 3243	1736

(a) Alpha form

The α form is separated first from the molten 1-monoglycerides (80-82) and has the lowest complete melting point. On the basis of X-ray measurements (single strong side spacing at 4.2\AA) Malkin et al (82) suggested that the α form exists as vertical rotating chains hexagonally packed. Lutton et al's (85) re-examination, however, showed that the chains were in fact tilted and this was confirmed by Larsson (96).

Dielectric measurements (93), broad line N.M.R. (91) and infra-red (90) spectroscopy have given further evidence for considerable freedom of motion of the alkyl chains not only about the chain axis but also longitudinally and laterally.

Using infra-red spectroscopy, Chapman (90) found that upon going from the liquid to the α form the H-bonding scheme altered. In the liquid state the H-bonds occurred between OH and C=O groups but in the α form the bonding was found to be preferentially between OH groups. This was inferred from the shift of the $\nu(\text{OH})$ band to lower frequency and the $\nu(\text{C=O})$ band to higher

frequency (table IV) upon going to the α form.

(b) Sub-alpha form

Malkin (82,86) stated that the α form was stable only near its melting point. Lutton et al (85) showed by X-ray diffraction, dilatometry and microscope examination that infact the α form was stable down to 25°C below the solidification point where a reversible transition took place to what was termed the sub- α form. The side spacings which characterized the sub- α form consist of one single strong line at 4.15Å with other medium lines at 3.9, 3.75 and 3.55Å. The sub- α is thought to have tilted chains with long spacings similar to the β' form. The reversibility of the transition as well as the X-ray data of Lutton et al (85) has been confirmed by Larsson (96) who showed that the angle of tilt of the chains to the end group planes was 55°.

Broad line N.M.R. (91) and dielectric (93) measurements have shown that just below the $\alpha \rightleftharpoons$ sub- α transition point the motion about the long axis ceases, though Crowe et al (93) explain the dielectric data from the sub- α form in terms of segment orientation, on which they do not elaborate.

Infra-red spectroscopic examination (90) showed that the α form was stable down to a lower transition temperature and changed into a form giving a spectrum of a crystalline modification; the sub- α form. However the bands were broad which is rather suggestive of some orientational freedom. The spectrum also shows a splitting of the single band at 719cm⁻¹ of the α spectrum, into two components (at 727cm⁻¹ and 719cm⁻¹). An analogous situation occurs in n paraffins. In the hexagonal form of the paraffin, similar to the α form of 1-monoglycerides, a single band exists near 720cm⁻¹. Below the transition point

to the crystal form the band is split into two (24). A similar situation occurs in polyethylene (19,98). Stein (99) showed that the splitting arises in n paraffins and polyethylene only when these materials are in a certain crystalline state, the two components being due to interaction of nearest neighbour CH_2 groups giving rise to the out-of-phase and in-phase components at different frequencies. From this Chapman (90) deduced that the sub- α form exists at least as a very ordered system and probably a crystalline lattice of the common orthorhombic type. Also from a shift of the $\nu(\text{OH})$ band to even lower frequency and the $\nu(\text{C}=\text{O})$ band to higher frequency (table IV) he was able to deduce that in the sub- α form the OH groups become more strongly H-bonded whilst the reverse occurred with the $\text{C}=\text{O}$ group.

More recently Lutton (97) using differential thermal analysis and X-ray diffraction has found evidence for the existence of a reversible transition $\text{sub-}\alpha_2 \rightleftharpoons \text{sub-}\alpha_1$ (indicated by Malkin et al (82) for 1-monostearin) below the reversible $\text{sub-}\alpha_1 \rightleftharpoons \alpha$ transformation for C_{18} to C_{22} compounds; it occurred at about 50°C and was found to be independent of chain length. The X-ray patterns of the sub- α_2 and sub- α_1 forms were found to be very similar. Lutton (97) found a value of the heat of transformation of the $\text{sub-}\alpha_2 \rightarrow \text{sub-}\alpha_1$ of 12.6Jg^{-1} compared with a value of 48Jg^{-1} of the $\text{sub-}\alpha_1 \rightarrow \alpha$ transition. It is still uncertain what the transition is due to.

Only five sub- α forms have been observed for 1-monomyristin (91), 1-monopalmitin and 1-monostearin (85,90, 91, 93), 1-monoarachidin and 1-monobehenin (97). Therefore whether this form exists for shorter chain 1-monoglycerides is open to conjecture.

(c) Beta-prime form

Malkin et al (82) obtained the β' form by a particular form of heat treatment of molten 1-monoglycerides. He showed that the melting points of the β' form of the 1-monoglycerides alternate as shown in figure 20. The X-ray analysis showed short spacings of 4.24 and 3.86Å whilst the long spacings were similar to the β form. It was therefore deduced that the structure consisted of non-rotating alkyl chains tilted at an angle of 59° in the bilayers. Lutton et al (85), Chapman (90) and Larsson (96) obtained the β' form by rapid crystallization from certain solvents. A single crystal of the β' form obtained by rapid recrystallization was examined by Larsson (96) using X-ray diffraction. He showed that the single crystal data was identical with that recorded for one form of 1-monoglycerides (96,100). Therefore Larsson (96) stated that the crystal form earlier known as the β' form was optically active and that the racemic form separated into antipode crystals on rapid crystallization and this β' form had nothing to do with the polymorphic transitions in racemic 1-monoglycerides. The principal arrangement of the molecules are directed head to head and the chain packing is the common orthorhombic. The angle of tilt of the chain is 55° and the direction of tilt alternated in successive double layers.

Dielectric (93) and broad line N.M.R. (91) measurements on the β' form have shown that the chains are indeed non-rotators.

Chapman (90) has studied the infra-red spectra of three 1-monoglycerides in the β' form. The spectra were more typical of the type of spectrum normally obtained with fully crystalline

materials, ie. the bands were narrow and sharp. This is more easily seen in figure 19. Also a further shift was observed of the $\nu(\text{OH})$ band to lower frequency (now split into two components), and the $\nu(\text{C}=\text{O})$ band was also shifted again to higher frequency (table IV). These two effects were taken to indicate a further decrease in the participation of the $\text{C}=\text{O}$ group in the H-bonding scheme in the β' form.

Lutton (97) using differential thermal analysis has recently determined a heat of transformation for the β' form to liquid at approximately 206 Jg^{-1} . This value compares favourably with the heats of transformation of the highly crystalline β form of even chain length fatty acids to melt (101) on a mole^{-1} basis.

(d) Beta form

The β form is the stable form with the highest melting point and can either be obtained by transformation via the α and β' forms or by slow crystallization from a suitable solvent. The alternation of melting points found for the β' forms is also found for the β form (82) and is shown in figure 20. X-ray diffraction (82, 85, 95, 96) has shown the structure to be rigid double layers of molecules with the alkyl chains packed in a monoclinic sub-cell with again an alternating angle of tilt of 55° in successive double layers. The short spacing which characterises this form is at 4.55\AA .

Dielectric (93) and broad line N.M.R. (91) measurements yielded values of dielectric constants, line widths and second moments which lead to the conclusion that the β form is a rigid structure with no appreciable motion occurring.

Several workers (90, 102-105) have obtained infra-red spectra of the β form. In these spectra the bands are, as in

the β' form, of a more crystalline nature. Chapman (90) observed that the $\nu(\text{OH})$ band was shifted even further to lower frequency (table IV). He deduced that this overall shift signified stronger H-bonds which could be correlated with the β form having the highest melting point and is therefore the most stable polymorph. Chapman (105) notes that the major differences between the spectra of the β form lie in the 1250cm^{-1} region where the vibrations are due to CH_2 wagging and twisting modes.

Lutton (97) using differential thermal analysis has found a value for the heat of transformation of the β form to liquid, similar to that of the β' form to liquid, of approximately 206Jg^{-1} .

(ii) Unsymmetrical trialkylphosphine oxides

No reports have been made, to date, of the structure of unsymmetrical trialkylphosphine oxides. Some information is available however from the studies made on the analogous unsymmetrical trialkyl-N-oxides (106, 107).

In the case of the X-ray measurements (107) spacings have been observed, but not distinct ones. Lutton (107) has suggested this is due to the presence of several different crystalline phases with different degrees of hydration. From the side spacing data it would appear that the N-oxides crystallize in the normal bimolecular layer structure of long chain compounds.

There is no evidence for the existence of different polymorphs in the unsymmetrical trialkylphosphine oxides.

(III) Hydration of Lipids

Polymorphism of a similar nature to that of 1-monoglycerides is observed in long chain alcohols (108, 109) and acids (110, 111). For fatty alcohols three principal crystal modifications have been distinguished α , β and γ forms. Similarly

the long chain acids also exhibit three different crystalline forms. These are A, B and C for even acids, and A', B' and C' for odd acids, although there has been recent spectral evidence of a fourth modification of some even acids (hexadecanoic and octadecanoic acids)(35,36).

Several workers whilst studying the polymorphism of these compounds have noted the effect of water. The techniques used in these studies were X-ray (112, 113, 114), dilatometry (115), thermal analysis (116, 117) and dielectric measurements (115,118, 119). It was found that small traces of water affected the polymorphic transitions.

A better understanding of the interaction of alcohols and acids with water was obtained later by Trapeznikov (120-129). He showed that in the bulk, higher aliphatic alcohols and acids interact with water and form hydrates characterized by definite physical properties such as the temperature of transition, melting and density. Also hydrates of these compounds exhibited sharply pronounced polymorphism, in particular formation of the liquid crystalline mesomorphic structure on surfaces.

Further evidence of hydrate formation was also obtained by Brookes et al (130,131) who used both monolayer pressure measurements as well as thermal analysis in their investigation of the effect of water on the polymorphic transition of tetradecanol and hexadecanol. They found a ratio of one water molecule to two alcohol molecules reduced the temperature of the α to β transition by a full 10°C . Lawrence et al (132) however in their study of the effect of water on the α form of long chain alcohols found a value of one water molecule to four alcohol molecules at saturation for alcohols above octanol. They also found that water in fact increases the freezing point from the liquid to

hexagonal form and reduces the transition temperature to the lower symmetry packing there by stabilizing the α form. Al-Mamun (12) obtained further evidence of the increased range of existence of the α form of alcohols in the presence of water using infra-red spectroscopy. Figure 21 shows the pure hexadecanol spectra when in the γ and α forms as well as that when saturated with water. Whereas at 39°C pure hexadecanol exists in the γ form, with water at the same temperature an α phase spectrum is obtained.

Even though this large volume of work has been carried out there is no X-ray evidence of the specific hydrate structure.

The existence of a monohydrate in the 1-monolaurin/water system has been proposed by Lawrence et al (133). The phase diagram for this system is shown as figure 22. The solid β modification of 1-monolaurin melts at 61°C and addition of water lowers this to a eutectic minimum at 41°C after which the phase boundary rises to a peak suggesting the formation of a monohydrate. Further evidence for this monohydrate was obtained from broad line N.M.R. measurements. The solid β modification has a second moment of $17.62(\pm 0.47)\text{G}^2$ whilst the value of the monohydrate was $19.41(\pm 0.31)\text{G}^2$. The value for the monohydrate is in agreement with what would be expected due to interaction of two or more protons on the water molecule with each other and the effect of H-bonding thereof. However there is no real evidence for any higher hydrate designated by the dotted line at approximately 16°C.

In the case of the unsymmetrical trialkyl-N-oxides there are several reports of their behaviour with water (106, 107, 134-139). Of the studies only Lawson et al (106) using broad line N.M.R. spectroscopy and Lutton (107) using X-ray diffraction have looked at the crystalline phase. In neither case was evidence



Figure 21.

Infra-red spectra of hexadecanol A- γ form(30°C), B-saturated with water at 39°C , C- α form(45°C).
Wavelength $6\text{-}18\mu$ and $2.75\text{-}3.25\mu$. (12)

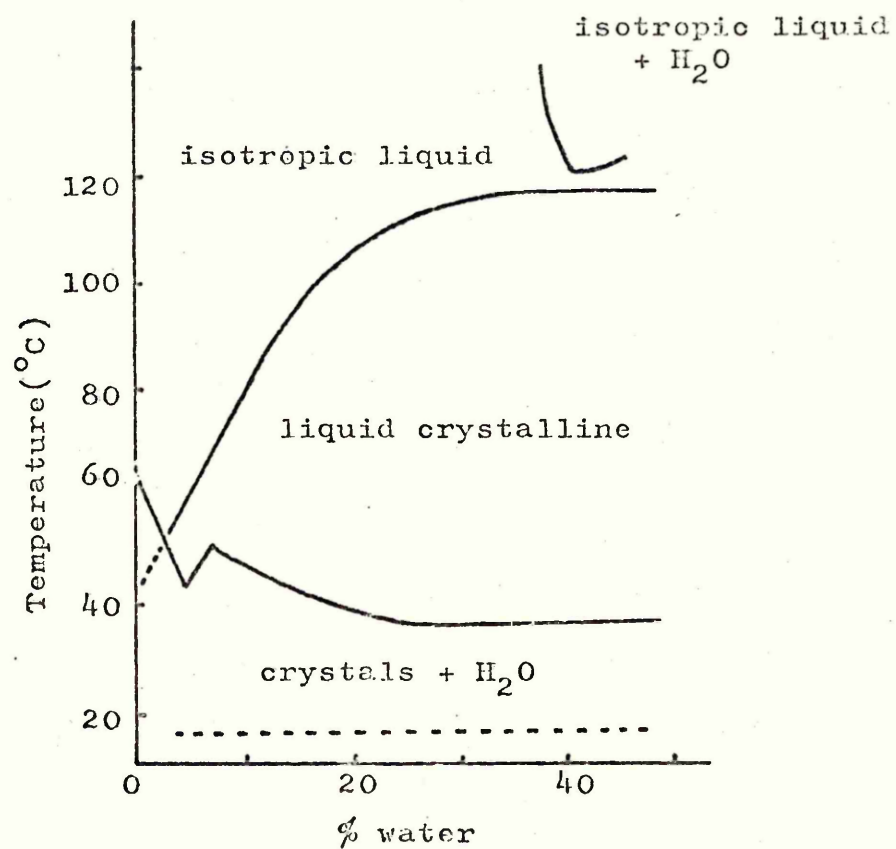


Figure 22

1-monolaurin/H₂O phase diagram. (133)

found for the presence of a hydrate although Lutton (107) has remarked that in the crystalline phases different degrees of crystal hydration seemed likely. In the case of the unsymmetrical trialkylphosphine oxides only two studies, to date, have been reported on the binary system with water (140, 141). In neither case was a study made of the crystalline regions of the phase diagram.

However in the case of the symmetrical trialkylphosphine oxide, trimethylphosphine oxide, Goubeau et al (142) have postulated the formation of various hydrates to account for the appearance of several $\text{P}=\text{O}$ stretching, $\nu(\text{P}=\text{O})$, bands in the infra-red spectra of the solid hydrated material. This spectral data was supported by vapour pressure measurements.

Also more recently evidence has been reported by O'Laughlin et al (143) for hydrate formation in the case of tri-n-octylphosphine oxide (T.O.P.O.). The extraction of water in CCl_4 solutions of T.O.P.O. was studied at various phosphine oxide concentrations. From infra-red and N.M.R. spectroscopic data as well as vapour pressure lowering data in addition to partition data it was found that T.O.P.O. extracts water to form a monohydrate for concentrations of T.O.P.O. of less than 0.1M.

(IV) Structure of Water from Infra-red and Raman Spectroscopy

Several reviews (144-146) have been produced on the structure of water, a subject which has attracted much attention in recent years from both biologists and physical chemists. Before a discussion of the structure of liquid water, it is necessary to consider what exactly is meant when talking about structure in connection with liquids.

In solids there is little doubt about the meaning of the word structure, a term used to describe the spatial relations

between molecules. Such descriptions are possible because spatial relations persist much longer than the time necessary for measuring these relations. As a result, uncertainties in average molecular (and atomic) positions are very small because measurements can be extended over periods of time many orders of magnitude longer than the correlation times of molecular motions. In liquids however, it is doubtful whether these prerequisites are fulfilled.

In liquid water the molecular motions may be divided into rapid oscillations and rotations and slower diffusional motion. Therefore the 'structure' depends on whether one considers a time interval short compared to the period of oscillation, or an interval longer than the period of an oscillation but less than the time for a displacement, or an interval considerably longer than the displacement time.

Spectroscopic techniques such as infra-red and Raman yield information about the so-called vibrationally-averaged (V) structure. This is because the periods of vibration (10^{-13} to 10^{-14} s) for both intra and intermolecular modes of water are short compared with the average time (10^{-11} to 10^{-12} s) between diffusional motions of molecules.

On the basis of a wide range of studies of liquid water, models have been postulated for liquid water. Most of these models can be grouped into two general categories, 'mixture' and 'continuum' models.

The mixture models (147-151) describe liquid water as an equilibrium mixture of molecular species with different numbers of H-bonds per molecule.

The continuum models (152-154) describe liquid water as a still essentially complete H-bonded network with a distribution

of H-bond energies and geometries. These models consider the average strength of H-bonds in water to be weaker than in ice as a result of irregular distortions and elongations both of which increase with temperature.

On the basis of the vibrational spectrum it should be possible to choose between the two types of models (as the frequency of OH stretching vibrations is known to decrease in a regular manner with increasing strength of H-bond (155)). If liquid water consisted of a mixture of molecules with broken and unbroken H-bonds then every OH stretching band would consist of two sub-bands. The sub-band corresponding to the non-H-bonded OH groups should occur at a frequency considerably higher than that of the sub-band due to the H-bonded OH groups and should be detectable. Moreover the relative intensity of this high frequency sub-band would increase rapidly with temperature as the proportion of broken H-bonds increased. If on the contrary, liquid water contains a continuous distribution of the H-bond energies, then a single broad band would be expected, which would shift gradually towards higher frequencies as the temperature is increased and the average strength of the H-bonding decreased.

However with the stretching bands of liquid water some complications arise. The frequencies of the two OH stretching vibrations, the OH symmetric (ν_1) and asymmetric (ν_3) stretch and the first overtone of the bending vibration (ν_2), $2\nu_2$, happen to be very close to one another in liquid H_2O . A similar, but even more complex situation holds for higher overtones and combination bands, so that the spectrum in fact consists not of single bands but of 'band clusters' which contain a rapidly increasing number of vibrational transitions. The situation in liquid D_2O is the same as in H_2O , all the vibrational frequencies

being simply reduced by a nearly constant factor of 1.36. The vibrations ν_1 and ν_3 enter into Fermi resonance with the overtone of ν_2 (156). Fermi resonance within each 'band cluster' may produce intensity borrowing and frequency shifts which will vary with temperature in a complex manner, since the frequencies of the three fundamentals vary differently with temperature. Finally intermolecular coupling occurs between like vibrations of neighbouring molecules and intramolecular coupling occurs between the closely spaced vibrational levels ν_1 and ν_3 leading to a general broadening and distortion of all band shapes.

However most of the above complications can be ruled out by the far simpler spectra of HDO (60, 156-158) produced by isotopic dilution of H_2O in D_2O or D_2O in H_2O , vice versa. The residual OH and OD stretching bands, $\nu(\text{OH})$ and $\nu(\text{OD})$, thus produced are said to be decoupled.

Figure 23 shows the decoupled $\nu(\text{OD})$ bands in liquid water obtained by Wall et al (60) and Walrafen (159) using Raman spectroscopy, along with that obtained by Falk et al (156) using infrared spectroscopy. Two interpretations were placed on the shape of the decoupled bands. The first was due to Wall et al (60), Falk et al (156) and Frank et al (160) all of whom emphasized that their results indicated an intensity distribution that was continuous and passed through a single maximum (except above the critical temperature at densities below 0.1g cm^{-3} , where rotational fine structure became important (160)).

The second interpretation of the shape of the decoupled Raman stretching bands shown in figure 23 was given by Walrafen (159, 161). Walrafen believes that the observed band shape arises from the superposition of two or three relatively broad overlapping gaussian component bands. Further support for Walrafen's interpretation has been reported by Hartmann (162) and Senior et al

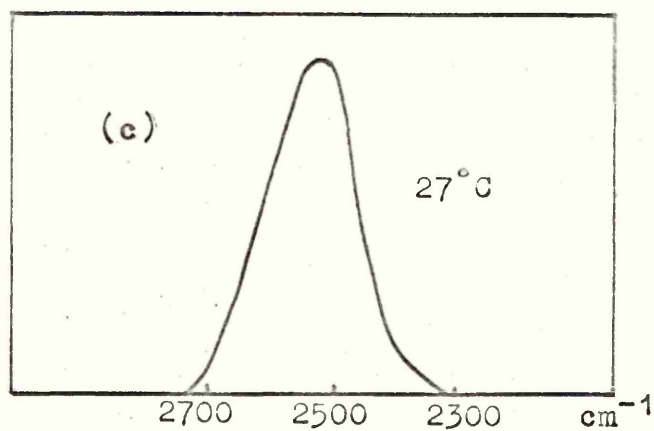
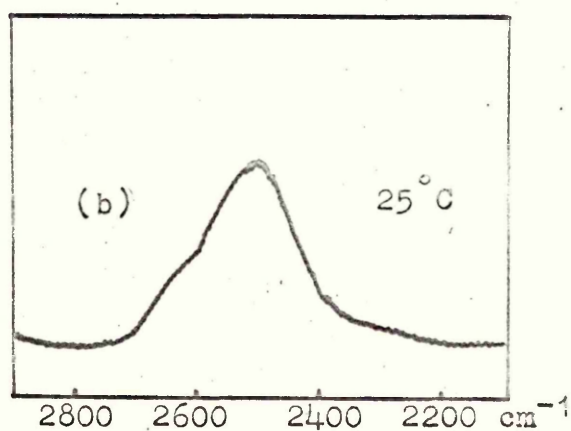
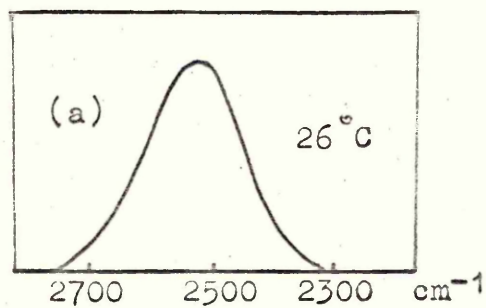


Figure 23.

Decoupled $\nu(\text{OD})$ bands of liquid water obtained by:-
 (a) Falk et al (156)(infra-red) , (b) Walrafen (159)
 (Raman) , (c) Wall et al (60)(Raman).

(164) using infra-red spectroscopy. However more recently doubt has been cast on the interpretation of Walrafen (146, 164). From information obtained from the studies on the decoupled stretching bands the present state of knowledge on the structure of liquid water can be summarized as follows:-

A range of OH environments, or H-bond strengths is present in liquid water. Water probably does not contain a small number of distinctly different molecular species, however the possibility is not ruled out that the liquid contains two or more species, each of which exhibits a wide range of molecular environments. Also the presence of some non-H-bonded OH groups in the liquid which have environments distinctly different from the majority of OH groups cannot be ruled out, although it seems unlikely.

(V) Lyotropic Liquid Crystalline Phases

Lyotropic liquid crystalline (l.c.) phases are formed by large numbers of lipids plus water at temperatures below their melting points.

The first lyotropic l.c. phase was observed in 1854 by Virchow (165) who in his own words 'soaked a piece of nerve tissue in water for a long time' and then saw this curious 'Newgate frill' of tubular looking excrescences which are now termed myelins. Later in 1863 Neubauer (166, 167) observed their formation when ammonium hydroxide solution was brought into contact with oleic acid.

The l.c. state has been the subject of six relatively recent reviews by Brown et al (168, 169), Christyakov (170), Winsor (171) Benedy (172) and Chandrasekhar et al (173).

The first step in the structure analysis of multicomponent systems is to characterize the different phases and determine their range of existence. This is carried out by determining the

phase diagram of the system as a function of temperature and composition. Condensed binary phase diagrams of various group II lipid/water systems have been reported. They include amine/water (174), amine oxide/water (107, 138), amine-hydrochloride/water (175, 176), alkyl-imide/water (177), dimethylalkylphosphine oxide/water (141), dodecylhexaoxyethylene glycol monoether/water (178), 1-monoglyceride/water (133, 178-183, 209), and lecithin/water (184) systems, two of which are shown in figures 22 and 24. A number of different l.c. phases have now been characterized the two most frequently encountered being the so called 'neat' and 'middle' phases.

(i) Neat phase

The presence of a neat phase is most easily detected by the birefringent textures which it shows under the polarizing microscope (185, 186) and the way in which these textures flow when pressure is applied to the microscope slide. The textures can take the form of myelins, batonnet and 'maltese cross' focal conics as well as many others, between crossed polarizers.

A large amount of X-ray data has been reported on the neat phase of many systems since the early measurements of Stauff (187) and Doscher et al (188). The systems studied include soap/water (189-199), amine-hydrochloride/water (195, 199), amine oxide/water (107, 137), alkyl-imide/water (200), 1-monoglyceride/water (180, 181, 182, 198, 201-203), dodecylhexaoxyethylene glycol monoether/water (178) and phospholipid/water (184, 195, 198, 201, 203-205) systems. In each system the neat phase was found to have a lamellar, smectic structure with the lipid lamellae separated by layers of water. This sort of arrangement is shown in figure 25, which also shows the X-ray parameters d_p and d used to characterize the structure.

It is found in the neat phase region of the above systems that

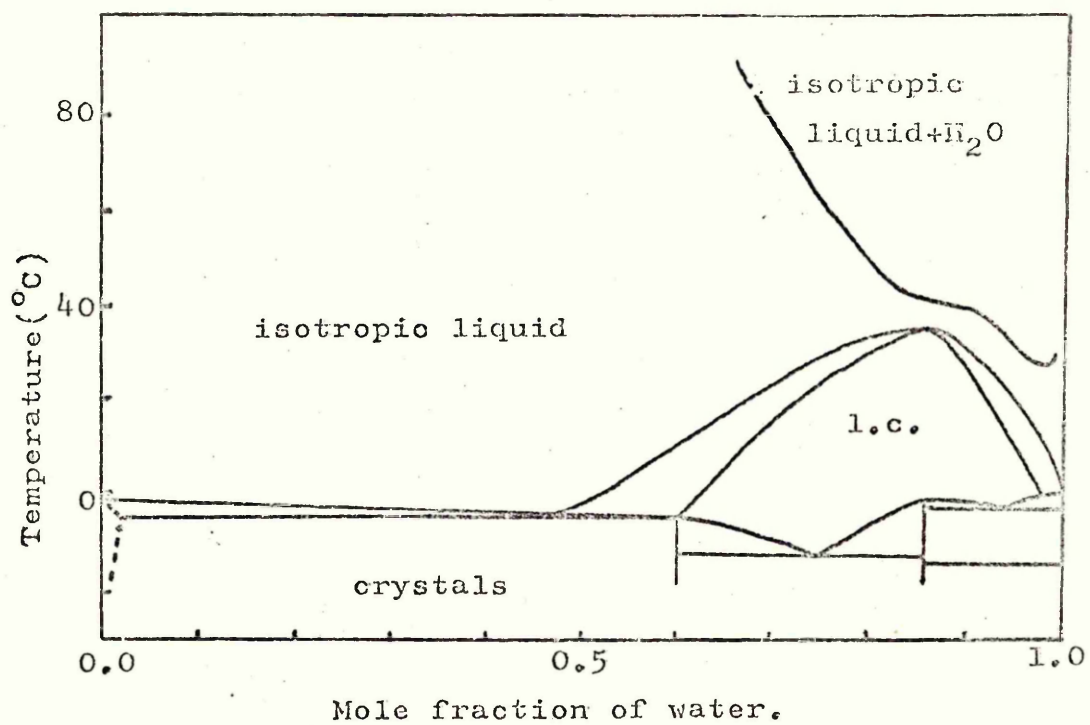


Figure 24
n-Octylamine/water phase diagram (174)

at constant temperature, d and s (the average surface area per hydrophilic group at the water interface) increase with increasing water content while d_l decreases. However if the water content is kept constant, s is again found to increase with increasing

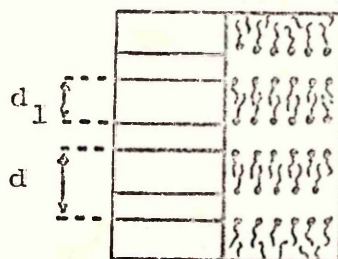


Figure 25
Structure of neat phase showing
X-ray parameters d_l and d .

temperature whilst d and d_l decrease. Luzzati et al (194) have also found that in general the bulkier the hydrocarbon chains the more extended is the neat phase range of stability, although other chemical factors also play a role such as the presence of double bonds in paraffin chains which increases s .

Gallot et al (195) determined the specific surface area, s , of polar groups in a number of soaps. They found at a constant temperature and for one cation, s was a function of the number of polar groups per volume of water present in the mixture, irrespective of the length of the hydrocarbon chain. They concluded, therefore, that the structure element dimensions are in the main determined by the interactions at the lipid/water interface, which in turn appears to be dependent on the concentration of the hydrophilic groups.

Recent X-ray data of Lawson et al (137) on the neat phase of the dimethyldodecylamine N-oxide/D₂O system indicated that the water is associated with and around the polar ends of the amine oxide molecules. By assuming that the surfactant and water are not incompletely separated layers but instead the oxygen of the amine oxide is incorporated into an ordered water lattice they derived an angle of tilt of 50-56° for the hydrocarbon chains.

The motion of the hydrocarbon chains is regarded as 'liquid like' by most workers. This conclusion has been reached on the basis of the rather broad and diffuse band at 4.5Å which is nearly identical with that found in liquid paraffins. However Luzzati (201) states that although the short range order is similar to that of liquid paraffins the disorder is not complete. This is concluded from an observed modulation, in some cases, of the intensity of the 4.5Å band showing that the movement of the chains are restricted. Further he states that since d_g decreases continuously as the temperature rises it is indicative of the polar groups in the plane of the water layer, and conformation of the chains being disordered. However, if as according to Lawson et al (137) the amine oxide groups order the water around themselves then a reciprocal ordering of the amine oxide groups is expected at the interface.

Direct confirmation of the layered structure of the neat phase has been obtained from the electron micrographs of anhydrous surface replicas (196,197,200), osmium tetroxide fixed sections (196,197,206) and negatively stained specimens (197,207). The step heights obtained from electron micrographs have been found to be in good agreement with the long spacing values obtained from X-ray diffraction.

Electron spin resonanance (208) and nuclear magnetic resonance (133,138,183,209-220) studies on the neat phase showed that there was a measurable degree of molecular ordering along a

direction perpendicular to the lamellar planes of the mesophase although there is a decrease in the degree of order down the chain from the polar head. The ordering of the water was found to be much smaller in magnitude and comparable to that previously observed in some hydrated silicates and fibrous material. Also the polar interface was not restricted to a planar surface but had a diffuse structure giving rise to an interface consisting, possibly, of the polar head group and 'ordered' water as well as one or two methylene groups. There was also found to be evidence for lateral diffusion of the molecules in the lipid bilayer.

Thermotropic liquid crystals have been studied by both polarized (221-225) and unpolarized (226-228) infra-red spectroscopy. Maier et al (224) using polarized infra-red spectroscopy made a quantitative measure of the degree of order in the nematic phase of some of the 4,4'-di-n-alkoxyazoxybenzenes, which compared favourably with that found by broad line N.M.R. spectroscopy. Unpolarized infra-red spectroscopy has been applied to the study of phospholipids (229, 230) and phospholipid/water mixtures in the l.c. state and membranes (230-234).

Figure 26 shows the spectrum at various temperatures of DL-dipalmitoylcephalin (m.pt. 195°C). At low temperature, -186°C, the spectrum shows a great deal of fine structure, eg, the band near 720cm^{-1} associated with the CH_2 rocking mode, $\omega(\text{CH}_2)$, is split into a doublet. At room temperature some of this fine structure has disappeared and now only a single band occurs at 720cm^{-1} . In the region 100°-120°C all the remaining fine structure disappears. This behaviour can be equated with the melting of the chains, the smearing out of the bands being related to possible isomerism. In a phospholipid containing an unsaturated alkyl chain, as in 2-oleoyl-3-stearoyl-L-1-phosphatidyl choline,

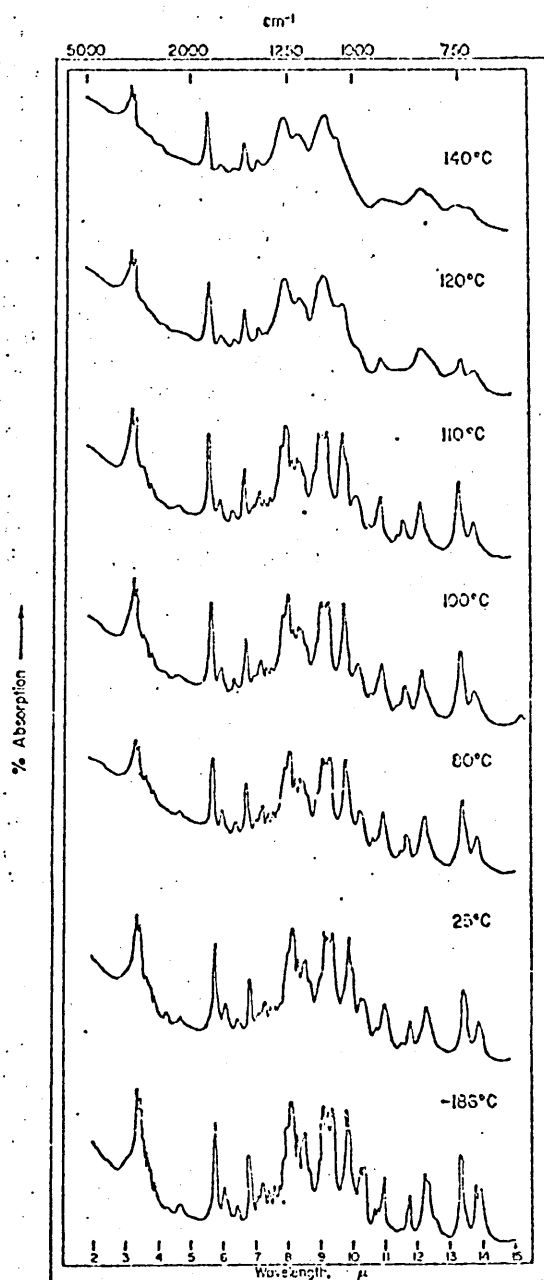


Figure 26
Infra-red spectra of 2,3 dipalmitoyl-DL-
1-phosphatidylethanolamine at different
temperatures. (230)

the alkyl chains were also shown, using infra-red spectroscopy, to be in this 'liquid like' state at room temperature.

Bulkin et al (227, 228) showed in their study of the l.c. phase of the phosphatidoyl ethanolamine/water system by infra-red and Raman spectroscopy, that the room temperature spectrum shows the 'liquid like' behaviour of the anhydrous spectrum at 140°C. Also by intensity alterations with temperature it was shown that infra-red and Raman spectroscopy were sensitive techniques for determining phase changes in these systems.

Friberg et al (235) have used infra-red spectroscopy to study the effect of octanoic acid on the l.c. phase of the octylamine/water system. They found that when the carboxylic acid was introduced into the l.c. phase of amine and water, an amine/acid salt was formed. This was evident from the infra-red spectrum in which the 1715cm^{-1} band due to non-ionized carboxylic acid groups was found to be absent.

(ii) Middle phase

As with the neat phase the presence of the middle phase can be most easily detected by the characteristic birefringent textures (185, 186) and the way in which the textures flow when pressure is applied to the microscope slide. When viewed between cross polarizers the sample appears bright. The consistency of the phase is strikingly stiff and it will not flow under the force of gravity.

Early observations using X-ray diffraction were carried out by Bernal et al (236) on tobacco mosaic virus and McBain (237) on the middle phase of the lauryl sulphonic acid/water system. According to McBain (237) the middle phase apparently consisted of fibres or long rods or elongated ellipsoids which lay parallel at a distance from each other in a hexagonal array. X-ray data has been reported on several systems including soap/water (190-197),

amine oxide/water (107, 137), alkyl-imide/water (200), dodecyl-hexaoxyethylene glycol monoether/water (178), 1-monoglyceride/water (180, 182), and phospholipid/water (194, 198, 205, 206) systems. The arrangement described by McBain (237) is shown as figure 27 which also shows the X-ray parameters d_l and d used to describe the structure.

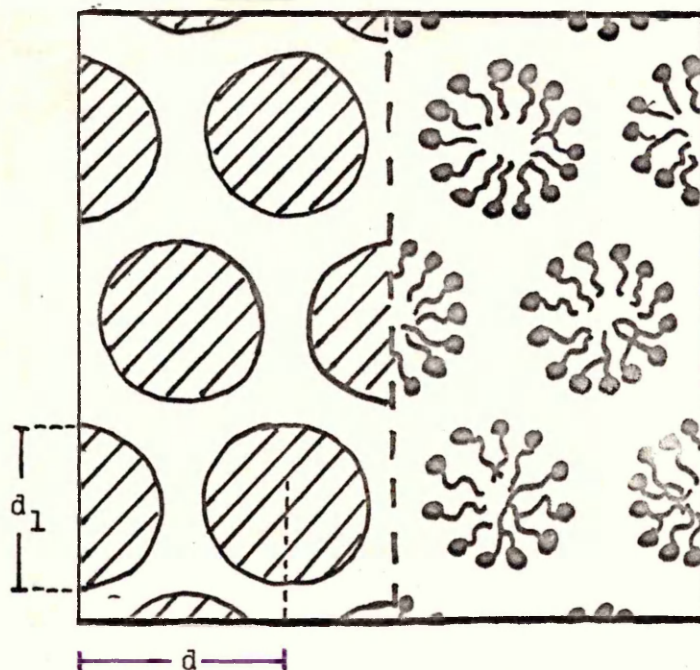


Figure 27.
Structure of middle phase showing
x-ray parameters d_l and d .

In the above systems it was found that d and s increase with increasing water content while d_l remained relatively constant. However the increase in s is small compared to the corresponding neat phase and the value of s was found to be independent of the length of the hydrocarbon chain.

Luzzati et al (194) have found that in general the bulkier the hydrophilic moiety then the more extended was the range of stability of the phase. Also Gallot et al (195) have shown that s is a function of the molal concentration of the polar groups in the water of the system for all soaps of the same cation.

In the phospholipid/water system studied by Luzzati et al (194) a reverse middle phase was observed similar to that shown in figure 27 in which the water was located on the interior of

the rods and the lipid molecules filled the gap between. This structure has conformation from the electron microscopy studies of Stoeckenius (206). In this case as the water content was increased, d , d_w (the diameter of the water cylinders) and s increased.

A controversy has arisen about the middle phase structure. This controversy centres around the details of the geometry of the rod like units. Luzzati et al (190-194) maintained on the basis of X-ray studies, that the units were uniform cylinders of a given diameter and definite length, Clunie et al (177) have suggested, recently, that the units 'consists of linearly aggregated spherical micelles' having the appearance of a string of beads. Their argument was based on the fact that they observed no abrupt changes in the X-ray spacings across the phase boundaries and on a consideration of the relative volume filling capabilities of spheres and cylinders.

More recently Lawson et al (137) have studied the middle phase of the dimethyldodecylamine N-oxide/water system by X-ray diffraction and attempted to fit the data to both the above models. Their results indicated that in their cases the middle phase consists of cylindrical units packed in a hexagonal lattice although on the information obtained, it was not possible to make a completely unambiguous choice between the models. The interface was viewed by Lawson et al (137) as a layer of 'ordered' water with the oxygen of the amine oxide group substituting for a water molecule in the layer. This is a contradiction of the statement of Luzzati et al (191) who believed that the water in the middle phase behaved as a continuous medium.

It is believed as in the case of the neat phase, that the motion of the hydrocarbon chains is again 'liquid like' but must be restricted to some extent by the anchoring of the polar groups

at the solvent/surfactant interface.

Confirmation of the hexagonal structure of the middle phase has been obtained from the electron micrographs of anhydrous surface replicas (197), osmium tetroxide fixed sections (197, 206), and negatively stained specimens (197). The interparticle spacings are in good agreement with the values found from X-ray measurements.

High resolution (137, 213) and broad line N.M.R. (215, 216) spectroscopic measurements have been carried out on the middle phase. The results of these studies indicated a looser packing of the chains than in the neat phase with a distribution of correlation times along the hydrocarbon chains. Also there is evidence of lower H-bond strength in the middle phase than in the neat phase.

To date no infra-red studies on the middle phase have been reported.

Summary

The structure of the neat and middle phases may be summarized as follows.

The neat phase is thought to consist of a conventional lamellar, smectic structure of equidistant bimolecular layers of an amphiphilic lipid separated by layers of water. The middle phase is envisaged as being a two dimensional array of equidistant cylinders or rods, the alkyl chains being located in the interior of the rods and the water filling the gap between (there is evidence that in certain systems the reverse structure does exist). In both cases the hydrophilic groups occupy the solvent interfaces and the water molecules are ordered by H-bonding to these polar head groups, although the H-bond strength is greater in the neat than the middle phase. The degree of order of the water in the

neat phase is similar to that found in some fibrous materials. In both cases the motion of the alkyl chains consists of restricted rotation with a distribution of correlation times, less motion near the polar head groups. There is also some evidence for chain diffusion in two dimensions.

The work incorporated in this part of the thesis was part of an overall study of the structure and H-bonding in anhydrous polar lipids and the solid and liquid crystalline phases produced in the hydrated state.

The polar lipids studied in this case were the l-monoglycerides and unsymmetrical trialkylphosphine oxides. The object of the work was to use polarized and unpolarized infra-red spectroscopy to investigate the structure of the lipids in the anhydrous and hydrated forms. This work was complementary to that carried out by Mr. W.E. Peel, who used broad line N.M.R. spectroscopy to study the anhydrous and hydrated forms of l-monoglycerides.

CHAPTER II

EXPERIMENTAL

(I) Preparation and purification of materials

(i) Preparation of l-monoglycerides

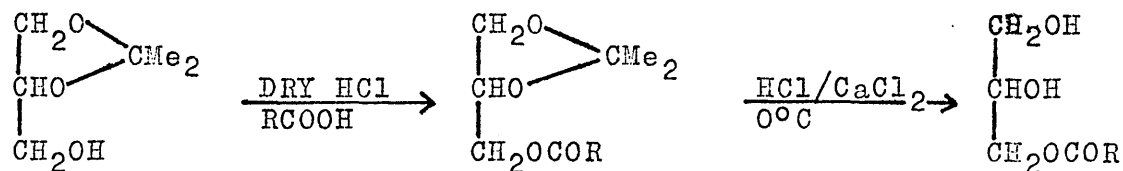
Racemic l-monoglycerides were prepared by Malkins' method (82), but using di-isopropyl ether in the extraction to reduce the loss of monoglycerides into the aqueous layer. The preparation of l-monooctanoin (MG8) is described in detail and the modification for the preparation of l-monoundecanoin (MG11) is given.

(a) MG8

Dry HCl was passed into a mixture of 25g of n-octanoic acid (Koch Light puriss., $\geq 99\%$ pure by G.L.C.) and 34g of isopropylidene glycerol (I.P.G.) (additive 'A', Laporte Industries Ltd.) until the solution became cloudy, and then for a further fifteen minutes. The resulting solution was cooled in ice, shaken with 100cm³ of ice-cold di-isopropyl ether, and allowed to stand in ice. The supernatant liquid was decanted from the glycerol which had settled out, shaken with a further 100cm³ of ice-cold di-isopropyl ether and poured into an ice-cold solution of 17g of anhydrous calcium chloride in 165cm³ of concentrated hydrochloric acid. The solution was shaken for two minutes, and treated with 200cm³ of ice-cold water and poured into a separating funnel. The ether layer was washed with three 200cm³ portions of ice-cold water to remove hydrochloric acid and calcium chloride and these retained. Each of the four aqueous layers was washed with 100cm³ of ice-cold di-isopropyl ether and all the ether

layers bulked. The ether was distilled off and the crude monoglyceride crystallised twice from 80cm³ of 40/60 petroleum ether at 0°C. The yield of pure MG8 was 70%. The melting point determined using a heating stage polarizing microscope and D.S.C. was 38°C (Literature value 38°C (82)).

The reaction scheme is shown below.



(b) MG11

For the preparation of MG11, 30g of I.P.G. and 25g of undecanoic acid (Koch Light pure, B.P. 58) were used. The undecanoic acid was found to be $\geq 99\%$ pure by G.L.C. The yield of pure MG11 was 75%. The melting point was 56°C (Literature value 56.5°C (82)).

(ii) Analysis of l-monoglycerides

Samples of the prepared l-monoglycerides were also checked for the presence of fatty acid, glycerol and di- and tri-glyceride impurities using thin layer chromatography (T.L.C.)(209).

The T.L.C. analysis was carried out on glass plates 20cm. x 20cm. coated with 0.25mm layer of Kieselgel G, which was activated by heating the plates in an oven at 110°C for half an hour. One of these plates was spotted with 200µg of MG8 and 200µg of MG11 in 40/60 petroleum ether using a micro-syringe. The plate was developed using a solvent system consisting of 106cm³ of 40/60 petroleum ether, 47cm³ of diethyl ether and 1.5cm³ of glacial acetic acid (238). The development time was 45 minutes. The plate was dried at room temperature and sprayed with a 0.2% solution of 2',7'-dichlorofluorescein in alcohol. The chromatogram

was observed under u.v. light of wavelength 350m μ and consisted of yellow spots on a green background. No other spots which would be caused by the presence of impurities could be seen. From the size of the spots used on the chromatogram it has been established (209) that impurities of approximately 1% could be detected.

The solvent system used did not separate different 1-mono-glycerides but this was considered unnecessary because of the high purity of the fatty acids used.

(iii) Deuteration of 1-monoglycerides

The 1-monoglycerides were shaken above their melting points with D₂O and cooled to the l.c. state. The l.c. phase was then freeze dried at liquid nitrogen temperatures. This process was repeated seven times after which the resultant deuteration was approximately 95% as found by comparative intensity measurements of the $\nu(\text{OH})$ band before and after deuteration.

(iv) Preparation of unsymmetrical trialkylphosphine oxide

The unsymmetrical trialkylphosphine oxide, dimethyldecylphosphine oxide (C₁₀PO) was prepared according to Laughlin. The synthesis initially involved the preparation of the phosphonate (239) with subsequent conversion, to the phosphine oxide (240) via a Grignard reaction.

(a) Preparation of diphenyl decylphosphonate

Decyl alcohol was distilled from freshly ignited calcium oxide, the fraction collected being that which came over at 229°C. Triphenylphosphite was dried over anhydrous magnesium sulphate and sodium iodide was dried in an oven at 100°C for twenty four hours.

32g of decyl alcohol, 62g of triphenylphosphite and 2.5g of sodium iodide were then placed in a one litre three necked flask equipped with a condenser, nitrogen inlet and stirrer. Water from

a 50°C reservoir was circulated through the condenser. The flask was lagged thoroughly and heated to a temperature of 240°C by a 300 watt isomantle while 2-3 cu.ft./hr. of nitrogen were swept over the reaction. Phenol began to distil from the reaction as the above temperature was reached. The total reaction time was approximately twenty hours, the contents of the flask remaining colourless throughout.

The reaction mixture was then distilled at a pressure of less than 0.05mm and taken up in ether. This solution was washed with 2N sodium hydroxide to remove the phenol, separated from the aqueous layer and dried over magnesium sulphate. The ether was then removed on a rotary evaporator and the remaining mixture distilled. The material collected came over at 180°C at a pressure of 0.01mm. The diphenyl decylphosphonate was a colourless liquid and the purity of it was shown to be greater than 98% by G.L.C. The yield of pure phosphonate was 53%.

(b) Preparation of C₁₀PO

(1) 200cm³ of ether, which had been dried over sodium, were used to cover 14.6g of magnesium turnings in a three necked one litre flask fitted with a cardice condenser, and stirrer. 57g of methyl bromide (b.pt. 4°C) were taken up in a 100cm³ of ether, both of which had been cooled separately in ice/salt. This ethereal solution was added dropwise to the magnesium/ether mixture, to which had been previously added one crystal of iodine. The reaction mixture was cooled by ice/salt and stirred during the addition. When the addition was completed the mixture was stirred for a further 30 minutes.

350cm³ of tetrahydrofuran (T.H.F.), which had been digested over and distilled from lithium aluminium hydride, were then added dropwise. During this addition the reaction mixture was stirred and cooled in ice/salt. The apparatus was modified

temporarily to permit distillation and the ether was distilled off until the liquid temperature reached 65-70°C. The reflux condenser was replaced and stage 2 of the preparation commenced.

(2) 37g of diphenyl decylphosphonate, in T.H.F. solution, was added slowly to maintain a steady reflux. The reaction was kept under a slightly positive pressure of nitrogen and refluxed for twelve hours. It was then cooled in ice and hydrolysed with 250cm³ of water, making sure during the addition of the water that the temperature did not rise above 15°C. To the slurry of salts was added approximately 60cm³ of concentrated hydrochloric acid. The pH of the aqueous layer measured 3. The combined layers were heated on a steam bath between 60-80°C and the upper layer decanted. The lower aqueous layer was kept hot and thoroughly extracted, by decantation, with chloroform. The solvents were then removed on a rotary evaporator.

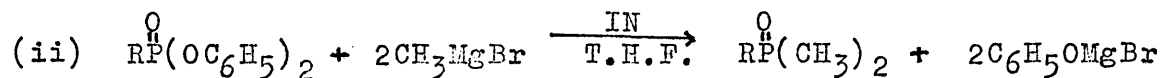
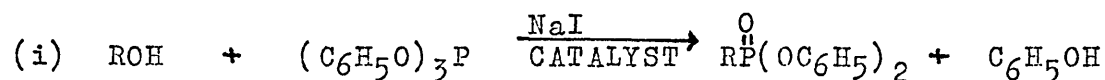
The product was transferred to a 250cm³ flask, immersed in an oil bath maintained at 120°C by a hot plate. Steam was passed through a trap, then with a ten turn 0.25inch copper coil also immersed in an oil bath maintained at 130°C and the phenol was steam distilled from the reaction mixture until the distillate no longer gave a ferric chloride test.

The residue was extracted by four times 100cm³ of hot benzene, the solvent removed on a rotary evaporator and the crude product taken up in 200cm³ of ether and dried with anhydrous magnesium sulphate. The solvent was again removed on a rotary evaporator and the crude product extracted with hot hexane which had been dried over sodium. C₁₈P₂O was then crystallized from the hexane at low temperature and finally recrystallized twice from hexane at room temperature. The melting point of this material was 75°C (Literature value 75°C (141)). The yield was 20%. Elemental analysis gave the following results:-

Calculated for $C_{12}H_{27}PO$: C, 66.06; H, 12.39%

Found : C, 66.05; H, 12.36%

The overall reaction scheme is shown below



(v) Other materials

Carbon tetrachloride, CCl_4 , (analar grade) used in solution studies was dried over magnesium sulphate.

Water used was purified as described on page 10.

Deuterium oxide (99.7%) was obtained from Koch light and used without further purification.

(II) Methods

(1) Thermal Analysis

The MG8, MG11 and $C_{10}PO$ samples were made by warming weighed mixtures to the temperature at which they formed isotropic solutions, shaking and then allowing them to cool. Samples containing D_2O were made up in a dry box.

(a) The investigations of the phase diagrams were carried out using the Du Pont 900 D.S.C. Because of the supercooling which occurred in these systems it was not possible to determine transition temperatures on cooling runs. All samples were therefore cooled to $-60^\circ C$ and allowed to warm up at a programmed rate of $3^\circ C/min.$ to record the thermogram. The transition temperatures were taken to be the onset of the peaks on the thermogram (figure 28)

To ensure that no water was absorbed or lost during the recording of a thermogram the sample pans were hermetically sealed. All the points on the phase diagrams were mean values from at least two thermograms.

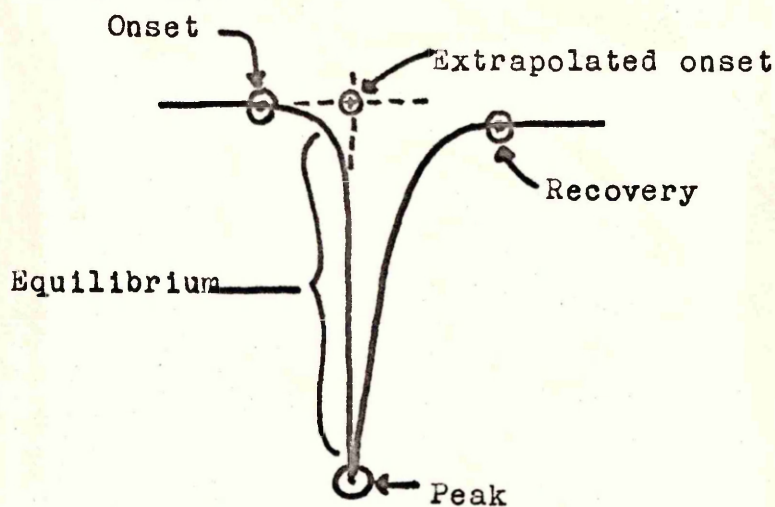


Figure 28.

The instrument was calibrated using the melting or decomposition points of the following substances.

C_6H_6	M. Pt.	$5.5^{\circ}C$
CH_3COOH	M. Pt.	$16.7^{\circ}C$
$Na_2SO_4 \cdot 10H_2O$	decomp. Pt.	$32.4^{\circ}C$
$NaBr \cdot 2H_2O$	decomp. Pt.	$50.7^{\circ}C$
$MnCl_2 \cdot 4H_2O$	decomp. Pt.	$58.1^{\circ}C$

(b) Transition at temperatures between $-60^{\circ}C$ and $60^{\circ}C$ were also observed using a polarizing microscope. The samples were sandwiched between two microscope slides precooled to $-60^{\circ}C$ by immersion in liquid nitrogen and allowed to warm up in air.

(c) Some of the transitions at high temperature including, i.e. melting points and dispersions to two liquid phases which gave very small or negligible D.S.C. peaks were also determined by direct observation of samples contained in sealed

glass tubes and heated in a stirred glycerol bath, the temperature being measured by a calibrated thermometer.

The agreement between transition temperatures determined by the different methods was always at least 1°C .

Methods (a) and (b) were used to investigate the polymorphism of the 1-monoglycerides, MG8, MG11, MG12 and MG18. Both heating and cooling runs were undertaken in that case to obtain the position and nature of the polymorphic transition.

(ii) Infra-red studies

The liquid and polycrystalline samples were produced as thin films between both sodium chloride and silver chloride windows.

The oriented neat l.c. films were produced by smearing the sample on silica or silver chloride windows and by successive translation of the windows in the direction of the long dimension of the plates. Polarized spectra were obtained on the oriented samples using the silver chloride polarizer in the position shown in figure 6. The sample positions are shown diagrammatically in figure 29 (plan view). No significant dichroisms were obtained upon rotation of the sample about the axis of the spectrometer beam ($V=0^{\circ}$). Dichroisms were obtained however when the sample was turned at 45° ($V=45^{\circ}$) to the beam, while still in a vertical plane.

The films of middle phase were produced by smearing the samples on silica or silver chloride windows but these samples could not be oriented so dichroisms were not obtained.

The partly deuterated samples were made up in a dry box.

Single crystals of solid anhydrous and partly hydrated C_{10}PO were grown from the melt between silver chloride and sodium chloride windows. During the crystallization the samples were

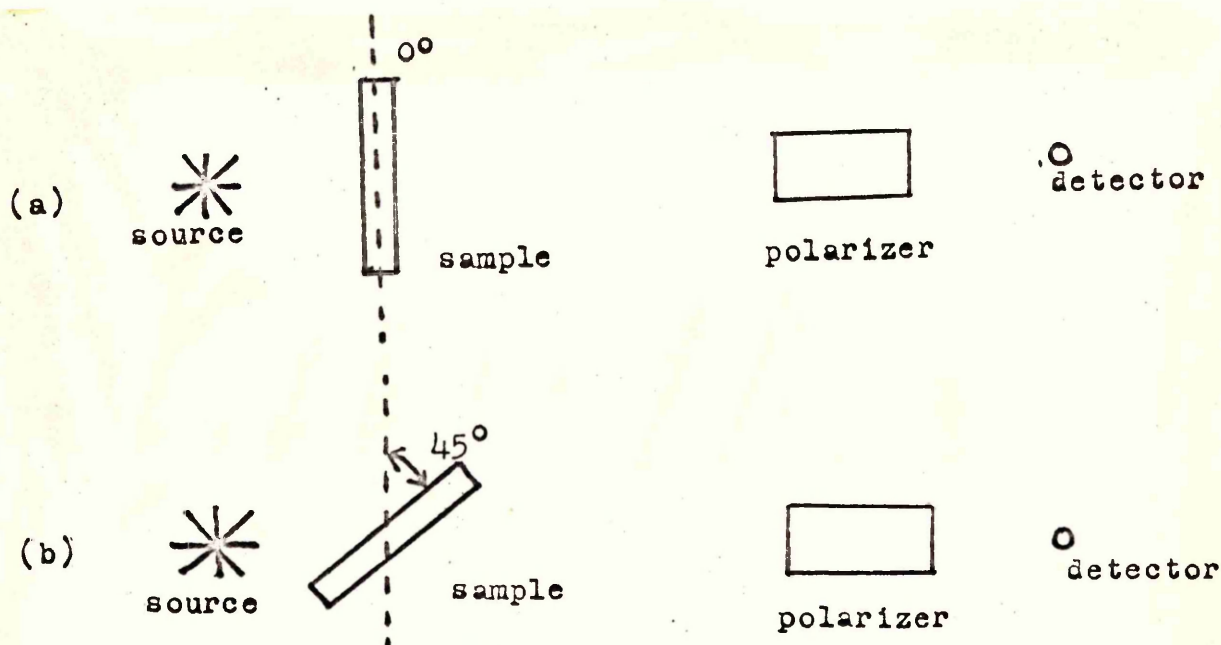


Figure 29.

Diagrammatic representation of position of oriented l.c. samples at:-

- (a) 0° ($V=0^\circ$)
- (b) 45° ($V=45^\circ$) to the beam.

kept at a constant temperature of 30°C . Single crystal portions were then detected under the polarizing microscope and the remainder of the cell blanked off with cardboard. Polarized spectra were recorded, as above, but only for the sample position $V=0^\circ$. Dichroisms were obtained by rotation of the sample.

Three methods were utilized for variable temperature runs.

(a) For temperatures in the range $15-50^\circ\text{C}$ cooling was effected by circulating water through a coil of copper tubing round the sample cell. The lowest temperatures were obtained using water from a reservoir of ethylene glycol/water cooled by a TECHNE (IU5) refrigeration unit.

(b) For temperatures higher than 50°C an electrically heated jacket ((J-2) - R11C) was used.

(c) For temperatures between -170°C and 15°C an R11C - VLT2 cell (figure 7) was used.

In cases (b) and (c) the temperature was controlled by the

TEM 1 (R11C) temperature controller. All temperatures measured were accurate to $\pm 2^{\circ}\text{C}$.

The samples used were all sealed around the edges as before.

Solution spectra in CCl_4 were obtained in a cell of path-length 1.5mm with sodium chloride windows and using a reference cell containing pure solvent.

All infra-red spectra were run on a Grubb Parsons 'Spectromaster' double beam spectrometer, the range of scan covered was $4000 - 550\text{cm}^{-1}$. The calibration of the instrument was accurate to $\pm 1\text{cm}^{-1}$.

CHAPTER III

ANHYDROUS LIPIDS

I) 1-MONOGLYCERIDES

(i) Results

(a) Thermal Analysis

When molten samples of the four 1-monoglycerides studied were allowed to cool, phase transitions observed by D.S.C. occurred at the temperatures given in table V. Typical thermograms are shown in figure 30 and it can be seen that there is no further transition down to -20°C . When the same samples were now heated phase transitions were observed at the temperatures given in table VI and the thermograms for MG11 and MG12 are shown in figure 31.

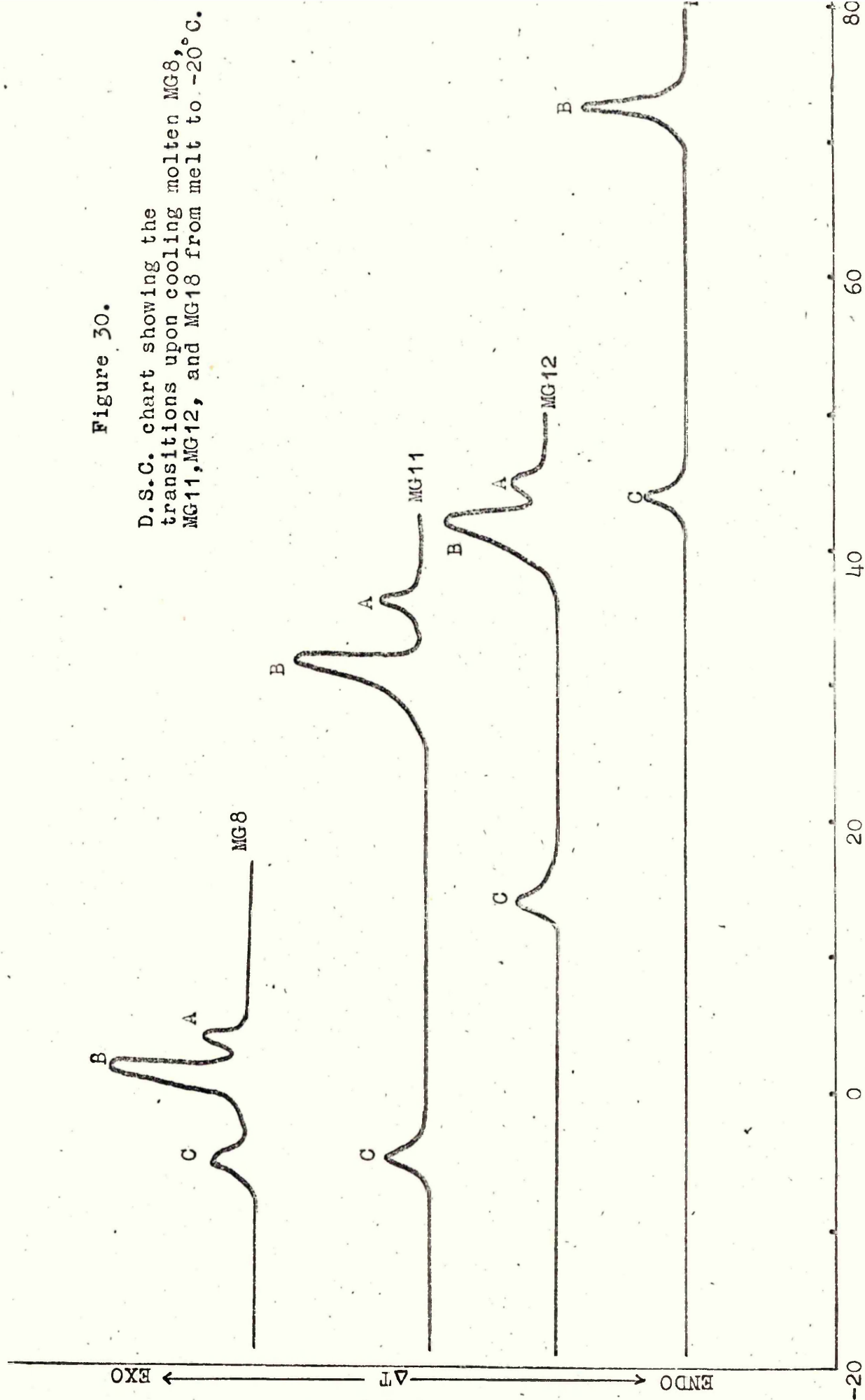
All the transitions which occurred at or above room temperature, except that of MG18 at 47°C , have also been observed using a heated stage polarizing microscope.

The first transition which occurred on cooling the molten 1-monoglycerides, except MG18, was the appearance of rings of structure in the liquid (transition A). A few degrees lower in temperature the samples assumed a variety of irregular birefringent shapes as described by Malkin (82). This latter transition, B, occurred directly from the melt in the case of MG18.

Samples of MG8 observed under the microscope after being melted and allowed to cool to room temperature, changed slowly to the highest melting form over a period of hours, whilst MG11

Figure 30.

D.S.C. chart showing the transitions upon cooling molten MG8, MG11, MG12, and MG18 from melt to -20°C .



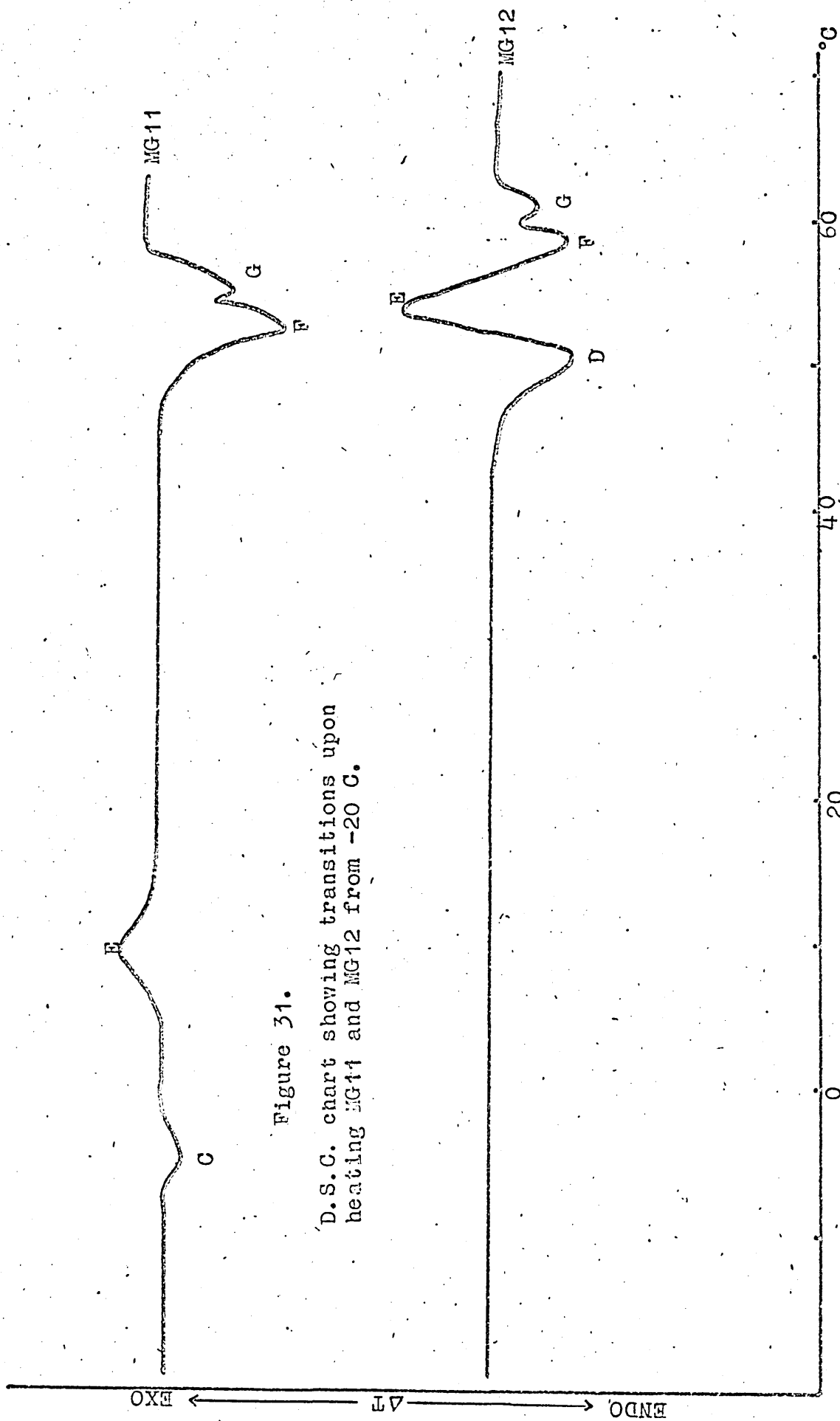


Figure 31.

D.S.C. chart showing transitions upon heating MG11 and MG12 from -20 C.

and MG12 took several days for the same change to occur. MG18 appeared to be indefinitely stable at room temperature in the form below C.

In the case of MG8, by holding the temperature just below each transition and then reheating, rapid conversion was observed on D.S.C. to the highest melting (most stable) form.

(b) Infra-red

The infra-red spectra of MG8 and DMG8 in the highest melting form were obtained at the beam temperature of 33°C and -170°C (figures 32 and 33). Liquid spectra of MG8 and DMG8 were obtained at 42°C (figure 34). The frequencies of the absorption bands together with proposed assignments are listed in tables VII and VIII.

Figures 35 and 36 show the spectra of MG18 above transition A (liquid), between B and C (α phase), below C (sub- α phase) and in the most stable form (β phase). MG11 and MG12 gave almost identical spectra in the liquid, α and β phases so these are not shown. In the case of MG11 samples were cooled down to -3°C and then heated to 20°C and the spectra just above transition E (β' phase) obtained (figure 37). In the case of MG12 a unique phase occurs below transition C and its spectrum is shown in figure 37.

Tables IX and X show the position of $\nu(\text{OH})$, $\nu(\text{C}=\text{O})$ and symmetric and asymmetric stretching of CH_2 and CH_3 groups, $\nu_s(\text{CH}_2)$, $\nu_a(\text{CH}_2)$ and $\nu_s(\text{CH}_3)$, $\nu_a(\text{CH}_3)$, respectively for the various phases.

It was not possible to obtain spectra of the phases between D and E, and E and F in the cases of MG12 because the lifetime of the phases was so short.

Spectra of the decoupled $\nu(\text{OH})$ of DMG8 in the stablest form

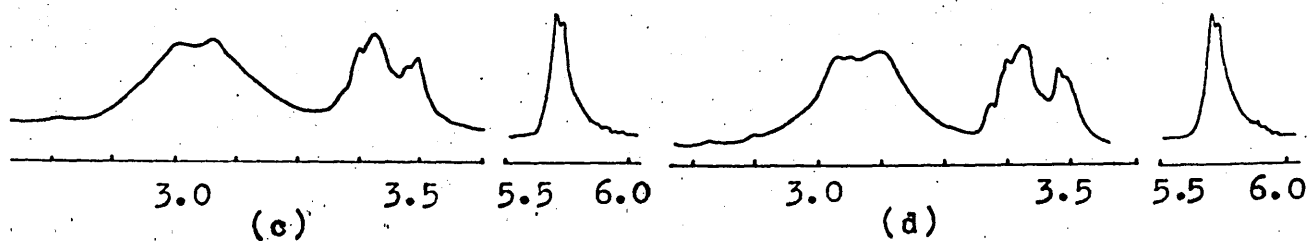
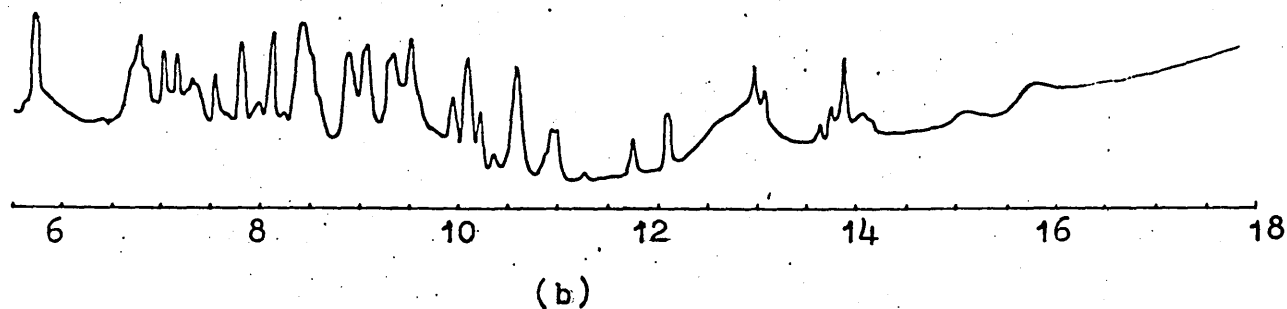
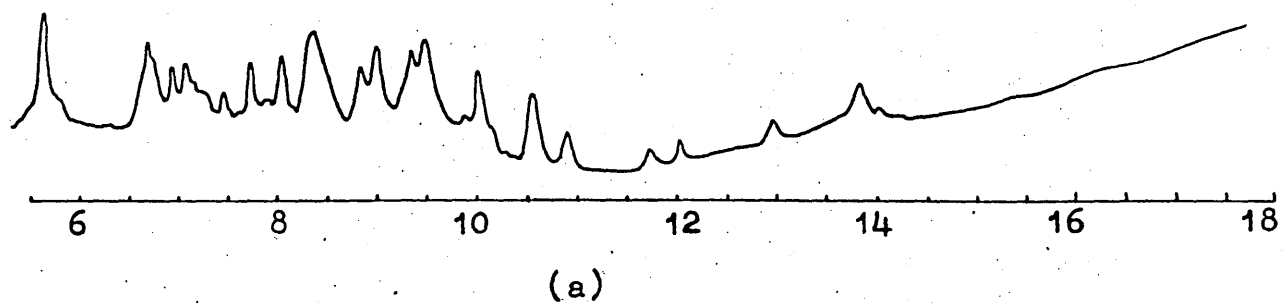
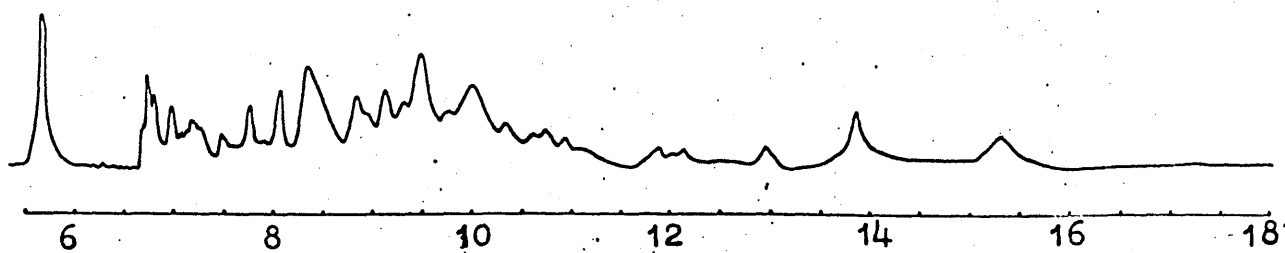
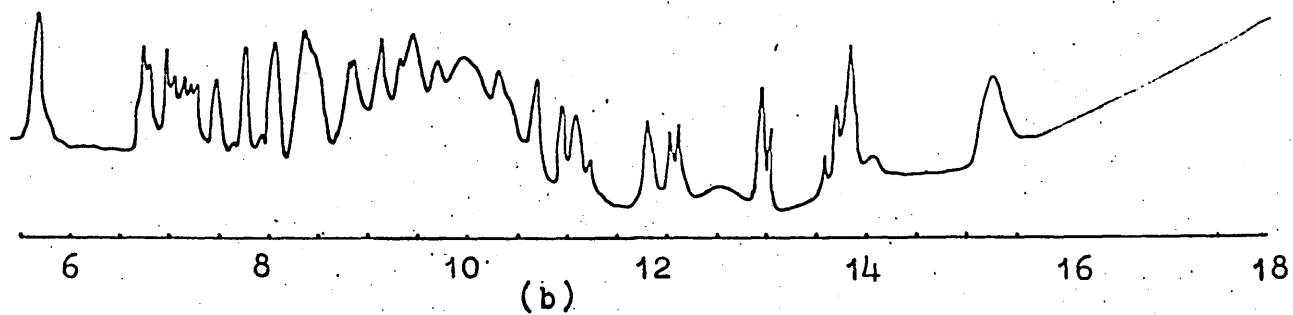


Figure 32.

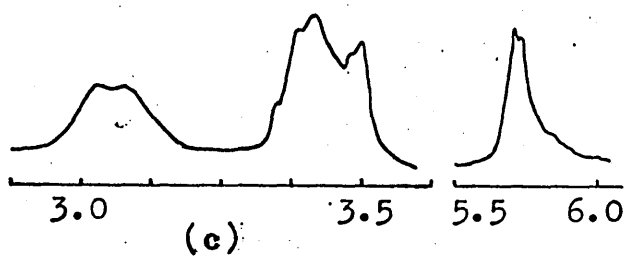
Infra-red spectra of MG8 at:- Beam temperature ,Wavelength(a) 6-18 μ ,
 (c) 2.75-3.625 and 5.5-6.0 μ .
 -170°C ,Wavelength(b) 6-18 μ , (d) 2.75-
 3.625 and 5.5-6.0 μ .



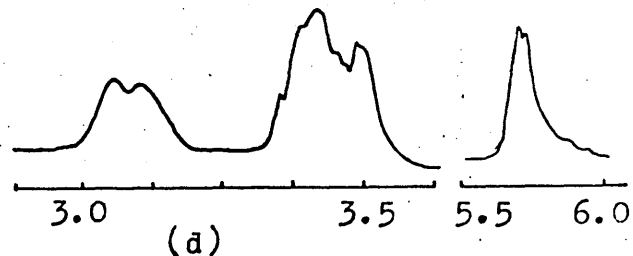
(a)



(b)



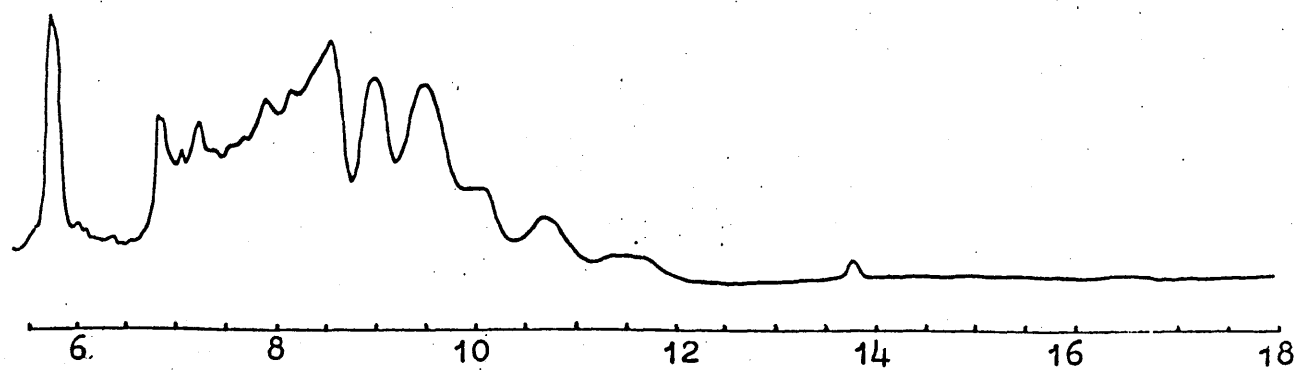
(c)



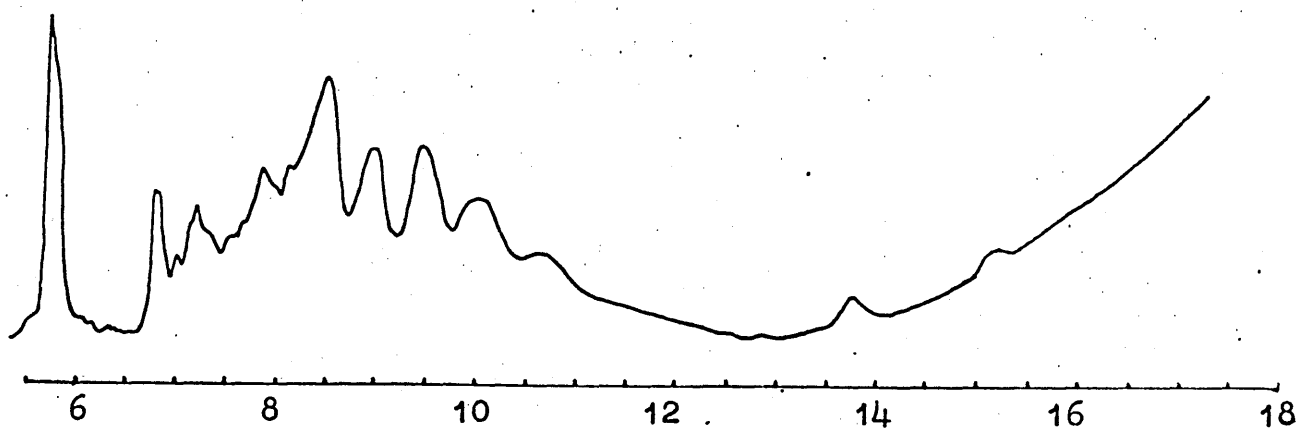
(d)

Figure 33.

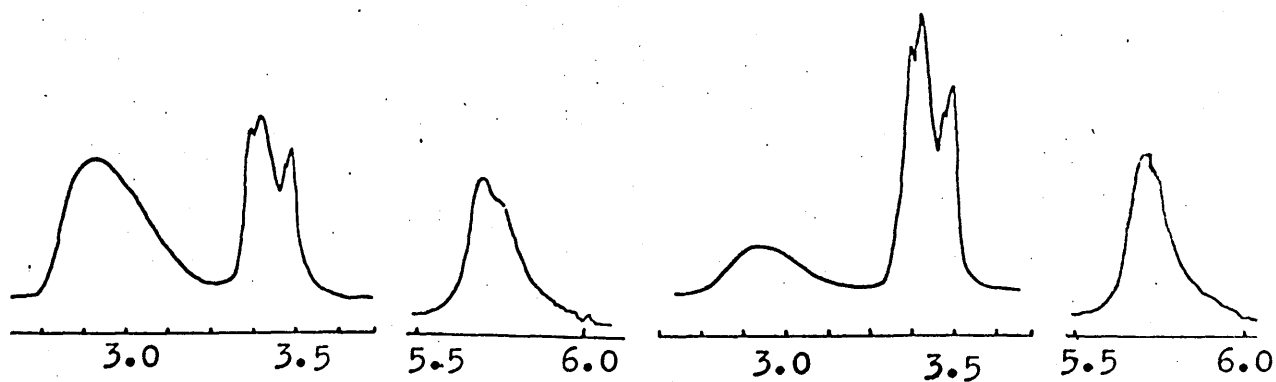
Infra-red spectra of DMG8 at: -Beam temperature, Wavelength (a) 6-18 μ ,
 (c) 2.875-3.625 and 5.5-6.0 μ .
 -170°C, Wavelength (b) 6-18 μ , (d) 2.875
 -3.625 and 5.5-6.0 μ .



(a)



(b)



(c)

(d)

Figure 34.

Infra-red spectra of liquid MG8(42°C), Wavelength(a) 6-18 μ , (c) 2.625-3.75 and 5.5-6.0 μ .
and of liquid DMG8(42°C), Wavelength(b) 6-18 μ , (d) 2.625-3.75 and 5.5-6.0 μ .

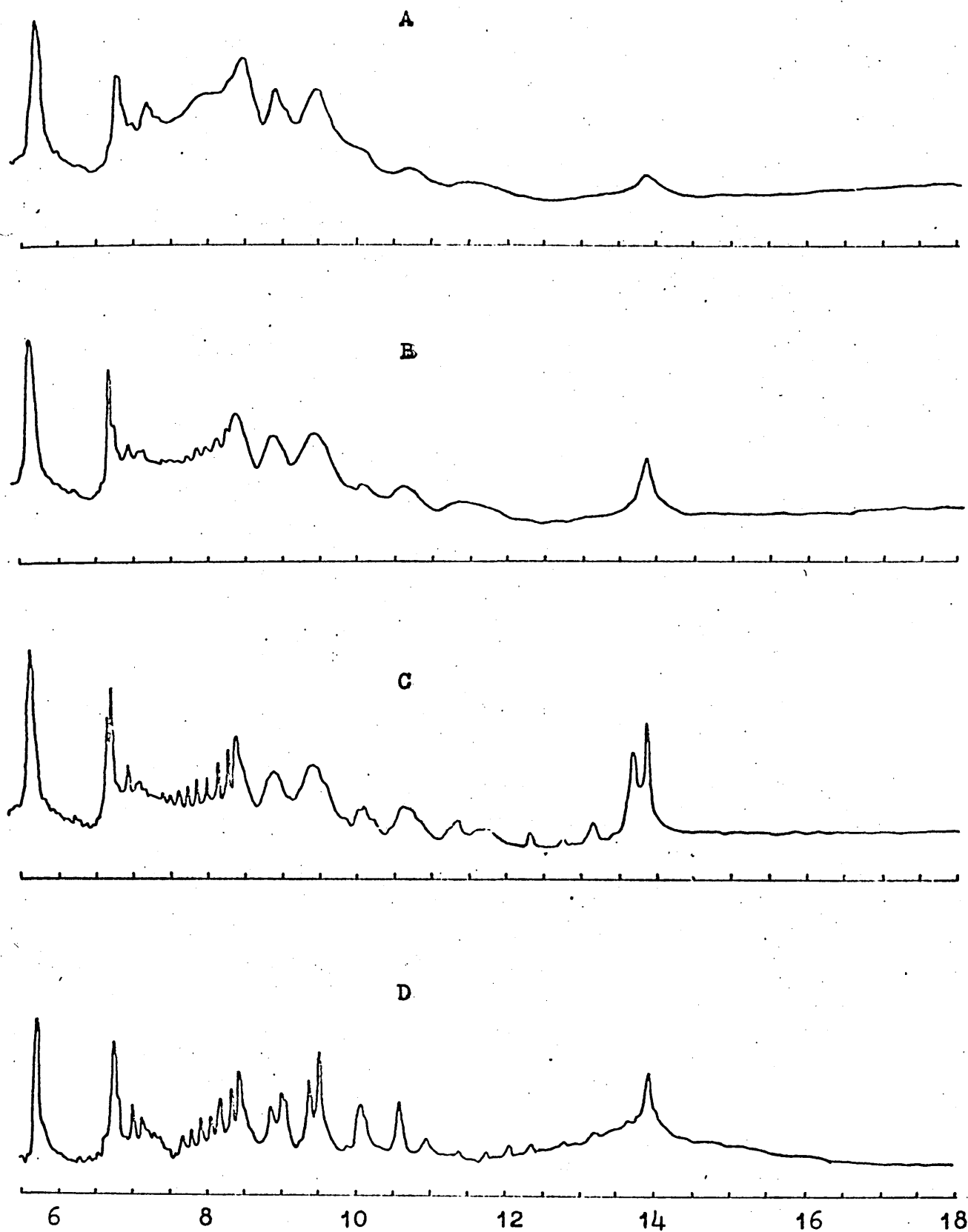
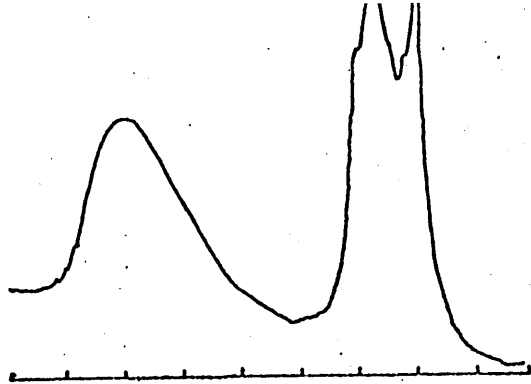
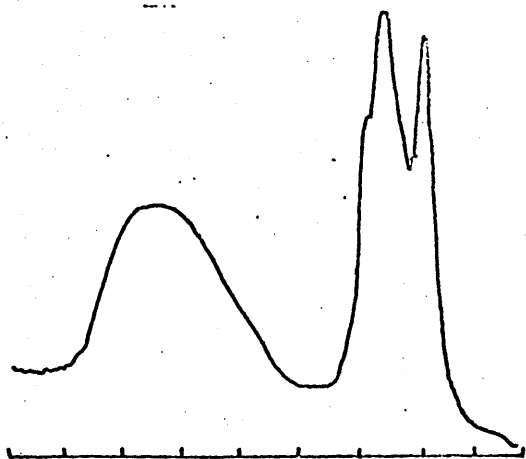
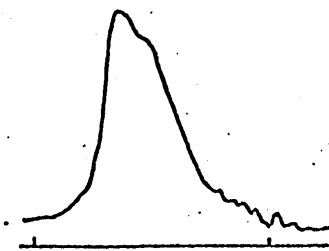


Figure 35.

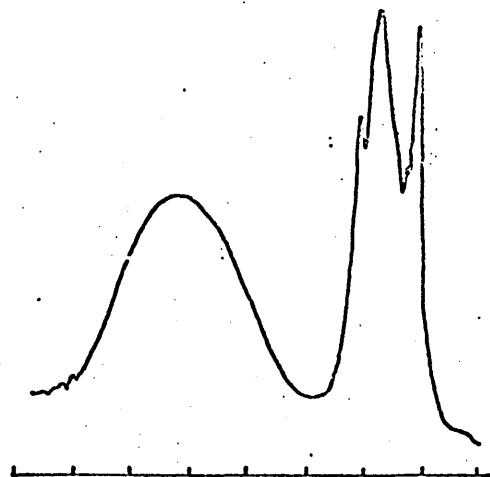
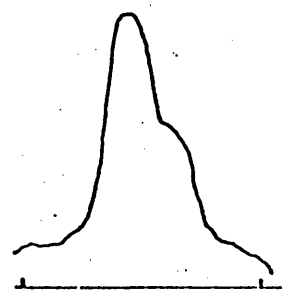
Infra-red spectra of the polymorphic forms of MG18,
A, Liquid; B, α ; C, Sub- α ; D, β ; Wavelength 6-18 μ .



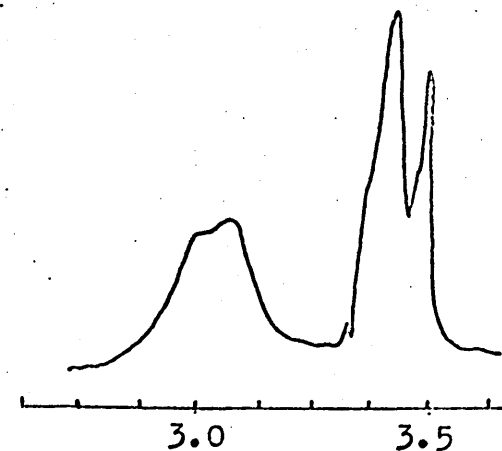
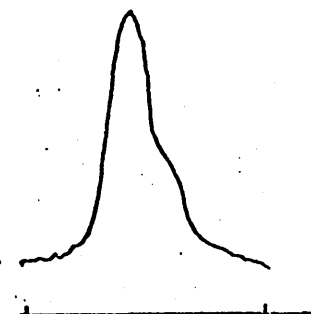
A



B



C



D

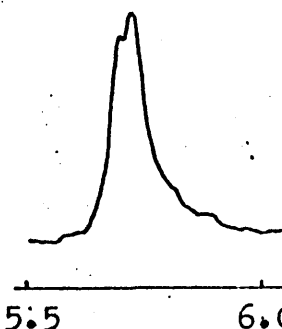


Figure 36.

Infra-red spectra of the polymorphic forms of MG18 ,
A, Liquid; B, α ; C, Sub- α ; D, β ; Wavelength 2.625-3.625 and 5.5-6.0 μ .

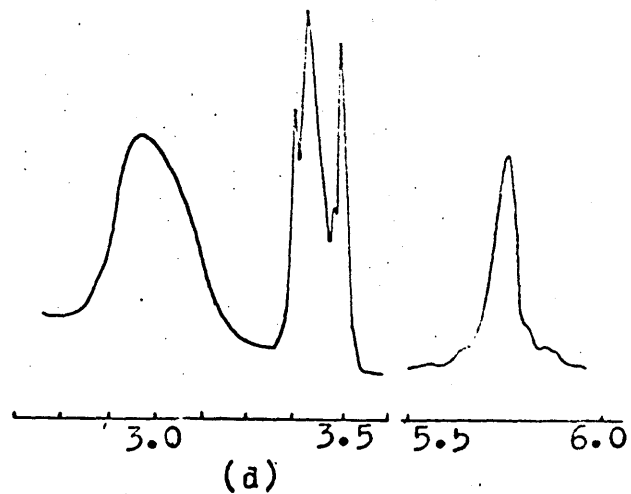
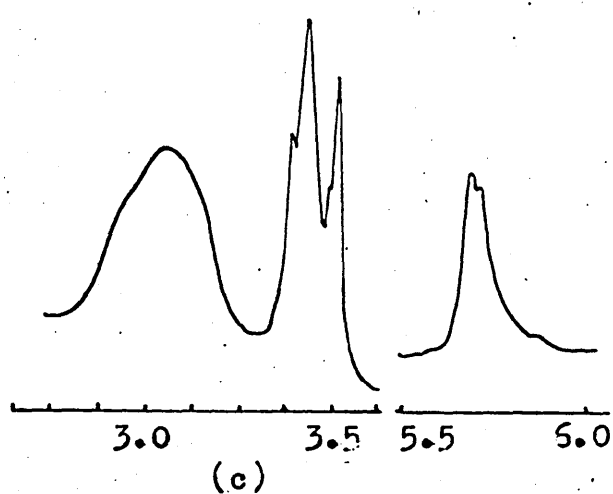
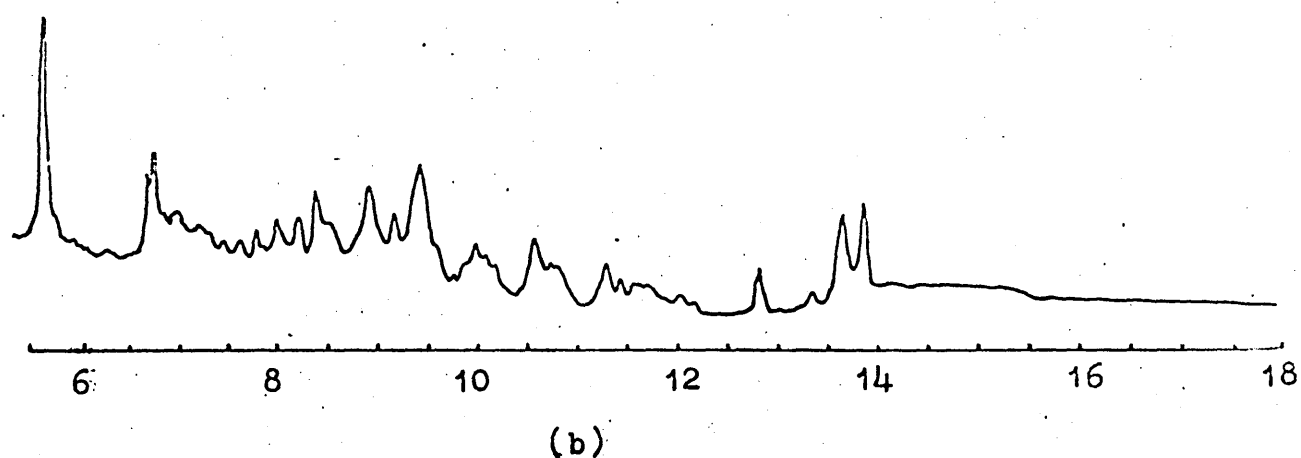
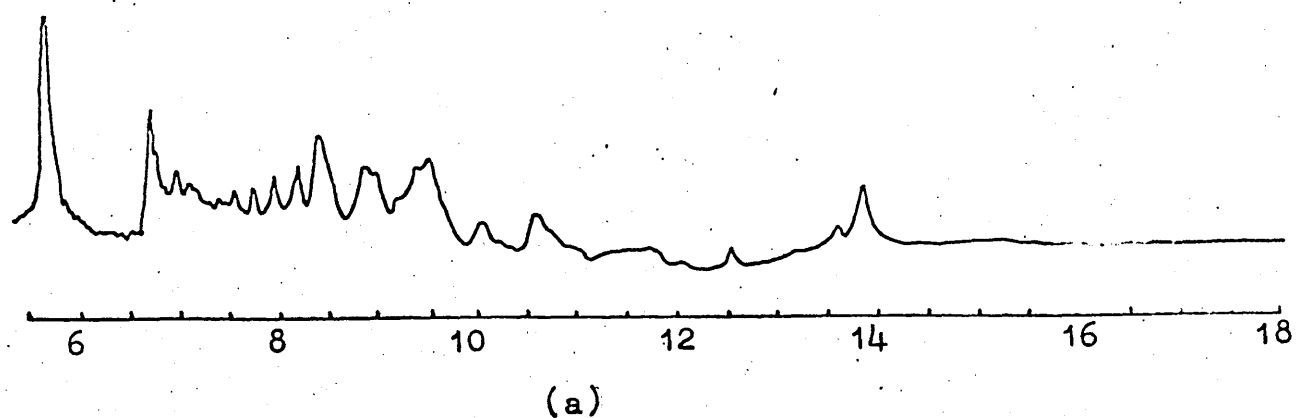


Figure 37.

Infra-red spectra of the β' form of MG11, Wavelength (a) 6-18 μ , (c) 2.625-3.625 and 5.5-6.0 μ .
 and the form below transition C for MG12, Wavelength (b) 6-18 ,
 (d) 2.625-3.625 and 5.5-6.0 μ .

were obtained at beam and low temperature and they are shown in figure 33.

Infra-red spectra were obtained of various concentrations of MG8 in CCl_4 and the $\nu(\text{OH})$ and $\nu(\text{C}=\text{O})$ regions are shown in figure 39. The concentration range covered was 0.0048 - 0.15M.

(ii) Discussion

(a) Polymorphism

The transitions observed on cooling the molten 1-monoglycerides agree to some extent with the results of Malkin on MG11-MG18 (82) and of Lutton on MG18 (85). However certain additional features have been observed and it has been possible to confirm some of these observations using infra-red spectroscopy.

1) Above transition A the 1-monoglycerides are in their liquid state. The spectrum of MG18 is almost identical to that of Chapman (90) shown in figure 38. The $\nu(\text{OH})$ absorption is broad at 3448cm^{-1} and a single band is observed at 720cm^{-1} for the lower limit of the CH_2 rocking mode, $\rho(\text{CH}_2)$, whilst there are four components in the CH stretch region due to the symmetric and asymmetric stretching of CH_2 and CH_3 groups.

However the $\nu(\text{C}=\text{O})$ band has been resolved as two components at 1739cm^{-1} and 1728cm^{-1} (figure 36) whereas Chapman (90) only reported a single band at 1706cm^{-1} .

The occurrence of two $\nu(\text{C}=\text{O})$ bands usually (50(e)) indicates the involvement of the carbonyl in H-bonding, the lower frequency component arising from the bonded carbonyl. It can be seen from table IX that the highest frequency component in the solid and liquid phases occurs regularly between 1736cm^{-1} and 1740cm^{-1} . The fact that in the solution spectrum a component occurs at 1754cm^{-1} makes it difficult to decide whether the

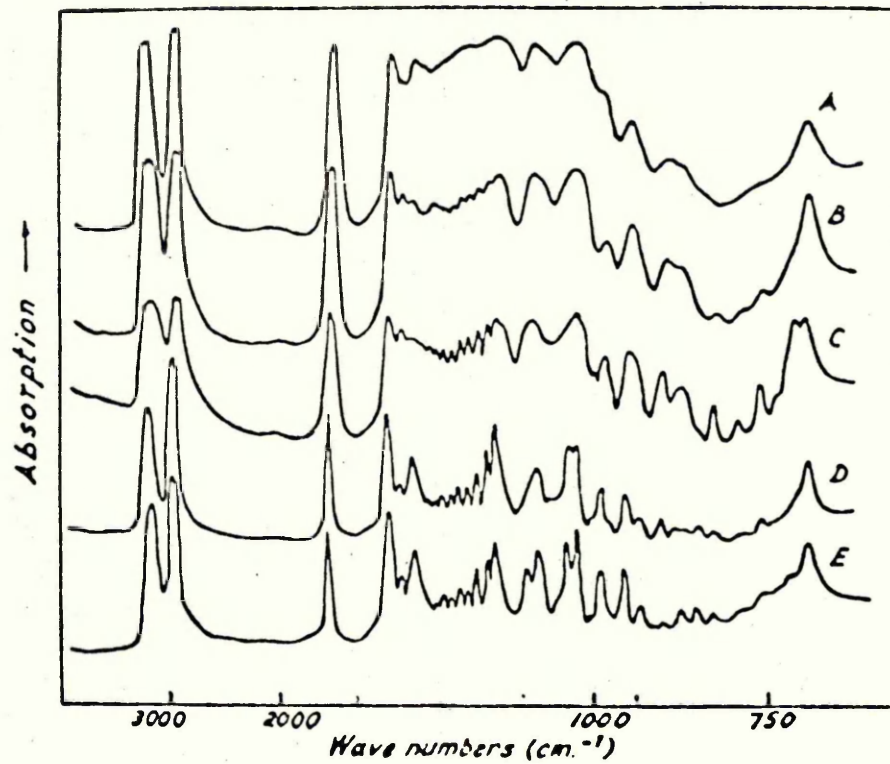


Figure 38.

- Polymorphic forms of 1-monostearin (MG18)
A, Liquid; B, α ; C, Sub- α ; D, β' ; E, β . (90)

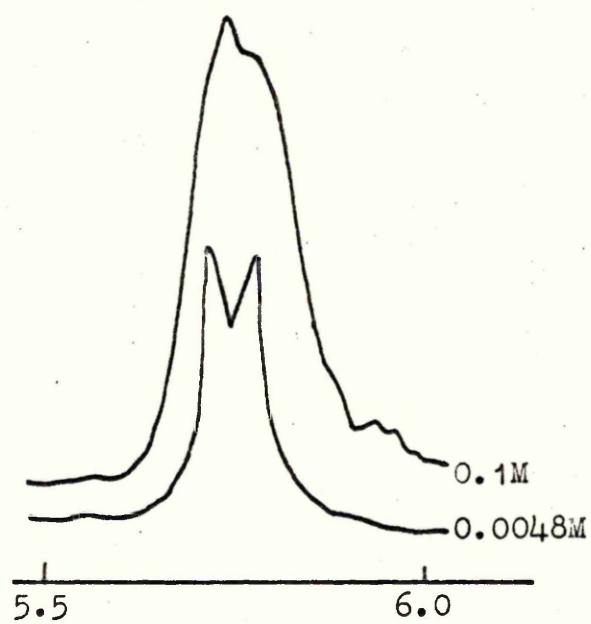
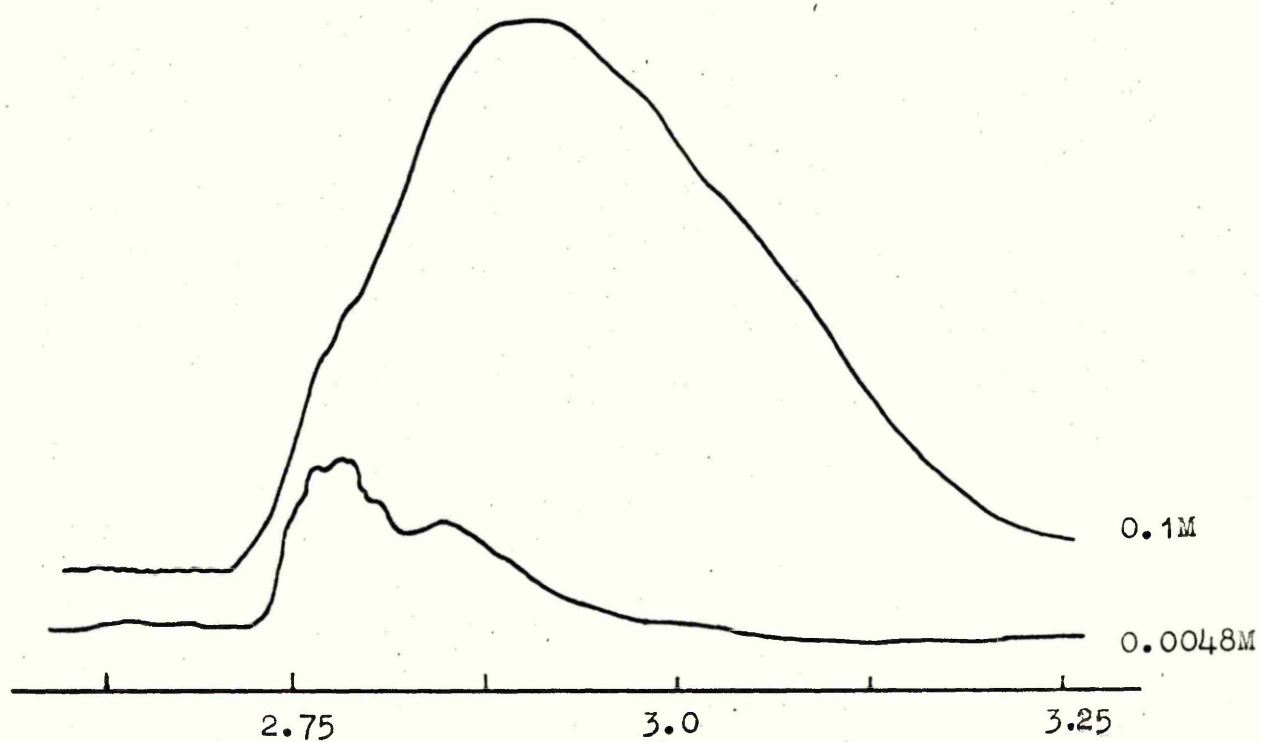


Figure 39.

$\nu(\text{OH})$ and $\nu(\text{C}=\text{O})$ bands of MG8 in CCl_4 solutions.
Wavelength 2.625-3.25 μ and 5.5-6.0 μ .

1736-1740 cm^{-1} band is due to free $\nu(\text{C}=\text{O})$ or another H-bonded species. In the present discussion we have merely considered the changes in the low frequency component of the $\nu(\text{C}=\text{O})$ doublet as being connected with the changes in the H-bonding. The possibility occurs that the 1736-1740 cm^{-1} band arises from the intramolecular H-bond referred to in part (b) of this discussion.

In this work the lower frequency component of $\nu(\text{C}=\text{O})$ appears as an intense shoulder at 1728 cm^{-1} to that at 1739 cm^{-1} . Two components have been resolved in the liquid state spectra for all the 1-monoglycerides studied (table IX).

2) At transition A for MG8, MG11 and MG12 the 1-monoglycerides pass through to a smectic l.c. phase the ring like structures observed under the polarizing microscope are 'stepped drops' which are formed by smectic phases under suitable conditions (241).

The α phase was regarded, by Malkin (82), to be formed first from the melt and to be stable near the melting point. He has described this phase as 'dark greyish pools which give a strong uniaxial interference figure'. It is almost certain that in this case he was observing the l.c. state.

Attempts were made to obtain infra-red spectra of samples of MG8, MG11 and MG12 in this state but the lifetime of the phase was too short to allow any measurements to be made.

3) At transition B the l.c. phase transforms into a solid phase which Malkin (82) describes as 'aggregates of molecules in all states from vertical rotating to tilted rigid'.

X-ray data (85,96), infra-red spectra (90) and P.M.R. line widths and second moments (91) have been reported for this solid and from this evidence it is considered to be an α phase in which the alkyl chains are hexagonally packed and rotating about

their chain axes. However more recently it has been suggested (209) from P.M.R. second moment calculations that the phase observed in the case of MG11 and MG12 is intermediate between a true α phase and a smectic l.c. phase in that rotation takes place but the chain axes are tilted with respect to the plane of the bilayers.

The infra-red spectrum of the α phase of MG18 (figure 35) is similar to that reported by Chapman (90). A series of bands occurs in the $1180\text{-}1340\text{cm}^{-1}$ region, which were not present in the liquid spectrum and are due to various vibrational modes of the CH_2 groups of the chain, although the appearance of the spectrum below 1170cm^{-1} is that more typical of a liquid. The series of bands between 1180cm^{-1} and 1340cm^{-1} in this study show more structure than in the earlier work (90) (figure 38). Similarly in figure 35 can be seen a very intense and sharp band at 1463cm^{-1} associated with the CH_2 bending mode, $\delta(\text{CH}_2)$ which is more typical of bands in the spectra of highly crystalline solids.

Even though there are the same number of components in the CH stretch region in this solid phase (figure 36) as in the liquid and in the same position (table X), those associated with asymmetric and symmetric stretching of the CH_2 groups, $\nu_a(\text{CH}_2)$ and $\nu_s(\text{CH}_2)$, at 2928cm^{-1} and 2854cm^{-1} , are much more intense in the solid. These differences in intensity of the $\nu_a(\text{CH}_2)$, $\nu_s(\text{CH}_2)$ and $\delta(\text{CH}_2)$ in the liquid and α phases are very striking in our spectra but are not visible in those of Chapman (90) and have not been reported previously.

In the earlier work (90) (figure 38) a single band was observed for $\nu(\text{C}=\text{O})$ at 1706cm^{-1} in the liquid which shifted

to 1721cm^{-1} in the α phase and on the basis of this and the shift of $\nu(\text{OH})$ to lower frequency upon going from liquid to the α phase, Chapman (90) drew the conclusion that the H-bonding was preferentially between OH groups in the solid phase.

We have not observed this single $\nu(\text{C}=\text{O})$ component. $\nu(\text{C}=\text{O})$ was resolved, as in the liquid, as a doublet (figure 36, table IX) with the lower frequency component having reduced intensity relative to its counterpart in the liquid, and moved to a lower frequency of 1718cm^{-1} whilst the other $\nu(\text{C}=\text{O})$ component is relatively unchanged in position at 1738cm^{-1} and has only a small increase in intensity. However $\nu(\text{OH})$ is broad and has shifted to a lower frequency of 3390cm^{-1} relative to the liquid at 3448cm^{-1} , which is similar to that previously observed (90). Therefore it may be deduced that the carbonyl has become less involved in the H-bonding scheme, although the H-bonds which are formed with the carbonyl are stronger. The H-bonding may therefore be predominantly between OH groups as Chapman (90) suggested.

These general observations have been made with the α phases of both MG11 and MG12.

4) Transition C has been the centre of a great deal of controversy between Malkin (82,86) and Lutton (85) as to whether the transition was reversible and the nature of the phase produced. Lutton (85) studied MG16 and MG18 and stated that at the lowest transition temperature a sub- α crystalline phase was produced and the transition was reversible. We have confirmed the reversibility of the transition C in the case of MG11 and MG18. The much lower value of transition C in MG11 than in MG12 (table V) is due to an alternation effect implying a greater mobility of the chains in the 1-monoglycerides

containing odd numbered chains.

The spectrum of the sub- α phase of MG18 obtained in this study is shown in figures 35 and 36 and the earlier spectrum in figure 38. Similarities are apparent but again there are marked differences as follows:-

i. More structure is observed, in this work, in the $1170\text{-}1340\text{cm}^{-1}$ region. The bands in this region now have the appearance of those of a crystalline solid.

ii. The 720cm^{-1} band is now split into two components at 730cm^{-1} and 721cm^{-1} and the intense single band at 1463cm^{-1} , due to $\delta(\text{CH}_2)$, in the α phase spectrum is now split into two components at 1466cm^{-1} and 1462cm^{-1} . This latter doublet has not been previously observed in the sub- α phase of MG18.

The splittings of the 720cm^{-1} and 1463cm^{-1} bands are thought (99) to arise because of the nearest neighbour CH_2 groups interacting to give the out-of-phase and in-phase modes. This sort of behaviour is found in the highly crystalline n-paraffins (24) and polyethylene (19,98) and it was therefore suggested (90), on the basis of the splitting of the 720cm^{-1} band, that the sub- α form had a crystalline lattice (or at least a very ordered system) possibly of the common orthorhombic type.

iii. Further evidence of the highly crystalline nature of the sub- α form can be seen in the splitting of the single band associated with $\nu_a(\text{CH}_2)$ at 2930cm^{-1} in the α form, into two components (table X and figure 36) and the general intensification and narrowing of the bands in the CH stretch region compared with the α form. This behaviour has not

previously been reported. The components observed here have similar relative intensities and positions to those found in triclinic n-C₂₀H₄₂ (29) although in that case a further component was resolved at 2922cm⁻¹.

iv. In the earlier work (90) a single $\nu(\text{C}=\text{O})$ band has been observed at 1730cm⁻¹ in the sub- α phase of MG18 (figure 38). This is a shift to a higher frequency relative to the α phase and on the basis of this and the shift of $\nu(\text{OH})$ to lower frequency upon going from the α to sub- α Chapman concluded that the H-bonds between OH groups are becoming stronger.

In this work (figure 36) the $\nu(\text{C}=\text{O})$ is still resolved as two components of a similar intensity to those of the α phase but narrower overall, with the lower frequency component now at a slightly higher frequency of 1722cm⁻¹. However $\nu(\text{OH})$ is broad and has shifted to a lower frequency at 3320cm⁻¹ which is similar to that previously observed. It would therefore appear that in this highly crystalline phase the contribution of the carbonyl to the H-bonding network is similar to that in the α form although the H-bonds formed are slightly weaker. Also the predominating H-bonds between OH groups have become stronger.

5) For the other 1-monoglycerides studied transition C was irreversible and several different types of behaviour have been observed when samples were reheated after cooling past this transition.

In the case of MG8 the cooled sample melted at the β melting point (transition G), indicating that below transition C the β form is obtained. There is no evidence from the D.S.C. measurements made that any intermediate form such as β' suggested by Malkin (82) occurs under these conditions.

For MG11 on heating past the reversible transition C, a

small exotherm (transition E) is observed at a variable temperature, probably determined by the number of seed crystals present and the previous thermal history of the sample. At transition E the β' and β forms are produced since partial melting now occurs at 52° and 56° (transitions F and G). The positions of these observed transitions agrees well with those of Malkin (82). The relative intensities of the two peaks indicate that the lower in temperature the sample is cooled the more β form is produced at transition E.

The infra-red spectra of the β' forms of MG18 and MG12 have previously been reported (90) and that of MG18 is shown as figure 38. The spectrum of the β' form of MG11 from this study is shown as figure 37. The spectra have general similarities but again there are differences from the earlier work.

The differences between the spectra may be due to the fact that the β' phase of the earlier work was obtained by rapid recrystallization and run as a nujol mull, whilst the present work involved the use of a heating cycle. In both cases there will undoubtedly be a certain small amount of the β form present.

In this work the overall resolution of the spectrum (figure 37) is much better than that previously reported by Chapman (90). The region $1470-700\text{cm}^{-1}$ shows more components generally than the sub- α although the split bands associated with $\delta(\text{CH}_2)$ and $\rho(\text{CH}_2)$ are now single components but still quite intense at 1461cm^{-1} and 722cm^{-1} respectively.

There are now five components in the CH stretch region, the intensity of the components due to $\nu_a(\text{CH}_2)$ and $\nu_s(\text{CH}_2)$ at 2919cm^{-1} and 2852cm^{-1} being similar to those of the α phase of MG11.

In the earlier work (90), $\nu(\text{C=O})$ is resolved as a single

band at 1736cm^{-1} , showing a significant shift from that in the sub- α phase, whilst $\nu(\text{OH})$ is now resolved as two broad components at 3342cm^{-1} (main component) and 3243cm^{-1} .

In this work $\nu(\text{C}=\text{O})$ is resolved as two components at 1739cm^{-1} and 1729cm^{-1} (figure 37). The lower frequency component now has increased intensity compared with the α and sub- α phases signifying an increase in the participation in the H-bonding scheme of this phase. However this component has moved to a higher frequency relative to the α and sub- α phases and shows therefore a decrease in the H-bond strength. Also $\nu(\text{OH})$ is resolved as two broad bands at 3408cm^{-1} and 3302cm^{-1} (main component).

The behaviour of MG12 upon reheating is more complex than that of any of the other 1-monoglycerides studied. At transition C, 26.5°C below the l.c.- α phase transition (B) a solid is formed, the spectrum of which is shown as figure 37. The spectrum is neither that of a sub- α , α or β' . It has pairs of bands at 1464cm^{-1} , 1460cm^{-1} and 728cm^{-1} , 721cm^{-1} for $\delta(\text{CH}_2)$ and $\rho(\text{CH}_2)$ modes respectively. The bands in the $1340\text{--}1180\text{cm}^{-1}$ region show a structure similar to the sub- α . There are seven components in the CH stretch region (figure 37, table X) showing a marked similarity in position and relative intensity to those of the sub- α although there is also a component at 2930cm^{-1} which is not present in the spectrum of the sub- α of MG18 (figure 36 and table X).

Also the $\nu(\text{OH})$ band is markedly asymmetric at 3347cm^{-1} possibly showing the presence of further $\nu(\text{OH})$ components whilst that of the sub- α of MG18 is symmetric. The $\nu(\text{C}=\text{O})$ absorption is present as a single component (figure 37) at 1738cm^{-1} which is in the same position as the higher frequency

$\nu(\text{C}=\text{O})$ component of the sub- α form. It would therefore appear that any H-bonding in this phase is taking place solely between OH groups.

By comparison of the spectrum of this phase with a sub- α spectrum of MG18 (figures 35, 36 and 37) it can be seen that this phase is possibly a modified sub- α structure with H-bonding only taking place between OH groups.

6) Transition G is due to the melting of the highest melting or β form. The β form has been studied extensively by X-ray (82,85,95,96), infra-red (90,102-105) and P.M.R. (91). From this evidence it is considered that the crystalline habit of the β form is monoclinic with layers of chains tilted at 55° (95) towards the end group plane with chain tilt alternating in successive double layers.

The spectrum of the β form of MG18 has been previously reported (90) and is shown as figure 38. The spectrum of β form of MG18 from this work is shown as figures 35 and 36. Again there are general similarities between the two, however the spectrum from this work is of a greater resolution and shows more detail especially in the region $1470\text{-}700\text{cm}^{-1}$.

There are seven components in the CH stretch region (figure 36 table X) however it was not possible to compare the intensity of these with any of the other phases of MG18 since the β spectrum was obtained as a nujol mull whilst the others of MG18 were obtained by suitable heating cycles. The intensities of the CH stretch components of the β and β' phases of MG11 were similar.

In the earlier work (90) a single component was observed for $\nu(\text{C}=\text{O})$ at 1736cm^{-1} in the β form of MG18 and two bands were observed for $\nu(\text{OH})$ at 3307cm^{-1} and 3243cm^{-1} (main component) (figure 38). This single $\nu(\text{C}=\text{O})$ band was also observed

in other 1-monoglycerides by Barcelo et al (103).

In this work the $\nu(\text{OH})$ absorption bands are present at 3292cm^{-1} and 3238cm^{-1} (main component) for MG18, which is a shift to a lower frequency for the components relative to the β' phase of MG11 signifying a further increase in the H-bond strength upon going to the β form. There is also an increase in intensity and narrowing of $\nu(\text{OH})$ components of the β form of MG11 relative to the β' form of MG11.

The $\nu(\text{C}=\text{O})$ absorption is resolved as a doublet in the β forms of all the 1-monoglycerides studied (table IX). The lower frequency component in the longer chain 1-monoglycerides (MG11, MG12, MG18) is of greater intensity than the other component whilst in the case of MG8 the reverse is found (figure 32). It therefore appears that the carbonyl may play a much larger role in the H-bonding scheme of the longer chain compounds than the shorter ones.

7) β form of MG8

Assignments of the bands was made by comparing the MG8 spectra with those of long chain saturated alcohols (12,13), n-paraffins (29,242), acids (30, 35) and ethylene glycol (57). Further help in the assignment of the bands was obtained from the spectra of DMG8. The following points arise:-

i. The β phase spectrum in figure 33 indicates that the OH has not been completely replaced by OD. New bands at 1025cm^{-1} and 800cm^{-1} are assignable to OD in plane vibrations, $\beta(\text{OD})$, corresponding to the bands previously found at 1398cm^{-1} (1437cm^{-1} in ethylene glycol (57)) and 1063cm^{-1} in the non-deuterated compound because the ratios of the frequencies between the two compounds, $r = 1398/1025 = 1.36$ and $1063/800 = 1.34$ respectively, are close to $\sqrt{2}$. In the low temperature spectrum

of DMG8 the bands in the vicinity of any residual $\beta(\text{OH})$ are intensified (figure 33) and split into a large number of components. It is possible that the band at 1403cm^{-1} is the residual $\beta(\text{OH})$ which has shifted to higher frequency due to the low temperature and appears more intense because of strong adjacent bands. Also in the low temperature spectrum of MG8 (figure 32) $\beta(\text{OH})$ at 1063cm^{-1} has increased in frequency and split into two components at 1075 and 1068cm^{-1} .

ii. In the beam temperature spectrum of DMG8 (figure 33) a very broad band, quite weak, appears at approximately 1030cm^{-1} upon which all the other bands in the region 1200 - 950cm^{-1} are superimposed. This broad band intensifies considerably at low temperature (figure 33) whilst remaining in the same position. Because of this alteration in intensity, bands in this region of the spectrum are drastically effected. The origin of this band is not known.

iii. In the low temperature spectrum of MG8 there are at least four $\gamma(\text{OH})$ bands (figure 32) at 633cm^{-1} , 668cm^{-1} , 775cm^{-1} and 800cm^{-1} and these bands are more intense than the two weak broad bands observed at 622cm^{-1} and 642cm^{-1} in the beam temperature spectrum (figure 32). These bands are not observed in the DMG8 spectra. The increase in frequency and intensity of $\gamma(\text{OH})$ vibrations with decreasing temperature and resolution into multiple bands was observed in the case of pinacol (part I, chapter III). In that case a broad band at 626cm^{-1} at beam temperature was replaced by at least three more intense components at 650cm^{-1} , 725cm^{-1} and 795cm^{-1} .

iv. A band at 656cm^{-1} is observed in the beam temperature spectrum of DMG8 (figure 33) which is not present in the spectrum of MG8 (figure 32). This band although it

intensifies at low temperature does not change in position. It is therefore unlikely to be a $\gamma(\text{OD})$ component.

v. Several other new bands appear in the deuterated spectrum at beam temperature (figure 33) and several are reduced in intensity. Some of the new bands are adjacent to bands which have greatly reduced intensity relative to the undeuterated compound spectrum at beam temperature (figure 32). Therefore it is reasonable to expect that these are not new bands but bands which are eclipsed by previously strong bands and helped to intensify these bands. New bands at 931cm^{-1} and 899cm^{-1} are both weak whereas adjacent bands which were previously strong at 944cm^{-1} and 916cm^{-1} in the undeuterated spectrum (figure 32) now have greatly reduced intensity at 943cm^{-1} and 915cm^{-1} .

vi. A strong band observed at 1105cm^{-1} in the spectrum of MG8 (figure 32) has reduced intensity at a lower frequency of 1093cm^{-1} in the DMG8 spectrum (figure 33). This band has been assigned to $\nu(\text{CO})$ (1111cm^{-1} in the pinacol spectrum). This shift to lower frequency on deuteration has been observed previously in the case of t-butyl alcohol (243). In the t-butyl alcohol spectrum $\nu(\text{CO})$ is shifted from 1214cm^{-1} to 1210cm^{-1} on deuteration.

In the low temperature spectrum of MG8 (figure 32) $\nu(\text{CO})$ is resolved as two components at 1113cm^{-1} and 1101cm^{-1} . The splitting of $\nu(\text{CO})$ at low temperature has been previously observed in the case of methanol (14).

vii. At lower temperatures in both the spectra of MG8 and DMG8 (figures 32 and 33) bands in the CH stretch region split into a large number of components.

viii. A weak band occurs at 2984cm^{-1} in the beam temperature spectrum (figure 32) of solid MG8 (2982cm^{-1} at low temperature) but not in the liquid spectrum (figure 34). This band is also present in the beam and low temperature spectra

(figure 33) of DMG8. This band could be due to :-

a. $\nu_a(\text{CH}_2)$ of CH_2 groups attached to the primary alcohol group of the glyceride residue.

b. $\nu_a(\text{CH}_2)$ of a CH_2 group adjacent to the carbonyl group.

c. Further component of $\nu_a(\text{CH}_3)$ due to interaction within the lattice.

This band is unaltered in position or intensity by deuteration and therefore is not associated with a. above. The shift from the general $\nu_a(\text{CH}_2)$ position is greater than would be expected for the CH_2 group attached to the carbonyl, although a weak band has been observed in the case of $\text{CH}_3\text{CH}_2\text{COCH}_2\text{CH}_3$ (244) at 2955cm^{-1} which has been associated with $\nu(\text{CH}_2)$. Therefore the 2985cm^{-1} band is thought not to be due to b. above.

Therefore the band is assigned tentatively as a further component of $\nu_a(\text{CH}_3)$ as in c. above.

8) Decoupled Spectra

There are three distinct peaks observed in the $\nu(\text{OH})$ region of the low temperature spectrum of the β modification of MG8 (figure 32) at 3275cm^{-1} , 3252cm^{-1} and 3187cm^{-1} whilst only two are observed in the decoupled spectrum at 3296cm^{-1} and 3213cm^{-1} (figure 33).

It has been shown (14) that the decoupled frequency should fall between the two observed frequencies for the coupled vibrations. Therefore taking account of this a fourth band would have been expected at 3317cm^{-1} in the normal spectrum of MG8 (figure 32).

The highest frequency peak of the coupled $\nu(\text{OH})$ occurs at 3275cm^{-1} which is much lower than the 'free' and intramolecular H-bond frequencies in the region $3646\text{--}3523\text{cm}^{-1}$ observed in dilute

solution of the MG8 in CCl_4 and also lower than the intramolecular frequency of 3564cm^{-1} in solid sucrose. It is therefore thought that there is no intramolecular H-bonding in the solid β modification of MG8 and if this is the case it is possible to use the correlation curve relating R_{O-O} to $\nu(\text{OH})$ in figure 15 and obtain R_{O-O} values corresponding to these decoupled $\nu(\text{OH})$ frequencies.

The appearance of two bands associated with the decoupled $\nu(\text{OH})$ indicates there are two distinct OH environments giving rise to R_{O-O} distances of 2.76\AA and 2.73\AA for the $\nu(\text{OH})$ frequencies 3296cm^{-1} and 3213cm^{-1} respectively.

In pinacol a value of 2.76\AA has been obtained associated with one of the components of the decoupled $\nu(\text{OH})$ at 3290cm^{-1} . Since in this compound only $\text{O}-\text{H}\cdots\text{O}$ intermolecular H-bonding can take place it is suggested that the value 2.73\AA is associated with the H-bond distance $\text{O}-\text{H}\cdots\text{O}=\text{C}$. However even though crystal studies have been carried out on the β form of 1-monostearin by Larson (96) using X-ray diffraction no structural information has been obtained about the end group configuration and therefore no confirmation for the type of H-bonding is available.

(b) Solution

1) Solution spectra have been obtained of 1-monoglycerides by Barcelo et al (103) but no information was obtained in that study as to the H-bonding. Studies have been made however by Debye et al (245,246) of the H-bonding taking place in 1-monoglyceride solutions. They assigned overlapping bands (at 3584cm^{-1} and 3460cm^{-1} in one paper and 3676 and 3572cm^{-1} in the second) to 'free' and 'bonded' OH groups, respectively, and found the ratio of the estimated intensities of these bands; OH free/OH bound decreased linearly with concentration in CCl_4

solution because of increasing molecular association. In chloroform and benzene, however, the ratio remained almost constant, indicating that association was taking place between glyceride and solvent molecules. Unfortunately, Debye does not distinguish between intra- and intermolecular H-bonding.

In this study of MG8 in CCl_4 solution eight components are observed in the OH stretch region (figure 39) in the most dilute solution in the range $3646\text{--}3523\text{cm}^{-1}$. The band at 3523cm^{-1} is broad. The concentration at which this spectrum was obtained, 0.0048M is so low that there is little possibility of intermolecular H-bonding (247).

Diols in dilute solution are known to give two bands (46). These bands are due to the 'free' $\nu(\text{OH})$ at around 3630cm^{-1} and intramolecular H-bonded $\nu(\text{OH})$ at approximately 3550cm^{-1} which is broader than the 'free' $\nu(\text{OH})$.

Also in the case of saturated alcohols which are incapable of intramolecular H-bonding asymmetry has been observed in the monomer band in dilute solution (248-255). This asymmetry has been resolved as definite component bands which have been interpreted in terms of OH groups in conformationally distinct environments in equilibrium (249,252-254). It has also been suggested that these bands are due to C-H---O intramolecular H-bonding (251,255). In the case of 1-propanol (251) a partially resolved triplet $\nu(\text{OH})$ absorption was observed at 3639cm^{-1} , 3633cm^{-1} and 3627cm^{-1} . In this study Krueger et al (251) proposed the band at 3627cm^{-1} was due to a C-H---O intramolecular H-bond between a methyl hydrogen and the lone pair of electrons on the oxygen atom. However there is a certain amount of scepticism concerning this hypothesis (252). That a very weak C-H---O-H lowers the $\nu(\text{OH})$ frequency is challenged by the observation

that a stronger OH---O-H bond in diols does not appear to affect the 'free' $\nu(\text{OH})$. When the OH oxygen of a diol serves as a proton acceptor the $\nu(\text{O-H})$ is the same as that of the corresponding methoxy alcohol (figure 41). Therefore the more generally accepted theory is that of conformational heterogeneity (249,252-254).

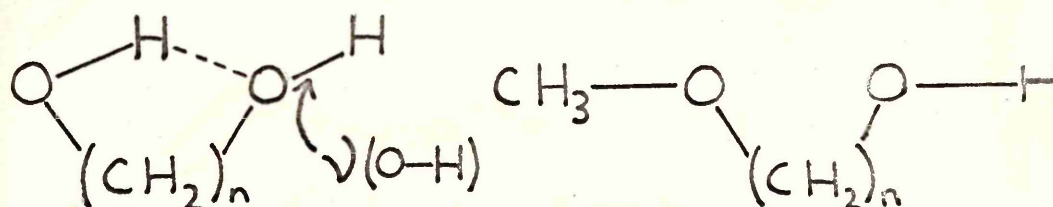
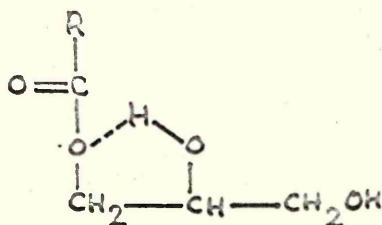
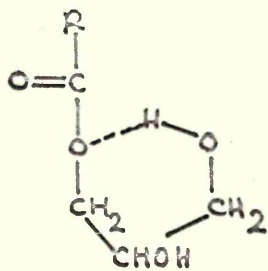
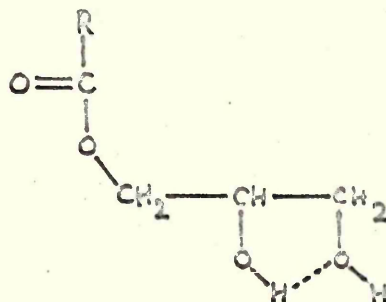
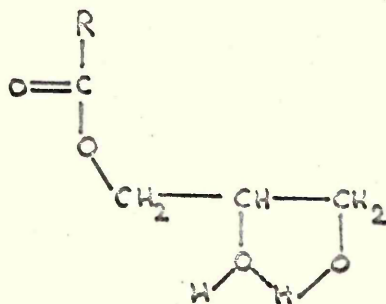
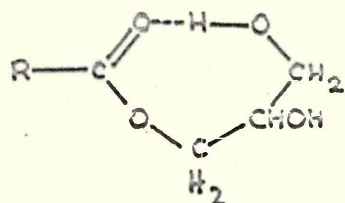
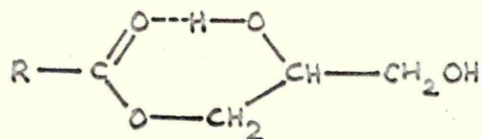


Figure 41.

1-Monoglycerides not only possess two hydroxyl groups in the 1,2 positions but also further acceptor sites in the carbonyl and alkoxy oxygen. Using these donor and acceptor sites participating in intramolecular H-bonding six possible structures exist. These are shown in figure 40.

The positions of 'free' and intramolecularly H-bonded $\nu(\text{OH})$ bands in compounds containing OH---OH, OH---O $\begin{smallmatrix} \text{R} \\ | \\ \text{R} \end{smallmatrix}$ and OH---O=C are in the ranges $3644\text{--}3600\text{cm}^{-1}$ and $3616\text{--}3460\text{cm}^{-1}$ respectively (247).

It may be therefore that the $\nu(\text{OH})$ bands of MGS in dilute solution at 3645cm^{-1} , 3636cm^{-1} , 3618cm^{-1} and 3597cm^{-1} are due to



R is $\text{CH}_3(\text{CH}_2)_6$

Figure 40.
Possible intramolecularly H-bonded
structures of 1-monooctanoin in
solution.

contributions from the structures shown in figure 40 with components present from the conformationally distinct 'free' OH groups. It is not feasible to assign the individual components here because of the complexity of the spectra and lack of data with which to correlate.

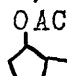
Also on present evidence it seems likely that the remaining bands at 3587cm^{-1} , 3571cm^{-1} , 3560cm^{-1} and 3523cm^{-1} may be due to the intramolecularly H-bonded $\nu(\text{OH})$ from species shown in figure 40.

2) It is well known that the carbonyl group participation in H-bonding in solution with donor molecules gives rise to $\nu(\text{C=O})$ bands at a lower frequency (256).

Evidence for the participation of the carbonyl in the H-bonding schemes shown in figure 40 can be seen from the observation of two equal intensity components of $\nu(\text{C=O})$ in very dilute solution (figure 39). These components are observed at 1753cm^{-1} and 1735cm^{-1} . In an 0.05M solution the bands occur at 1750cm^{-1} and 1734cm^{-1} and the addition of a small amount of D_2O caused the lower frequency H-bonded component to increase in intensity relative to the 'free' component.

When the concentration of MG8 in CCl_4 was increased the relative intensities of the $\nu(\text{C=O})$ components altered. The 'free' $\nu(\text{C=O})$ at higher concentrations is of greater intensity than the H-bonded component and also there is a small shift of the 'free' component from 1753cm^{-1} to 1750cm^{-1} . It is apparent

from measurements in the $\nu(\text{OH})$ region of the spectrum (figure 39) over this concentration range that as the concentration of MG8 is increased intermolecular H-bonding takes place.

Upon altering the type of association taking place, from intra-to intermolecular, it might be expected that by analogy with the shifts in $\nu(\text{OH})$ an increased shift to lower frequency of $\nu(\text{C=O})$ might occur. For example when ethanol is added to n-hexane solutions of ethyl acetate (257) a shift is observed of $\nu(\text{C=O})$ of 17cm^{-1} relative to the 'free' $\nu(\text{C=O})$. However a similar size shift is observed in $\nu(\text{C=O})$ when intramolecular H-bonding takes place in the compound  OH in CCl_4 (258).

Therefore it may be that any intermolecular $\nu(\text{C=O})$ components present at higher concentration in 1-monoglyceride solutions would not in fact be observed as separate low frequency $\nu(\text{C=O})$ bands since they are likely to occur at the same frequency as the intramolecular bands. Thus even though there appears to be more intermolecular H-bonding at higher concentrations it is not possible to infer this from the carbonyl bands.

3) Evidence of alkoxy oxygen participation in intramolecular H-bonding schemes of aryloxyacetic acids has been shown by Oki et al (259). In dilute solutions various aryloxyacetic acids showed bands at $\approx 3525\text{cm}^{-1}$ and 3490cm^{-1} due to structures I and II (figure 42).

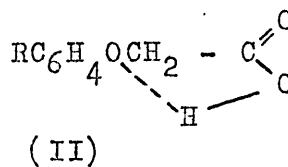
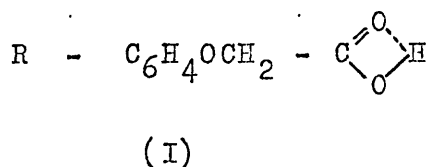


figure 42.

Evidence for the participation of the alkoxy oxygen in triglyceride H-bonding scheme was obtained from the following

observations on trilaurin-ethanol in CCl_4 solutions. Trilaurin contains only two acceptor sites, a carbonyl and an alkoxy oxygen. In a range of solutions from 0.005 - 0.1M in CCl_4 , the $\nu(\text{C=O})$ band appeared as a single intense band (figure 43) at 1750cm^{-1} .

A dilute solution of ethyl alcohol (0.005M) in CCl_4 showed only a single 'free' $\nu(\text{OH})$ at 3636cm^{-1} (figure 43). When solutions were made up containing 0.1M trilaurin and 0.005M ethyl alcohol in CCl_4 and run against a reference solution containing only 0.1M trilaurin in CCl_4 a 'free' $\nu(\text{OH})$ was observed at 3636cm^{-1} and also an association band which was much broader at 3570cm^{-1} (figure 43). This association band could only be due to either $\text{O-H}\cdots\text{O}=\text{C}$ or $\text{OH}\cdots\text{O}$ or both interactions since the concentration of ethanol was only sufficient to produce a 'free' $\nu(\text{OH})$ band. In the mixed solution the $\nu(\text{C=O})$ band was found to be the same intensity and in the same position as found for the comparable concentration of trilaurin alone. Therefore the association band must have arisen because of $\text{OH}\cdots\text{O}$ interaction.

4) At the higher concentrations of MG8 (figure 39) the broad band at 3523cm^{-1} intensifies in 0.1M solution, broadens and shifts to a lower frequency of 3448cm^{-1} whilst shoulders appear at 3376cm^{-1} and 3310cm^{-1} . In the butane diols three distinct bands are observed (46) which are unambiguously assigned to the stretching vibration of the 'free', intramolecularly and intermolecularly H-bonded OH groups. The latter is at a considerably lower frequency than the others.

It is thought therefore that the two broad bands at 3376cm^{-1} and 3310cm^{-1} in MG8 solutions are probably due to formation of dimers and higher multimers either of the linear or cyclic type.

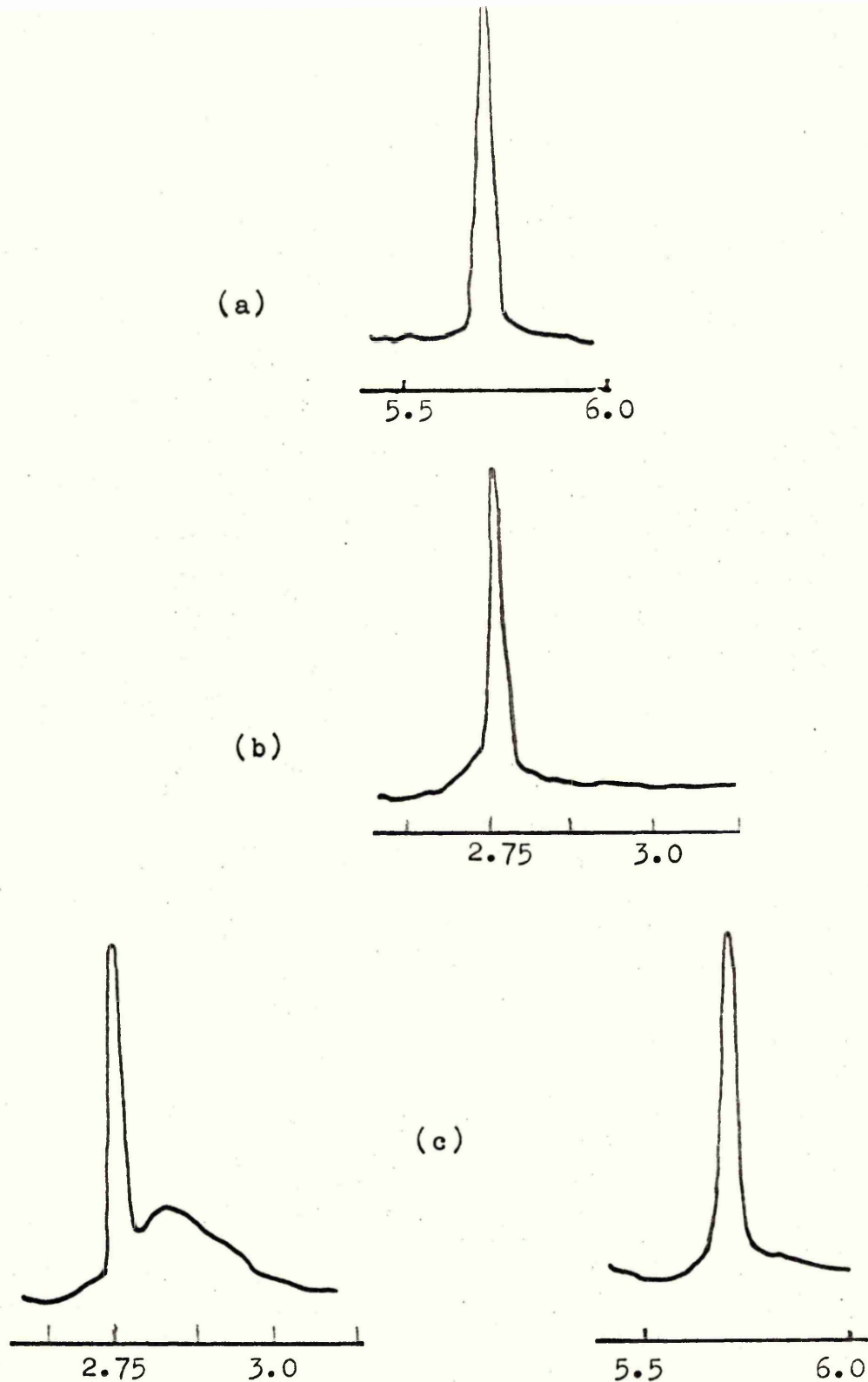


Figure 43.

- (a) $\nu(\text{C}=\text{O})$ of 0.1M solution of trilaurin in CCl_4 .
 (b) $\nu(\text{OH})$ of 0.005M solution of ethanol in CCl_4 .
 (c) $\nu(\text{OH})$ and $\nu(\text{C}=\text{O})$ bands of solution containing 0.1M trilaurin and 0.005M ethanol in CCl_4 .
 Wavelength 2.625-3.125 μ and 5.5-6.0 μ .

TABLE V

DSC Transition Temperatures - Cooling from the melt.

1-monoglyceride	Temperature (°C)		
	A	B	C
MG8	5.5 (rs)	2.5 (rs)	-3.5
MG11	36.5 (rs)	34 (rs)	-5 (rs)
MG12	45 (rs)	44 (rs)	17.5
MG18		74 (rl)	47 (rl)

All transitions are exothermic.

rs indicates transition is reversible over a short period of time (minutes or sometimes hours).

rl indicates transition is reversible over a long period of time (weeks).

All other transitions are irreversible.

TABLE VI

DSC Transition Temperatures - Heating from -20°C.

1-monoglyceride	Temperature (°C)					
	C	B	D	E	F	G
MG8						38
MG11	-5			0-19(exo)*	52	56
MG12			49	53(exo)	59	62.5
MG18	47	74				

All transitions are endothermic except where stated.

* The temperature at which this transition occurred depended on the lowest temperature to which the MG11 sample was cooled, i.e.

MG11 cooled to (°C)	Transition E Temperature (°C)
-3	19
-10	7
-20	0

Table VII

Assignments of the absorption bands of the MG8 spectrum.

Liquid 42°C		Solid Beam Temp.		Solid -170°C		(b) Assignments
cm ⁻¹	(a) Intensity	cm ⁻¹	(a) Intensity	cm ⁻¹	(a) Intensity	
3466	s.br.	3291	s	3275	s	ν(OH)
		3249	s	3252	s	
				3187	s	
		2984	w	2982	w	ν _a (CH ₃)
		2962	m	2963	m	
2957	m			2955	m	
		2952	s	2949	s	ν _a (CH ₂)
				2936	s	
2929	s	2930	s	2928	s	
				2922	s	ν _s (CH ₃)
		2914	s	2914	s	
				2910	s	
				2899	m	ν _s (CH ₂)
				2883	m	
2878	m	2873	m	2868	m	
				2857	m	ν(C=O)
2854	s	2853	s	2852	s	
1739	s	1739	s	1739	s	
1733	sh	1732	s	1732	s	δ _a (CH ₃)
		1478	sh	1477	sh	
1468	m	1468	s	1469	s	
1460	sh	1458	sh	1454	m	δ(CH ₂)
				1437	w	
				1430	v.w.	
1422	w	1425	m	1423	m	β(OH)
		1398	w	1393	w	
1385	m	1385	w	1389	w	
		1370	w	1375	w	δ _s (CH ₃)
				1366	w	
				1346	v.w.	
		1330	w	1329	w	W(CH ₂)
				1312	v.w.	
		1301	v.w.	1302	v.w.	
		1282	m	1283	m	and T(CH ₂)
1272	m	1253	v.w.	1255	v.w.	
				1250	v.w.	
				1238	v.w.	T(CH ₂)
1232	m	1233	m	1230	m	
		1220	v.w.	1218	v.w.	
				1212	v.w.	

cont.

- 93 -

Liquid 42°C		Solid Beam Temp.		Solid -170°C		(b) Assignments
cm ⁻¹	(a) Intensity	cm ⁻¹	(a) Intensity	cm ⁻¹	(a) Intensity	
		1189	s.br.	1188	s	} ν(COC)
				1183	s	
1174	s.br.			1175	m	
		1125	m	1125	m	} ν(CO) ^s
1113	m.br.			1113	m	
		1105	m	1101	sh	
				1075	sh	} β(OH)
				1068	m	
		1063	m.s.			
1053	m.br.	1049	s	1053	m.s.	s
				1036	v.w.	s
				1031	v.w.	s
				1026	v.w.	s
		1010	v.w.	1008	w	s
990	w	993	m.s.	993	m	s
		980	v.w.	980	w	
		970	v.w.	967	v.w.	
				964	v.w.	
		944	m	947	m	
935	w.br.			936	v.w.	
		916	m	916	w	ρ(CH ₂)
				912	w	ρ(CH ₂)
		895	v.w.	889	v.w.	ρ(CH ₃)
870	w.br.					
		852	w	853	w	ρ(CH ₂)
		826	w	830	w	ρ(CH ₂)
				800	sh	} δ(OH)
				775	m.br.	
		773	w	773	m	} ρ(CH ₂)
		769	sh	767	m	
				736	v.w.	
				730	w	
726	v.w.	723	w	723	m	
				711	v.w.	
				706	v.w.	
		651	w.br.	668	w.br.	} γ(OH)
		626	w.br.	633	w.br.	

Table VIII

Assignments of the absorption bands of the DMGS spectrum.

Liquid 42°C		Solid Beam Temp.		Solid -170°C		(b) Assignments
cm ⁻¹	(a) Intensity	cm ⁻¹	(a) Intensity	cm ⁻¹	(a) Intensity	
3418	w	3306	w	3296	w	} $\nu(\text{OH})$
		3252	w	3213	w	
		2984	w	2982	w	} $\nu_a(\text{CH}_3)$
		2962	m	2963	m	
2957	m			2955	m	
		2952	s	2950	s	} $\nu_a(\text{CH}_2)$
2929	s	2930	s	2936	s	
				2926	s	
				2920	s	
		2916	s	2914	s	
				2909	s	
				2898	m	} $\nu_s(\text{CH}_3)$
				2883	m	
2870	m	2873	m	2867	m	} $\nu_s(\text{CH}_2)$
				2857	m	
2853	s	2854	s	2852	s	} $\nu(\text{OD})$
2527	s.br.					
		2462	s	2442	s	
				2410	s	
		2417	s	2370	s	} $\nu(\text{C=O})$
1739	s	1739	s	1739	s	
1733	sh	1732	s	1732	s	} $\delta_a(\text{CH}_3)$
		1477	sh	1477	sh	
1468	m	1468	m	1468	s	} $\delta(\text{CH}_2)$
1459	m	1456	m	1456	m	
				1449	w	
				1433	v.w.	
1422	w	1422	w	1423	m	} $\beta(\text{OH})$
				1411	m	
		1408	w	1403	m	} $\delta_s(\text{CH}_3)$
		1398	v.w.	1391	m	
		1388	w	1383	m	
1385	m			1375	m	} $\nu(\text{CH}_2)$
		1379	w	1372	sh	
		1372	w	1364	m	
				1332	w	
		1331	w	1320	m	} and
		1325	w	1312	sh	
				1304	v.w.	
				1294	v.w.	
		1282	m	1277	m.s.	} $\text{T}(\text{CH}_2)$
1272	m			1256	v.w.	
		1257	v.w.	1250	v.w.	
				1232	m	} $\text{T}(\text{CH}_2)$
1232	m	1233	m	1227	m	

cont.	Liquid 42°C	Solid Beam Temp.	Solid -170°C	
cm ⁻¹	(a) Intensity	cm ⁻¹	(a) Intensity	(b) Assignments
1174	s.br.	1193 s 1179 sh	1190 s 1184 sh	} $\nu(\text{COC})$
			1174 sh	
			1133 m	
			1124 m	
		1127 m	1121 sh	
1111	m.br.	1114 w	1117 sh	
		1093 w	1093 s	} $\nu(\text{CO})$
			1083 sh	
1050	w.br.	1073 w	1073 m	
		1052 s	1056 s	
			1037 m	s
		1025 w		$\beta(\text{OD})$
1000	w.br.	998 m.br.	1003 m	s
			994 w	s
			991 w	s
			985 sh	
		967 w	966 m	
			959 m	
939	w.br.	943 w	945 v.w.	
		931 w	932 m	
		915 w	914 m	$\rho(\text{CH}_2)$
		899 w	899 m	$\rho(\text{CH}_3)$
			889 m	} $\rho(\text{CH}_2)$
			879 v.w.	
849	w.br.	845 w	845 m	
		831 w	830 m	
		825 w	824 m	$\rho(\text{CH}_2)$
		800 w	795 w.br.	$\beta(\text{OD})$
		774 w	772 m	} $\rho(\text{CH}_2)$
		770 w	769 m	
			735 w	
			729 m	
724	w	722 w	723 s	
			708 w	
		658 w.br.	658 m	

(a) The following abbreviations are used:

s - strong, m - medium, w - weak, v - very, sh - shoulder,
br - broad.

(b) The meanings of the symbols used are as follows:

ν - stretching

δ - bending

β - in-plane bending

s - skeletal

cont.

ρ - rocking

γ - out-of-plane bending

T - twisting

W - wagging

These bands may be combination bands (35).

TABLE IX Frequencies of the $\nu(\text{OH})$ and $\nu(\text{C=O})$ in the different phases of 1-monoglyceride

Phase	1-monoglyceride	T°C	$\nu(\text{OH})$ cm ⁻¹	$\nu(\text{C=O})$ cm ⁻¹
Liquid	MG8	42	3422	1739 1733
	MG11	65	3428	1739 1732
	MG12	70	3430	1740 1730
	MG18	93	3448	1739 1728
B → C (α)	MG11	30	3361	1736 1717
	MG12	40	3361	1739 1718
	MG18	65	3390	1738 1718
Below C	MG12	15	3347	1738
	MG18 (sub- α)	28	3320	1738 1722
E → F (β')	MG11	20	3408 } 3302 }	1739 1729
	MG8	30	3291 } 3249 }	1739 1732
Highest Melting form (β)	MG11	30	3292 } 3253 }	1739 1731
	MG12	45	3292 } 3259 }	1738 1731
	MG18	30	3292 } 3238 }	1740 1732

Table X

Frequencies (cm^{-1}) of the components of $\nu(\text{CH}_2)$ and $\nu(\text{CH}_3)$ for the different polymorphic forms of 1-monoglycerides.

Liquid	B $\xrightarrow{\quad}$ C (α form)	Below C		E $\xrightarrow{\quad}$ F	Highest Melting form	Assignm- ents
MG11, MG12 MG18	MG11, MG12 MG18	MG12	MG18 (sub- α) form	MG11 (B' form)	MG11, MG12 MG18	
					2983(w)	} $\nu_a(\text{CH}_3)$
		2963(sh)	2963(sh)	2963(sh)	2962(sh)	
2954(m)	2954(m)	2954(m)	2953(m)	2954(m)	2952(m)	
2928(s)	2930(s)	2930(s)			2930(s)	} $\nu_a(\text{CH}_2)$
				2919(s)*		
		2915(s)	2916(s)		2913(s)	
		2899(m)*	2899(m)*			
2870(m)	2870(m)	2870(m)	2868(m)	2868(m)	2872(m)	$\nu_s(\text{CH}_3)$
2853(s)	2854(s)	2850(s)	2852(s)	2852(s)	2854(s)	$\nu_s(\text{CH}_2)$

* These bands may be combination bands (35). Intensities of these bands are shown in parenthesis.

For the meaning of the abbreviations used see footnote to Table VIII.

The frequencies quoted, where more than one 1-monoglyceride is shown, are those of MG18. The others agree to $\pm 3\text{cm}^{-1}$ with respect to the frequencies shown.

(II) Unsymmetrical Trialkylphosphine Oxides

(i) Results

Infra-red spectra of the liquid and polycrystalline $C_{10}PO$ were obtained at $80^{\circ}C$ and beam temperature whilst those of $C_{12}PO$ were obtained at $90^{\circ}C$ and beam temperature respectively. These spectra are shown as figures 44 and 45. Single crystal spectra of $C_{10}PO$ were obtained at the beam temperature and are shown in figure 44. Proposed assignments of the bands in these spectra are given in tables XI and XII. From the observed dichroisms the direction of the alkyl chain axis was deduced and has been marked (figure 46). Parallel dichroisms are taken to be parallel to the chains.

Long spacing values for anhydrous $C_{10}PO$ and $C_{12}PO$ are given in table XIII.

(ii) Discussion

(a) A structure analysis of trimethylphosphine oxide has been made in the gas phase using electron diffraction (260). The bond angles and bond lengths obtained in this study are shown in figure 47.

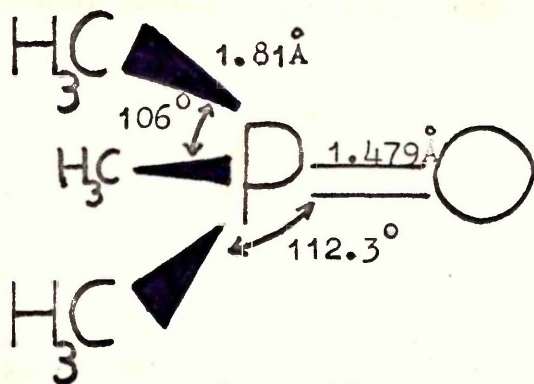


Figure 47.

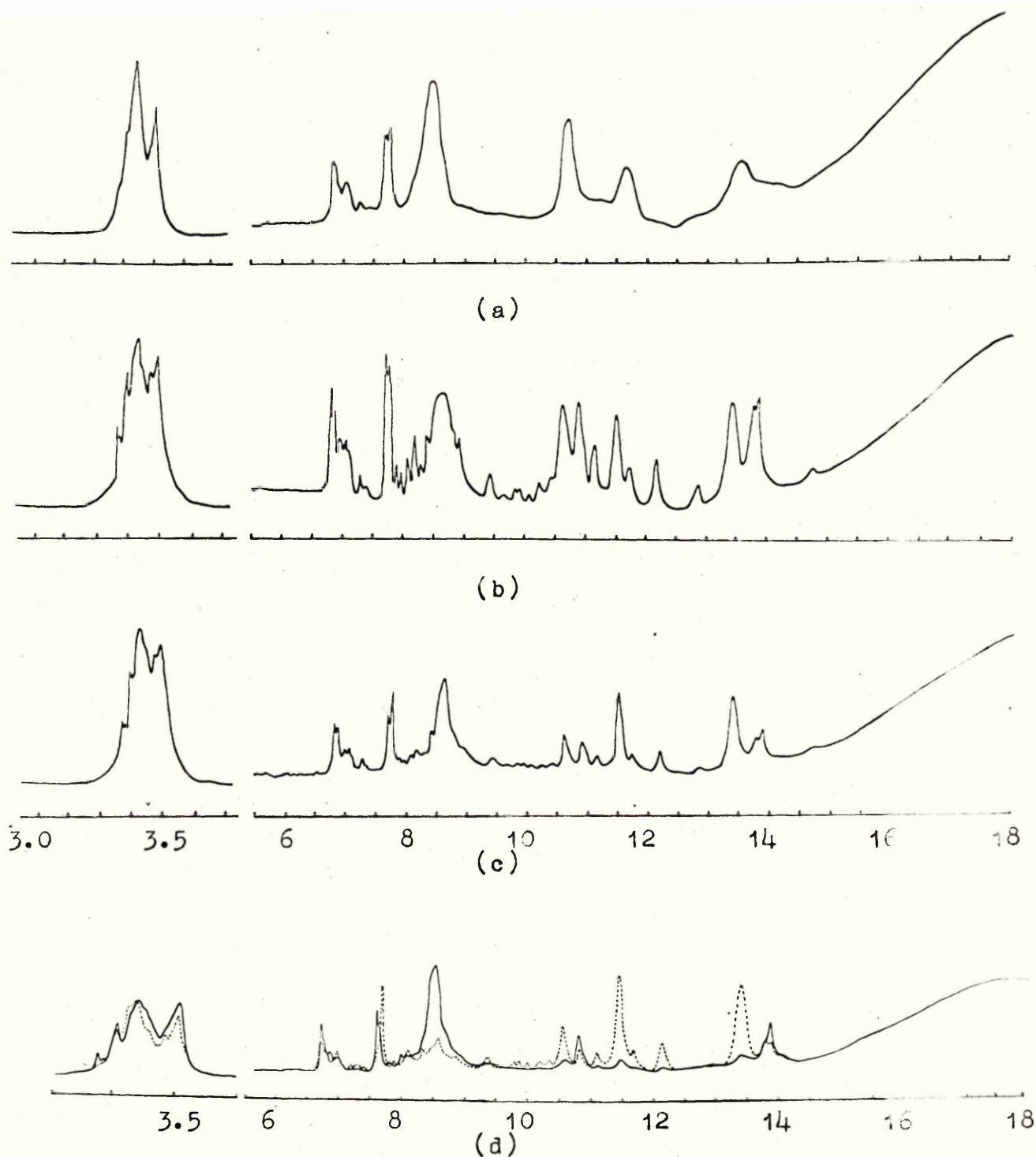


Figure 44.

Infra-red spectra of $C_{10}PO$, (a) Liquid ($80^{\circ}C$), Wavelength $3.0-3.75$ and $6-18\mu$, (b) polycrystalline (beam temperature), Wavelength $3.0-3.75$ and $6-18\mu$, (c) unpolarized single crystal (beam temperature), Wavelength $3.0-3.75$ and $6-18\mu$, (d) polarized single crystal (beam temperature), $3.25-3.625$ and $6-18\mu$: electric vector parallel to chains ----, and perpendicular to chains —.

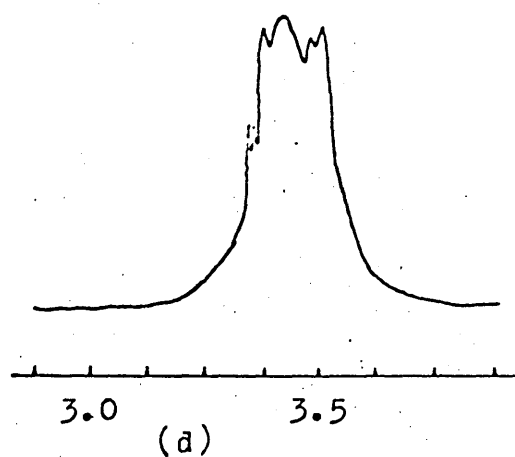
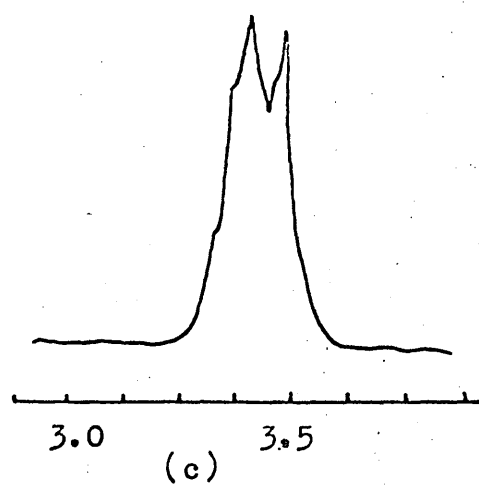
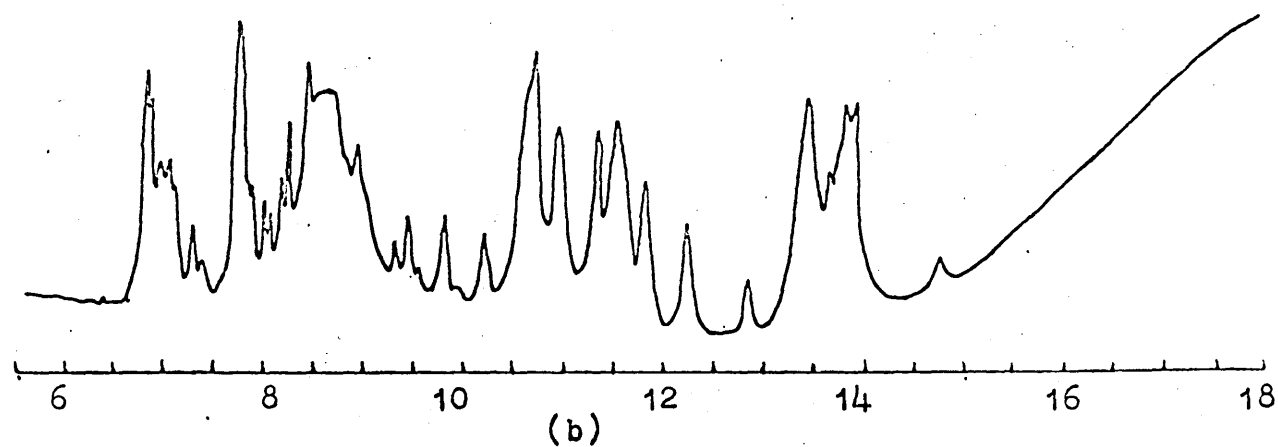
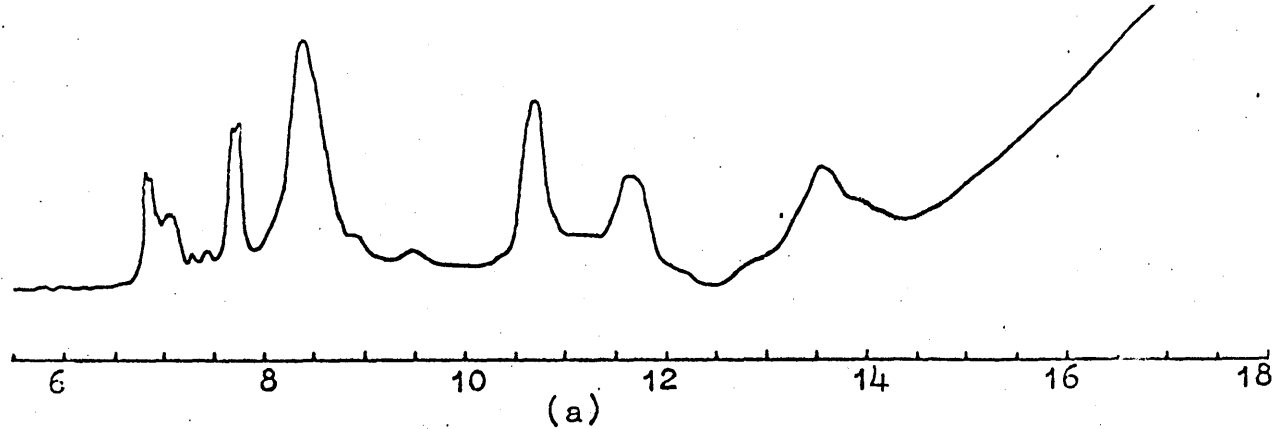


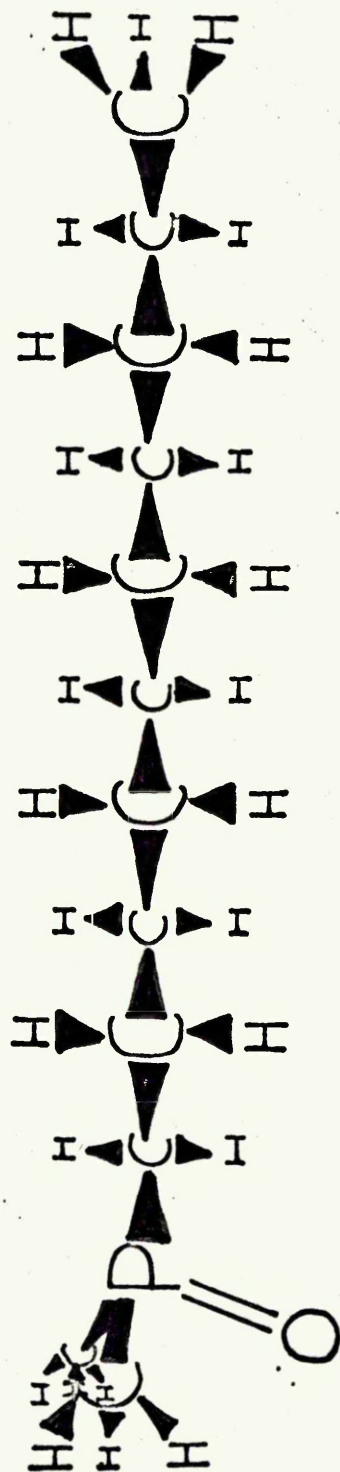
Figure 45.

Infra-red spectra of $C_{12}PO$, Liquid($90^{\circ}C$), Wavelength(a) $6-18\mu$, (c) $2.875-2.875\mu$.
Solid (beam temperature), Wavelength(b) $6-18\mu$, (d) $2.875-3.875\mu$.

Figure 46.
Model structure of $C_{10}PO$.

Electric vector perpendicular
and parallel to chains

$E \perp$ $E \parallel$



Assuming that in the long chain phosphine oxides studied in the solid state, a similar C-P length of 1.81\AA is present then the average distance parallel to the chain axis between the adjacent C and P atoms is approximately 1.18\AA . Also assuming that the chains pack in a zig-zag manner with C \hat{C} C angles of $109^{\circ}28'$ with the average distance parallel to the chain axis between adjacent C atoms being approximately 1.26\AA (261), then the spacings obtained for $C_{10}PO$ and $C_{12}PO$ (table XIII) are too great to correspond with the length of a single molecule (12.52\AA and 15.04\AA for $C_{10}PO$ and $C_{12}PO$ respectively). However they are consistent with a double molecule and therefore indicate that $C_{10}PO$ and $C_{12}PO$ crystallize in bimolecular layers as do n paraffins (262), 1-monoglycerides (82,96) and fatty alcohols (263).

(b) The proposed assignments of the $C_{10}PO$ and $C_{12}PO$ spectra are given in tables XI and XII and were made with reference to their liquid spectra (figure 44 and 45) as well as the single crystal spectra of $C_{10}PO$ (figure 44). Also analogy was made with assigned spectra of trimethylphosphine oxide (142), long chain hydrocarbons (29,242), fatty acids (30,35) and long chain alcohols (12,13). Some of the very weak bands observed in the polycrystalline spectra of $C_{10}PO$ have not been observed in the single crystal spectra because the single crystal was too thin. Differences between the unpolarized polycrystalline and single crystal spectra of $C_{10}PO$ (figure 44) may be attributed to the regularity of molecular orientation in the latter case.

(c) In the polarized spectra of $C_{10}PO$ (figure 44):-

1. Significant dichroisms, in the same direction, have been observed for the bands associated with the CH_2 bending mode, $\delta(CH_2)$, at 1464cm^{-1} , the lower limit CH_2 rocking mode, $\rho(CH_2)$ at 719cm^{-1} and the CH_2 twisting modes, $T(CH_2)$, at

1269cm⁻¹, 1239cm⁻¹, 1206cm⁻¹ and 1190cm⁻¹ whilst opposite dichroisms are observed for the bands associated with the CH₂ wagging modes, W(CH₂), at 1355cm⁻¹, 1339cm⁻¹, 1258cm⁻¹ and 1223cm⁻¹, and skeletal modes, S, in the range 1121-943cm⁻¹.

Similar, but not identical dichroisms have been observed previously for these modes in the polarized spectra of single crystals of n-C₁₈H₃₈ (29), orthorhombic n-C₂₄H₅₀ (29), and the B form of octadecanoic acid (35) and were related to directions parallel and perpendicular to the alkyl chain axis in these crystals.

Therefore it seems likely from our dichroisms that the single crystal of C₁₀PO has formed with the alkyl chains aligned either in the plane of the sodium chloride plates or tilted at an angle less than 45° to them.

This is in contrast with the work of Suzi (30,31) who obtained single crystals of various long chain acids between sodium chloride plates by gradient cooling. In that work the axes of the alkyl chains were almost perpendicular to the plane of the plates.

2. Relatively small dichroisms are observed for the bands associated with the hydrocarbon chain CH₂ and CH₃ symmetric and asymmetric stretch, $\nu_s(\text{CH}_2)$, $\nu_a(\text{CH}_2)$ and $\nu_s(\text{CH}_3)$, $\nu_a(\text{CH}_3)$ (figure 44) in the region 2987-2851cm⁻¹. All these bands should show appreciable dichroisms if the skeletal plane was in the plane of the plates. It would therefore appear that these skeletal planes are approximately parallel to the incident beam and therefore perpendicular to the plates.

3. The phosphoryl absorptions, $\nu(\text{P=O})$, at 1168cm⁻¹ and 1156cm⁻¹ have strong dichroisms in the same directions as those of $\delta(\text{CH}_2)$ and $\rho(\text{CH}_2)$ and it thus appears that the transition

moments have a similar direction. Therefore it is thought that the phosphoryl group lies as shown in figure 46 and is approximately perpendicular to the chain axis.

As previously mentioned a structure analysis has been carried out on trimethylphosphine oxide (260) in the gas phase. In this compound the phosphorus atom has formed four approximately tetrahedral sp^3 bonds to the three carbon atoms and the oxygen atom. A 'd' orbital on the phosphorus atom may then overlap with a 'p' orbital on the oxygen atom to give a multiple bond. It would therefore be expected that the $C-\hat{P}=O$ bond angles in this compound would be greater in agreement with the view (260) that the electrons in a double bond repel those in a single bond, as in $POCl_3$. No structure analysis of trimethylphosphine oxide has been carried out in the solid state.

In the phosphine oxides studied in this work one of the methyl groups attached to phosphorus has been replaced by a hydrocarbon chain. It would be expected that the phosphorus atom would be at the centre of an approximate tetrahedron with the $C-\hat{P}=O$ angles greater than the $109^\circ 28'$ for a perfectly sp^3 hybridized system and possibly of the order of that shown for trimethylphosphine oxide with $C-\hat{P}-C$ bond angles being smaller than this value. Therefore the methyl groups might be expected to take up a position relative to the phosphoryl group as shown in figure 46 at 16° to the axis of the chain.

(d) The bands due to $\nu(CH_2)$ and $\nu(CH_3)$ lie in the range $3000 - 2850cm^{-1}$ (50(b)). In the spectrum of trimethylphosphine oxide a medium strong band has been assigned to $\nu_a(PCl_3)$ at $2955cm^{-1}$ (142). Weak bands occur in the unpolarized $C_{10}PO$ spectrum (figure 44) at $2987cm^{-1}$ and $2980cm^{-1}$. However in the spectrum of the liquid (figure 44) the band at $2987cm^{-1}$

is not present and therefore may have been due to crystal splitting of the $\nu_a(\text{CH}_3)$ mode. The band at 2980cm^{-1} is therefore assigned to $\nu_a(\text{PCH}_3)$ and shows a small perpendicular dichroism.

In the polycrystalline spectrum of C_{12}PO (figure 45) weak bands are observed at 2990cm^{-1} and 2981cm^{-1} . In the spectrum of the liquid (figure 45) the band at 2990cm^{-1} is not present. Therefore the bands at 2990cm^{-1} and 2981cm^{-1} have again been assigned to $\nu_a(\text{CH}_3)$ and $\nu_a(\text{PCH}_3)$ respectively.

(e) A band at 2898cm^{-1} has been observed by Krimm et al (22) in the case of monoclinic $n\text{-C}_{36}\text{H}_{74}$ and some controversy has arisen as to the assignment of this band. In the work of Krimm et al (22) the band was assigned to the 'b' polarized component of $\nu_a(\text{CH}_2)$ whilst in the case of triclinic $n\text{-C}_{20}\text{H}_{42}$ (29) where no interchain coupling could occur, the band was assigned to a combination band of Raman and infra-red active $\delta(\text{CH}_2)$ modes.

In the polarized single crystal spectra of $n\text{-C}_{20}\text{H}_{42}$ (29) the polarized radiation was thought to be incident approximately parallel to the chain axis and dichroisms were observed perpendicular and parallel to the skeletal planes. Other bands were observed in this region at 2922cm^{-1} showing a parallel dichroism whilst a band at 2916cm^{-1} has a perpendicular dichroism. The band at 2916cm^{-1} was assigned to $\nu_a(\text{CH}_2)$ whilst the band at 2922cm^{-1} was assigned with the band at 2898cm^{-1} to a combination band. These bands have also been observed by Al-Mamun (12) in the spectrum of hexadecanol and have been similarly assigned.

In the polycrystalline spectrum of C_{10}PO (figure 44) a strong band occurs at 2922cm^{-1} with a shoulder of medium intensity at 2900cm^{-1} . In the polarized spectra (figure 44) in the parallel position an intense band is observed at 2922cm^{-1} with a weak shoulder at 2898cm^{-1} . In the perpendicular position an intense band is observed at 2916cm^{-1} with an intense shoulder at

2904 cm^{-1} . It is thought that the band at 2900 cm^{-1} has an apparently strong dichroism because it enters into Fermi resonance with the band at 2922 cm^{-1} when in the perpendicular position. This interpretation fits in with the relatively small dichroisms which occur throughout this region. The bands at 2922 cm^{-1} and 2900 cm^{-1} have been assigned to combination bands as previously described in the case of $n\text{-C}_{20}\text{H}_{42}$ (29).

(f) In the spectrum of $n\text{-C}_{20}\text{H}_{42}$ (29) bands at 2953 cm^{-1} and 2962 cm^{-1} have strong dichroisms perpendicular and parallel to the skeletal planes respectively. Bands in the same position have also been observed in the spectrum of hexadecanol with a much smaller dichroism which is perpendicular to the chain axis. These bands have been assigned to $\nu_a(\text{CH}_3)$.

In the polycrystalline spectrum of C_{10}PO (figure 44) a medium intensity band at 2955 cm^{-1} which shows a very small perpendicular dichroism has a shoulder at 2963 cm^{-1} which shows no observable dichroism. These bands have been assigned to $\nu_a(\text{CH}_3)$ of the CH_3 group of the hydrocarbon chain.

In the spectrum of C_{12}PO (figure 45) a medium intensity band at 2954 cm^{-1} with a shoulder at 2963 cm^{-1} have been similarly assigned to $\nu_a(\text{CH}_3)$.

(g) In the spectrum of $n\text{-C}_{20}\text{H}_{42}$ (29) bands at 2851 cm^{-1} and 2872 cm^{-1} have very strong dichroisms parallel to the skeletal planes. Bands are observed in the spectrum of hexadecanol (12) in the same positions but show a much smaller dichroism which is perpendicular to the chain axis. These bands were assigned to $\nu_s(\text{CH}_2)$ and $\nu_s(\text{CH}_3)$ respectively.

In the spectrum of C_{10}PO (figure 44) medium and strong bands are observed at 2873 cm^{-1} and 2851 cm^{-1} which have been assigned to $\nu_s(\text{CH}_3)$ and $\nu_s(\text{CH}_2)$ respectively and show small dichroisms

perpendicular to the chain axis.

In the spectrum of $C_{12}PO$ (figure 45) a medium band at 2874cm^{-1} and a strong band at 2850cm^{-1} have been assigned to $\nu_s(\text{CH}_3)$ and $\nu_s(\text{CH}_2)$ respectively.

(h) In the polycrystalline spectrum of $C_{10}PO$ (figure 44) a strong band is observed at 2931cm^{-1} . Strong bands associated with $\nu_a(\text{CH}_2)$ usually lie in the range $2936-2916\text{cm}^{-1}$ (54(c)). This band has been assigned to $\nu_a(\text{CH}_2)$ and has a small parallel dichroism. Also a strong band at 2934cm^{-1} in the polycrystalline spectrum of $C_{12}PO$ (figure 45) has been assigned as $\nu_a(\text{CH}_2)$.

(i) Weak bands associated with $\delta_s(\text{CH}_3)$ are found in the region of 1380cm^{-1} (52). A very weak parallel band at 1374cm^{-1} in the polarized spectrum of $C_{10}PO$ (figure 44) has also been assigned to $\delta_s(\text{CH}_3)$ of the CH_3 group of the hydrocarbon chain. Also this band is found in the same position in the spectrum of $C_{12}PO$ (figure 45).

In the spectrum of the A form of octadecanoic acid (35) a medium intensity band was observed at 1450cm^{-1} with a dichroism perpendicular to the skeletal planes. This band was assigned to the CH_3 asymmetric deformation, $\delta_a(\text{CH}_3)$. In the spectra of $C_{10}PO$ (figure 44) a medium intensity shoulder is observed at 1456cm^{-1} with a dichroism perpendicular to the chain axis and this has been assigned to $\delta_a(\text{CH}_3)$.

A medium intensity band is observed in the spectrum of $C_{12}PO$ (figure 45) at 1458cm^{-1} which has also been assigned to $\delta_a(\text{CH}_3)$.

(j) The presence of a P-CH_3 linkage in a molecule is usually characterized by three sets of absorptions in the regions 1420cm^{-1} , 1300cm^{-1} , 900cm^{-1} (264).

Near 1420cm^{-1} bands which are weak due to the CH_3 asymmetric

deformation, $\delta_a(\text{PCH}_3)$, generally occur (264). In the case of trimethylphosphine oxide (142) bands associated with $\delta_a(\text{PCH}_3)$ have been observed in the range $1486\text{--}1411\text{cm}^{-1}$ and are of medium strong intensity. There are weak bands in this region of the unpolarized spectra of C_{12}PO (figure 45) and C_{10}PO (figure 44) at 1425cm^{-1} , 1418cm^{-1} and 1408cm^{-1} . In the polarized spectra of C_{10}PO these bands possess small parallel, parallel and perpendicular dichroisms respectively (figure 44). All these bands have been assigned to $\delta_a(\text{PCH}_3)$.

In the spectrum of trimethylphosphine oxide (142) bands of medium strong intensity were observed in the range $1336\text{--}1259\text{cm}^{-1}$ and these have been assigned to the symmetric CH_3 deformation, $\delta_s(\text{PCH}_3)$. Bands of medium to very strong intensity occur in the unpolarized spectrum of anhydrous C_{10}PO (figure 44) at 1299cm^{-1} , 1290cm^{-1} and 1287cm^{-1} , have been assigned to $\delta_s(\text{PCH}_3)$ and possess perpendicular, perpendicular and parallel dichroisms respectively. In the spectrum of C_{12}PO (figure 45) bands of medium to very strong intensity associated with $\delta_s(\text{PCH}_3)$ occur at 1297cm^{-1} , 1294cm^{-1} and 1290cm^{-1} .

The third characteristic band due to P- CH_3 linkage lies within the limits $930\text{--}840\text{cm}^{-1}$ (264) and is usually of medium or strong intensity. This absorption is due to the CH_3 rocking mode, $\rho(\text{PCH}_3)$. In the case of trimethylphosphine oxide (142) strong bands are observed at 944cm^{-1} , 870cm^{-1} and 863cm^{-1} which have been assigned to $\rho(\text{PCH}_3)$. In the unpolarized spectrum of C_{10}PO , two bands occur one of medium intensity at 919cm^{-1} with a perpendicular dichroism and another at 868cm^{-1} also of medium intensity with a parallel dichroism, and in C_{12}PO (figure 45) bands are observed at 917cm^{-1} and 870cm^{-1} and are of medium

intensity. These bands have been assigned to $\rho(\text{PCH}_3)$.

The dichroisms may be explained in terms of the model (figure 46) where it can be seen that if the two methyl groups are at approximately 16° to the chain axis then when they 'breathe' in-phase there will be a larger component of the transition moment in a direction parallel to the chain axis. When they 'breathe' out-of-phase there will be a larger component of the transition moment perpendicular to the chain axis.

Also when these methyl groups rock in-phase there will be a larger component of the transition moment perpendicular to the chain axis but when they rock out-of-phase it would appear that the components of the transition moment perpendicular and parallel to the chain axis are the same. That more than two bands are present in some of the above cases is possibly due to crystal splitting.

(k) On present evidence (264) it can be said that the phosphoryl absorption, $\nu(\text{P=O})$, range is about $1415\text{-}1080\text{cm}^{-1}$. In trimethylphosphine oxide an intense band was found by Goubeau et al (142) at 1160cm^{-1} and by Daasch et al (265) at 1170cm^{-1} which have been assigned to $\nu(\text{P=O})$. In the latter reference a low frequency shoulder is observed to the $\nu(\text{P=O})$ band which, by the presence of strong bands associated with water is undoubtedly due to the H-bonded component of $\nu(\text{P=O})$. Goubeau et al (142) also observed weak bands in the spectrum of trimethylphosphine oxide at 1180cm^{-1} and 1102cm^{-1} which they have also assigned to $\nu(\text{P=O})$ and the appearance of all the $\nu(\text{P=O})$ bands at a much lower frequency than the gas phase at 1228cm^{-1} has been interpreted in terms of the associations such as those shown in figure 48.

Dipole - dipole association of the phosphoryl groups of

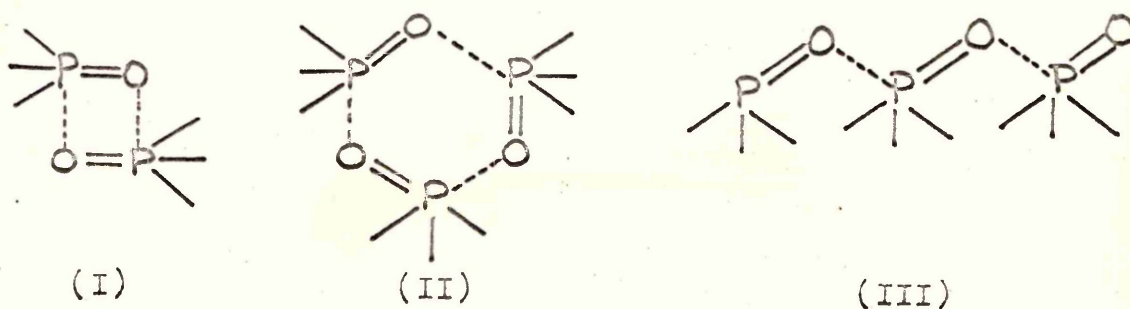


Figure 48.

type III (figure 48) has also been postulated (266) to account for the large frequency shift of $\nu(\text{P}=\text{O})$ in the tri-*n*-octylphosphine oxide spectrum, upon going from the dilute solution in CS_2 to the solid state. In dilute solution $\nu(\text{P}=\text{O})$ occurs at 1170cm^{-1} and moves to 1142cm^{-1} in the solid.

In this work two intense bands are observed at 1156cm^{-1} and 1168cm^{-1} for C_{10}PO in the solid whilst in dilute solution in CCl_4 the band moves to 1190cm^{-1} . In the case of C_{12}PO only one intense band (figure 45) is observable at 1166cm^{-1} due to the presence of a strong band superimposed upon it at 1190cm^{-1} . These bands have been assigned to $\nu(\text{P}=\text{O})$. It is thought that in the case of C_{10}PO that the large shift in frequency of $\nu(\text{P}=\text{O})$ upon going from solution to solid is due to dipole-dipole association, the two bands in the solid being due to types I and III (figure 48). As mentioned earlier the strong perpendicular dichroism of these bands has assisted in determining the orientation of the molecules in the specimen.

(1) Absorptions occur in compounds containing P-C linkages due to the P-C stretching mode, $\nu(\text{PC})$, in the range 770-650 cm^{-1} (264). In the spectrum of trimethylphosphine oxide (142) three bands have been assigned to $\nu_a(\text{PC})$ at 741 cm^{-1} , 777 cm^{-1} and 805 cm^{-1} which are of strong, medium and weak intensity respectively. In the spectrum of C_{10}PO (figure 44) two bands are observed at 744 cm^{-1} and 821 cm^{-1} of medium and weak intensity respectively which have been assigned to $\nu_a(\text{PC})$ and whose parallel dichroisms agree with expectation. In the spectrum of C_{12}PO (figure 45) bands associated with $\nu_a(\text{PC})$ are observed at 746 cm^{-1} and 819 cm^{-1} and are of medium strong and weak intensity respectively.

Also a band is observed in the spectrum of trimethylphosphine oxide (142) at 664 cm^{-1} of very weak intensity and this was assigned to $\nu_s(\text{PC})$. Very weak bands are observed at 676 cm^{-1} and 679 cm^{-1} in the spectra of C_{10}PO and C_{12}PO (figures 44 and 45) respectively which have been assigned to $\nu_s(\text{PC})$.

(m) Further absorptions have been noted previously due to the deformation of a CH_2 group adjacent to phosphorus (54(c)), $\delta(\text{PCH}_2)$, in the region 1440 cm^{-1} . Weak bands occur at 1449 cm^{-1} and 1437 cm^{-1} in the spectrum of anhydrous C_{10}PO and these have been assigned to $\delta(\text{PCH}_2)$ modes. These bands have the same perpendicular dichroisms as those due to $\delta(\text{CH}_2)$. In the spectrum of C_{12}PO weak bands associated with $\delta(\text{PCH}_2)$ occur at 1445 cm^{-1} and 1437 cm^{-1} .

(n) The infra-red spectra of most long chain molecules show very regular progressions of absorption bands in the approximate region of 1380-1180 cm^{-1} and 1300-1170 cm^{-1} (267) due to the $\text{W}(\text{CH}_2)$ and $\text{T}(\text{CH}_2)$ modes respectively. These bands are usually weak in intensity in the case of n paraffins but in the case of

molecules having a polar head group the intensity may be increased somewhat (267,268).

In the spectra of $C_{10}PO$ (figure 44) and $C_{12}PO$ (figure 45) a series of weak and very weak bands are observed in the frequency range $1380-1170\text{cm}^{-1}$.

The very weak parallel bands at 1355cm^{-1} and 1339cm^{-1} in the polarized spectrum of $C_{10}PO$ (figure 44) and the very weak bands at 1356cm^{-1} and 1328cm^{-1} in the spectrum of $C_{12}PO$ (figure 45) have been assigned to $W(\text{CH}_2)$.

Below 1280cm^{-1} several bands of very weak and weak intensity are observed in both spectra, six in the case of $C_{10}PO$ and eight in the case of $C_{12}PO$, although two bands in the spectrum of $C_{12}PO$ at 1217cm^{-1} and 1190cm^{-1} are of medium and strong intensity. This increase in the number of bands within this region of the spectrum with increase in chain length is to be expected and is observed in long chain fatty acids (269,270) and alcohols (13) as well as in n paraffins (242,267). In the polarized spectrum of $C_{10}PO$ (figure 44) the six bands observed in this region have alternate perpendicular and parallel dichroisms. Since the $T(\text{CH}_2)$ mode is an out of plane mode it is expected to be polarized perpendicularly and therefore the very weak perpendicular bands at 1269cm^{-1} , 1239cm^{-1} , 1206cm^{-1} and a weak perpendicular band at 1190cm^{-1} have been assigned tentatively to $T(\text{CH}_2)$ whilst the parallel bands at 1258cm^{-1} and 1223cm^{-1} which are of very weak and weak intensity respectively have been assigned to $W(\text{CH}_2)$.

Bands in this region of the $C_{12}PO$ spectrum (figure 45) below 1280cm^{-1} have been assigned to $W(\text{CH}_2)$ and $T(\text{CH}_2)$ modes. The reason for the strong intensity of the 1190cm^{-1} band associated with $W(\text{CH}_2)$ is not known.

(o) In the spectra of n paraffins weak bands due to the

skeletal modes, S, usually occupy the range $1150-950\text{cm}^{-1}$ (242). These bands are much stronger in the spectra of molecules such as the straight chain alcohols where the participation of the polar C-O bond in the skeletal vibrations causes a marked increase in the intensity of these bands (267). In alcohols the majority of the skeletal frequencies lie between about 1070cm^{-1} and 950cm^{-1} . Bands assigned to skeletal vibrations are found in n-C₂₄H₅₀ in the range $1121-1038\text{cm}^{-1}$ (29) are of weak intensity and have dichroisms parallel to the chain axis although a very weak band at 1051 assigned to a skeletal vibration has a perpendicular dichroism. A series of weak and very weak parallel bands is observed in the spectra of C₁₀PO (figure 44) in the range $1121-962\text{cm}^{-1}$ and these have been assigned tentatively to skeletal vibrations. In this spectrum a band at 943cm^{-1} of medium intensity also shows a parallel dichroism and this has been assigned to a skeletal vibration since its intensity may have been increased by the presence of the polar phosphoryl group. Similarly bands in the range $1124-943\text{cm}^{-1}$ in the polycrystalline spectrum of C₁₂PO (figure 45) have been assigned to skeletal vibrations.

(p) Bands due to $\rho(\text{CH}_2)$ occur in long chain compounds in the range $1050-720\text{cm}^{-1}$ (267). The set of bands due to $\rho(\text{CH}_2)$ is more prominent in the spectra of n paraffins than in the spectra of polymethylene compounds particularly those with polar groups (267). The lower limit of the distribution is well defined and occurs at approximately 720cm^{-1} (267). A band associated with $\delta(\text{CH}_2)$ is usually found in the region of 1460cm^{-1} . It has already been mentioned that pairs of bands occur for $\delta(\text{CH}_2)$ and the lower limit of $\rho(\text{CH}_2)$ in long chain compounds with orthorhombic chain packing. In addition to the pairs of

bands observed in the $C_{10}PO$ spectrum (figure 44) for $\delta(CH_2)$ and $\rho(CH_2)$ at $1473cm^{-1}$, $1464cm^{-1}$ and $727cm^{-1}$, $719cm^{-1}$ pairs of bands are observed at the same position in the spectrum of $C_{12}PO$ (figure 45). It therefore appears that the chains are similarly packed in an orthorhombic sub-cell in both cases.

In the polarized spectra of the B form of octadecanoic acid (35) bands associated with $\rho(CH_2)$ in the region $991-733cm^{-1}$ possess perpendicular dichroisms. In the polarized spectra of $C_{10}PO$ no further bands occur with perpendicular dichroisms. This is not surprising since as previously stated only a small perpendicular dichroism is observed for the strong $\rho(CH_2)$ band at $719cm^{-1}$ in the polycrystalline spectrum of $C_{10}PO$ and therefore even smaller perpendicular dichroisms might be expected for weaker $\rho(CH_2)$ bands. Weak bands at $780cm^{-1}$ and $735cm^{-1}$ which are seen as very weak bands in the unpolarized single crystal spectrum of $C_{10}PO$ (figure 44) and show no observable dichroism have been assigned as further $\rho(CH_2)$ components. Weak bands at $781cm^{-1}$ and shoulders at $735cm^{-1}$ and $730cm^{-1}$ in the spectrum of $C_{12}PO$ have been similarly assigned to $\rho(CH_2)$.

(q) A band occurs about $890cm^{-1}$ in the spectra of even n paraffins of C_{12} chain length and above (242). This band is said to consist of a mixture of CH_3 in-plane rocking and stretching of terminal C-C bonds (242). In the shorter even members two components are observed, one extremely weak whilst the other is quite strong. Two components of $\rho(CH_3)$ are also observed in the spectra of even and odd chain length alcohols (13).

In the spectrum of n- $C_{10}H_{22}$ (242) a medium band is observed at $897cm^{-1}$ with an extremely weak shoulder at $904cm^{-1}$ and these have been assigned to $\rho(CH_3)$. Also in the spectrum of n- $C_{12}H_{26}$ (242) a medium intensity band associated with $\rho(CH_3)$ is observed

at 893cm^{-1} although two very weak bands have been assigned to $\rho(\text{CH}_3)$ at 878cm^{-1} and 891cm^{-1} in $\text{C}_{12}\text{H}_{25}\text{OH}$ (13).

A medium intensity band at 887cm^{-1} in the spectrum of $n\text{-C}_{24}\text{H}_{50}$ (29) shows a parallel dichroism as does a weak band at 894cm^{-1} in the spectrum of the B form of octadecanoic acid (35). These bands have been assigned to $\rho(\text{CH}_3)$ rocking parallel to the skeletal planes.

A parallel band of weak intensity is observed in the polarized spectra of C_{10}PO (figure 44) at 897cm^{-1} and this band has been assigned to $\rho(\text{CH}_3)$ rocking parallel to the skeletal planes. In the spectrum of C_{12}PO (figure 45) a medium intensity band is observed at 890cm^{-1} and this has been assigned similarly to $\rho(\text{CH}_3)$.

Table XI Assignments of liquid and crystalline C₁₀PO

Liquid (cm ⁻¹)	Intensity ^a	Crystal (cm ⁻¹)	Intensity ^a	Polarization ^b	Interpretation ^c
		2987	w	1	$\nu_a(\text{CH}_3)$
2981	w	2980	w	1	$\nu_a(\text{PCH}_3)$
		2963	sh	-	$\nu_a(\text{CH}_3)$
2955	m	2955	m	1	$\nu_a(\text{CH}_3)$
		2931	s	11	$\nu_a(\text{CH}_2)$
2923	s	2922	s	-	} combination bands
2899	m.sh.	2900	m.sh.	1	
2873	m.sh.	2873	m	1	$\nu_s(\text{CH}_3)$
2855	m.s.	2851	s	1	$\nu_s(\text{CH}_2)$
		1473	m.sh.	-	} $\delta(\text{CH}_2)$
1465	m	1464	m.s.	1	
1456	m	1456	m.sh.	1	$\delta(\text{CH}_3)$
		1449	w	1	$\delta_a(\text{PCH}_2)$
1437	w	1437	w	1	} $\delta_a(\text{PCH}_3)$
1427	w	1425	w	11	
1418	v.w.	1418	w	11	
		1408	w	1	
1374	v.w.	1374	v.w.	11	$\delta(\text{CH}_3)$
		1355	v.w.	11	$\delta_w(\text{CH}_2)$
1343	v.w.				
		1339	v.w.	11	$w(\text{CH}_2)$
1335	v.w.				
1299	m	1299	v.s.	1	} $\delta_s(\text{PCH}_3)$
		1290	m	1	
1287	m.s.	1287	v.s.	11	} $\begin{matrix} T(\text{CH}_2) \\ W(\text{CH}_2) \\ T(\text{CH}_2) \\ W(\text{CH}_2) \\ T(\text{CH}_2) \\ T(\text{CH}_2) \end{matrix}$
		1269	v.w.	1	
		1258	v.w.	11	
1238	v.w.sh.	1239	v.w.	1	
1224	w.sh.	1223	w	11	
		1206	v.w.	1	
		1190	w	1	
1180	s.br.	1168	s(br)	1	
		1156	s(br)	1	} $\nu(\text{P=O})$
		1136	w.sh.	1	
1117	v.w.	1121	w	-	s
		1062	v.w.	11	s
1058	v.w.br.	1052	v.w.	-	s
		1037	v.w.	-	s
		1017	v.w.	11	s
		1008	v.w.	11	s
		996	v.w.	11	s
		978	v.w.	11	s
		962	w	11	s
		943	m	11	s
935	m.s.				
		919	m	1	$\rho(\text{PCH}_3)$
894	w.br.	897	w	11	$\rho(\text{CH}_3)$
		868	m	11	$\rho(\text{PCH}_3)$
858	w.br.				
		853	v.w.	11	

cont.

Table XI Assignments of liquid and crystalline C₁₀PO

Liquid (cm ⁻¹)	Intensity ^a	Crystal (cm ⁻¹)	Intensity ^a	Polarization ^b	Interpretation ^c
		821	w	11	$\nu_a(\text{PC})$
776	v.w.br.	780	v.w.	-	$\rho_a(\text{CH}_2)$
		744	m	11	$\nu_a(\text{PC})$
736	w.br.	735	w.sh.	-	$\rho_a(\text{CH}_2)$
		727	m	-	}
725	v.w.	719	s	1	
708	v.w.	676	v.w.		$\nu_s(\text{PC})$

Table XII Assignments of liquid and crystalline $C_{12}PO$

Liquid (cm^{-1})	Intensity ^a	Crystal (cm^{-1})	Intensity ^a	Interpretation ^c
		2990	w	$\nu_a(CH_2)$
2982	w	2981	w	$\nu_a(PCH_2)$
		2963	sh	$\nu_a(CH_3)$
2956	m	2954	m	$\nu_a(CH_3)$
		2934	s	$\nu_a(CH_2)$
2926	s	2923	s	} combination bands
		2900	m.sh.	
2873	m	2874	m	$\nu_s(CH_3)$
2851	s	2850	s	$\nu_s(CH_2)$
		1473	m	} $\delta(CH_2)$
1465	m	1464	s	
1460	m	1458	m	$\delta_a(CH_3)$
		1445	w	$\delta(PCH_2)$
		1437	w	} $\delta_a(PCH_3)$
1425	v.w.	1425	w	
1412	v.w.	1418	w	
		1408	w	
1376	v.w.	1374	v.w.	$\delta_s(CH_3)$
1370	v.w.			
1352	v.w.	1356	v.w.	$\nu(CH_2)$
		1328	v.w.	$\nu(CH_2)$
1299	m.s.	1297	v.s.	} $\delta_s(PCH_3)$
		1294	v.s.	
1292	m.s.	1290	m.sh.	
		1279	w	
		1272	w	} $\nu(CH_2)$ and $\tau(CH_2)$
1256	w	1254	w	
		1245	v.w.	
		1225	w	
		1217	m	
		1200	w	
		1190	s	$\nu(CH_2)$
1190	s.br.	1166	m.s.br.	$\nu(P=O)$
		1136	w	
1117	w	1124	w	s
		1076	v.w.	s
1058	w	1063	w	s
		1050	v.w.	s
		1027	v.w.	s
		1020	w	s
1008	v.w.	1008	v.w.	s
987	v.w.	983	w	s
		980	w.sh.	s
		943	m.s.sh.	s

cont.

Table XII Assignments of liquid and crystalline $C_{12}PO$

Liquid (cm^{-1})	Intensity ^a	Crystal (cm^{-1})	Intensity ^a	Interpretation ^c
935	m.s.	935	s	
		917	m	$\rho(PCH_3)$
898	v.w.br.	890	m	$\rho(CH_3)$
		870	m	$\rho(PCH_3)$
860	w.br.	850	m	
		819	w	$\nu_a(PC)$
		781	v.w.	$\rho(CH_2)$
778	v.w.br.	752	m.sh.	
		746	m.s.	$\nu_a(PC)$
738	w.br.	735	m	$\rho(CH_2)$
		730	m.sh.	$\rho(CH_2)$
723	sh.	727	m.s.	$\rho(CH_2)$
		719	m.s.	$\rho(CH_2)$
709	v.w.	679	v.w.	$\nu_s(PC)$

- a. For the meaning of the abbreviations used, see footnote to table VIII.
- b. The symbols l and ll indicate that the bands are polarized perpendicular and parallel to the alkyl chain axis.
- c. The meaning of the symbols used are as follows:

ν , stretching

δ , bending

W , wagging

T , twisting

s. , skeletal

ρ , rocking

Table XIII X-ray long spacings of $C_{10}PO$ and $C_{12}PO$

Phosphine oxide	$d(\text{\AA})$
$C_{10}PO$	25.5
$C_{12}PO$	28.9
$C_{10}PO + 0.5$ mole fraction of D_2O	25.5

CHAPTER IV

PHASE BEHAVIOUR

(I) Results

T_{pen} has been determined for MG11 and this value along with values determined by Peel (209) and Lawrence et al (79) are given in table XIV.

Table XIV

<u>1-monoglyceride</u>	<u>T_{pen} ($^{\circ}\text{C}$)</u>	<u>Reference</u>
MG8	12.5	209
MG10	30.0	209
MG11	35.0	This work
MG12	41.0	209
MG14	49.5	79
MG18	65.0	79, 209

The phase diagrams of the MG11/ D_2O and $\text{C}_{10}\text{PO}/\text{H}_2\text{O}$ systems are shown as figures 49 and 50. Transition temperatures for the samples studied are given in tables XV and XVI. The phase diagram of $\text{C}_{10}\text{PO}/\text{H}_2\text{O}$ can be compared with that determined by Hermann et al (141) shown in figure 51, whilst that of MG11/ D_2O can be compared with that determined by Lawrence et al (133) for MG12/ H_2O and Peel (209) for MG8/ D_2O shown in figures 22 and 52 respectively.

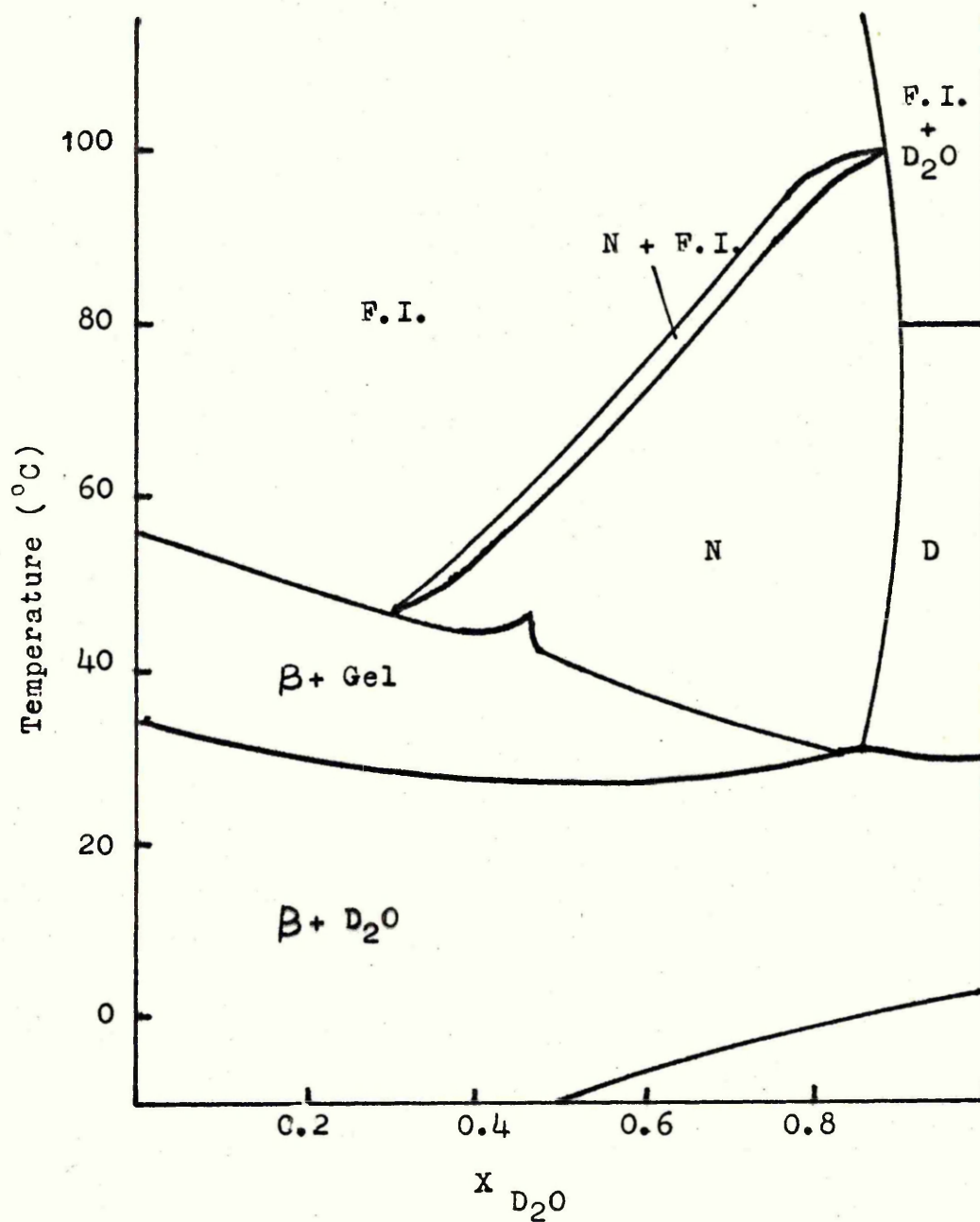


Figure 49.

1- monoundecanoin/D₂O phase diagram.

N - Neat phase

D - Dispersion

F.I.- Fluid isotropic

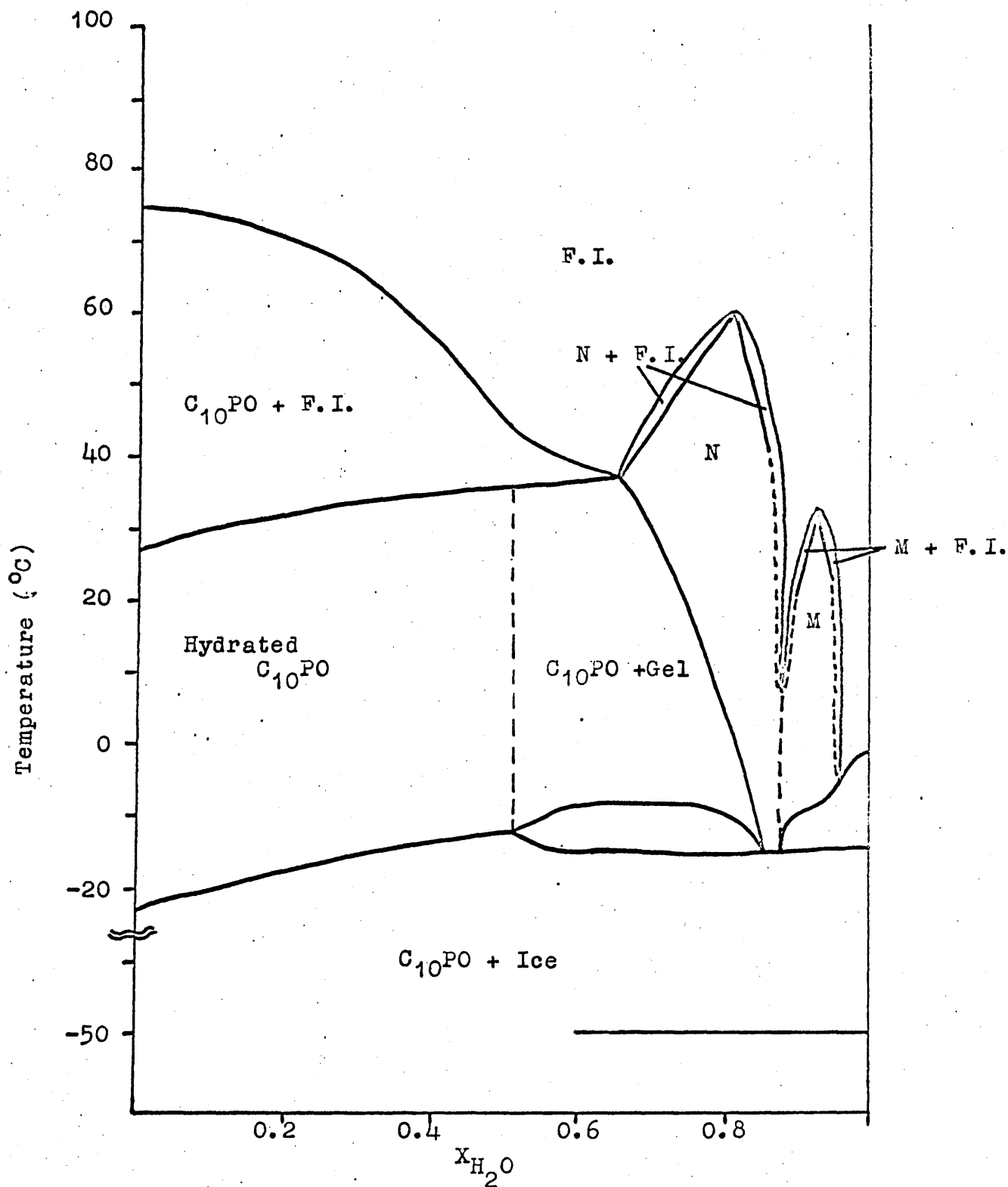


Figure 50.

Dimethyldecylphosphine oxide/H₂O phase diagram

M - Middle phase

See figure 49 for other abbreviations.

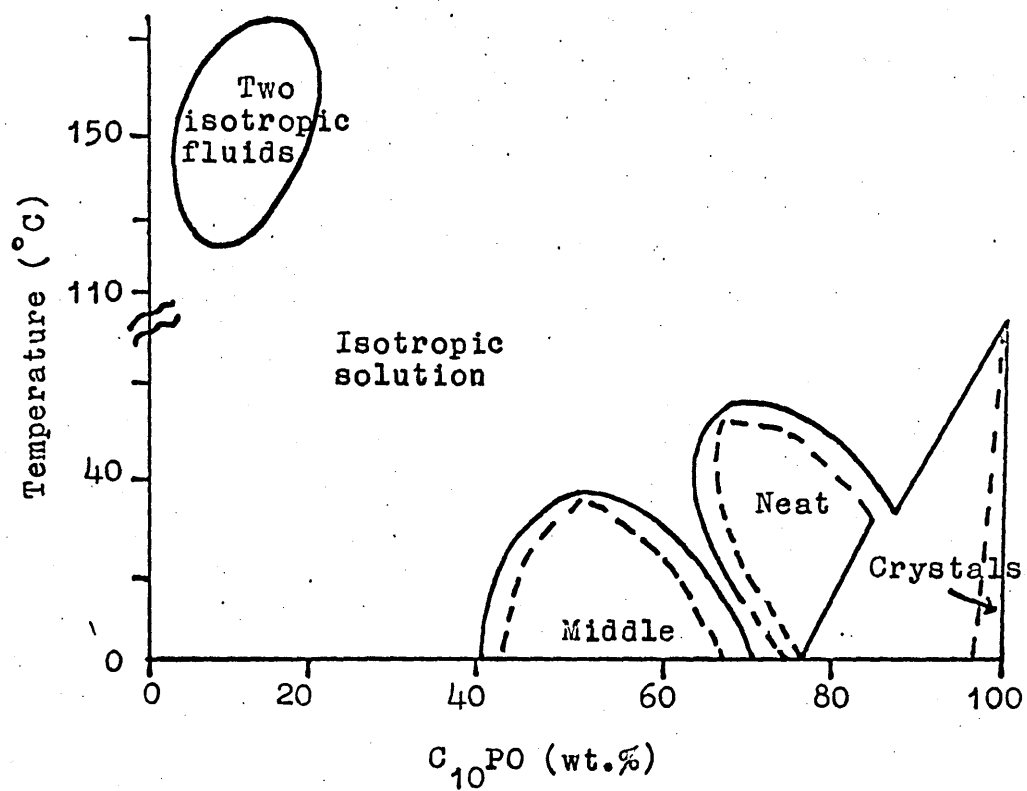


Figure 51.

Dimethyldodecylphosphine oxide($C_{10}PO$)/ H_2O
phase diagram.(141)

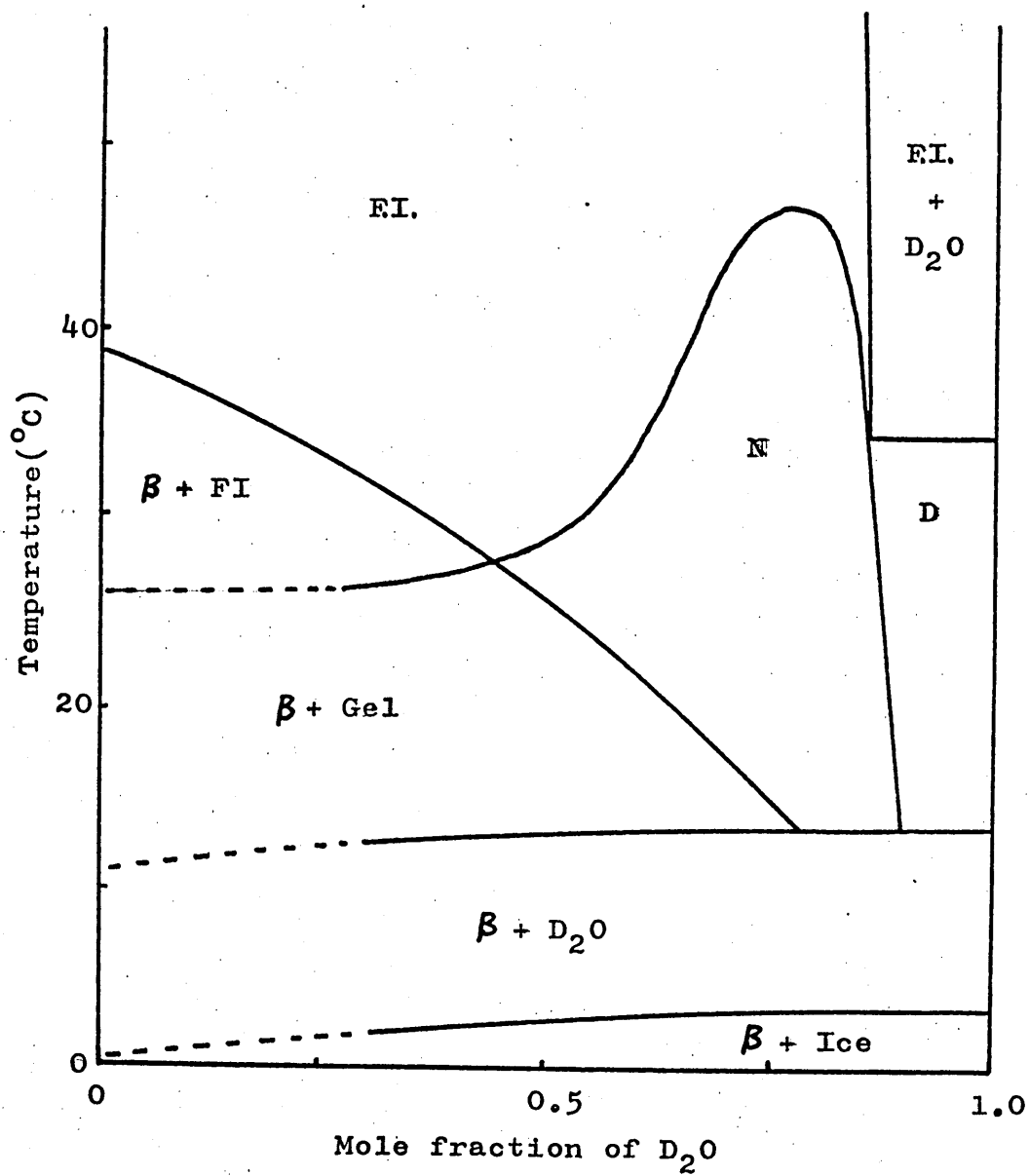


Figure 52.

1-monooctanol/ D_2O phase diagram.(209)

(II) Discussion

(i) MG11/D₂O system

(a) In figure 53 T_{pen} for the β form is shown as a function of alkyl chain length for the six 1-monoglycerides shown in table XIV. T_{pen} does not appear to alternate or correlate with any transition in the anhydrous 1-monoglycerides. However in the cases of MG8 and MG11 T_{pen} correlates well with the lowest temperature at which the l.c. phase in the 1-monoglyceride/D₂O systems is stable as shown by the phase diagrams (figures 52 and 49).

Since water is observed to penetrate along the edges of the crystals it is assumed that penetration is occurring between layers of polar groups.

T_{pen} seems likely to be that temperature at which thermal motion of the 1-monoglyceride molecules is great enough to cause a breakdown of the H-bonding system between the hydroxyl groups in the crystal lattice and the subsequent incorporation of water into a new and more stable H-bonding system. At the same time the thermal motion has reduced the Van der Waals' interaction between alkyl chains so as to allow them to move laterally and longitudinally to expand the crystal lattice for water to be incorporated.

Lawrence et al (79) has also determined T_{pen} values for the penetration of water into the α phases of two 1-monoglycerides and these are also shown in figure 53. T_{pen} for the α phases occur at a lower temperature than those for the β form.

In the α phase the alkyl chains are rotating about their long axes and therefore the spacing between adjacent alkyl chains will be greater than in the β form. Therefore the H-bonding system between the hydroxyl groups will be more dynamic perhaps

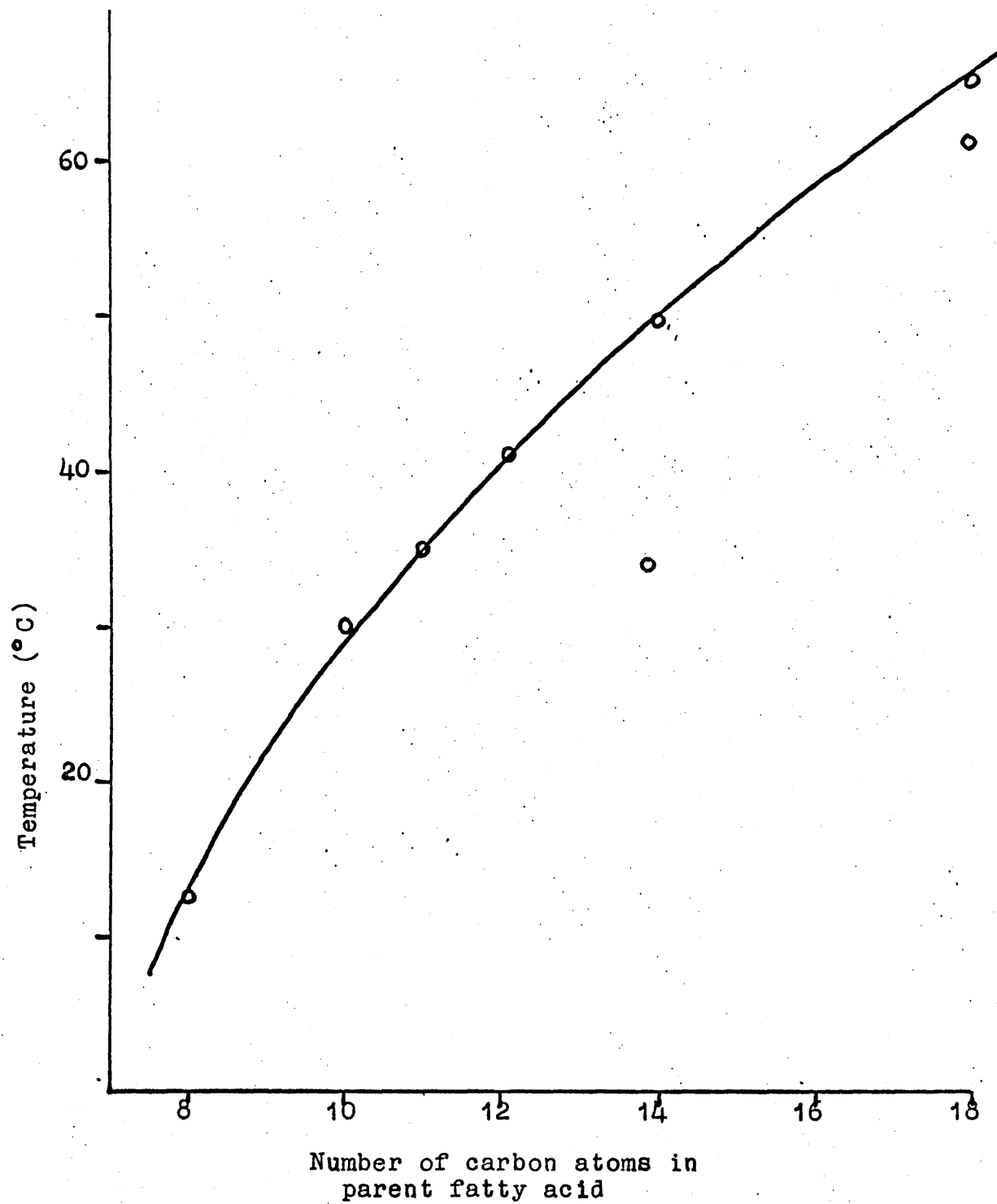


Figure 53.

Tpen v's. 1-monoglyceride chain length.

therefore allowing penetration of water to occur at a lower temperature.

(b) The main features of the MG11/D₂O phase diagram are similar to those of the part phase diagram of MG12/H₂O determined by Lawrence et al (133) and that of MG8/D₂O determined by Peel (209) (figures 22 and 52).

The solid β modification melts at 56.5°C and addition of water lowers this to the eutectic minimum at 43°C after which the gel to l.c. phase boundary rises to a peak at 0.47 mole fraction indicating the formation of a monohydrate. This sort of behaviour has been previously observed by Lawrence et al (133) (figure 22) in the case of MG12/H₂O. Further evidence of the existence of this hydrate was found in the following way. Samples containing below 0.47 mole fraction of D₂O were homogenised as isotropic fluid and then cooled to temperatures below -50°C using D.S.C. No transition was observed either on cooling or the subsequent heating runs, which could be associated with D₂O freezing or melting (figure 54). However above this mole fraction of D₂O peaks were observed (figure 54), the melting peak moving steadily from -11.5°C at 0.475 mole fraction of D₂O and increasing in size.

The gel phase is thought by Larsson (180) to have the same structure as the α crystal form of 1-monoglycerides. If this is so, it is possible that at certain water contents the structure of the gel phase may have an optimum stability as reflected in the higher melting point. This sort of thing occurs in the α phases of long chain alcohols (132) which take up a quarter mole of water with an increase in melting point of up to 3°C.

The shorter chain alcohols do not show this behaviour and therefore stable hydrated crystals would not be expected to form

Figure 54.

D.S.C. chart showing various MG11
mole fractions heated from -60 C



in the MG8/D₂O system since the hydrocarbon chains are probably too short for sufficiently strong Van der Waals forces to stabilize these crystals as they do in MG11 and MG12. Infact Peol (209) observed a 'free' D₂O peak on the D.S.C. at all mole fractions of D₂O.

(c) The changes occurring during a heating run on samples of MG11 with low D₂O content are firstly a transition to a gel phase and β crystals between 27°C and 34°C. This gel phase melts at a temperature which decreases from 56.5°C as the amount of D₂O is increased up to 0.3 mole fraction of D₂O giving a fluid isotropic phase. The fact that no further transition is observed before finally melting to the fluid isotropic phase as is observed in the MG8/D₂O phase diagram at low D₂O content (figure 52) may be due to increased stability of the gel phase with increased chain length.

Samples above 0.3 but below 0.47 mole fraction of D₂O transform from the gel phase to the neat l.c. phase, N. This takes place at a temperature which initially shows a small decrease from 47.5°C to 43°C between 0.3 and 0.4 mole fraction of D₂O, but finally rises to a peak at a temperature of 45.4°C and 0.47 mole fraction of D₂O.

(d) Above 0.47 mole fraction of D₂O the first change which occurs is the melting of D₂O ice initially at -11.5°C and increasing to 3°C at a mole fraction of 0.98 and then the penetration of the liquid D₂O into the hydrate crystals at temperatures between 27°C and 30°C to give a gel phase with crystalline inclusions. This gel phase then transforms to the l.c. phase, N, at a temperature which decreases to 32.5°C at 0.825 mole fraction of D₂O.

(e) At higher D₂O contents the β crystals and D₂O

transform directly to the l.c. phase, N, at 32.5°C at 0.825 mole fraction of D_2O without forming an intermediate gel phase. In the MG8/ D_2O system the position at which this occurs, 0.8 mole fraction of D_2O , corresponds to a distinct position of maximum melt indicating possibly that an MG8.4 D_2O aggregate is particularly stable although there is no evidence from the N.M.R. and phase studies (209) of a solid tetrahydrate.

In the case of the MG11/ D_2O system the melting point of the l.c. phase, N, increases with increasing water content until the system forms two phases at 0.86 mole fraction of D_2O . The maximum melting point is 99.0°C and is of a lower value than 108°C for MG10/ H_2O (180) and 115°C for MG12/ H_2O (133) systems. It is not clear why the maximum melting point in the case of the MG11/ D_2O system should be so low. However it may be due in part to some sort of chain length alternation effect in addition to the use of D_2O rather than H_2O .

(f) From 0.3 to 0.87 mole fraction of D_2O the l.c. phase, N, partially melts to give a two phase region labelled, N + F.I., consisting of regions of l.c. phase, N, floating in fluid isotropic, F.I. The maximum temperature range over which this region is stable is 4°C . This two phase region melts to give a fluid isotropic phase. This transition can only be observed visually and is completely undetectable on the D.S.C.

(g) For samples containing more than 0.88 mole fraction of D_2O , at T_{pen} , a dispersion is formed. Larsson (180) concluded from X-ray diffraction and optical microscopy studies on the MG8/ H_2O system that the structure consists of concentric bimolecular shells of 1-monoglyceride molecules alternating with water shells.

At 79.5°C the dispersion becomes two liquids, fluid

isotropic and D_2O . The phase boundary between fluid isotropic and fluid isotropic + D_2O rises almost vertically from the composition $MG11 + 0.91$ mole fraction of D_2O . The steepness of this phase boundary is indicated by the fact that a sample containing 0.85 mole fraction of D_2O became two phase at $115^\circ C$ whilst a sample containing 0.83 mole fraction of D_2O was still one phase at $150^\circ C$.

(ii) $C_{10}PO/H_2O$ system

The $C_{10}PO/H_2O$ phase diagram was determined in order to discover the exact range of stability of the neat and middle l.c. phase regions since we wished to carry out infra-red investigations in these regions.

The $C_{10}PO/H_2O$ phase diagram is similar to that determined by Hermann et al (141) above $0^\circ C$ except that the phase marked 'two isotropic fluids' (figure 51) was not investigated in this work so it has not been included in the phase diagram. The phases below $0^\circ C$ have not been reported previously. Certain other points have been noted and are discussed below.

(a) The solid $C_{10}PO$ melts at $75^\circ C$ and addition of water lowers this to a eutectic minimum of $37^\circ C$ at 0.66 mole fraction of H_2O . Above this concentration of H_2O a neat l.c. phase, N, is formed. The phase boundary between the l.c. phase, N, and the fluid isotropic phase rises to a peak at 0.8 mole fraction of H_2O whilst that between the l.c. phase, N, and gel descends to a minimum at $-14^\circ C$ and 0.86 mole fraction of H_2O . This latter phase transition has only been observed visually.

Samples containing less than 0.46 mole fraction of H_2O were cooled below $-60^\circ C$ using D.S.C. and one exotherm was observed at $-37^\circ C$ which increased in size with increasing H_2O content.

For samples containing 0.46 to 0.52 mole fraction of H_2O an additional minute exotherm was observed at approximately $-13^{\circ}C$. When these samples were heated only one endotherm was observed at $-17^{\circ}C$ at 0.2 mole fraction of H_2O rising to $-12^{\circ}C$ at 0.52 mole fraction of H_2O and the size of the peak increased with increasing H_2O content. Between 0.52 and 0.86 mole fraction of H_2O , two exotherms were observed upon cooling at approximately $-12^{\circ}C$ and $-34^{\circ}C$, the higher temperature peak increasing in size relative to the lower temperature peak as the amount of H_2O increased. Two endotherms were then observed upon subsequent heating at $-14.5^{\circ}C$ and $-8.5^{\circ}C$, the high temperature peak increasing in size relative to the low temperature peak as the amount of H_2O increased. At 0.86 mole fraction of H_2O only a single exotherm was observed at $-32^{\circ}C$ on cooling and an endotherm at $-14^{\circ}C$ on heating.

All this indicates that up to 0.52 mole fraction of H_2O the first change taking place during a heating run is concurrent melting and penetration of H_2O into the $C_{10}PO$ lattice in the vicinity of the polar group giving rise to a hydrated crystalline solid. Between 0.52 - 0.86 mole fraction of H_2O it is possible that the 1:1 hydrated solid is produced first at $-14.5^{\circ}C$ followed at $-8.5^{\circ}C$ by a further melt and concurrent penetration of excess H_2O to produce a gel phase.. At 0.86 mole fraction transformation from crystalline solid + ice takes place directly to the neat l.c. phase, N, and this has been confirmed visually.

(b) The changes occurring at higher temperatures during a heating run on samples containing less than 0.52 mole fraction of H_2O are a transformation between $33^{\circ}C$ and $36^{\circ}C$ to crystals and fluid isotropic. Samples finally became fluid isotropic at a temperature which decreased with increasing H_2O

content. Between 0.52 and 0.66 mole fraction of H_2O , the gel phase goes through the same two transformations.

(c) The maximum melt of the l.c. phase, N, occurs at 0.8 mole fraction of H_2O indicating that a $C_{10}PO:4H_2O$ aggregate is particularly stable, although there is no evidence from the phase studies of a solid tetrahydrate.

(d) The $C_{10}PO/H_2O$ system shows a region of middle l.c. phase, M, existing between 0.88 and 0.96 mole fraction of H_2O . It has been shown by X-ray diffraction studies (190) that the middle phase structure consists of a two dimensional array of equidistant cylinders or rods arranged in a hexagonal form, the alkyl chains being located in the interior of the rods and the water filling the gaps between. However there is evidence (194) that in certain systems the reverse structure does exist.

(e) At 0.88 mole fraction of H_2O the first transition which occurs upon heating is directly from the crystalline $C_{10}PO + H_2O$ ice to the l.c. phase, M, at $-14^\circ C$ and this transition can be seen by D.S.C. as well as visually. The l.c. phase, M, then melts at $11^\circ C$ to give a fluid isotropic phase but the transition does not show on the D.S.C. For samples containing this mole fraction of H_2O no two phase region, M + F.I., was detected. At $24^\circ C$ zones of l.c. phase, N, appear in the fluid isotropic phase as the system passes through the two phase region, N + F.I., and disappears at $34^\circ C$.

(f) The two phase region, N + F.I., appears at both sides of the peak of the l.c. phase, N, at 0.8 mole fraction of H_2O and can only be seen visually. However it was not observed in the case of samples containing 0.87 mole fraction of H_2O (figure 50).

Similarly the two phase region, M + F.I., appears at both

sides of the peak of the l.c. phase, M, at 0.925 mole fraction of H_2O . In this case no two phase region was observed in samples containing 0.88 or 0.95 mole fraction of H_2O .

(g) No direct transition has been observed visually or on D.S.C. of the l.c. phase M to N and the transition is only drawn in tentatively as an almost vertical dotted line.

(h) Samples containing more than 0.88 mole fraction of H_2O were cooled below $-60^{\circ}C$ using D.S.C. and two exotherms were observed at approximately $-12^{\circ}C$ and $-34^{\circ}C$, the higher temperature peak increasing in size relative to the lower temperature peak as the amount of H_2O was increased. Two endotherms were observed upon subsequent heating, one at $-14^{\circ}C$ and the other at $-9^{\circ}C$ rising to $-0.5^{\circ}C$ and increasing in size relative to the lower temperature peak as the amount of H_2O increased. It would therefore appear that during heating runs the changes taking place here are firstly concurrent melting and penetration of H_2O into the $C_{10}PO$ lattice to produce the 1:1 hydrated solid. This is followed by further melting and penetration of excess H_2O to produce the l.c. phase, M, up to 0.96 mole fraction of H_2O where transformation directly to the fluid isotropic phase takes place. The latter transition can be observed visually.

When the H_2O content is increased from 0.88 mole fraction the phase boundary between the two phase region, M + F.I., and the fluid isotropic phase rises to a maximum at $33^{\circ}C$ at 0.925 mole fraction of H_2O . This boundary then decreases to a shallow eutectic minimum of $-5^{\circ}C$ at 0.96 mole fraction of H_2O .

(i) For all samples containing more than 0.61 mole fraction of H_2O an endotherm is observed at $-49.5^{\circ}C$ for all heating runs. It is thought that this transition may be due to a polymorphic transition at this temperature. This transition cannot be seen in the thermograms of anhydrous $C_{10}PO$.

TABLE XV

Data points for Mg11/D₂O phase diagram.

x_{D_2O}		Transition Temperatures (°C)			
0.12		32.5	51.8		
0.29		29.5	48.2		
0.31		29.2	47.0		
0.36		28.0	43.5	49.7	51.5
0.44		27.5	43.0	54.5	59.5
0.47		27.2	45.4	58.0	62.5
0.475	-11.5	27.0	42.8	58.3	62.8
0.49	-11.0	27.0	42.0	60.3	64.0
0.52	-10.3	27.5	41.4	62.5	66.5
0.525	- 8.6	27.3	40.5	63.1	66.4
0.55	- 7.5	27.6	40.8	65.3	68.6
0.62	- 5.2	27.7	37.5	74.0	78.0
0.71	- 3.5	28.0	33.0	84.0	88.0
0.79	- 1.8	30.0	32.0	92.5	95.5
0.825	- 1.2	32.5		96.0	98.5
0.85	- 0.8	32.5		97.8	99.0 115
0.87	- 0.6	32.4		97.4	99.2
0.88	0.3	31.5	41.0		98.6
0.89	0.5	30.5	45.0		99.0
0.90	1.3	30.0	50.0		99.0
0.91	1.8	29.8		79.5	
0.93	2.7	29.6		80.0	
0.95	2.8	30.0		79.5	
0.97	2.9	29.0		79.5	
0.98	3.0	29.7		79.5	

TABLE XVI

Data points for $C_{10}PO/H_2O$ phase diagram.

x_{D_2O}	Transition Temperature ($^{\circ}C$)					
0.20		-17.0	33.0	72.0		
0.31		-15.0	34.5	63.5		
0.39		-14.5	35.0	62.5		
0.46		-12.0	35.5	48.0		
0.52		-12.0	36.0	42.0		
0.61	-49.5	-14.5	-8.0	37.0	40.0	
0.66	-49.5	-14.0	-8.5	37.0		
0.70	-49.5	-14.5	-8.5	30.0	43.0	46.0
0.76	-49.5	-14.5	-8.5	17.0	53.0	56.0
0.80	-49.5	-14.5	-8.5	12.0		59.5
0.84	-50.0	-14.5	-8.5		54.0	57.5
0.86	-49.5	-14.0			45.0	48.0
0.87	-50.0	-14.5				
0.88	-49.5	-14.0		11.0		
0.895	-49.5	-14.5	-9.0	22.0	27.5	
0.925	-49.5	-14.0	-8.5		33.0	
0.94	-49.5	-14.0	-7.5	28.0	32.5	
0.95	-49.5	-14.0	-6.5		13.0	
0.96	-49.5	-14.0	-5.0			
0.97	-50.0	-14.0	-3.0			
0.98	-49.5	-14.0	-0.5			
0.99	-49.5	-14.5	-0.5			

- 150 -

CHAPTER V

HYDRATED DIMETHYLDECYLPHOSPHINE OXIDE

(I) Results

Infra-red spectra have been obtained of single crystal samples of $C_{10}PO$ containing up to 0.48 mole fraction of H_2O at the beam temperature and $-3^\circ C$. Unpolarized and polarized spectra of a sample containing 0.48 mole fraction of H_2O at the beam temperature are shown as figure 55. Also polarized and unpolarized spectra of the decoupled $\nu(OH)$ have been obtained at this mole fraction of H_2O at the beam temperature and these spectra are also shown in figure 55. Attempts were made to grow single crystals of samples containing higher mole fraction of H_2O but without success. Also attempts were made to obtain low temperature polarized spectra. The lowest temperature at which single crystal spectra were obtained was $-3^\circ C$.

The effect of temperature on a sample containing 0.48 mole fraction of H_2O has been studied. Figure 56 shows the absorption spectrum of this sample over the ranges $4000-3000cm^{-1}$ and $1300-1000cm^{-1}$ at $-13^\circ C$ and $-45^\circ C$ along with the spectra taken in these regions at the beam temperature.

(II) Discussion

(i) The X-ray long spacing values for the anhydrous and hydrated $C_{10}PO$ (table XIII) are identical and it is concluded that the introduction of water in the vicinity of the phosphoryl group has not affected the hydrocarbon chain packing to any observable extent.

This is born out by spin-lattice, T_1 , and spin-spin, T_2 , relaxation times which were obtained for the alkyl chain protons in the anhydrous and hydrated state of $C_{10}PO$. If upon addition of water any change in molecular motion in the frequency ranges

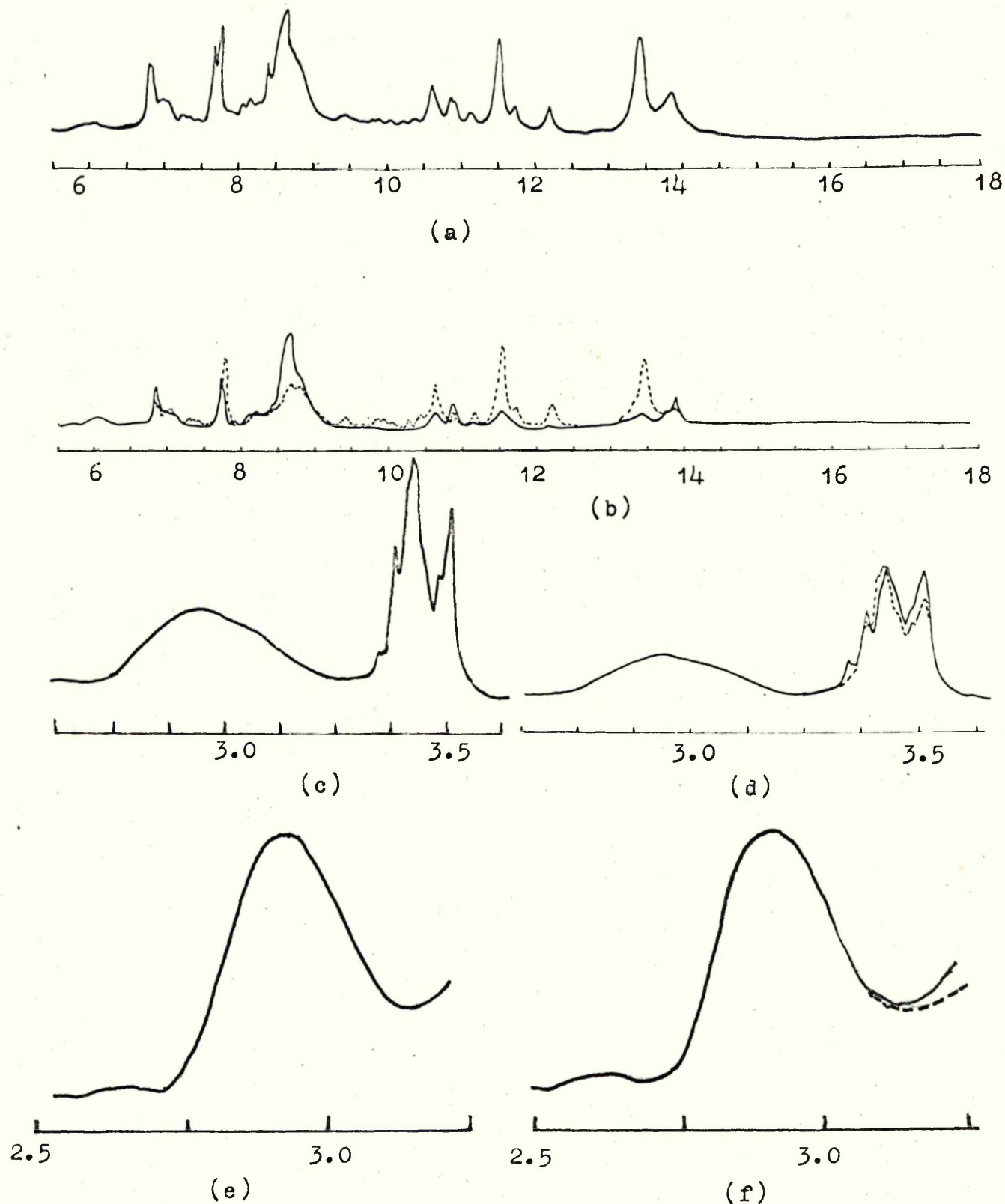


Figure 55.

Infra-red spectra of $C_{10}PO + 0.48$ mole fraction of H_2O at beam temperature, Wavelength unpolarized spectra (a) $6-18\mu$, (c) $2.625-3.625\mu$. Polarized spectra (b) $6-18\mu$, (d) $2.625-3.625\mu$. Also decoupled $\nu(OH)$ for this mole fraction at the same temperature (e) unpolarized, (f) polarized, Wavelength $2.5-3.25\mu$: electric vector parallel to chains ----, and perpendicular to chains —.

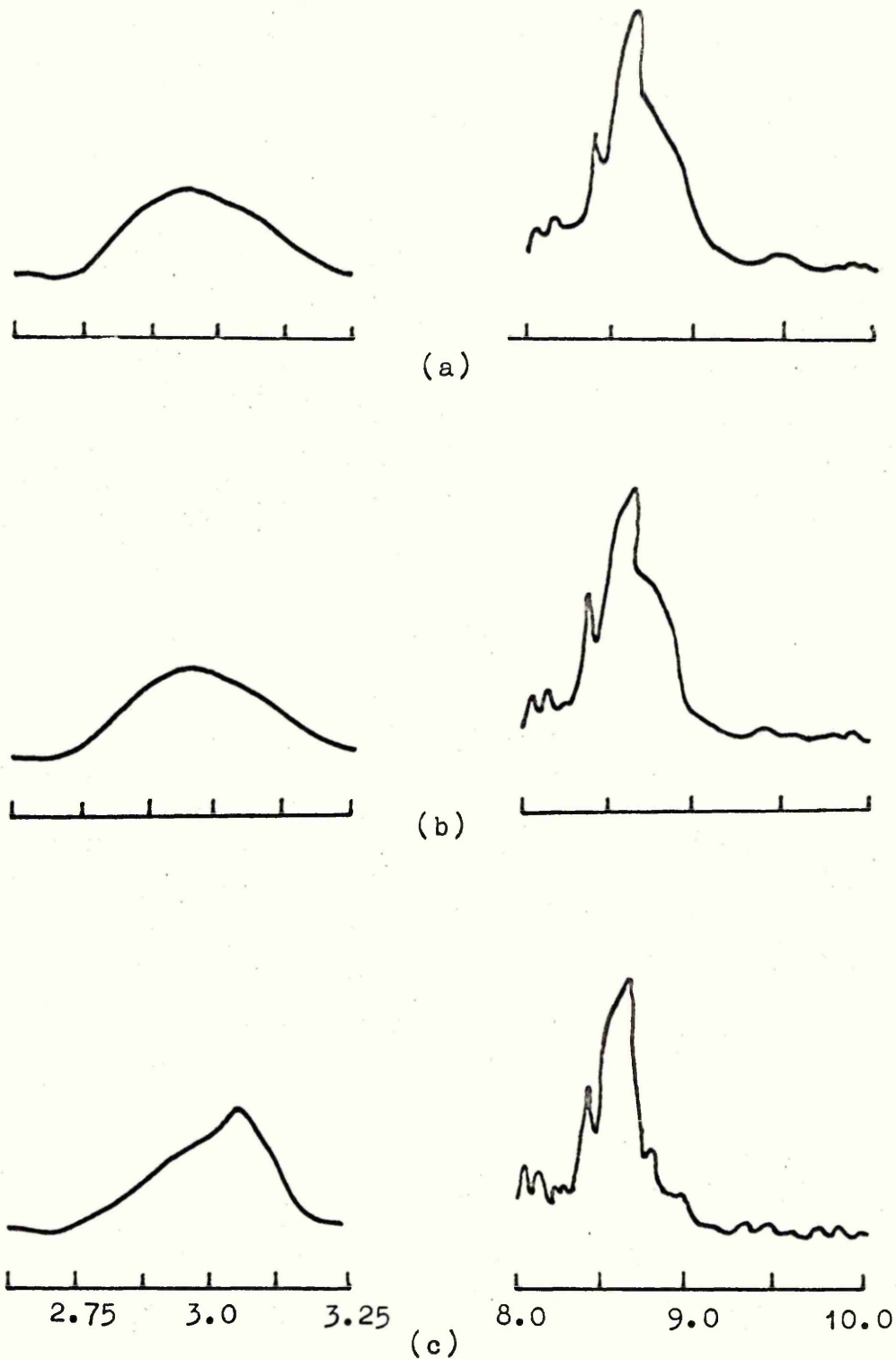


Figure 56.

$\nu(\text{OH})$ and $\nu(\text{P=O})$ bands in $\text{C}_{10}\text{PO} + 0.48$ mole fraction of H_2O at :-

- (a) beam temperature
- (b) -13°C
- (c) -45°C

Wavelength $2.625\text{--}3.25\mu$ and $8.0\text{--}10.0\mu$.

10^7 or 10^5 had occurred then this would have been reflected in an increase in the values of T_1 and T_2 relative to the anhydrous material. However the values for T_1 and T_2 of 0.7 seconds and 10 μ seconds respectively remained constant showing no apparent loosening had taken place.

The value of T_2 found here for both the anhydrous and hydrated material compares very favourably with the theoretical value of approximately 6 μ seconds for a hydrocarbon chain calculated from the theoretical line width of 15 gauss (271) using the standard relationship (272).

$$\text{Line width} = \frac{1}{\sqrt{2\pi} \cdot T_2}$$

T_1 and T_2 measurements for the methyl group protons adjacent to phosphorus show the same effect. Upon going from the anhydrous to hydrated form T_1 shows a marked increase from 50-150 μ seconds as does T_2 from 75-150 μ seconds. The dichroisms of bands associated with the various vibrational modes of these methyl groups are almost identical in the hydrated (figure 55) and anhydrous $C_{10}PO$ (figure 44).

The lengthening of the relaxation times is consistent with a greater freedom of motion of the methyl groups. This increase in motion does not appear to alter the observed dichroisms.

(ii) The infra-red spectra obtained for the hydrated material (figure 55) when compared with the anhydrous $C_{10}PO$ spectra (figure 44) also reinforce the conclusion that the addition of water has very little effect upon the structure of $C_{10}PO$. The general features of the spectra as to band position, relative intensity and dichroisms are the same. This also indicates that the hydrated crystal has formed with the molecules of $C_{10}PO$ having the same orientation relative to the polarized beam as those in the anhydrous case. However there are differences apparent

between the spectra as follows:-

(a) In the anhydrous $C_{10}PO$ spectrum (figure 44), at the beam temperature, strong broad bands associated with $\nu(P=O)$ are observed at 1168cm^{-1} and 1156cm^{-1} . In the spectrum of the hydrated material (figure 55) there is also a shoulder at 1138cm^{-1} which increases in intensity as the amount of H_2O is increased. This shoulder has been assigned to the H-bonded component of $\nu(P=O)$.

This shift of $\nu(P=O)$ to a lower frequency when participating in H-bond formation with a donor atom has been previously observed in solution (273-274) as well as in the solid state (142,265).

Goubeau et al (142) observed three bands in the spectrum of anhydrous trimethylphosphine oxide which they interpreted in terms of various phosphoryl dipole association species. Upon addition of water they observed five bands in the range $1175-1103\text{cm}^{-1}$ which they have interpreted in terms of the phosphoryl group H-bonded with water as shown in figure 57.

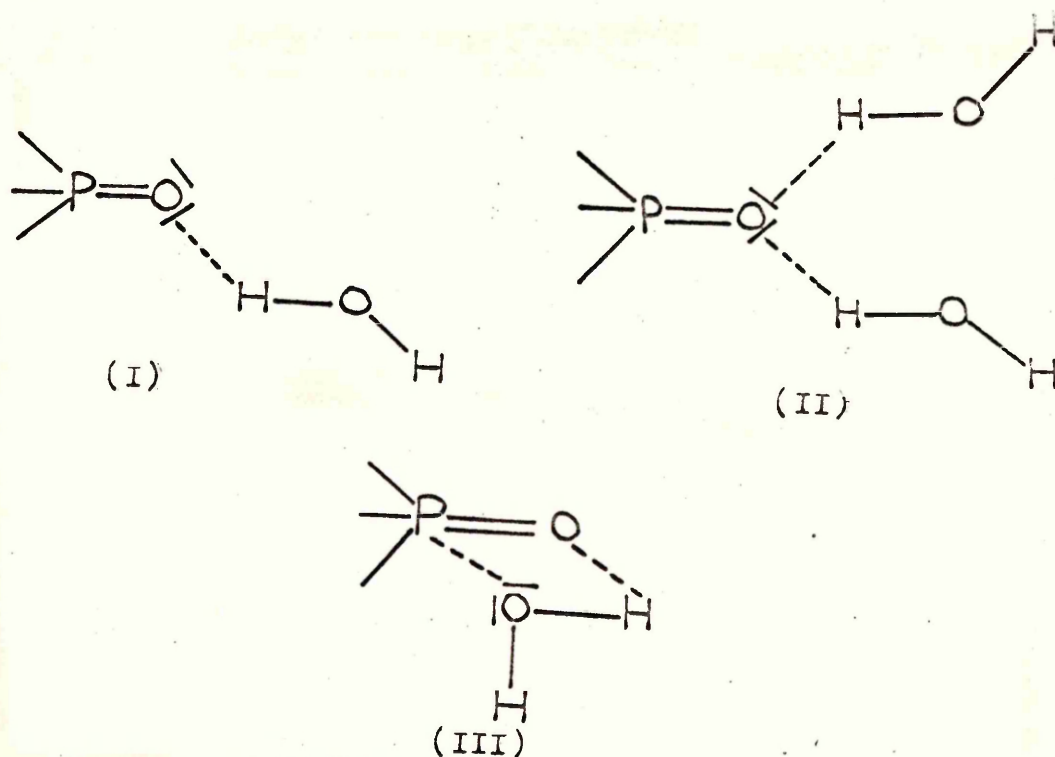


Figure 57.

In the spectrum of hydrated $C_{10}PO$ (figure 55) since the mole fraction of H_2O does not exceed 0.5, the low frequency shoulder at $1138cm^{-1}$ is probably due to the H-bonded species of the type shown as I and III in figure 57.

The dichroism observed for the shoulder at $1138cm^{-1}$ due to the H-bonded $\nu(P=O)$ is only very small in contrast to the large dichroisms shown by the stronger higher frequency $\nu(P=O)$ bands.

At a temperature of $-3^{\circ}C$ the bands at $1168cm^{-1}$ and $1156cm^{-1}$ remain in the same position but the shoulder moves to $1136cm^{-1}$. The dichroisms obtained at this lower temperature are almost identical with those at beam temperature.

(b) A very broad medium intensity $\nu(OH)$ band is observed at $3425cm^{-1}$ (figure 55) which is markedly asymmetric at $3306cm^{-1}$ in the hydrated $C_{10}PO$. This band does not show an observable dichroism (figure 55) even at the lower temperature of $-3^{\circ}C$.

A spectrum of liquid water has been obtained at beam temperature and $\nu(OH)$ from this spectrum is shown as figure 58. The band maximum occurs at $3408cm^{-1}$ and the band is extremely broad and markedly asymmetric at $3306cm^{-1}$.

The decoupled $\nu(OH)$ in the hydrated form of $C_{10}PO$ (figure 55) at the beam temperature, appears to have a single maximum at $3396cm^{-1}$ and is very broad with $\Delta\nu_{\frac{1}{2}}$ of $275cm^{-1}$. This band also shows no observable dichroism. In liquid water the decoupled $\nu(OH)$ band (figure 58) appears to have a single maximum at $3410cm^{-1}$ and is also broad with $\Delta\nu_{\frac{1}{2}}$ of $268cm^{-1}$.

No other bands associated with liquid water were observed in the hydrated spectrum of $C_{10}PO$.

From this data it would appear that the water incorporated in $C_{10}PO$ up to a mole fraction of 0.48 is in a liquid state.

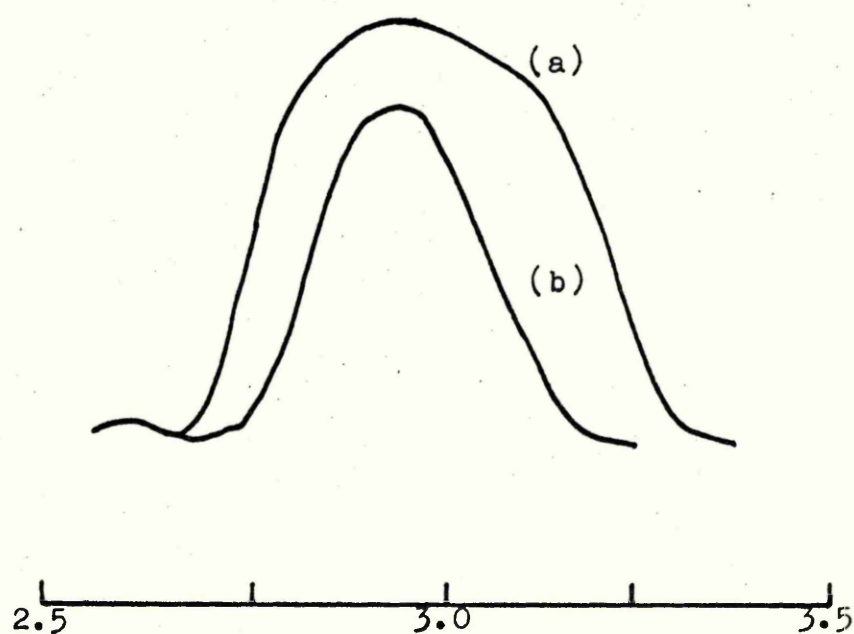


Figure 58.

$\nu(\text{OH})$ bands of liquid ^{water} at beam temperature: (a) coupled,
(b) decoupled. Wavelength $2.5\text{--}3.5\mu$.

However from the shift of the decoupled $\nu(\text{OH})$ band to lower frequency in the hydrated C_{10}PO spectrum compared to liquid water it does appear to have a distribution of H-bonds on the average stronger than in liquid water.

In the spectrum shown by Daasch et al (265) for trimethylphosphine oxide a strong band is observed at 3410cm^{-1} which is undoubtedly due to $\nu(\text{OH})$ of water incorporated in the phosphine oxide. This band appears to have shoulders at 3320cm^{-1} and 3500cm^{-1} . However this band is not mentioned in their paper.

Goubeau et al (142) observed a very strong band at 3260cm^{-1} which moves to 3400cm^{-1} as the amount of H_2O is increased. These bands again are not referred to in their paper.

(c) At a temperature of -13°C , $\nu(\text{OH})$ in the unpolarized spectrum of the hydrated C_{10}PO (figure 56) shifts to a lower frequency of 3394cm^{-1} and is asymmetric at 3294cm^{-1} whilst the H-bonded component of $\nu(\text{P=O})$ shifts to 1136cm^{-1} , is better resolved but has the same intensity as the shoulder at the beam temperature. The bands at 1168cm^{-1} and 1156cm^{-1} at the beam temperature (figure 55) due to $\nu(\text{P=O})$ are also better resolved at this lower temperature but remain in the same position.

At a temperature of -45°C the spectrum of $\nu(\text{OH})$ reverts to that shown in figure 56 with a main component at 3296cm^{-1} and shoulders at 3320cm^{-1} and 3150cm^{-1} . This spectrum may be compared with that obtained for ice I by Falk et al (49) at -160°C where $\nu(\text{OH})$ has a main component at 3220cm^{-1} and shoulders at 3380cm^{-1} and 3150cm^{-1} . These spectra are very similar the differences probably being due to the different temperatures at which the spectra were obtained.

At this temperature of -45°C the H-bonded component of $\nu(\text{P=O})$ reduces in intensity at 1136cm^{-1} (figure 56). It is not

surprising that a small band remains at 1136cm^{-1} since there is a band at this frequency in the spectrum of the anhydrous C_{10}PO (figure 44).

Generally at -45°C the spectrum of the hydrated material is identical with that of the anhydrous C_{10}PO except for the presence of bands due to ice I in the former spectrum. It would therefore appear that at a temperature of -45°C the water in the hydrated material freezes out as ice I giving the region indicated on the phase diagram as, crystalline $\text{C}_{10}\text{PO} + \text{Ice}$ (figure 50).

CHAPTER VI

LIQUID CRYSTALLINE PHASES

(I) Neat phase

(i) Results

(a) Both polarized and unpolarized spectra have been obtained of oriented samples of MG8/H₂O, DMG8/D₂O at 15°C, and MG11/H₂O, DMG11/D₂O, at 45°C in the composition range of the lamellar l.c. region of the phase diagrams. The neat l.c. phase is stable in systems containing 0.5-0.9 and 0.3-0.9 mole fraction of D₂O for the MG8/D₂O (figure 52) and MG11/D₂O (figure 49) systems respectively.

The absorption spectra of samples containing 0.45 mole fraction of H₂O with MG8 and D₂O with DMG8, at 15°C, are shown in figure 59. The frequencies and the proposed assignments of the absorption bands are listed in tables XVII and XVIII.

Significant dichroisms have only been observed in the case of the decoupled $\nu(\text{OH})$ for samples containing 0.45 and 0.8 mole fraction of D₂O with DMG8 upon going from sample position $V=0^\circ$ to $V=45^\circ$ (figure 29) between silica plates. However this procedure could not be carried out satisfactorily with silver chloride plates since transmission was too greatly reduced when they were used at 45° to the beam. It was only possible therefore to obtain spectra in the 3000cm^{-1} region since the silica plates do not transmit satisfactorily below this frequency. The polarized and unpolarized spectra, at 15°C, of the 0.45 and 0.89 mole fraction samples are shown in figure 60. Similar dichroisms have been observed for the decoupled $\nu(\text{OH})$ of the DMG11/D₂O neat phase in samples containing 0.52 and 0.73 mole fraction of D₂O at 45°C, and the values of the $\nu(\text{OH})$ frequency, half band width,

$\Delta\nu_{\frac{1}{2}}$, and intensity ratios, D_{45}/D_0 , for the sample positions $V=0^\circ$ and $V=45^\circ$ are shown in table XIX for the two systems studied.

Also the effect of temperature on the dichroisms observed in the DMG11/D₂O samples has been studied and the polarized spectra for the decoupled $\nu(\text{OH})$ at 75°C along with that at 45°C for the 0.73 mole fraction sample, for sample positions $V=0^\circ$ and $V=45^\circ$ are shown in figure 61. The unpolarized spectra of the decoupled $\nu(\text{OH})$ bands for this sample at 45°C and 75°C are also shown in figure 61.

(b) Both polarized and unpolarized infra-red spectra have been obtained on oriented samples of C₁₂PO/H₂O at 45°C in the composition range of the lamellar l.c. region of the phase. The neat l.c. phase is stable in systems containing 0.82 - 0.92 mole fraction of H₂O (figure 62).

The absorption spectrum of samples containing 0.84 mole fraction of H₂O with C₁₂PO at 45°C is shown in figure 63. The frequencies and proposed assignments of the absorption bands are listed in table XX. No significant dichroisms have been observed, however the polarized and unpolarized spectra of the decoupled $\nu(\text{OH})$ of samples containing 0.84 mole fraction of D₂O with C₁₂PO at 45°C are shown in figure 64.

The neat l.c. phase of the C₁₀PO/H₂O system is stable in systems containing 0.66 - 0.87 mole fraction of H₂O (figure 50). The unpolarized spectra of the decoupled $\nu(\text{OH})$ at 4°C and beam temperature are shown in figure 64 for samples containing 0.86 mole fraction of D₂O with C₁₀PO.

(c) The unpolarized spectra of the decoupled $\nu(\text{OH})$ of liquid water has been obtained at 4°C , 15°C , beam temperature and 75°C and the bands are shown in figure 64. Also the polarized spectra at 4°C have been obtained for sample positions $V=0^\circ$ and

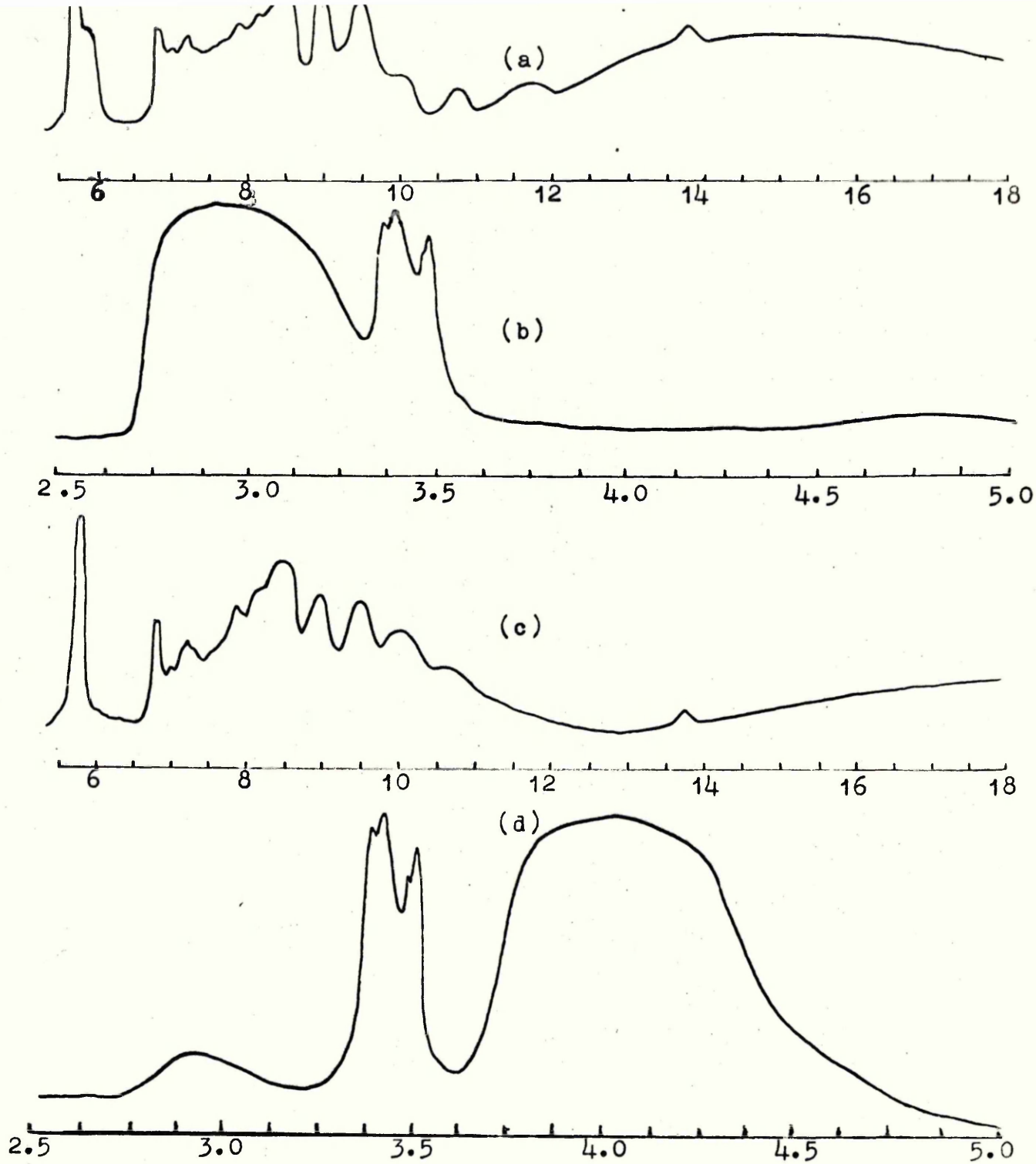


Figure 59.

Infra-red spectra of: MG8+0.45 mole fraction of H_2O (15°C), Wavelength
 (a) 6-18 μ , (b) 2.5-5.0 μ .
 DMG8+0.45 mole fraction of D_2O (15°C), Wavelength
 (c) 6-18 μ , (d) 2.5-5.0 μ .

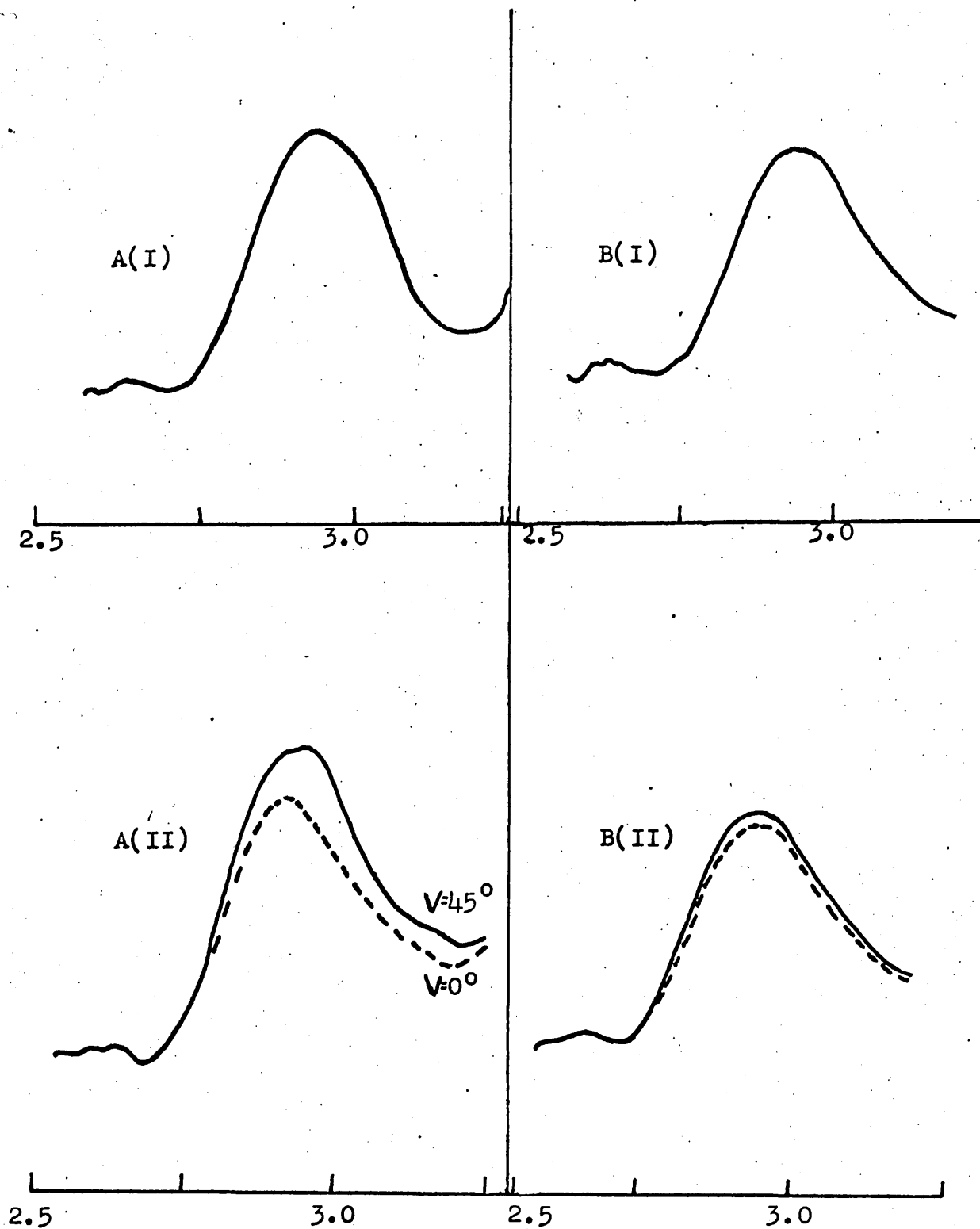


Figure 60

Decoupled $\nu(\text{OH})$ bands in DMG8 containing A- 0.45 mole fraction D_2O , (I) unpolarized (II) polarized. B- 0.89 mole fraction D_2O , (I) unpolarized (II) polarized. Wavelength $2.5\text{--}3.25\mu$. Temperature 15°C .

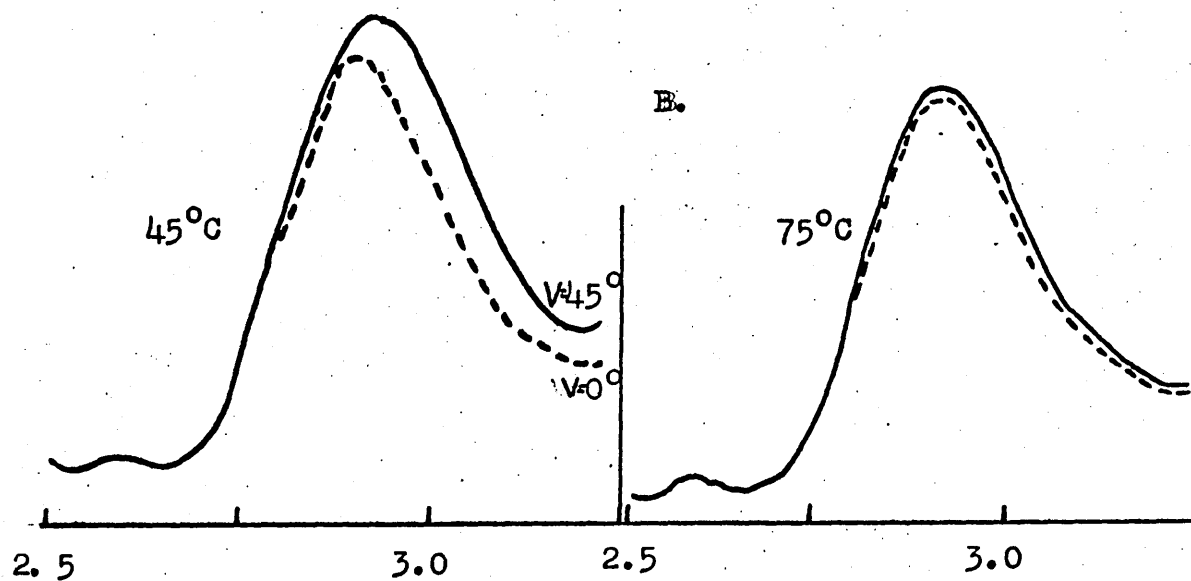
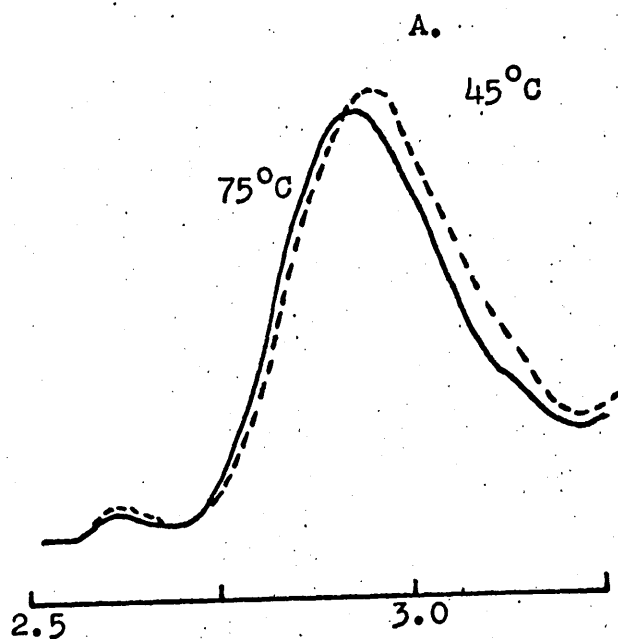


Figure 61.

Decoupled $\nu(\text{OH})$ bands in DMG11 containing 0.73 mole fraction of D_2O . A-unpolarized, B-polarized. Wavelength 2.5-3.25 μ .

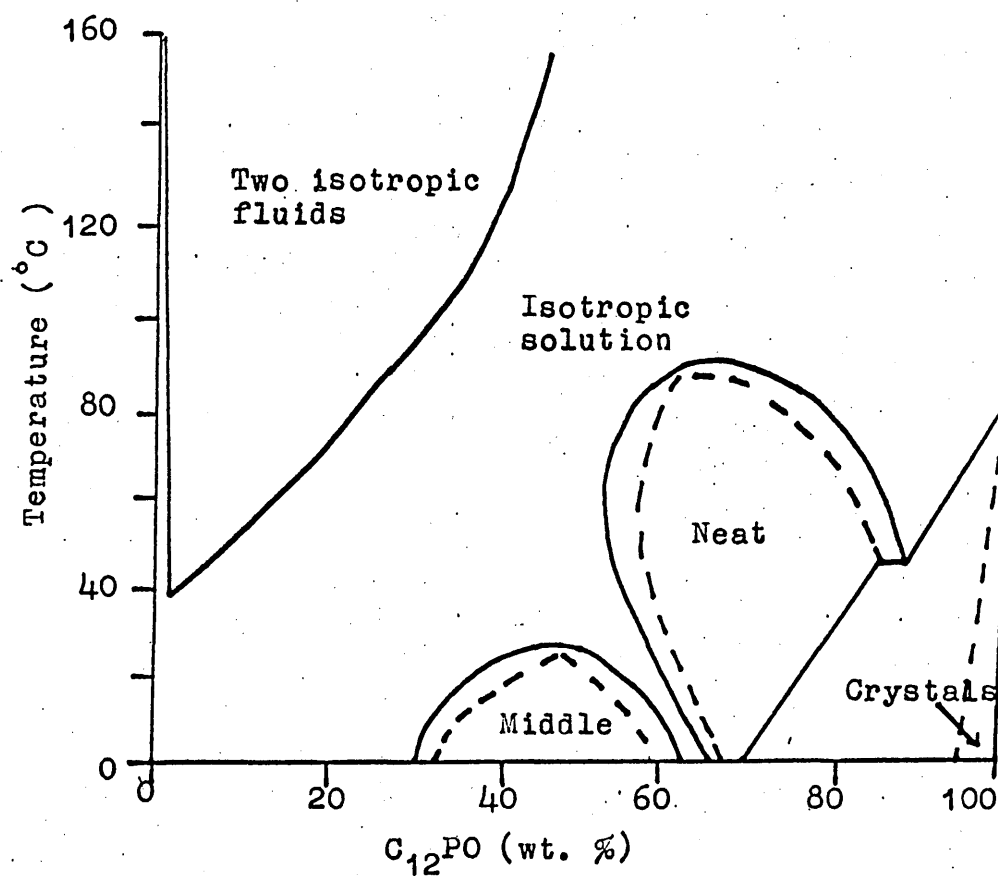


Figure 62.

Dimethyldodecylphosphine oxide($C_{12}PO$)/ H_2O
phase diagram (14)

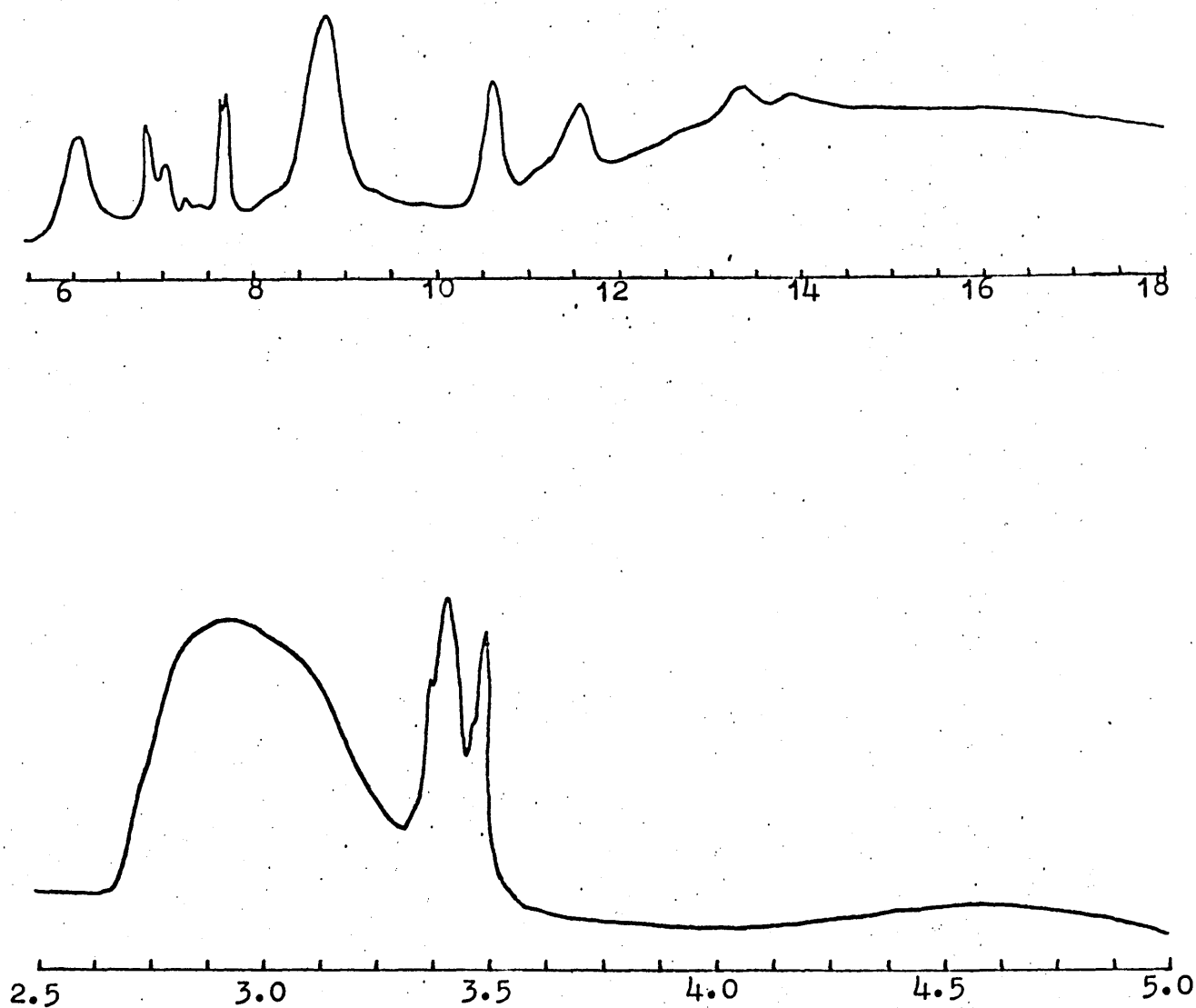


Figure 63.

Infra-red spectrum of $C_{12}PO$ + 0.84 mole fraction of H_2O
at $45^\circ C$. Wavelength 2.5-5.0 and 6-18 μ .

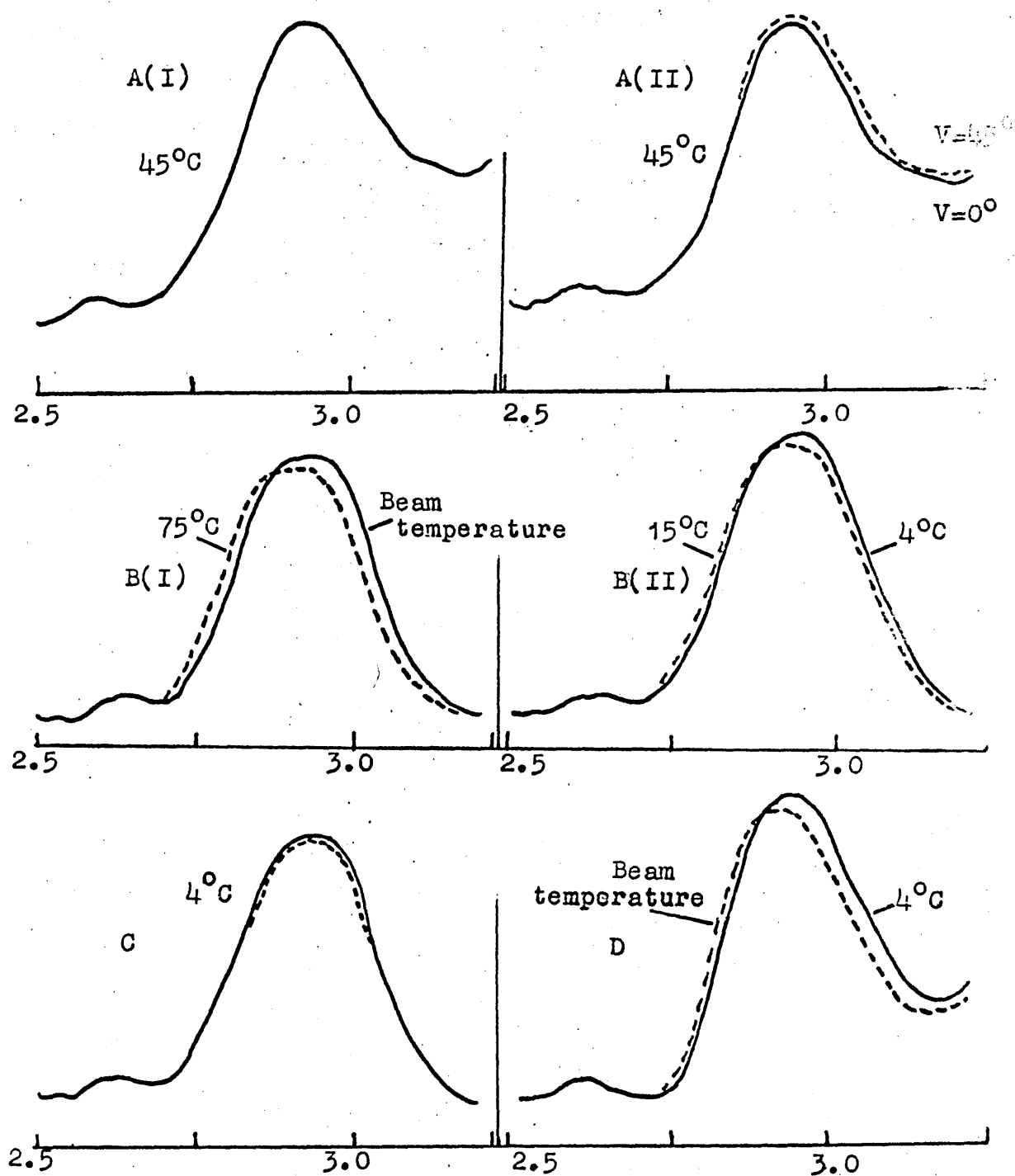


Figure 64.

Decoupled $\nu(\text{OH})$ bands of A- $\text{C}_{12}\text{PO} + 0.84$ mole fraction D_2O (45°C), (I) unpolarized, (II) polarized. B- Liquid water (unpolarized) at (I) beam temperature and 75°C, (II) 4 and 15°C. C- Liquid water (polarized) at 4°C. D- $\text{C}_{10}\text{PO} + 0.86$ mole fraction D_2O at 4°C and beam temperature. Wavelength 2.5-3.25 μ .

$V=45^\circ$ for the decoupled $\nu(\text{OH})$ band and these spectra are also shown in figure 64. No differences are observed in the spectra at $V=0^\circ$ and $V=45^\circ$.

Table XXI shows the various spectral parameters for the decoupled $\nu(\text{OH})$ of liquid water with those for the l.c. phases at the various temperatures.

Unpolarized spectra of liquid H_2O and D_2O were obtained at the beam temperature and are shown as figure 65.

(ii) Discussion

The structure of the neat l.c. phase in 1-mono-glyceride/water systems was shown to be lamellar by Larsson (180) and Reiss Husson (198) using X-ray diffraction.

The identification of this phase in the case of the $\text{C}_{12}\text{PO}/\text{H}_2\text{O}$ and $\text{C}_{10}\text{PO}/\text{H}_2\text{O}$ systems was carried out by Hermaun et al (141) using a polarizing light microscope. They observed the textures characteristic of a lamellar structure reported by Rosevear (185) and this identification has been confirmed in the present work.

(a) Structure of the water layer

(1) $\nu(\text{OH})$

The $\nu(\text{OH})$ band of the samples containing 0.45 mole fraction of H_2O with MG8 (figure 59), 0.52 mole fraction of H_2O with MG11, and 0.84 mole fraction of H_2O with C_{12}PO (figure 63) is extremely broad, has its maximum at approximately 3410cm^{-1} , and is markedly asymmetric at approximately 3300cm^{-1} . The breadth of this band is so great ($\Delta\nu_{\frac{1}{2}} > 400\text{cm}^{-1}$) that there is considerable overlap with bands associated with $\nu(\text{CH}_2)$ and $\nu(\text{CH}_3)$ in the region of 3000cm^{-1} . The shape and position of $\nu(\text{OH})$ is unchanged by increasing the concentration of H_2O present.

This band is very similar in appearance to that observed in liquid water (figure 65). In liquid water the band envelope of $\nu(\text{OH})$ is made up of contributions from the following components

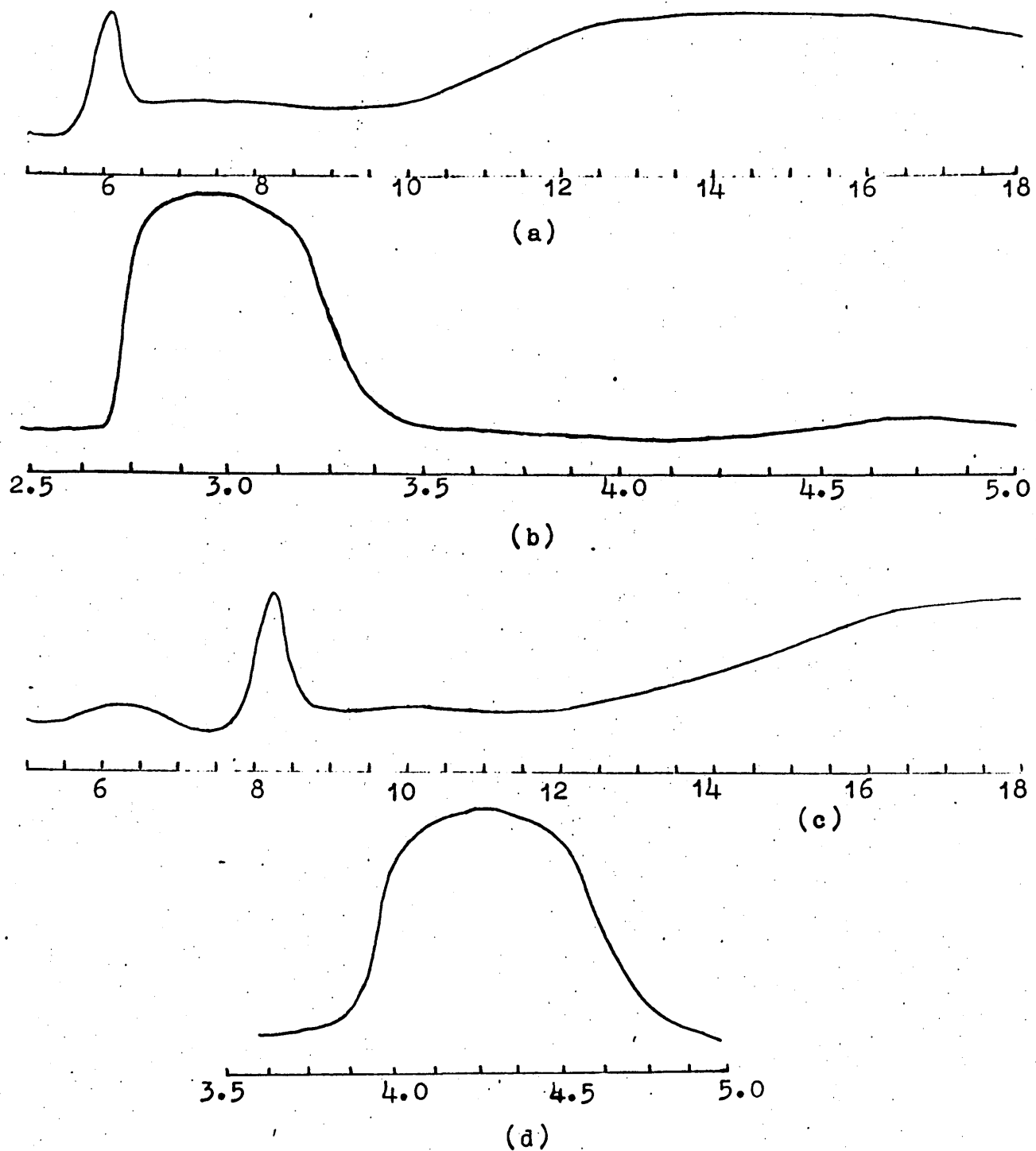


Figure 65.

Infra-red spectra of liquid water:- H_2O , Wavelength (a) 5-18 μ ,
 (beam temperature) (b) 3.5-5.0 μ .
 D_2O , Wavelength (c) 5-18 μ ,
 (d) 3.5-5.0 μ .

(156):-

- i. OH asymmetric stretch, ν_3 .
- ii. OH symmetric stretch, ν_1 .
- and iii. the first overtone of the bending vibration, $2\nu_2$.

Each of these components is broad and hence overlap takes place giving rise to the observed broad asymmetric band. In the case of 1-monoglycerides, in addition to the components listed there is also a contribution in some part from the glyceride residue OH groups.

From a comparison of these spectra it would appear that the water incorporated in the neat l.c. phase is in a similar state to liquid water.

(2) Decoupled $\nu(\text{OH})$

i. The decoupled $\nu(\text{OH})$ bands in the unpolarized spectra of DMG8 and DMG11/D₂O samples occur at 3410cm^{-1} (15°C) and 3419cm^{-1} (45°C) and are broad with $\Delta\nu_{\frac{1}{2}}$ of 262cm^{-1} and 268cm^{-1} respectively. In the decoupled $\nu(\text{OH})$ spectra of 0.45 and 0.80 mole fraction of D₂O with DMG8 (figure 60) and 0.52 mole fraction of D₂O with DMG11 the bands appear to have a single maximum and are markedly asymmetric at the low frequency side of the band envelope, at 3358cm^{-1} and 3368cm^{-1} respectively, whilst those of the 0.89 mole fraction of D₂O with DMG8 (figure 60) and 0.73 and 0.86 mole fraction of D₂O with DMG11 are symmetric.

Spectra of samples of DMG11 containing 0.73 mole fraction of D₂O were also obtained at 75°C (figure 61). The decoupled $\nu(\text{OH})$ band is broad and symmetric with a value of $\Delta\nu_{\frac{1}{2}}$ of 270cm^{-1} and shifted to a higher frequency of 3424cm^{-1} . There is also a decrease in the intensity relative to the lower temperature spectrum.

In liquid water the decoupled $\nu(\text{OH})$ is a symmetric band (figure 64), appears to have a single maximum at 3398cm^{-1} (15°C),

3410cm^{-1} (beam temperature), and 3415cm^{-1} (75°C) and has $\Delta\nu_{\frac{1}{2}}$ values of 265cm^{-1} , 268cm^{-1} and 273cm^{-1} respectively. There is also a gradual decrease in the intensity with increasing temperature (figure 64). This sort of behaviour is to be expected at higher temperatures because of the weakening of the H-bond interaction. Similar spectra have been obtained previously in the case of liquid water (156) with similar band widths and frequency positions.

It would therefore appear that at high mole fractions of D_2O in both neat phases studied, the decoupled $\nu(\text{OH})$ not only occurs in a similar position, has a similar $\Delta\nu_{\frac{1}{2}}$, but also has a similar temperature behaviour as well as observed band shape as liquid water. Although from the positions of the decoupled $\nu(\text{OH})$ bands the average H-bond strength in the neat phase appears to be slightly lower than in liquid water.

At lower mole fractions, however, even though the band maxima are in the same position as the high water content samples and $\Delta\nu_{\frac{1}{2}}$ is similar, the bands have not the same shape, being markedly asymmetric at the low frequency side. The asymmetry may be due to contributions directly from the water molecules associated with the glyceride hydroxyl groups. It is known that H-bonding between alcoholic hydroxyl groups and water molecules is stronger than that between the hydroxyl groups or water molecules alone (275). It would therefore be expected that the $\nu(\text{OH})$ of groups involved in such bonding would occur at a lower frequency.

At the low water contents all water molecules would, say, be attached fleetingly to one or other of the 1-monoglyceride molecules, but as the water content is increased there will be an increasing number of water molecules instantaneously attached only to other water molecules therefore swamping the former effect and hence giving a more symmetrical, liquid water like,

band envelope.

Further evidence for this orientation of the water was found in the 1-monoglyceride systems studied in this thesis by McDonald et al (220) using broad line N.M.R. on oriented l.c. samples. A narrow doublet associated with the protons on the water molecules was observed indicating a degree of anisotropy in the motion of the water molecules. This anisotropy was also seen to decrease with increasing concentration of water.

ii. The peak of the neat l.c. phase of the MG8/D₂O phase diagram (figure 52) occurs at a composition of MG8.4D₂O suggesting that a complex of that composition is particularly stable in the l.c. phase. The maximum is at a mole fraction of 0.8 in D₂O. If it is assumed that the 0.8 mole fraction complex is a type of hydrate then comparison with other hydrates may be made. Using the correlation curve shown in figure 15 relating R_{O-O} distances to $\nu(\text{OH})$ frequencies, a value of 2.82 Å is found to correspond to the $\nu(\text{OH})$ frequency of 3410 cm⁻¹ for this sample.

From the decoupled $\nu(\text{OD})$ frequencies of pinacol hexahydrate, R_{O-O} values of 2.77 Å and 2.74 Å were obtained via the $\nu(\text{OD})$ v's R_{O-O} correlation curve (figure 16). Thus the average value of the l.c. R_{O-O} is much higher than either of the values obtained for pinacol hexahydrate. An average value for 20 hydrates (155) is 2.80 Å and probably represents a reliable estimate of the H-bond lengths in organic hydrates. The l.c. R_{O-O} value compares very favourably with this average value. There is however no evidence from other sources that such a hydrate exists.

iii. In the MG11/D₂O phase diagram (figure 49) there is a small peak in the phase boundary between the gel and l.c. region at MG11 + 0.47 mole fraction of D₂O, suggesting the presence of a monohydrate.

A comparison of the unpolarized spectrum of the decoupled $\nu(\text{OH})$ in samples containing 0.47 mole fraction of D_2O (figure 66) can be made with samples containing 0.53 mole fraction of D_2O (figure 66) at 45°C . Both decoupled $\nu(\text{OH})$ bands appear to have a single maximum at 3419cm^{-1} but the former band is much more symmetrical and has $\Delta\nu_{\frac{1}{2}}$ of 226cm^{-1} which is a reduction of approximately 40cm^{-1} compared with the latter band.

In liquid water the breadth of the decoupled $\nu(\text{OH})$ bands was concluded by Wall et al (60) to be due to structural disorder. In liquid water the decoupled $\nu(\text{OH})$ has a value of $\Delta\nu_{\frac{1}{2}}$ of 268cm^{-1} whilst in the case of ice I (49) and $\text{CaSO}_4 \cdot 2\text{H}_2\text{O}$ (11), $\Delta\nu_{\frac{1}{2}}$ values are 50cm^{-1} and 30cm^{-1} respectively. It would be expected therefore that an increase in the structure would give rise to narrower bands in the decoupled spectra. This narrowing effect has been observed in the spectrum of DMG11 + 0.47 mole fraction of D_2O and suggests that the monohydrate is stable in the l.c. phase.

The frequency of the decoupled $\nu(\text{OH})$ band, 3419cm^{-1} , for the DMG11 + 0.47 mole fraction of D_2O samples corresponds to an R_{0-0} value of 2.83\AA (figure 15). This value compares very favourably with the average value previously quoted for organic hydrates at 2.80\AA (155). However it is much higher than those previously obtained for pinacol monohydrate from the $\nu(\text{OD})$ v's R_{0-0} correlation curve (figure 16) which lie in the range $2.75 - 2.72\text{\AA}$.

iv. Polarized spectra

1. Dichroisms have been observed in the polarized spectra of the decoupled $\nu(\text{OH})$ of DMG8/ D_2O and DMG11/ D_2O (figures 60 and 61) neat l.c. samples upon going from sample positions $V=0^\circ$ to $V=45^\circ$.

For samples containing 0.45 and 0.80 mole fraction of D_2O

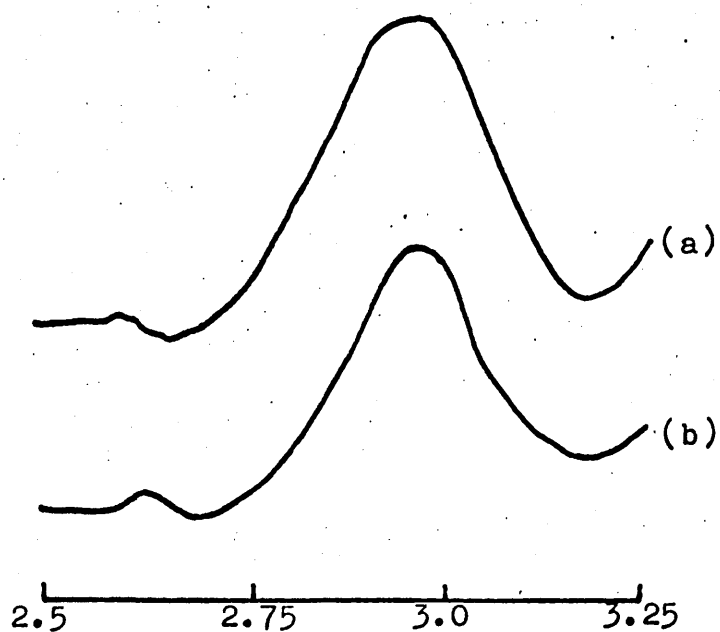


Figure 66.

Decoupled $\nu(\text{OH})$ bands in DMG11 containing
(a) 0.53 and (b) 0.47 mole fraction of D_2O
at 45°C . Wavelength $2.5\text{--}3.25\mu$.

with DMG8 for sample position $V=0^\circ$ broad bands are observed with a single maximum at 3406cm^{-1} and 3404cm^{-1} respectively. Upon going to sample position $V=45^\circ$ single broad bands are again observed with similar $\Delta\nu_{\frac{1}{2}}$ values but with increased intensity at 3382cm^{-1} and 3385cm^{-1} respectively. The decoupled $\nu(\text{OH})$ of liquid water showed none of these effects.

At higher D_2O mole fractions, 0.89, with DMG8 single broad bands are observed at 3404cm^{-1} and 3403cm^{-1} for sample positions $V=0^\circ$ and $V=45^\circ$ respectively, with only a very small increase in intensity between sample positions (table XIX).

Similar behaviour is observed in the case of the DMG11/ D_2O neat l.c. phase (table XIX).

This data may be interpreted in the following way: Considering the samples containing 0.45 and 0.80 mole fraction of D_2O with DMG8 (0.52 and 0.73 in the case of the DMG11/ D_2O system), the OH groups of the glyceride residue are 'anchored' at the interface and this will probably mean the OH bond direction is effectively parallel to the direction of propagation of the incident radiation and give rise to a general ordering effect of the water molecules, at the interface, in a direction perpendicular to the interface. Then any contribution of the resultant transition moment for the interface structure, to the spectrum in the $V=0^\circ$ position would be expected to be very small. The observed band at this sample position is therefore the contribution from the 'liquid like' water molecules.

However at $V=45^\circ$ the incident radiation now interacts with any resultant transition moment at an angle which would give rise to a considerable contribution to the $\nu(\text{OH})$ band envelope in addition to the liquid like water contribution. This contribution would be at a lower frequency due to the fact that the H-bonds formed by the water associated with the OH groups of the

- 44 -

residue at the interface are stronger. This would also account, in part, for the increase in intensity of the decoupled $\nu(\text{OH})$ band at this sample position, relative to $V=0^\circ$.

When the concentration of D_2O in the system increases it leads to an increase in the thickness of the water layer (180) but not in the number of molecules instantaneously H-bonded to the monoglyceride OH groups. Therefore in the case of samples containing 0.89 mole fraction of D_2O with DMG8 (0.86 in the case of DMG11/ D_2O system) it would be expected that the relative intensity of the low frequency vibration would diminish and in fact the differences between the two polarized spectra decrease with increasing water content (table XIX).

To test the above interpretation it was decided to examine also a long chain lipid which did not possess a hydroxyl group and which formed a neat l.c. phase which was stable at, or about, room temperature. An unsymmetrical trialkylphosphine oxide was chosen for this purpose. In the $\text{C}_{12}\text{PO}/\text{H}_2\text{O}$ system the neat l.c. phase is stable in systems containing 0.82 to 0.92 mole fraction of H_2O (figure 62).

The decoupled $\nu(\text{OH})$ band in the unpolarized spectrum (figure 64) of samples containing 0.84 mole fraction of D_2O in C_{12}PO appears to have a single maximum at 3414cm^{-1} (45°C) and is broad with $\Delta\nu_{\frac{1}{2}}$ of 268cm^{-1} and symmetrical.

The decoupled $\nu(\text{OH})$ bands in the polarized spectra (figure 64) showed no shift in frequency upon going from sample position $V=0^\circ$ to $V=45^\circ$, the frequency of the bands being 3408cm^{-1} . These bands have the same behaviour as the polarized spectra obtained in the case of the DMG8/ D_2O (figure 60) and DMG11/ D_2O systems for the samples containing the highest mole fraction of D_2O .

In this study of the $\text{C}_{12}\text{PO}/\text{H}_2\text{O}$ neat l.c. system, broad line N.M.R. has been used on oriented l.c. samples. No dipolar splitting of the water molecule resonance has been observed in this

system at the lowest mole fraction of H_2O for which the l.c. phase is stable, thus showing that in the case of this neat phase there is no observable ordering of the water by the phosphoryl end group. Whereas in the case of the l-monoglycerides studied by W.E. Peel (209) a small splitting was observed even at the highest water concentration for which the neat l.c. phases are stable. Also the angular dependence of the doublet splitting in this case (209) showed that there was a measurable degree of molecular ordering along a direction perpendicular to the lamellar planes of the mesophase.

Therefore comparing both infra-red and N.M.R. data on the $C_{12}PO/H_2O$ system with that obtained for the l-monoglyceride systems it would seem that the interpretation placed upon the observed dichroisms is reasonable.

2. Polarized spectra for samples containing 0.73 mole fraction of D_2O with DMG11 were obtained at $75^\circ C$ as well as at $45^\circ C$ (figure 61). Details of the various spectral parameters are given in table XIX. For sample position $V=0^\circ$, at $75^\circ C$, the broad band is observed at $3418cm^{-1}$. Upon going to sample position $V=45^\circ$, at this temperature, a single broad band is again observed with a similar $\Delta\nu_{\frac{1}{2}}$ (table XIX) at $3414cm^{-1}$ (3418 and $3396cm^{-1}$ respectively in the same sample at $45^\circ C$). There is an increase in intensity in the sample position $V=45^\circ$ but the ratio (D_{45}/D_0) (table XIX) is reduced compared with that observed for the lower temperature spectra and indeed is tending to the value obtained for the much higher water concentration, 0.86 mole fraction, at a lower temperature of $45^\circ C$.

The effects produced on the $\nu(OH)$ band by an increase of temperature are due to a greater relative decrease in the numbers of the most strongly associated species which give rise to the

low frequency vibration, similar to that occurring in alcohols and other hydroxylic substances.

v. Calculation of average O-O distance

The decoupled $\nu(\text{OH})$ band in the unpolarized spectrum of C_{10}PO containing 0.86 mole fraction of D_2O (figure 64) at 4°C is broad with $\Delta\nu_{\frac{1}{2}}$ of 270cm^{-1} , symmetrical and appears to have a single maximum at 3391cm^{-1} , whilst at the beam temperature $\nu(\text{OH})$ occurs at 3412cm^{-1} with $\Delta\nu_{\frac{1}{2}}$ of 273cm^{-1} . The corresponding bands in liquid water are found at 3389cm^{-1} and 3410cm^{-1} and these bands have $\Delta\nu_{\frac{1}{2}}$ values of 263cm^{-1} and 268cm^{-1} respectively (figure 64).

Both sets of bands appear to have similar frequency positions and band shapes as well as undergoing similar alterations with increasing temperature. It is assumed that, as in the case of liquid water (60), the breadth of the decoupled bands in the C_{10}PO neat phase is due to structural disorder and the shape of these bands is due to a continuous distribution of nearest neighbour O-O separations, then it is possible to obtain an average value for this distance, $R_{\text{O-O}}$, by invoking the correlation between $\nu(\text{OH})$ and the intermolecular distance, $R_{\text{O-O}}$ (71) (figure 15).

Wall et al (60) have recently utilized a curve of this type to obtain a radial distribution type of curve, similar to those obtained by X-ray spectroscopists in their studies of liquids (276), for liquid water from a Raman study of the decoupled $\nu(\text{OH})$ band. Ice I fitted on the correlation curve and they justified the extension of the use of a correlation curve, referring to crystals, to liquid water on the basis of the nature of the interaction in water and ice being qualitatively identical. Van Eck et al (61) estimated the o-o distance in water from the frequency of the infra-red absorption maximum of HDO . In both cases the

correlation with X-ray data was excellent.

If it is now assumed that the degree of interaction within the water layer of the neat phase l.c. and water are identical then extension of the correlation curve to the water region of the l.c. phase appears valid.

In construction of the correlation curves used by Van Eck et al (67,277,278) and Wall et al (6,67,277) some of the data utilized has since been found to be unreliable (71). The correlation curve used in this present study is that of Efimov et al (71) (figure 15).

To convert the vibrational spectra to a distribution function, the lineal height of the infra-red band at each frequency (actually at 30cm^{-1} intervals) is taken as a measure of the number of oscillators with that frequency at any instant. The ordinate in the distribution functions is lineal band height multiplied by the slope of the correlation curve ($\delta^2/\delta r$) at the point in question.

To test the validity of the use of this particular procedure the decoupled $\nu(\text{OH})$ bands of liquid water at 4°C and 75°C were analysed in the above manner. The resulting distribution functions are shown in figure 67 and it can be seen that the short distance side of the curves rise sharply and the peaks occur at $2.82(1)$ and 2.84\AA respectively.

Narten et al (276) have obtained distribution functions for liquid water at various temperatures, including 4°C and 75°C , using the X-ray technique. They observed a gradual increase in the average R_{0-0} values from the peaks of the functions of 2.82\AA at 4°C and 2.94\AA at 200°C . If this is a gradual increase then a value of approximately 2.86\AA would be expected at 75°C .

A comparison of the values obtained from this band analysis, with the values from the X-ray study, at 4°C and 75°C shows

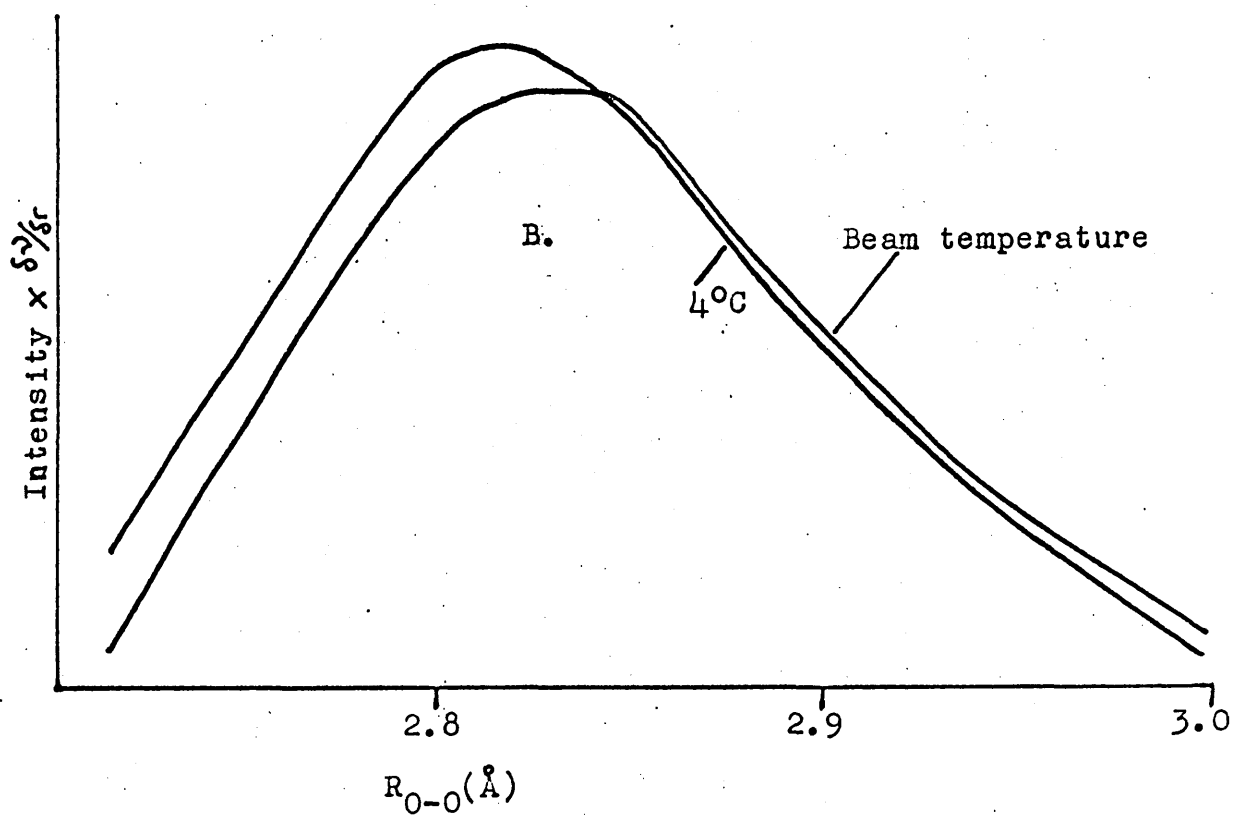
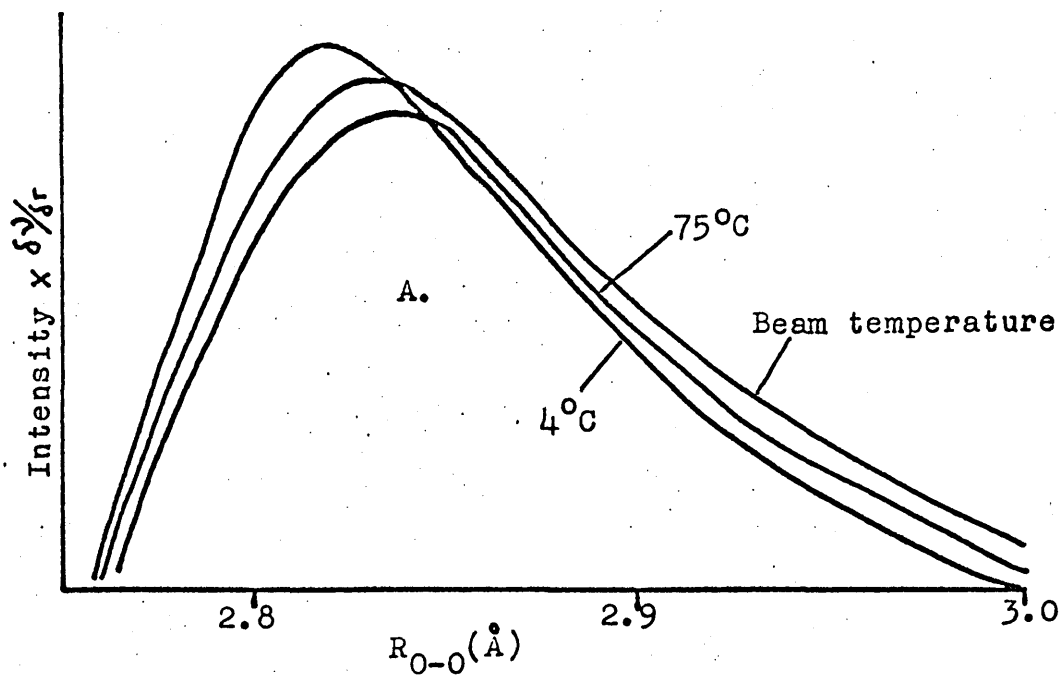


Figure 67

Distribution function for the decoupled $\nu(\text{OH})$ bands of:-
 A. Liquid water at 4°C, beam temperature and 75°C, and
 B. $\text{C}_{10}\text{PO} + 0.86$ mole fraction of D_2O at 4°C and beam temperature.

excellent agreement, although there is a difference of 0.02\AA at the higher temperature. On the basis of this agreement it seemed reasonable to utilize the infra-red R_{O-O} analysis technique further.

The distribution functions for the decoupled $\nu(\text{OH})$ bands of samples containing 0.86 mole fraction of D_2O in C_{10}PO at 4°C and beam temperature are shown in figure 67, along with those for the decoupled $\nu(\text{OH})$ bands of liquid water at the same temperatures. The resulting average R_{O-O} distances obtained from the peaks of these functions are given in table XXII.

The distribution curves and the average R_{O-O} distances are very similar in the two cases. However the distribution curve of the neat phase is rather broader and indicates a greater proportion of shorter R_{O-O} distances compared with those for liquid water. This may be due to participation of the phosphoryl group, present at the interface, in the nearest neighbour interaction in the neat phase causing an increase in the numbers of species with shorter R_{O-O} distances.

(3) Other bands associated with liquid water.

i. In the unpolarized spectra of samples of MGS containing 0.45 mole fraction of H_2O (figure 59) at 15°C a very weak broad band is observed at 2130cm^{-1} , whilst in the case of samples of 0.52 mole fraction of H_2O with MG11, and 0.84 mole fraction of H_2O with C_{12}PO (figure 63) at 45°C the band occurs at 2118cm^{-1} . This band in liquid water (figure 65) has its maximum near 2125cm^{-1} and is the counterpart of the association band, ν_A , which occurs in ice I at 2270cm^{-1} (49). It is thought that this band is composed of overtones of intermolecular modes, or a combination of the HOH deformation, ν_2 , at 1645cm^{-1} with an intermolecular mode or both. Williams (279) proposed the assignment $(\nu_2 + \nu_L - \nu_t)$ for this band, where ν_L is the librational

mode, ν_t is the translational mode usually found at approximately 685cm^{-1} and 193cm^{-1} (280) respectively, in the spectrum of liquid water. The intensity of this band increases as the amount of H_2O is increased but it remains in the same position.

ii. In the unpolarized spectra of samples of MG8 containing 0.45 mole fraction of H_2O (figure 59), ν_2 occurs at 1656cm^{-1} compared with 1648cm^{-1} in liquid water (figure 65) and 1650cm^{-1} in ice I (49).

In the DMG8 sample (figure 59) the band due to $\nu_2(\text{D}_2\text{O})$ appears at approximately 1216cm^{-1} in the region of $\text{W}(\text{CH}_2)$ and $\text{T}(\text{CH}_2)$ which compares with the value of liquid D_2O of 1215cm^{-1} (figure 65).

A similar effect is observed in the case of the neat phase spectra of the MG11/ H_2O and D_2O samples at 45°C .

In the case of the spectra of the 0.84 mole fraction of H_2O with C_{12}PO at 45°C ν_2 occurs at 1648 (figure 63).

The higher frequency in the MG8 and MG11/ H_2O case is probably due to the presence of $\nu(\text{C}=\text{O})$.

iii. Recently a previously unreported absorption maximum in the infra-red spectrum of liquid water at 1350cm^{-1} in H_2O and at 1000cm^{-1} in D_2O has been assigned to the first overtone of the far infra-red ν_L band (281). This band lies between ν_2 and ν_L for liquid water and is clearly visible in the spectra of liquid H_2O and D_2O shown in figure 65.

In the neat l.c. phase spectra shown of the samples of 0.45 mole fraction of H_2O and D_2O with MG8 and DMG8 (figure 59) this band is not observed due to the fact that superimposed over this region of the spectra are the bands arising from various modes associated with the hydrocarbon chain. This band is not observed in the neat l.c. spectra of MG11/ H_2O or the $\text{C}_{12}\text{PO}/\text{H}_2\text{O}$ samples for similar reasons.

iv. The librational mode (ν_L) in the spectra of samples of MG8, MG11 and C₁₂P0 containing 0.45 (figure 59), 0.52 and 0.84 (figure 63) mole fraction of H₂O respectively is a broad band and occurs at approximately 686cm⁻¹ which is approximately the same position as in liquid water at 685cm⁻¹ (figure 65). In ice I ν_L is at 846cm⁻¹ (49). Therefore the position in the neat l.c. phases of these systems would give the impression that the strength of the H-bond is on average the same order of magnitude as that in liquid water. This band remains in approximately the same position with increase in concentration of water in all systems.

(4) $\nu(C=O)$

At 15°C in the unpolarized spectra of samples containing 0.45 mole fraction of D₂O with DMG8, $\nu(C=O)$ is resolved into two components at 1746cm⁻¹ and 1735cm⁻¹ the former being the stronger band. Changes occur in the $\nu(C=O)$ doublet on increasing the amount of D₂O present. The $\nu(C=O)$ bands of the various DMG8 hydrated phases are shown diagrammatically in figure 68. The frequencies of these components of $\nu(C=O)$ for the DMG8 and DMG11/D₂O neat phases are shown in table XXIII.

In very dilute solution in CCl₄ the $\nu(OH)$ spectrum indicated that there was no intermolecular H-bonding, and a doublet associated with $\nu(C=O)$ was observed at 1754cm⁻¹ and 1735cm⁻¹ and these components were assigned to 'free' and intramolecular H-bonded $\nu(C=O)$ (chapter III (b)).

The lowest frequency $\nu(C=O)$ band in the neat phases of MG8 and MG11/D₂O systems occurs in the same position as the lowest frequency component in solution and it could therefore be due to intramolecular H-bonded carbonyl groups. However as mentioned earlier $\nu(C=O)$ for intermolecularly H-bonded carbonyl groups

sometimes occurs at this frequency and therefore an unequivocal assignment cannot be made.

The relative intensity of the low frequency component in the neat phase of MG8/D₂O system (figure 68) is seen to increase with increasing D₂O content of the sample and this sequence also occurs with increasing content of D₂O in the l.c. phase of the MG11/D₂O system. In the MG11 system increasing D₂O content causes increased melting point of the l.c. phase (figure 49) but in the MG8 system (figure 52) the melting point goes through a maximum at approximately 0.8 mole fraction of D₂O. Since the relative intensity of the low frequency component of the carbonyl band continues to increase above 0.8 mole fraction of D₂O it seems that the H-bonding in which the carbonyl group is involved is not important to the stability of the lamellar phase.

(5) $\nu(\text{P}=\text{O})$

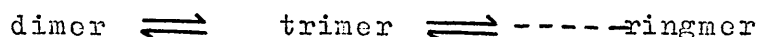
Several authors have studied the complex formation of phosphine oxides with various proton donors in CCl₄ solution (143,273,274,282,283).

Mroczek et al (282) have suggested from shifts observed in the $\nu(\text{P}=\text{O})$ and changes in $\nu(\text{OH})$ of tri-n-octylphosphine oxide (T.O.P.O.) and various other phosphine oxides in H₂O saturated solutions of CCl₄ certain aggregates were formed, in particular 2T.O.P.O..H₂O. More recently in the case of T.O.P.O. it was postulated by O'laughlin et al (143) on the basis of infra-red, N.M.R. and vapour pressure measurements that a 1:1 complex is formed in solutions containing less than 0.1M of T.O.P.O.

Gramstad et al (274) have studied the pentafluorophenol (P.F.P.) and triphenylphosphine oxide (T.P.P.O.) mixtures in CCl₄ solution. Alterations in the $\nu(\text{OH})$ spectrum of P.F.P. with concentration changes in T.P.P.O. have been correlated with the formation of complexes of the 1:1, 1:2 and 2:1 ratio of donor

to acceptor and ΔH , as well as ΔS values for these complexes have been calculated. Furthermore in the trimethylphosphine oxide/methanol system in CCl_4 (273), ΔH values were found to be dependent upon concentration. This was thought to be due to the formation of molecular aggregates of a similar nature to those found by Gramstad et al (274). Support for the existence of such complexes was found in the spectra of Riltsev et al (273), figure 69, which show that the addition of methanol causes changes in the complexity of $\nu(P=O)$ of trimethylphosphine oxide.

A study has been made, using high resolution N.M.R. (283), of solutions of water in tri-n-butylphosphate (T.B.P.). The chemical shift of the H_2O protons, was found to increase almost linearly with increase in H_2O concentration. This was interpreted in terms of strong interactions of the water molecules with the organic base and the following model equilibria were postulated.



Increasing T.B.P. \leftarrow \rightarrow increasing H_2O content

The $\nu(P=O)$ bands of the mole fractions of H_2O covering the concentration range for which the neat phase of the $C_{12}PO/H_2O$ system is stable are shown diagrammatically in figure 70. The frequencies of these components are shown in table XXIV.

In the neat l.c. phase of $C_{12}PO/H_2O$ system, initially at a H_2O mole fraction of 0.84 at $45^\circ C$ a broad band is observed at $1138cm^{-1}$. This is a shift of $18cm^{-1}$ from that observed in the solid state at $1156cm^{-1}$. An intense shoulder is also observed at $1148cm^{-1}$ (figure 70, table XXIV). When the concentration of water was increased a further component was resolved at the low frequency side of the principal band, now at $1136cm^{-1}$, at $1120cm^{-1}$, whilst the shoulder at $1148cm^{-1}$ has much reduced intensity at $1149cm^{-1}$ (figure 70). Finally at the maximum concentration of water for which the l.c. phase is stable (0.90 mole

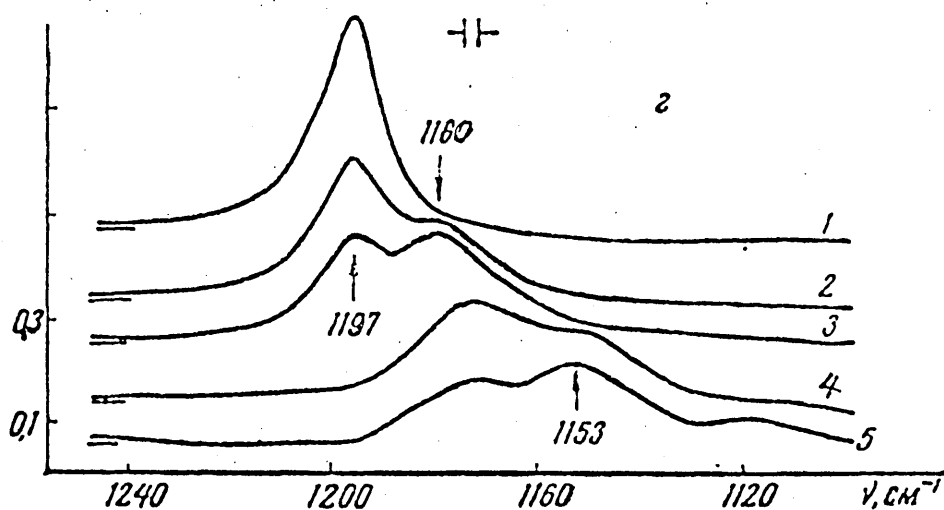


Figure 69.

$\nu(\text{P}=\text{O})$ bands of trimethylphosphine oxide, 0.01M, in CCl_4 (1), also 0.01M in CCl_4 solutions containing methanol concentrations, 0.045M (2), 0.09M (3), 0.45M (4), 1.9M (5). (273)

fraction), the principal band is now observed at 1137 cm^{-1} whilst the shoulder on the high frequency side is now found at 1148 cm^{-1} (figure 70). At this concentration of water no distinct low frequency shoulder is observed.

The three new components associated with $\nu(\text{P}=\text{O})$ can be discussed in the terms of the complex species present. It is thought that complexes of phosphine oxide and water with a composition 2:1, 1:1 and 1:2 could be involved corresponding to the components observed at 1148 cm^{-1} , 1138 cm^{-1} and 1120 cm^{-1} respectively. The possible structures of these complexes are shown in figure 71.

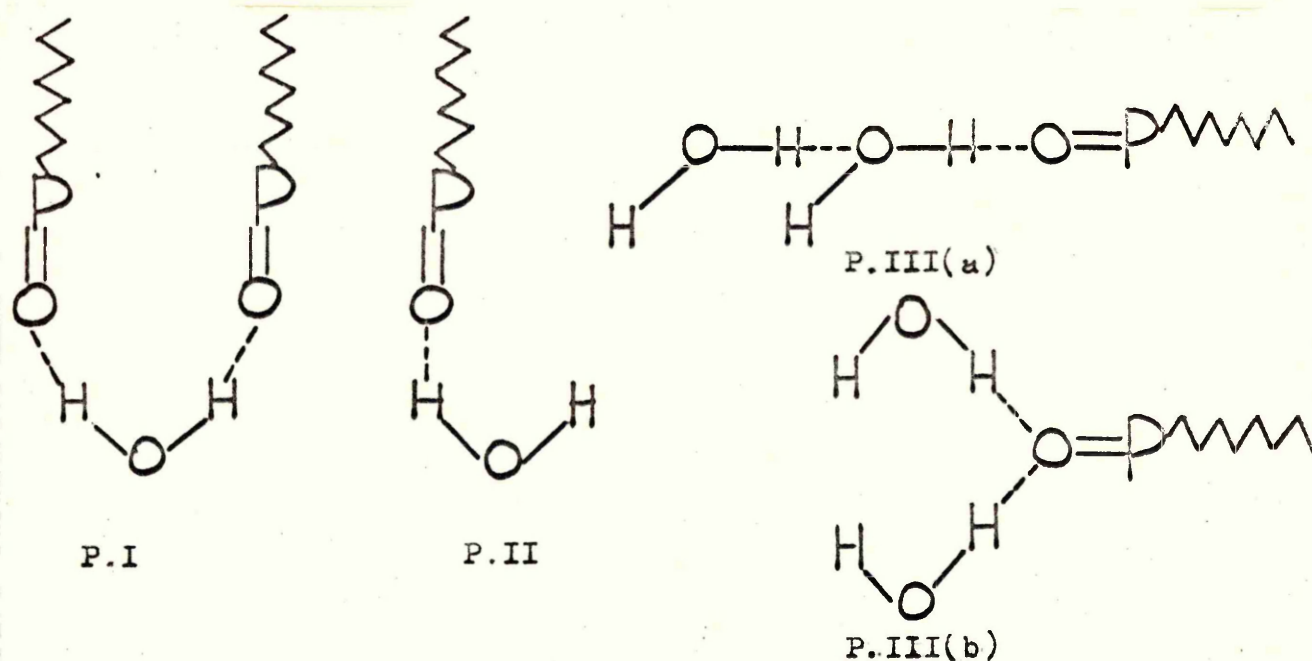


Figure 71.

It is difficult to make an unequivocal choice between the two structures shown for the 1:2 complex (structures P.III(a) and (b), figure 71). Some assistance is obtained from a consideration of the behaviour of $\nu(\text{C}=\text{O})$. In the study of the effect of p-cresol upon acetone and acetophenone, in CCl_4 solution where Whetsel et al (284) observed the appearance of two new bands associated with $\nu(\text{C}=\text{O})$ and correlated them with 1:1 and 1:2 complexes of the type shown in figure 72.

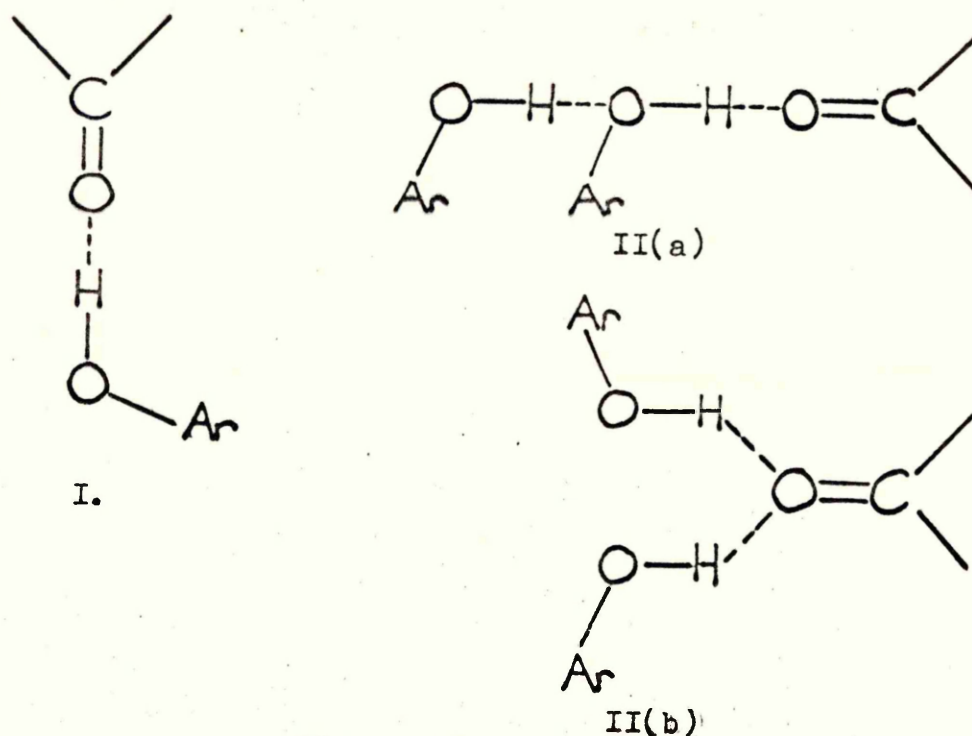


Figure 72.

Of the two structures which represent the 1:2 complexes, structure II(a) in figure 72 was chosen as the most favourable because of a small frequency shift that resulted from the addition of the second p-cresol molecule. With cyclohexanone for example, the shift amounted to only 5.3cm^{-1} , while the shift of the 1:1 complex (structure I in figure 72) band from the 'free' ketone band was 16.8cm^{-1} .

Therefore on this basis it is considered that because of the relatively large frequency shift that resulted from the addition of the second molecule of H_2O in the C_{12}PO system the structure which best represents the 1:2 complex is that shown as structure P.III(b) in figure 71.

From the observed spectra (figure 70) it can be seen that the participation of the different H-bonded species alters as the amount of H_2O is increased. Even though at all concentrations all the structures postulated are present to some extent, it appears that at low H_2O concentration structures PI and PII predominate whilst at higher H_2O concentrations structures PII and PIII(b) predominate.

(b) Lipid layer

It has been well established that the neat l.c. phase has a bilayer structure (180,195,197,198,201). The motion of the hydrocarbon chains within the bilayer is regarded as 'liquid like' by most workers. This has been confirmed in the systems studied in this thesis.

Generally the spectra obtained for the various neat l.c. systems (figures 59 and 63) have the appearance of those obtained for the liquid anhydrous material (figures 34 and 45), the frequencies of the observed absorption bands being in approximately the same positions (tables XVII and XX). The bands which have been assigned to the various vibrational modes of the CH₂ groups of the hydrocarbon chain, are rather broad and diffuse. In the liquid states of polymethylene compounds the molecules are generally bent and curled into a variety of different conformations and thus give rise to diffuse spectra.

Furthermore dichroisms of the bands associated with the hydrocarbon chains have not been observed in any of the systems studied.

W.E. Peel (209) has used broad line N.M.R. to study the motion and orientation of the hydrocarbon chains in the l-monoglyceride/H₂O neat l.c. phases studied here. His results both on oriented and non-oriented samples have indicated that the lipid molecules are rotating about their long axes with a significant increase in the freedom of the rotational motion occurring at four methylene groups along the alkyl chains from the polar head group of the saturated lipid. The dipolar splitting associated with the N.M.R. spectrum of the first few methylene groups of the l-monoglyceride hydrocarbon chains also indicated that the motion of these methylene groups was virtually a simple rotation.

One might therefore have expected to observe dichroisms from these more ordered segments of the hydrocarbon chain but not from the remainder in which there must also be torsional and flexing motion as well as simple rotation.

Table XVII

Assignments of the absorption bands MG8/H₂O neat phase spectrum (0.45 mole fraction of H₂O)

Liquid MG8 (42°C)		Neat phase MG8/H ₂ O (15°C)		Assignments (b)
cm ⁻¹	Intensity (a)	cm ⁻¹	Intensity (a)	
3466	s.br.	3410	s.br.	} $\nu(\text{OH})$ $\nu_a(\text{CH}_3)$ $\nu_a(\text{CH}_2)$ $\nu_s(\text{CH}_2)$ $\nu_s(\text{CH}_2)$ $\nu_A(\text{H}_2\text{O})$
2957	m	2959	m	
2929	s	2929	s	
2878	m	2878	m	
2854	s	2855	s	
		2130	v.w.br.	} $\nu(\text{C}=\text{O})$ $\nu_2(\text{H}_2\text{O})$ $\delta(\text{CH}_2)$ $\text{T}(\text{CH}_2)$ & $\text{W}(\text{CH}_2)$ $\nu(\text{COC})$ $\nu(\text{CO})$ s s
		1746	s	
1739	s	1734	sh	
1733	sh	1656	m	
1468	m	1469	m	
1460	m	1460	m	} $\nu(\text{C}=\text{O})$ $\nu_2(\text{H}_2\text{O})$ $\delta(\text{CH}_2)$ $\text{T}(\text{CH}_2)$ & $\text{W}(\text{CH}_2)$ $\nu(\text{COC})$ $\nu(\text{CO})$ s s
1422	w	1422	w	
1385	m	1385	m	
1272	m	1272	m	
1232	m	1233	m	
1174	s.br.	1174	s.br.	} $\nu(\text{C}=\text{O})$ $\nu_2(\text{H}_2\text{O})$ $\delta(\text{CH}_2)$ $\text{T}(\text{CH}_2)$ & $\text{W}(\text{CH}_2)$ $\nu(\text{COC})$ $\nu(\text{CO})$ s s
1113	m.br.	1114	m.br.	
1053	m.br.	1053	m.br.	
990	w.br.	990	w.br.	
935	w.br.	936	w.br.	
870	w.br.	868	w.br.	} $\nu(\text{C}=\text{O})$ $\nu_2(\text{H}_2\text{O})$ $\delta(\text{CH}_2)$ $\text{T}(\text{CH}_2)$ & $\text{W}(\text{CH}_2)$ $\nu(\text{COC})$ $\nu(\text{CO})$ s s
726	v.w.	725	v.w.	
		686	s.br.	

Table XVIII

Assignment of the absorption bands DMG8/D₂O neat phase spectrum (0.45 mole fraction)

Liquid DMG8 (42°C)		Neat phase DMG8/D ₂ O (15°C)		Assignments (b)
cm ⁻¹	Intensity (a)	cm ⁻¹	Intensity (a)	
3418	w	3410	w	} ν (OH)
2957	m	2956	m	
2929	s	2930	s	} ν_a { CH ₃ } ν_a { CH ₂ } ν_s { CH ₃ } ν_s { CH ₂ }
2870	m	2870	m	
2853	s	2853	s	
2527	s.br.			
		2500	s.br.	} ν (OD)
		1558	v.w.br.	
		1746	s	} ν_a (H ₂ O)
1739	s			
1733	s	1735	sh	} ν (C=O)
1468	m	1469	m	
1459	m	1460	m	} δ (CH ₂)
1422	w	1423	w	
1385	m	1385	m	
1272	m	1272	m	
1232	m			} ν_2 { D ₂ O } ν { C=O } ν { CO }
1174	s.br.	1215	m	
1111	m.br.	1175	s.br.	
1050	w.br.	1112	m.br.	
1000	w.br.	1052	w.br.	s
938	w.br.	1000	w.br.	s
849	w.br.	940	w.br.	
724	w	852	w.br.	
658	w.br.	725	w	ρ (CH ₂)

(a) For the meanings of the abbreviations used see the footnote to Table VIII.

(b) The meanings of the symbols used are as follows:-

ν	Stretching
δ	Bending
s	Skeletal
ρ	Rocking
T	Twisting
W	Wagging

Table XIX

Frequencies, half band widths, $\Delta\nu_{\frac{1}{2}}$, and intensity ratios, D_{45}/D_0 , for the decoupled $\nu(\text{OH})$ bands (Polarized) for the MG8 and MG11/ D_2O neat phases.

1-Monoglyceride	Temperature (°C)	X D_2O	Sample position				D_{45}/D_0
			$\nu(\text{OH})$ (cm^{-1})	$\Delta\nu_{\frac{1}{2}}$ (cm^{-1})	$\nu(\text{OH})$ (cm^{-1})	$\Delta\nu_{\frac{1}{2}}$ (cm^{-1})	
MG8	15	0.45	3406	269	3382	275	1.2130
	15	0.80	3404	267	3385	272	1.2269
	15	0.89	3404	271	3403	268	1.0311
MG11	45	0.52	3418	265	3404	269	1.2565
	45		3418	270	3396	272	1.2988
	75	0.73	3418	272	3414	275	1.0535
	45	0.86	3416	264	3414	270	1.0423

Table XX

Assignments of the absorption bands of the $C_{12}PO/H_2O$
neat phase spectrum (0.84 mole fraction of H_2O)

Liquid $C_{12}PO$ (90°C)		Neat phase $C_{12}PO/H_2O$ (45°C)		Assignments (b)
cm ⁻¹	Intensity (a)	cm ⁻¹	Intensity (a)	
2982	w	3410	s.br.	ν (OH)
2956	m	2956	m	ν_a (PCH)
2926	s	2929	s	ν_a (CH ₃)
2873	m	2875	m	ν_a (CH ₂)
2851	s	2852	s	ν_s (CH ₃)
		2118	v.w.br.	ν_s (CH ₂)
		1648	m.br.	ν_A (H ₂ O)
1465	m	1465	m	ν_2 (H ₂ O)
1460	m	1462	m	δ^2 (CH ₂)
1425	w	1425	w	} δ_a (PCH ₃)
1412	v.w.	1412	v.w.	
1376	v.w.	1397	v.w.	} δ_s (CH ₃)
1370	v.w.	1370	v.w.	
1352	v.w.	1350	v.w.	} δ_s (PCH ₃)
1299	m.s.	1298	m.s.	
1292	m.s.	1293	m.s.	
1256	w	1256	v.w.	
1190	s.br.	1148	sh	} ν (P=O)
		1138	s.br.	
1117	w	1058	w	s
1058	w	1008	w	s
1008	v.w.	987	v.w.	s
987	v.w.	935	m	
935	m.s.	896	v.w.br.	
898	v.w.br.	863	w.br.	
860	w.br.	778	v.w.br.	ρ (CH ₂)
778	v.w.br.	740	w.br.	ν_a (PC)
738	w.br.	723	v.w.br.	ρ (CH ₂)
723	sh	686	s.br.	ν_L (H ₂ O)
709	v.w.			

(a) For the meanings of the abbreviations used see footnote to Table VIII.

(b) The meanings of the symbols used are as follows:-

ν	Stretching
δ	Bending
s	Skeletal
ρ	Rocking

Table XXI

Frequencies and half band widths, $\Delta\nu_{\frac{1}{2}}$, of decoupled $\nu(\text{OH})$ (unpolarized) of liquid water MG8, MG11/D₂O and C₁₀PO/H₂O neat phases.

Temperature (°C)	Liquid water		Neat phase	
	$\nu(\text{OH})$ (cm ⁻¹)	$\Delta\nu_{\frac{1}{2}}$ (cm ⁻¹)	$\nu(\text{OH})$ (cm ⁻¹)	$\Delta\nu_{\frac{1}{2}}$ (cm ⁻¹)
4	3389	263	3391 (a)	270
15	3398	265	3410 (b)	262
33	3410	268	3412 (a)	273
45			3419 (c)	268
75	3415	273	3424 (c)	270

(a) C₁₀PO/H₂O

(b) MG8/D₂O

(c) MG11/D₂O

Table XXII

Average Ro-o values for liquid water and the $C_{10}PO/H_2O$ neat phase.

Temperature (°C)	Ro-o (Å)	
	liquid water	neat phase (0.86 mole fraction)
4	2.821	2.818
33	2.829	2.826
75	2.84	

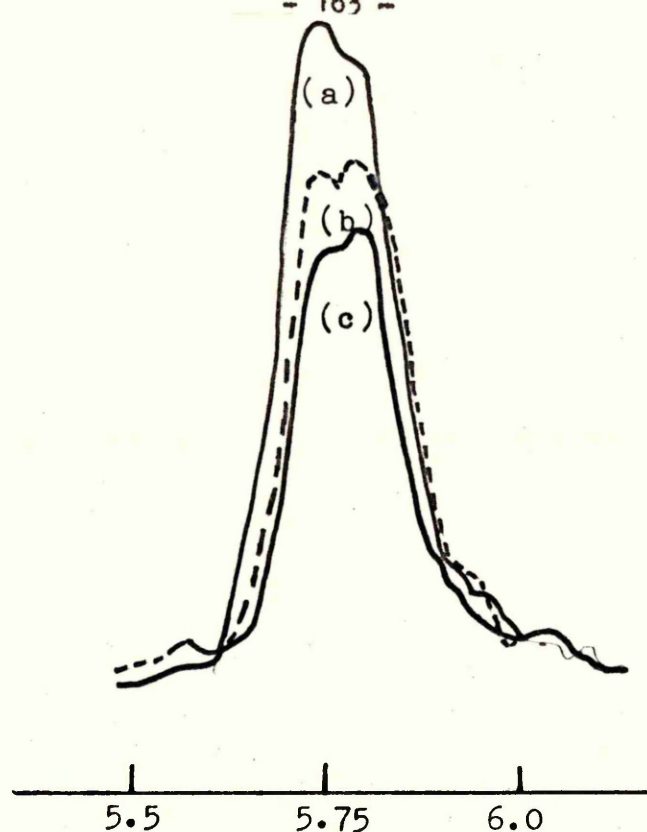


Figure 68.

$\nu(\text{C}=\text{O})$ bands in the neat l.c. phase of the DMG8/D₂O system, temperature 15°C,

(a) 0.45
(b) 0.80
(c) 0.89

mole fraction D₂O

Wavelength 5.5-6.0 μ.

Table XXIII

Frequencies of the $\nu(\text{C}=\text{O})$ bands for MG8 and MG11/D₂O neat phases.

l-monoglyceride	Temperature (°C)	X D ₂ O	$\nu(\text{C}=\text{O})$ (cm ⁻¹)
MG8	15	0.45	1746, 1735
	15	0.80	1745, 1734
	15	0.89	1745, 1734
MG11	45	0.52	1744, 1733
	45		1745, 1734
	75	0.73	1745, 1733
	45	0.86	1744, 1734

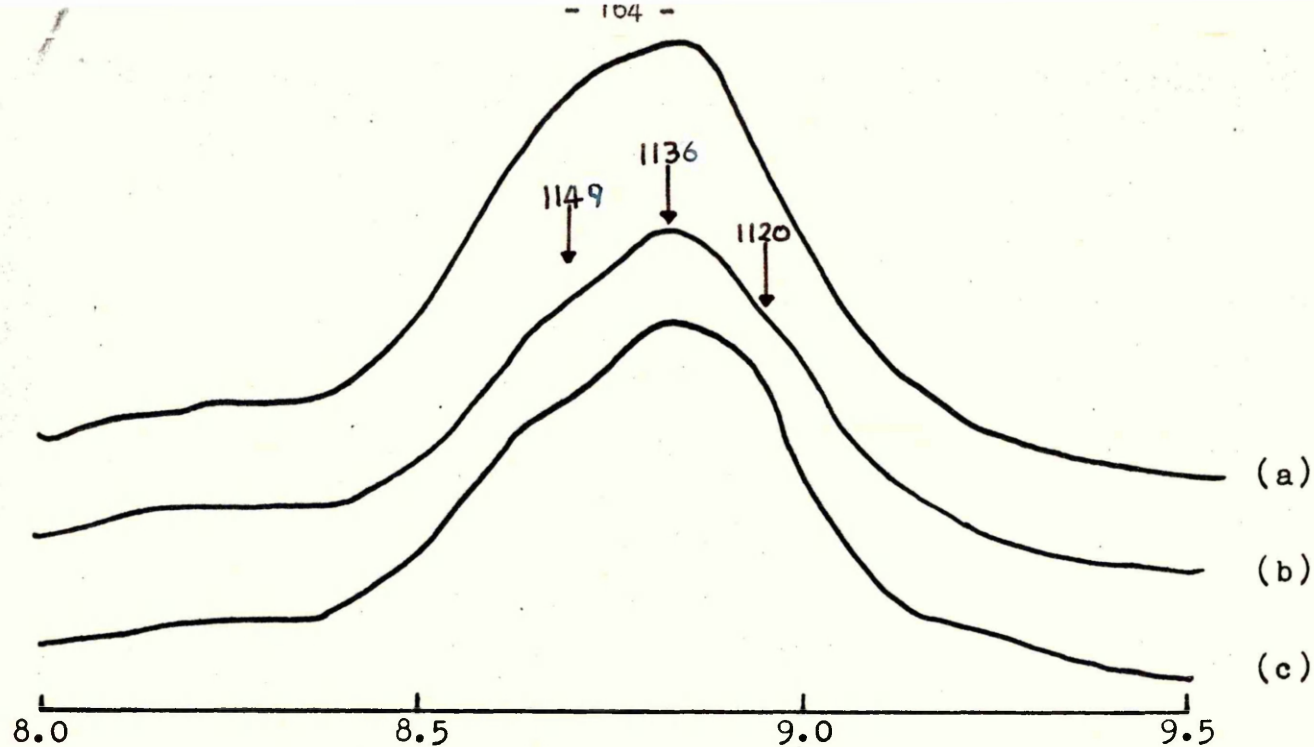


Figure 70.

$\nu(P=O)$ bands in the neat l.c. phase of the $C_{12}PO/H_2O$ system.

temperature $45^\circ C$,

$\left. \begin{array}{l} (a) 0.84 \\ (b) 0.87 \\ (c) 0.90 \end{array} \right\}$ mole fraction D_2O

Wavelength $8.0-9.5\mu$.

Table XXIV

Frequencies of the $\nu(P=O)$ bands for the $C_{12}PO/H_2O$ neat phase at $45^\circ C$.

x_{H_2O}	$\nu(P=O)$ (cm^{-1})
0.84	1148, 1138
0.87	1149, 1136, 1120
0.90	1148, 1137

(II) Middle Phase

(i) Results

Unpolarized infra-red spectra have been obtained of samples of $C_{12}PO$ at $15^{\circ}C$ in the composition range of the middle l.c. region of the phase diagram (figure 62). The middle phase is stable in systems containing 0.90 and 0.95 mole fraction of H_2O .

The absorption spectrum of the samples containing 0.90 mole fraction of H_2O with $C_{12}PO$ at $15^{\circ}C$ is shown in figure 73. The frequencies and proposed assignments of the absorption bands are listed in table XXV.

The unpolarized absorption spectrum of the decoupled $\nu(OH)$ of samples containing 0.94 mole fraction of D_2O with $C_{10}PO$ at $15^{\circ}C$ has been obtained and is shown, along with the decoupled $\nu(OH)$ of liquid water at the same temperature in figure 74.

(ii) Discussion

The structure of the middle phase in various lipid/ H_2O systems is envisaged (137,190-193) as being a two dimensional array of equidistant cylinders or rods, the alkyl chains being located in the interior of the rods and the water filling the gap between, although there is evidence that in certain systems the reverse structure does exist (194).

The identification of the middle phase, M, in the case of the $C_{12}PO/H_2O$ and $C_{10}PO/H_2O$ systems was carried out by Hermann et al (141) using a polarizing light microscope. They reported the textures characteristic of this phase reported by Rosevear (185). This identification has been confirmed in this work.

(a) Bands associated with the water/lipid interface

(1) $\nu(OH)$

The $\nu(OH)$ band of the 0.90 mole fraction of H_2O in $C_{12}PO$ spectrum (figure 73) at $15^{\circ}C$ is extremely broad,

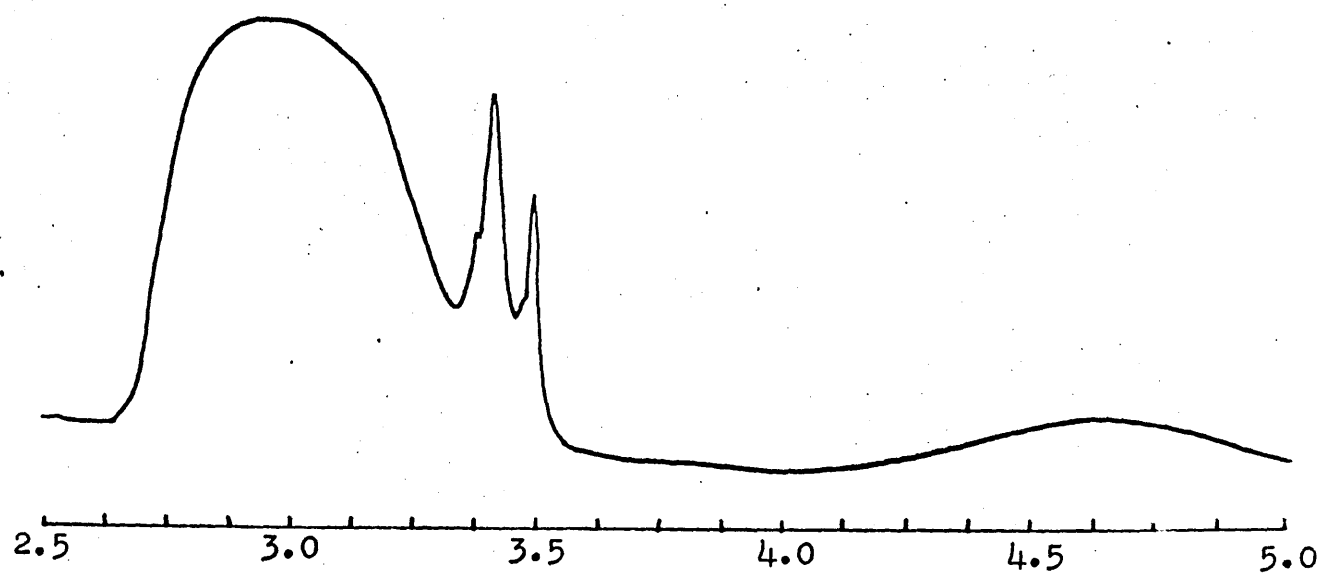
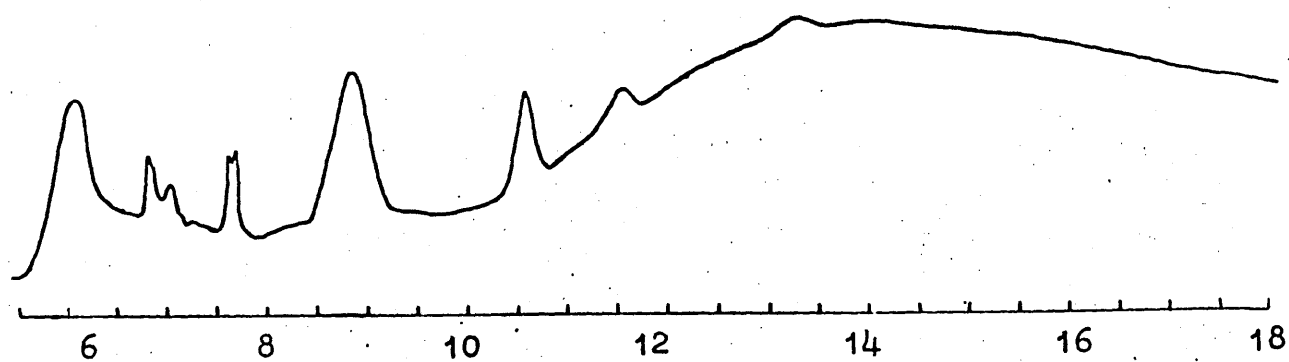


Figure 73.

Infra-red spectrum of $C_{12}PO$ + 0.90 mole fraction of H_2O
at $15^\circ C$ Wavelength 2.5-5.0 and 6-18 μ .

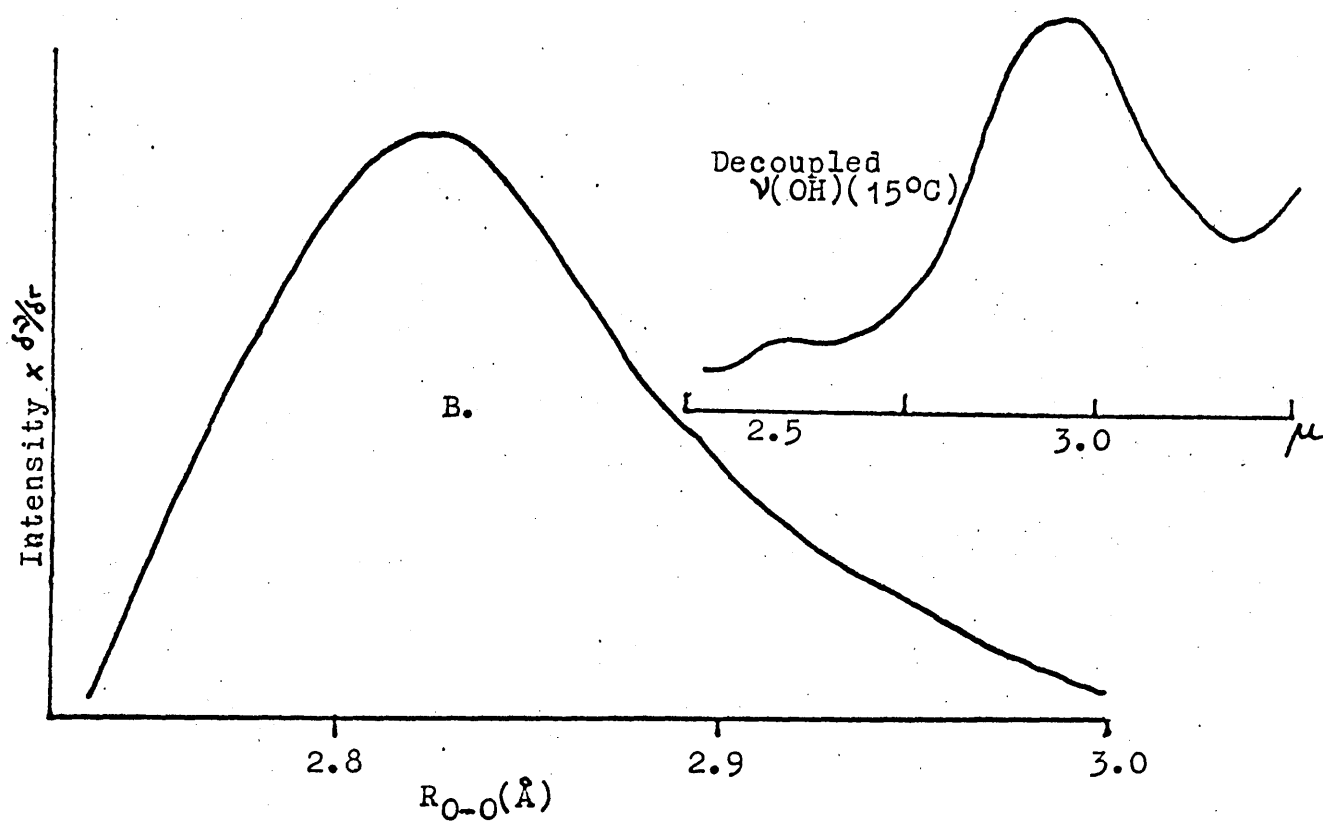
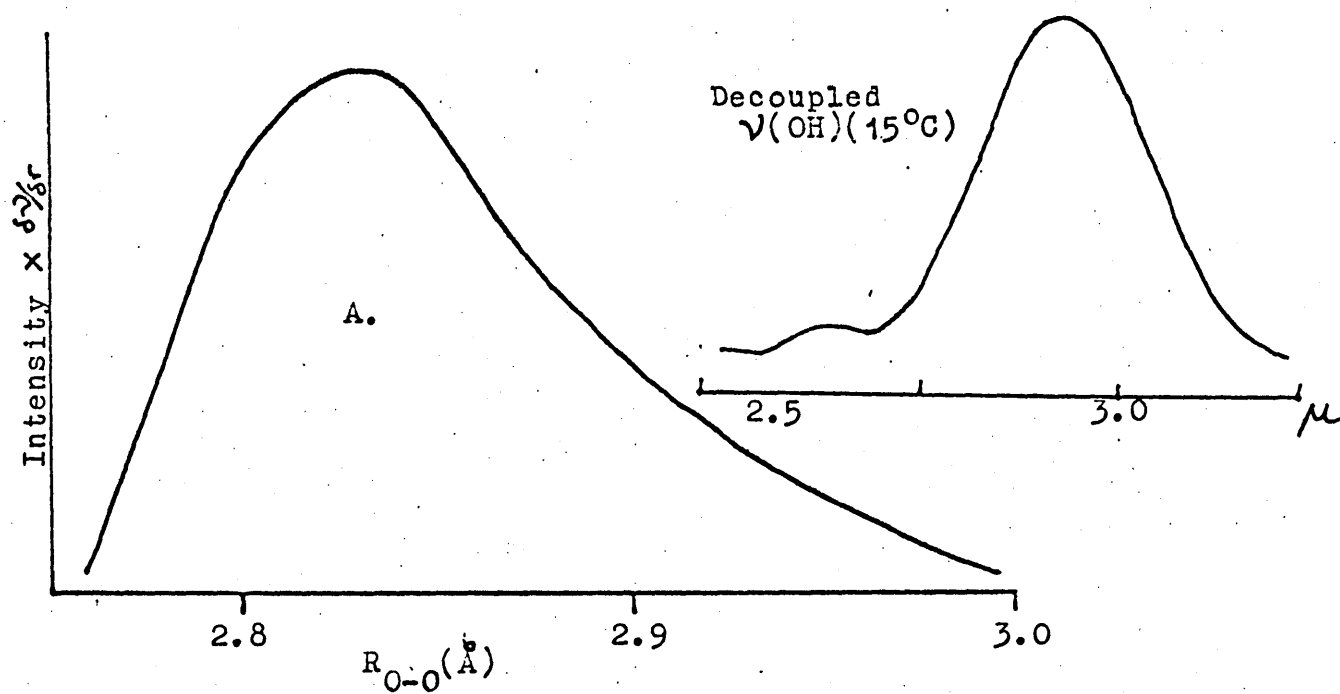


Figure 74.
Distribution functions of the decoupled $\nu(\text{OH})$ bands of:-
A. Liquid water at 15°C and B. $\text{C}_{10}\text{PO} + 0.94$ mole fraction of D_2O at 15°C .

has its maximum at approximately 3404cm^{-1} and is markedly asymmetric at approximately 3300cm^{-1} . As in the case of the $\nu(\text{OH})$ band of the l.c. phase observed in the case of $\text{MG8}/\text{H}_2\text{O}$, $\text{MG11}/\text{H}_2\text{O}$ and $\text{C}_{12}\text{PO}/\text{H}_2\text{O}$ systems (figures 59 and 63) the breadth of this band is so great, with $\Delta\nu_{\frac{1}{2}}$ in excess of 400cm^{-1} , that there is considerable overlap with bands associated with $\nu(\text{CH}_2)$ and $\nu(\text{CH}_3)$ in the region of 3000cm^{-1} and the general shape and position of this band at this temperature is unchanged on increasing the concentration of H_2O .

From a comparison of this spectrum with that of liquid water (figure 65) it would appear that as in the neat phase studied, the water incorporated in this middle phase is in a similar state to liquid water.

(2) Decoupled $\nu(\text{OH})$

The decoupled $\nu(\text{OH})$ band in the unpolarized spectrum of C_{10}PO samples containing 0.94 mole fraction of D_2O (figure 74) at 15°C appear to have a single maximum at 3394cm^{-1} . These bands are broad and symmetrical with a $\Delta\nu_{\frac{1}{2}}$ of 269cm^{-1} , like those of the neat phase of the $\text{C}_{10}\text{PO}/\text{H}_2\text{O}$ system and high water content neat phase samples of the $\text{MG8}/\text{D}_2\text{O}$ and $\text{MG11}/\text{D}_2\text{O}$ systems (figure 60) and liquid water (figure 74).

In liquid water at 15°C the decoupled $\nu(\text{OH})$ band appears to have a single maximum at 3398cm^{-1} and has a value of $\Delta\nu_{\frac{1}{2}}$ of 265cm^{-1} .

Assuming that the degree of interaction within the water incorporated in the middle phase of the $\text{C}_{10}\text{PO}/\text{H}_2\text{O}$ system is identical to that in liquid water itself then it is possible, utilizing the band analysis technique employed in the previous section of this chapter to obtain an average $R_{\text{O}-\text{O}}$ distance from this band. The distribution function for this sample is shown in figure 74 along with that obtained from the decoupled $\nu(\text{OH})$

of liquid water, at this temperature.

In both cases, the short distance side of the curves rise sharply and the peaks occur at $2.82(4)\text{\AA}$ and $2.82(2)\text{\AA}$ for liquid water and middle phase respectively.

Also the general shape of the distribution curve is more similar to that of water than that of the neat phase (section (I) part V. of this chapter). This is to be expected since in this phase there is more water present and therefore the contribution of the phosphoryl group to the nearest neighbour interaction would be proportionately smaller.

This data does not assist in determining whether or not the water is located in the interior of the rods or between them.

(3) Other bands associated with liquid water

In the unpolarized spectra of samples of $C_{12}PO$ containing 0.90 mole fraction of H_2O at $15^\circ C$ (figure 73) the other bands associated with liquid water are found in the following positions:-

- i. ν_A , a broad very weak band at 2125cm^{-1}
(2130cm^{-1})
- ii. ν_2 , a broad band of medium intensity at
 1649cm^{-1} (1648cm^{-1})
- iii. ν_L , an extremely broad and intense band at
approximately 682cm^{-1} (686cm^{-1}).

All the bands i-iii increase in intensity upon increasing the amount of H_2O , but do not alter their position. The frequencies of these bands in liquid water (figure 65) are shown in parenthesis after the frequency positions shown for the middle phase counterparts.

The band associated with the first overtone ν_L , as in the neat phase spectra previously discussed, is not observed.

(4) $\nu(P=0)$

The $\nu(P=0)$ bands for the various mole fractions of H_2O covering the $C_{12}PO$ middle phase, are shown diagrammatically as figure 75. The frequencies of these components of $\nu(P=0)$ within the middle phase are shown in table XXVI.

In this study of $\nu(P=0)$ bands in the middle l.c. phase of the $C_{12}PO/H_2O$ system, initially at a mole fraction of 0.90 of H_2O at $15^\circ C$ a broad band is observed at $1134cm^{-1}$ with shoulders at $1119cm^{-1}$ and $1147cm^{-1}$ (figure 75). This particular composition also exists as a neat phase at a temperature of $45^\circ C$. A comparison of the two spectra (figure 75) shows that the component at $1147cm^{-1}$ is much weaker in the middle phase spectra, whilst the asymmetry observed in the neat phase spectra in the vicinity of $1120cm^{-1}$ has increased in intensity in the middle phase spectrum and is now present as a definite shoulder at $1119cm^{-1}$. The intensity of the broad band at $1137cm^{-1}$ in the neat phase, now found at $1134cm^{-1}$ in the middle phase is unchanged.

The three components are observed in the same relative positions with the same relative intensity at a mole fraction of 0.94. However at a water mole fraction of 0.95, the highest mole fraction for which the middle l.c. phase is stable, the high frequency shoulder disappears completely. The principal band is now observed at $1132cm^{-1}$ whilst an intense shoulder is observed at $1119cm^{-1}$ (figure 75).

It would appear that upon reducing the temperature from $45^\circ C$ to $15^\circ C$ and hence changing the structure from neat to middle phase the relative proportions of the types of $C_{12}PO.H_2O$ complexes are altered. In the middle phase at $15^\circ C$ there appears to be an increase in the amount of the 1:2 complex (structure PIII(b), figure 71) and a corresponding decrease in the amount of the 2:1 complex (structure PI, figure 71) relative to the neat phase.

There is also a shift to lower frequency of the $\nu(\text{P}=\text{O})$ bands which might be expected with increased H-bond strength at lower temperature.

When the amount of H_2O is increased, within the phase, eventually this high frequency shoulder associated with the 2:1 complex disappears and it seems therefore reasonable to assume that complexes present are almost entirely of the 1:1 and 1:2 type (structures PII and PIII(b), figure 71). However the presence of components from the 2:1 complex may still be present as part of the rather extended high frequency tail of the broad $\nu(\text{P}=\text{O})$ bands remaining.

(b) Bands associated with the hydrocarbon chain

It is believed, as in the case of the neat phase, that the motion of hydrocarbon chains is again 'liquid like'. This has been confirmed in the middle phase of the $\text{C}_{12}\text{PO}/\text{H}_2\text{O}$ system. The spectra obtained for the middle phase have the appearance of those obtained in the neat phase of this system (figures 63 and 73) as well as the anhydrous liquid material (figure 45), the frequencies of the observed broad and diffuse absorption bands being in approximately the same positions (table XXV).

Table XXV

Assignments of the absorption bands of the $C_{12}PO/H_2O$
middle phase spectrum (0.95 mole fraction of H_2O)

Liquid $C_{12}PO$ (90°C)		Middle phase $C_{12}PO/H_2O$ (15°C)		Assignments (b)
cm ⁻¹	Intensity (a)	cm ⁻¹	Intensity (a)	
2982	w	3404	s.br.	ν (OH)
2956	m			ν_a (PCH)
2928	s	2956	m	ν_a (CH ₃)
2873	m	2930	s	ν_a (CH ₂)
2851	s	2876	m	ν_s (CH ₃)
		2851	s	ν_s (CH ₂)
		2125	v.w.br.	ν_a (H ₂ O)
		1649	m.br.	ν_2 (H ₂ O)
1465	m	1465	m	} δ (CH ₂)
1460	m	1462	m	
1425	w	1424	w	} δ_a (PCH ₃)
1412	v.w.	1411	v.w.	
1376	v.w.	1376	v.w.	} δ_s (CH ₃)
1370	v.w.	1369	v.w.	
1352	v.w.	1350	v.w.	} δ_s (PCH ₃)
1299	m.s.	1298	m.s.	
1292	m.s.	1293	m.s.	
1256	w	1256	v.w.	
1190	s.br.			} ν (P=O)
		1132	s.br.	
		1119	sh.	
1117	w			
1058	w	1057	w	s
1008	v.w.	1008	w	s
987	v.w.	987	v.w.	s
935	m.s.	935	m	
898	v.w.br.	897	v.w.br.	
860	w.br.	862	w.br.	
778	v.w.br.	778	v.w.br.	ρ (CH ₂)
738	w.br.	740	w.br.	
723	sh	723	v.w.br.	ρ (CH ₂)
709	v.w.			ν_L (H ₂ O)
		682	s.br.	

(a) For the meanings of the abbreviations used see footnote to Table VIII.

(b) The meanings of the symbols used are as follows:-

ν	Stretching
δ	Bending
s	Skeletal
ρ	Rocking

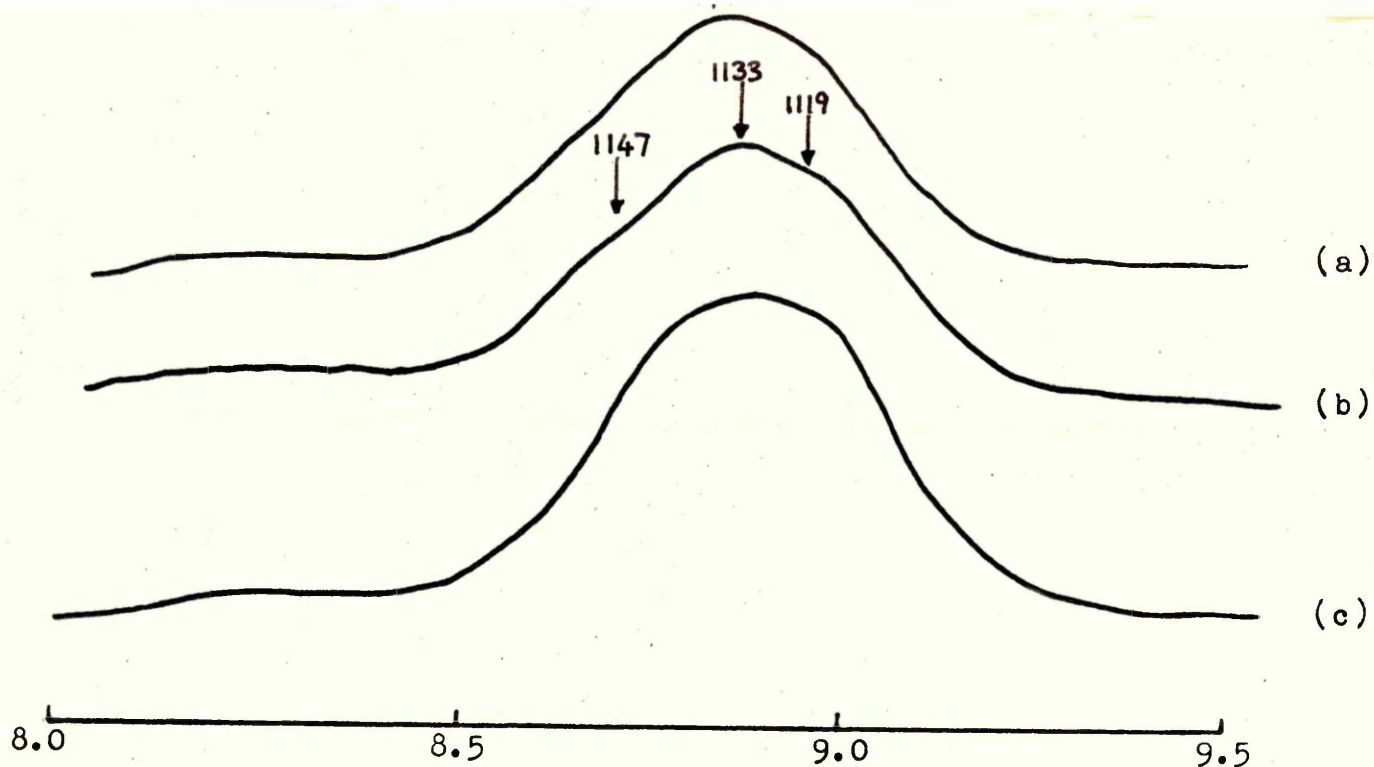


Figure 75.

$\nu(\text{P}=\text{O})$ bands in the middle l.c. phase of the $\text{C}_{12}\text{PO}/\text{H}_2\text{O}$ system
temperature 15°C ,

$\left. \begin{array}{l} \text{(a) } 0.90 \\ \text{(b) } 0.94 \\ \text{(c) } 0.95 \end{array} \right\} \text{ mole fraction } \text{H}_2\text{O}$

Wavelength $8.0\text{--}9.5\mu$.

Table XXVI

Frequencies of the $\nu(\text{P}=\text{O})$ bands for the $\text{C}_{12}\text{PO}/\text{H}_2\text{O}$ middle phase
at 15°C .

$x_{\text{H}_2\text{O}}$	$\nu(\text{P}=\text{O})$ (cm^{-1})
0.90	1147, 1134, 1119
0.94	1147, 1133, 1119
0.95	1132, 1119

CHAPTER VII

CONCLUSIONS

(I) Anhydrous Lipids

(i) 1-monoglycerides

(a) Polymorphism

The polymorphic forms of MG18, obtained by thermal treatment, and their transition temperatures observed in this work using D.S.C. are in good agreement with those reported previously using cooling and heating curves and differential thermal analysis. It has been confirmed that the polymorphic transitions are reversible and the polymorphs are stable over their reported temperature ranges. Also the infra-red spectra of these polymorphs are in good agreement with those obtained previously. However certain differences have been observed.

These include evidence from the structure of the $\nu(\text{C=O})$ band for the participation of the carbonyl in the H-bonding scheme in all the polymorphs obtained, and from a doublet $\delta(\text{CH}_2)$ band and bands in the CH stretch region in a similar position to highly crystalline n paraffins further evidence of the crystalline nature of the sub- α phase.

Two new polymorphic forms produced by thermal treatment have been observed for MG8 and MG12. Characterization of the phase in the case of MG8 proved impossible due to the exceedingly short life time but in the case of MG12 an infra-red spectrum of the new phase was obtained and appears to be that of a modified sub- α phase.

Unpolarized infra-red spectra of MG8 and DMG8 have been obtained of the liquid and polycrystalline states and most of the bands have been assigned tentatively to vibrational modes. Two

decoupled $\nu(\text{OH})$ bands are observed in the spectrum of DMG8 and indicate that the OH groups are present in two different environments. A comparison of the $R_{0-0}(\text{\AA})$ values, obtained for these bands, with those of pinacol indicate that the OH groups of MG8 are probably involved in $\text{O-H}\cdots\text{O-H}$ and $\text{O-H}\cdots\text{O}=\text{C}$ H-bonding.

(b) 1-monooctanoin in solution

Concentration changes in $\nu(\text{OH})$ and $\nu(\text{C}=\text{O})$ have been observed and indicate that there is a considerable amount of intramolecular H-bonding occurring in dilute solutions of MG8. Several possible H-bonded structures are discussed and measurements on a triglyceride/alcohol system in solution have been made in order to investigate the possible involvement of the alkoxy oxygen in the H-bonding scheme of MG8.

(ii) Structure of unsymmetrical trialkylphosphine oxides

The observed dichroisms in the polarized infra-red spectra of C_{10}PO have assisted in deciding the orientation of the molecules in the single crystal samples. The molecules are aligned with the alkyl chains in, and making an angle of less than 45° with, the plane of the plates, the alkyl chain skeletons being approximately at right angles to this plane. The phosphoryl groups also lie in the plane of the plates and are approximately at right angles to the alkyl chains. Also the dichroisms have assisted in the assignment of the bands of C_{10}PO and C_{12}PO spectra. The complexity of the $\nu(\text{P}=\text{O})$ bands has been discussed in terms of dipole-dipole association species.

X-ray long spacings of C_{10}PO and C_{12}PO indicate that the molecules crystallize in a bilayer structure and from the infra-red spectra it would appear that the alkyl chains pack in an orthorhombic sub-cell.

(II) Hydrated dimethyldecylphosphine oxide

The infra-red spectra, X-ray and T_1 and T_2 measurements indicate that the presence of water up to a mole fraction

of 0.5 does not effect the crystallization of $C_{10}PO$ in its bimolecular layer lattice. Differences do occur between the spectra of the hydrated and unhydrated material which indicate that H-bonding is taking place between the phosphoryl group and water. Also the water at normal temperatures is liquid like below a mole fraction of 0.5 although the slight shift to low frequencies of the decoupled $\nu(OH)$ band suggests a slightly higher H-bond strength than in liquid water.

However when the temperature is reduced to $-45^{\circ}C$ changes occur in $\nu(P=O)$ and $\nu(OH)$ which show the water is now present as ice I in the phase ($C_{10}PO + \text{ice I}$).

(III) Liquid Crystalline Phases

(i) The water/lipid interface

The unpolarized infra-red spectra of the bands associated with water in the l-monoglyceride and $C_{12}PO$ systems studied indicate that water in the neat and middle l.c. phases is liquid like.

In both l.c. phases the decoupled $\nu(OH)$ bands are broad. The shape of the bands in the case of the l-monoglyceride neat phase is found to alter with mole fraction of water. They are markedly asymmetric at low water content and symmetric at high concentrations, the bands looking like those of liquid water. No dichroisms are observed for these bands by rotation of the l-monoglyceride neat phase samples in the $V=0^{\circ}$ position. However when the samples are turned to $V=45^{\circ}$ to the beam whilst still in a vertical plane a shift to lower frequency and increase in intensity of the decoupled $\nu(OH)$ bands is observed in the low water content polarized spectra whilst at high water content these effects are not observed.

The asymmetry of the unpolarized decoupled $\nu(OH)$ bands at low water contents and the dichroic effects in the polarized

spectra are both due to the structuring effects of the 1-mono-glyceride OH groups within the water layer of the mesophase. The validity of this interpretation has been checked by observations on the decoupled $\nu(\text{OH})$ bands of the neat phase of the $\text{C}_{12}\text{PO}/\text{H}_2\text{O}$ system.

Effects similar to those observed on increasing the water content are observed when a low water content sample of MG11 + H_2O neat phase is heated to a higher temperature. These effects are due to a greater relative decrease in the numbers of the most strongly associated species which give rise to the low frequency vibration.

Evidence has been obtained for the stable monohydrate, indicated by a small peak in the phase diagram of the MG11/ D_2O system from a significant narrowing of the decoupled $\nu(\text{OH})$ band at that composition.

Evidence has also been obtained in the MG8 and MG11/ D_2O neat phases for the participation of the carbonyl in the H-bonding scheme but it seems that the H-bonding in which the carbonyl is involved is not important in the stability of the neat phase.

The presence of several $\nu(\text{P=O})$ bands in both neat and middle phases of $\text{C}_{12}\text{PO}/\text{H}_2\text{O}$ system is explained in terms of the presence of 2:1, 1:1, and 1:2 acceptor to donor H-bonding complexes. At all water contents all these complexes are present to some extent. However at low water contents complexes of the 2:1 and 1:1 type predominate whilst at higher water concentrations, in the middle phase, the 1:1 and 1:2 complexes predominate.

The decoupled $\nu(\text{OH})$ bands of the C_{10}PO neat and middle phases and liquid water have been analysed to produce radial distribution curves. The average $R_{\text{O}-\text{O}}(\text{\AA})$ values indicate that the water in both phases is liquid like, although the shape of

the distribution function is broader in the case of the neat phase, relative to water, due to the appreciable participation of the phosphoryl groups in the nearest neighbour interaction.

(ii) The hydrocarbon chains

Comparison of the spectra of the liquid anhydrous lipids with those of the neat and middle phases indicate that the motion of the hydrocarbon chains is liquid like. Dichroisms have not been observed for bands associated with the hydrocarbon chains for sample positions $V = 0^\circ$ or $V = 45^\circ$ in all the neat phases studied.

REFERENCES

1. H.H. Hatt, Rev. Pure Appl. Chem., 6, 153, 1956.
2. N.A. Pushin and A.A. Glagoleva, J. Chem. Soc., 121, 2816, 1922.
3. A.J. O'Connor, M.Sc. Thesis, Sheffield University, 1969.
4. H.E. Petch, N. Sheppard and H.D. Megaw, Acta Cryst., 2, 29, 1956.
5. J.M. Janik, G. Pytasz and S. Staneck, Acta Phys. Pol., 65, 997, 1969.
6. J. Schiffer, Ph.D. Thesis, Princeton University, 1963.
7. L.J. Bellamy, M. Blandamier, M.C.R. Symons and D. Waddington, Trans. Faraday Soc., 67, 3435, 1971.
8. J. Schiffer and D.F. Hornig, Natl. Bur. Std. (U.S.), Spec. Publ., 301, 257, 1969.
9. R.A. Fifer and J. Schiffer, J. Chem. Phys., 52, 2664, 1970.
10. R. Kling and J. Schiffer, J. Chem. Phys., 54, 5331, 1969.
11. V. Seidl, O. Knop and M. Falk, Can. J. Chem., 47, 1361, 1969.
12. M.A. Al-Mamun, Ph.D. Thesis, Sheffield University, 1969.
13. M. Tasumi, T. Shimanouchi, A. Watanabe and R. Goto, Spectrochim. Acta., 20, 629, 1964.
14. M. Falk and E. Whalley, J. Chem. Phys., 34, 1554, 1961.
15. Y. Mikaya, J.W. Brasch and R.J. Jakobsen, Spectrochim. Acta, 27A, 529, 1971.
16. R.J. Jakobsen, Y. Mikaya and J.W. Brasch, Nature, 215, 1071, 1967.
17. R.J. Jakobsen, J.W. Brasch and Y. Mikaya, J. Mol. Struct., 1, 309, 1967.
18. G. Renner, Fette Seifen, Anstrichmittel, 67, 918, 1965.
19. A. Elliott, E.J. Ambrose and R.B. Temple, J. Chem. Phys., 16, 877, 1948.
20. J.R. Nielsen and R.F. Holland, J. Mol. Spectroscopy, 4, 488,

1960.

21. J.R. Nielsen and R.F. Holland, J.Mol. Spectroscopy, 6, 394, 1961.
22. S. Krimm, C.Y. Liang and G.B.B.M. Sutherland, J.Chem. Phys., 25, 549, 1956.
23. S. Krimm, J. Chem. Phys., 22, 567, 1954.
24. R.S. Stein and G.B.B.M. Sutherland, J.Chem.Phys., 22, 1993, 1954.
25. M.C. Tobin and M.J. Carrano, J. Chem. Phys., 25, 1044, 1956.
26. M.P. McDonald and I.M. Ward, Polymer, 2, 341, 1961.
27. W.H.T. Davison, J.Chem. Soc., 3270, 1955.
28. H. Aminoto, J. Polym. Sci., A, 2, 2283, 1964.
29. R.F. Holland and J.R. Nielsen, J.Mol.Spectroscopy, 8, 383, 1962.
30. H. Susi and A.M. Smith, J. Amer. Oil Chem. Soc., 37, 431, 1960.
31. H. Susi, J. Amer. Chem. Soc., 81, 1535, 1959.
32. J. Mann and H.W. Thompson, Proc. Roy. Soc. (London), A192, 489, 1948.
33. E.J. Ambrose, A. Elliott and R.B. Temple, Proc. Roy. Soc. (London), A206, 192, 1951.
34. H. Susi, Spectrochim. Acta, 12, 1063, 1959.
35. R.F. Holland and J.R. Nielsen, J. Mol.Spectroscopy, 2, 436, 1962.
36. R.F. Holland and J.R. Nielsen, Acta Cryst., 16, 902, 1963.
37. A.R.H. Cole and R.N. Jones, J. Opt. Soc. Amer., 42, 348, 1952.
38. Y. Mikaya, J.W. Brasch and R.J. Jakobsen, J. Mol. Spectroscopy, 3, 103, 1969.
39. H. Susi, Anal. Chem., 31, 910, 1959.
40. C.A. Coulson, Spectrochim. Acta, 14, 161, 1959.
41. R. Newman and R.S. Halford, Rev.Sci.Inst., 19, 270, 1948.

43. A. Elliott, E.J. Ambrose and R.B. Temple, J. Opt. Soc. Am., 38, 212, 1948.
44. E. Charney, J. Opt. Soc. Am., 45, 980, 1955.
45. A. Yamaguchi, I. Ichishima and S. Mizushima, Spectrochim. Acta, 12, 294, 1958.
46. L.P. Kuhn, J. Amer. Chem. Soc., 74, 2492, 1952.
47. S.N. Vinogradov and R.H. Linnell, Hydrogen Bonding, P.252., Van Nostrand Reinhold, New York, 1971.
48. D. Eisenberg and W. Kauzmann, The Structure and Properties of Water, P.229, Oxford University Press, Oxford, 1969.
49. J.E. Bertie and E. Whalley, J. Chem. Phys., 40, 1637, 1964.
50. C.N.R. Rao, Chemical Applications of Infra-red Spectroscopy P,(a) 187, (b) 132, (c) 137, (d) 143, (e) 209, Academic Press, 1963.
51. A.V. Stuart and G.B.B.M. Sutherland, J.Chem. Phys. 24, 559, 1956.
52. L.J. Bellamy, Advances in Infra-red Group Frequencies, P.9, Methuen, 1968.
53. N. Sheppard and D.M. Simpson, Quart. Rev., 7, 19, 1953.
54. N.B. Colthup, L.H. Daly and S.E. Wiberley, Introduction to Infra-red and Raman Spectroscopy, P, (a) 195, (b) 274, (c) 197, Academic Press, 1964.
55. G.J. Karabatsos, J. Org. Chem., 25, 1409, 1960.
56. H.A. Ory, Anal. Chem., 32, 509, 1960.
57. H. Matsuura and T. Myazawa, Bull. Chem. Soc. Japan, 40, 85, 1967.
58. J.P. Perchard and M.L. Josein, J.Chim. Phys., 65, 1856, 1968
59. G.C. Pimentel and A.L.McClellan, The Hydrogen Bond, P.129, Freeman, San Francisco, 1960.
60. T.T. Wall and D.F. Hornig, J.Chem.Phys., 43, 2079, 1965.
61. C.L.Van Eck, H. Mendel and J. Fahrenfort, Proc. Roy. Soc. (London), A247, 472, 1958.

62. C.A. Coulson, Valence, Oxford Univ. Press, London, 1961.
63. E. Schwarzmann, Z. Anorg. Allg. Chem., 317, 176, 1962.
64. V. Seidl, O. Knopp and M. Falk, Can. J. Chem., 47, 1361, 1969.
65. R.E. Rundle and M. Parasol, J. Chem. Phys., 20, 1487, 1952.
66. R.C. Lord and R.E. Merrifield, J. Chem. Phys., 21, 166, 1953.
67. K. Nakamoto, M. Margoshes and R.E. Rundle, J. Amer. Chem. Soc., 77, 6480, 1955.
68. O. Glemser and E. Hartert, Naturiss., 42, 534, 1955.
69. G.C. Pimentel and C.H. Sederholm, J.Chem.Phys., 24, 639, 1956.
70. H. Ratajczack and W.J. Orville-Thomas, J. Mol. Structure, 1, 449, 1967-68.
71. Y.Y. Efimov and Y.I. Naberukhin, Z. Strukt.Khim., 12, 540, 1971.
72. W.C. Hamilton and J.A. Ibers, Hydrogen Bonding in Solids, W.A. Benjamin, New York, 1968.
73. K.J. Jauer and W.N. Lipscombe, Acta Cryst., 5, 606, 1952.
74. K. Lonsdale, Proc. Roy. Soc. (London), A247, 424, 1958.
75. J.S. Cook and R.J. Meakins, Trans. Faraday Soc., 51, 1483, 1955.
76. A.S.C. Lawrence, Mol. Cryst. Liquid Cryst., 7, 1, 1969.
77. D. Chapman, Introduction to Lipids, McGraw-Hill, 1969.
78. D. Small, J. Amer. Oil. Chem. Soc., 45, 108, 1968.
79. A.S.C. Lawrence, A. Bingham, C.B. Capper and I.K. Hume, J. Phys. Chem., 68, 3470, 1964.
80. E. Fischer, M. Bergmann and H. Barwind, Ber., 53, 1589, 1920
81. R.S. Rewadikar and H.E. Watson, J. Indian Inst.Sci., 13A, 128, 1930.
82. T. Malkin and M.R. El Shurbagy, J. Chem. Soc., 1628, 1936.

83. B.F. Daubert and A.R. Baldwin, J. Amer. Chem. Soc., 66, 997, 1944.
84. M.G.R. Carter and T. Malkin, J. Chem. Soc., 554, 1947.
85. E.S. Lutton and F.L. Jackson, J. Amer. Oil Chem. Soc., 70, 2445, 1948.
86. T. Malkin, Progress in the Chemistry of Fats and other Lipids, Pergamon Press, London, Vol.2, Ch.1, 1954.
87. A.T. Gross and R.O. Feuge, J. Amer. Oil Chem. Soc., 34, 239, 1957.
88. L.J. Filer, Jr., S.S. Sidhu, B.F. Daubert and H.E. Longenecker, J. Amer. Chem. Soc., 66, 1333, 1944.
89. D. Chapman, Nature, 176, 216, 1955.
90. D. Chapman, J. Chem. Soc., 55, 1956.
91. D. Chapman, R.E. Richards and R.W. Yorke, J. Chem. Soc., 436, 1960.
92. A. Bhide and R.J. Bhide, J. Univ. Bombay, 8, 220, 1939.
93. R.W. Crowe and C.P. Smyth, J. Amer. Chem. Soc., 72, 4427, 1950.
94. D. Chapman, Chem. Rev., 62, 433, 1962.
95. K. Larsson, Arkiv Kemi, 23, 29, 1964.
96. K. Larsson, Arkiv Kemi, 23, 35, 1964.
97. E.S. Lutton, J. Amer. Oil Chem. Soc., 48, 778, 1971.
98. H.W. Thompson and P. Torkington, Proc. Roy. Soc. (London), 184A, 3, 1945.
99. R.S. Stein, J. Chem. Phys., 23, 734, 1955.
100. S. Abrahamsson, S. Aleby, G. Larsson and K. Larsson, Acta Cryst., 13, 1044, 1960.
101. M.C. Phillips, R.M. Williams and D. Chapman, Chem. Phys. Lipids, 3, 234, 1969.
102. N.H. Kurht, E.A. Welch, W.P. Blum, E.S. Perry and W.H. Weber, J. Amer. Oil Chem. Soc., 29, 261, 1952.

103. J.R.Barcelo and C.S. Martin, J. Phys. Radium, 5, 403, 1954.
104. R.T. O'Connor, E.F. Dupre and R.O. Feuge, J. Amer. Oil Chem. Soc., 32, 88, 1955.
105. D. Chapman, J. Amer. Oil Chem. Soc., 37, 73, 1960.
106. K.D. Lawson and T.J. Flautt, J. Phys. Chem., 72, 2066, 1968.
107. E.S. Lutton, J. Amer. Oil Chem. Soc., 43, 28, 1966.
108. D.G. Kolp and E.S. Lutton, J. Amer. Oil Chem. Soc., 72, 5593, 1951.
109. S. Abrahamson, G. Larsson and E. Von Sydow, Acta Cryst., 13, 770, 1960.
110. S.H. Piper, T. Malkin and H.E. Austin, J. Chem. Soc., 2310, 1926.
111. S.H. Piper, T. Malkin and H.E. Austin, Trans Faraday Soc., 25, 348, 1929.
112. J.D. Bernal, Z. Krist, 83, 153, 1932.
113. S.H. Piper, A.C. Chibnall and E.F. Williams, J. Biochem, 28, 2175, 1934.
114. S.H. Piper, A.C. Chibnall and E.F. Williams, J. Biochem, 25, 2072, 1931.
115. K. Higasi and M. Kubo, Sci. Paps. Inst. Phys. Chem. Res. (Japan), 36, 286, 1939.
116. W.E. Garner, F.C. Madden and J.E. Rushbrooke, J.Chem. Soc., 2491, 1926.
117. W.C. Philips and S.A. Munford, J. Chem. Soc., 1732, 1932.
118. J.D. Meyer and E.E. Reid, J. Amer. Chem. Soc., 55, 1574, 1933.
119. J.D. Hoffman and C.P. Smyth, J. Amer. Chem. Soc., 71, 431, 1949.
120. A. Trapeznikov, Acta Physiochim., 19, 553, 1944.
121. A. Trapeznikov, Compt. Rend. Acad. Sci., U.R.S.S., XLVII, 275, 1945.

122. A. Trapeznikov, Doklady Acad. Nauk. S.S.S.R., 227, 1945.
123. A. Trapeznikov, Comp. Rend. Acad. Sci., U.R.S.S., 47, 417, 1945.
124. A. Trapeznikov. Doklady Acad. Nauk., S.S.S.R., 435, 1945.
125. A. Trapeznikov, Zhur. Fiz. Khim., 19, 228, 1955.
126. A. Trapeznikov, 2nd. Int. Cong. Surface Activity, 1, 109, 1957.
127. A. Trapeznikov, 2nd. Int. Cong. Surface Activity, 1, 129, 1957.
128. A. Trapeznikov, and T.A. Lomonosava, Doklady Acad. Nauk, S.S.S.R., 155, 1419, 1964.
129. A. Trapeznikov and T.A. Lomonosava, Zhur. Fiz. Khim., 41, 277, 1967.
130. J.H. Brookes and A.E. Alexandre, Retardation of Evaporation by Monolayers, Ed., V. La-Mer, N.Y., 1963.
131. J.H. Brookes and A.E. Alexandre, J. Phys. Chem., 66, 1851, 1962.
132. A.S.C. Lawrence, H.A. Al-Mamun and M.P. McDonald, Trans. Faraday Soc., 63, 2789, 1967.
133. A.S.C. Lawrence and M.P. McDonald, Mol. Cryst., 1, 205, 1966
134. J.M. Corkhill and K.W. Hermann, J. Phys. Chem., 67, 935, 1963.
135. K.W. Hermann, J. Phys. Chem., 68, 1540, 1964.
136. L. Benzamin, J. Phys. Chem., 68, 3575, 1964.
137. K.D. Lawson, A.J. Mabis and T.J. Flautt, J. Phys. Chem., 72, 2058, 1968.
138. K.D. Lawson and T.J. Flautt, Mol. Cryst. 1, 241, 1966.
139. J.R. Hanson and K.D. Lawson, Nature, 225, 542, 1970.
140. L. Benzamin, J. Phys. Chem., 70, 3790, 1966.
141. K.W. Hermann, J.G. Brushmiller and W.L. Courchene, J. Phys. Chem., 70, 2909, 1966.

142. V.J. Goubeau and W. Berger, *Zeits. Anorg. Chem.*, 304, 148, 1960.
143. J.W. O'laughlin, J.J. Richard, J.W. Ferguson and C.V. Banks, *Anal. Chem.*, 40, 146, 1968.
144. D.J.G. Ives and T.H. Lennon, *R.I.C. Rev.*, 1, 62, 1968.
145. D.P. Stevenson, *Structural Chemistry and Molecular Biology*, Ed. A. Rich and N. Davidson, Freeman, 1968.
146. D. Eisenberg and W. Kauzmann, *The Structure and Properties of Water*, Oxford 1969.
147. L. Pauling, *Hydrogen Bonding*, Ed. D. Hadzi, Pergamon Press, P.1, 1959.
148. G. Nemethy and H.A. Scheraga, *J. Chem. Phys.*, 36, 3382, 1962.
149. R.P. Marchi and H. Eyring, *J. Phys. Chem.*, 68, 221, 1964.
150. W. Luck, *Ber. Bunsenges Physik. Chem.*, 67, 186, 1963.
151. M.D. Danford and H.A. Levy, *J. Amer. Chem. Soc.*, 84, 3965, 1962.
152. J.A. Pople, *Proc. Roy. Soc. (London)*, 205A, 163, 1951.
153. D.N. Glew, *J. Phys. Chem.*, 66, 605, 1962.
154. J.A. Barker, *Ann. Rev. Phys. Chem.*, 14, 229, 1963.
155. G.C. Pimentel and A.L. McClellan, *The Hydrogen Bond*, Freeman, San Francisco, 1960.
156. M. Falk and T.A. Ford, *Can. J. Chem.*, 44, 1699, 1966.
157. D.F. Hornig, *J. Chem. Phys.*, 40, 3119, 1964.
158. R.D. Waldron, *J. Chem. Phys.*, 26, 809, 1957.
159. G.E. Walrafen, *J. Chem. Phys.*, 48, 244, 1968.
160. E.U. Franck and K. Roth, *Disc. Faraday Soc.*, 43, 108, 1967.
161. G.E. Walrafen, *J. Chem. Phys.*, 47, 114, 1967.
162. K.A. Hartman, *J. Phys. Chem.*, 70, 270, 1966.
163. W.A. Senior and R.E. Verall, *J. Phys. Chem.*, 73, 4242, 1969.
164. M. Falk and H.R. Wyss, *J. Chem. Phys.*, 51, 5727, 1969.
165. R. Virchow, *Archiv.*, 6, 502, 1854.

166. Neubauer, *Analyst. Zeit.*, 6, 189, 1863.
167. Neubauer, *Liter. Centralbl.*, 491, 1863.
168. G.H. Brown and W.G. Shaw, *Chem. Rev.*, 57, 1049, 1957.
169. G.H. Brown, J.W. Doane and V.D. Neff, *Crit. Revs. in Solid State Sci.*, 1, 303, 1970.
170. J.G. Christyakov, *Soviet Physics Cryst.*, 5, 917, 1961.
171. P.A. Winsor, *Chem. Rev.*, 68, 1, 1968.
172. H. Benedy, *Chem. Anlagen. Verfahren.*, 11, 85, 1971.
173. S. Chandrasekhar and N.V. Madhusudana, *App. Spec. Revs.*, 6, 193, 1973.
174. A.W. Ralston, C.W. Hoerr and E.J. Hoffman, *J. Amer. Chem. Soc.*, 64, 1516, 1942.
175. F.K. Broome, C.W. Hoerr and H.J. Harwood, *J. Amer. Oil Chem. Soc.*, 72, 3350, 1951.
176. R.R. Balmbra, J.S. Clunie and J.F. Goodman, *Nature*, 222, 1159, 1969.
177. J.S. Clunie, J.M. Corkhill and J.F. Goodman, *Proc. Roy. Soc. A285*, 520, 1965.
178. J.S. Clunie, J.F. Goodman and P.C. Symons, *Trans. Faraday Soc.*, 65, 287, 1969.
179. E.S. Lutton, *J. Amer. Oil Chem. Soc.*, 42, 1068, 1965.
180. K. Larsson, *Zeit. Phys. Chem.*, 56, 173, 1967.
181. N. Krog and J. Andreasen, *Nord. Symp. Graenselfadekemi Fortryk Foredrag*, 3rd., 1, 1967.
182. N. Krog and K. Larsson, *Chem. Phys. Lipids*, 2, 129, 1968.
183. B. Ellis, M.P. McDonald, A.S.C. Lawrence and W.E. Peel, *Liquid Crystals and Ordered Fluids*, Ed., J.F. Johnson and R.S. Porter, Plenum Press, New York, 1970.
184. D.M. Small, *J. Lipid Research*, 8, 551, 1967.
185. F.B. Rosevear, *J. Amer. Oil Chem. Soc.*, 31, 628, 1954.
186. F.B. Rosevear, *J. Soc. Cosmetic Chemists*, 12, 581, 1968.

187. J. Stauff, Kolloidzeitschrift, 89, 224, 1939.
188. T. Doscher and R. Vold, J. Phys. Colloid Chem., 52, 97, 1948.
189. W. Philippoff and J.W. McBain, Nature, 164, 885, 1949.
190. V. Luzzati, H. Mustacci and A. Skoulios, Nature, 180, 600, 1957.
191. V. Luzzati, H. Mustacci and A. Skoulios, Disc. Faraday Soc., 25, 43, 1958.
192. V. Luzzati, H. Mustacci, A. Skoulios and F. Husson, Acta Cryst., 13, 660, 1960.
193. F. Husson, H. Mustacci and V. Luzzati, Acta Cryst., 13, 668, 1960.
194. V. Luzzati and F. Husson, J. Cell Biology, 12, 207, 1962.
195. B. Gallot and A.E. Skoulios, Kolloidzeitschrift, 208, 37, 1966.
196. R.R. Balmbra, J.S. Clunie and J.F. Goodman, Mol. Cryst., 3, 281, 1967.
197. D.A.B. Bucknall, J.S. Clunie and J.F. Goodman, Mol. Cryst., Liquid Cryst., 7, 215, 1969.
198. F. Reiss-Husson, J. Mol. Biology, 25, 363, 1967.
199. A. Skoulios, Advan. Colloid Interface Sci., 1, 79, 1967.
200. R.R. Balmbra, J.J. Clunie and J.F. Goodman, Proc. Roy. Soc., A285, 534, 1965.
201. V. Luzzati, Biological Membranes, Ch. 3, Ed. D. Chapman, Academic Press, 1969.
202. J.W. McBain and S.S. Marsden, J. Chem. Phys., 15, 211, 1947.
203. S.S. Marsden and J.W. McBain, J. Phys. Colloid Chem., 52, 110, 1948.
204. V. Luzzati, F. Reiss-Husson, E. Rivas and T. Gulik-Krzywicki Ann. N.Y. Acad. Sci., 137, 409, 1966.
205. T. Gulik-Krzywicki, E. Rivas and V. Luzzati, J. Mol. Biology, 27, 303, 1967.

206. W. Stoeckenius, J. Cell Biology, 12, 221, 1962.
207. A.D. Bagham and R.W. Horne, J. Mol. Biology, 8, 660, 1964.
208. J. Seelig, J. Amer. Chem. Soc., 92, 3881, 1970.
209. W.E. Peel, Ph. D. Thesis, Sheffield Polytechnic, 1972.
210. M.P. McDonald, Arch. Sci. (Geneva), 12, 141, 1959.
211. C.A. Gilchrist, J. Rogers, G. Steel, E.G. Vaal and P.A. Winsor, J. Colloid Interface Sci., 25, 409, 1967.
212. J.M. Corkhill, J.F. Goodman and J. Wyer, Trans. Faraday Soc., 65, 9, 1969.
213. K.D. Lawson and T.J. Flautt, J. Phys. Chem., 72, 2066, 1968.
214. K.D. Lawson and T.J. Flautt, J. Phys. Chem., 69, 4256, 1965.
215. J. Charvolin and P. Rigny, J. Phys. (Paris), 30, C4-76, 1969.
216. R. Blinc, K. Easwaran, J. Pirs, M. Volfan and I. Zupaneic, Phys. Revs. Letters, 25, 1327, 1970.
217. J.J. deVries and H.J.C. Berendsen, Nature, 221, 1139, 1969.
218. T. Drakenberg, A. Johansson and S. Forsen, J. Phys. Chem., 74, 4528, 1970.
219. G.J.T. Tiddy, Nature, 230, 136, 1971.
220. M.P. McDonald and W.E. Peel, Trans. Faraday Soc., 67, 890, 1971.
221. W. Maier and G. Englert, Z. Physik. Chem. (N.F.), 12, 123, 1957.
222. W. Maier and G. Englert, Z. Electrochem., 62, 1020, 1958.
223. W. Maier and G. Englert, Z. Physik. Chem. (N.F.), 19, 168, 1959.
224. W. Maier and G. Englert, Z. Elektrochem., 64, 689, 1960.
225. V.D. Neff, L.W. Gulrich and G.H. Brown, Liquid Crystals, Proc. 1st. Int. Liquid Crystal Conf., Eds. G.H. Brown, G.J. Dienes, and M.M. Labes, Gordon and Breach, New York, London and Paris, 1967, P. 21.
226. B.J. Bulkin, D. Grunbaum and A.V. Santoro, J. Chem. Phys., 51, 1602, 1969.

227. B.J. Bulkin and N.I. Krishnamachari, Biochim. Biophys. Acta., 211, 592, 1970.
228. B.J. Bulkin and N.I. Krishnamachari, J. Amer. Chem. Soc., 94, 1109, 1972.
229. P. Byrne and D. Chapman, Nature, 202, 987, 1964.
230. D. Chapman, The structure of Lipids, Methuen, London, 1965.
231. A.H. Maddy and B.R. Malcolm, Science, N.Y., 150, 1616, 1965.
232. D.F.H. Wallach and P.H. Zahler, Proc. Natl. Acad. Sci., U.S.A., 56, 1552, 1966.
233. J.L. Kavanu, Science, N.Y., 153, 213, 1966.
234. D. Chapman, V.B. Kamat and R.J. Levene, Science, N.Y., 160, 314, 1968.
235. S. Friberg and G. Saderland, Kolloid Polymere, 243, 56, 1971.
236. J.D. Bernal and S. Frankacheu, J. Gen. Physiol, 25, 111, 1941.
237. J.W. McBain, J. Amer. Chem. Soc., 70, 1973, 1948.
238. D.C. Mabis and H.K. Mangold, J. Amer. Oil Chem. Soc., 37, 383, and 576, 1960.
239. R.G. Laughlin, J. Org. Chem., 27, 3644, 1962.
240. R.G. Laughlin, J. Org. Chem., 30, 1322, 1965.
241. G. Friedel, Ann. de Physique, 18, 300, 1922.
242. R.G. Snyder and J.H. Schachtschneider, Spectrochim. Acta, 19, 85, 1963.
243. J.G. Pritchard and H.M. Nelson, J. Phys. Chem., 64, 795, 1960.
244. L.J. Bellamy, Infra-red Spectra of Complex Molecules, Methuen, P. 17, 1964.
245. P. Debye and W. Prins, J. Colloid Sci., 13, 86, 1958.
246. P. Debye and H. Coll, J. Colloid Sci., 17, 220, 1962.
247. M. Tichy, Adv. Org. Chem., 5, 115, 1965.

248. T.D. Flynn, R.L. Werner and B.M. Graham, Aust. J. Chem., 12, 575, 1959.
249. F. Dalton, G.D. Meakins, J.H. Robinson and W. Zaharia, J. Chem. Soc., 1566, 1962.
250. J. Stevens, Ph.D. Thesis, Sheffield University, 1970.
251. P.J. Krueger and H.D. Mattee, Can. J. Chem., 42, 347, 1964.
252. L. Jons, P.N. Schleyer and E. Osawa, Tetrahedron, 24, 4759, 1968.
253. R. Piccolini and S. Winstein, Tetrahedron Letters, No. 13, 4, 1959.
254. M. Oki and H. Iwamura, Bull. Chem. Soc. Japan, 32, 950, 1959
255. E.L. Saier, L.R. Cousins and M.R. Basila, J. Chem. Phys., 41, 40, 1964.
256. L.J. Bellamy, Advances in Infra-red Group frequencies, Methuen, P. 151, 1968.
257. R.E. Kagarise and K.B. Whetsel, Spectrochim. Acta, 18, 341, 1962.
258. T.C. Briuce and T.H. Fife, J. Amer. Chem. Soc., 84, 1973, 1962.
259. M. Oki and M. Hirota, Bull. Chem. Soc. Japan, 34, 374, 1961.
260. J.J. Daly, Persp. in Struct. Chem., Ed. J.D. Duniltz and J.A. Ibers, John Wiley, VIII, 165, 1970.
261. D. Chapman, The structure of lipids, Methuen, P. 233, 1965.
262. A. Muller, Proc. Roy. Soc., 138A, 514, 1932.
263. T. Seto, Mem. Coll. Sci. (Kyoto University), 30A, 89, 1962.
264. D.E.C. Corbridge, Topics in Phosphorus Chem., Interscience, 6, 235, 1959.
265. L.W. Daasch and D.C. Smith, J. Chem. Phys., 19, 22, 1951.
266. C.D. Miller, R.C. Miller, and W. Rogers, Jr., J. Amer. Chem. Soc., 80, 1562, 1958.

267. N. Sheppard, *Advances in Spectroscopy*, Interscience, 1, 289, 1959.
268. R.G. Snyder, *J. Mol. Spect.*, 4, 411, 1960.
269. E. Von Sydow, *Acta Chem. Scand.*, 9, 1119, 1955.
270. R.G. Sinclair, A.F. McKay and R.N. Jones, *J. Amer. Chem. Soc.*, 74, 2575, 1952.
271. E.R. Andrew, *J. Chem. Phys.*, 18, 607, 1950.
272. E.R. Andrew, *Nuclear Magnetic Resonance*, Cambridge University Press, 1955.
273. E.V. Riltsev, *Zuhm. Priklad. Spektr.*, 15, 889, 1971.
274. T. Gramstad and G.V. Binst, *Spectrochim. Acta*, 22, 1681, 1966.
275. N.N. Ugarova, L. Radic and I. Nemes, *Russ. J. Phys. Chem.*, 41, 835, 1967.
276. A.H. Narten, M.D. Danford and H.A. Levy, *Disc. Faraday Soc.*, 42, 97, 1967.
277. O. Glemser and E. Hartert, *Z. Anorg. Allgem. Chem.*, 283, 111, 1956.
278. E.R. Lippincott and R. Schroeder, *J. Chem. Phys.*, 23, 1099, 1955.
279. D. Williams, *Nature*, 210, 194, 1966.
280. D.A. Draeger, N.W.B. Stone, B. Cumutte and D. Williams, *J. Opt. Soc. Am.*, 56, 64, 1966.
281. R. Oder and D.A.J. Goring, *Spectrochim. Acta*, 27A, 2285, 1971.
282. J.E. Mrochek, J. Richard and C.V. Banks, *J. Inorg. Nucl. Chem.*, 27, 625, 1965.
283. E. Bullock and D.G. Tuck, *Trans. Faraday Soc.*, 59, 1293, 1963.
284. K.B. Whetsel and R.E. Kagarise, *Spectrochim. Acta*, 18, 315, 1962.

Postgraduate course of studies

The following series of lectures given to postgraduate students at the University of Sheffield were attended.

1. Structure of membranes, by Professor D. Chapman (6 lectures).
2. X-ray crystallography, by Dr. N. A. Bailey (6 lectures).
3. Computing and chemistry, Dr. D. B. Cook (6 lectures)